ATOMIC AND PLASMA–MATERIAL INTERACTION DATA FOR FUSION

VOLUME 7 PART B

INTERNATIONAL
ATOMIC ENERGY AGENCY
VIENNA, 2001

ATOMIC AND PLASMA–MATERIAL INTERACTION DATA FOR FUSION

VOLUME 7

PART B

INTERNATIONAL ATOMIC ENERGY AGENCY, VIENNA, 2001

The volumes of ATOMIC AND PLASMA–MATERIAL INTERACTION DATA FOR FUSION are published by the International Atomic Energy Agency normally once a year.

For these volumes, papers, letters and reviews are accepted which deal with the following topics:

- Elementary collision processes in fusion plasmas involving photons, electrons, ions, atoms and molecules;
- Collision processes of plasma particles with surfaces of fusion relevant materials;
- Plasma-material interaction phenomena, including the thermophysical response of materials.

Each submitted contribution should contain fusion relevant data and information in either of the above areas. Original contributions should provide new data, using well established methods. Review articles should give a critical analysis or evaluation of a wider range of data. They are normally prepared on the invitation by the Editor or on prior mutual consent. Each submitted contribution is assessed by two independent referees.

Every manuscript submitted must be accompanied by a *disclaimer* stating that the paper has not been published and is not being considered for publication elsewhere. If no copyright is claimed by the authors, the IAEA automatically owns the copyright of the paper.

Guidelines for the preparation of manuscripts are given on the inside back cover. Manuscripts and correspondence should be addressed to: The Editor, ATOMIC AND PLASMA–MATERIAL INTERACTION DATA FOR FUSION, International Atomic Energy Agency, Wagramer Strasse 5, P.O. Box 100, A- 1400 Vienna, Austria.

Publisher: International Atomic Energy Agency, Wagramer Strasse 5, P.O. Box 100, A-1400 Vienna, Austria

---

ATOMIC AND PLASMA–MATERIAL INTERACTION DATA FOR FUSION, VOLUME 7
IAEA, VIENNA, 2001
STI/PUB/023/APID/07/B

EDITORIAL NOTE

The present volume of Atomic and Plasma-Material Interaction Data for Fusion is devoted to a critical review of the physical sputtering and radiation enhanced sublimation (RES) behaviour of fusion plasma-facing materials, in particular carbon, beryllium and tungsten. The present volume is intended to provide fusion reactor designers a detailed survey and parameterization of existing, critically assessed data for the chemical erosion of plasma-facing materials by particle impact. The survey and data compilation is presented for a variety of materials containing the elements C, Be and W (including dopants in carbon materials) and impacting plasma species. The dependencies of physical sputtering and RES yields on the material temperature, incident projectile energy, and incident flux are considered. The main data compilation is presented as separate data sheets indicating the material, impacting plasma species, experimental conditions, and parameterizations in terms of analytic functions.

This volume of Atomic and Plasma-Material Interaction Data for Fusion is the result of a five year Co-ordinated Research Project on "Plasma-surface interaction induced erosion of fusion reactor materials" in the period 1992-1997. A companion volume was published in 1998, which provided a critical review and data compilation for chemical erosion induced by fusion plasma particle impact.

The International Atomic Energy Agency expresses its appreciation to the contributors to this volume for their dedicated effort and co-operation.

Vienna, December 2000

Particle Induced Erosion of Be, C and W in Fusion Plasmas.

Part B: Physical Sputtering and Radiation-Enhanced Sublimation.

W. Eckstein[a], J. A. Stephens[b], R. E. H. Clark[b], J. W. Davis[c], A. A. Haasz[c], E. Vietzke[d], and Y. Hirooka[e]

[a] *Max-Planck-Institut für Plasmaphysik, EURATOM Association, D-85748 Garching bei München, Germany*

[b] *Division of Physical and Chemical Sciences, Nuclear Data Section, International Atomic Energy Agency, P.O. Box 100, Wagramer Strasse 5, A-1400 Vienna, Austria*

[c] *Fusion Research Group, University of Toronto, Institute for Aerospace Studies, 4925 Dufferin Street, Toronto, Ontario, Canada, M3H 5T6*

[d] *Institut für Plasmaphysik, Forschungszentrum Jülich (KFA), EURATOM Association, D-52425 Jülich, Germany*

[e] *National Institute for Fusion Science, 322-6, Oroshi-cho, Toki-shi, Gifu-ken, 509-5292 Japan*

CONTENTS

1 INTRODUCTION

1.1 Motivations and Scope

Extensive literature is available on the erosion of a wide spectrum of materials that have – over the years – been considered for plasma-facing applications in fusion reactors. The term 'erosion', in itself, encompasses processes such as physical sputtering, chemical reactions leading to the formation of volatile particles, radiation-enhanced sublimation (which occurs for carbon-based materials), and thermal sublimation. The major deleterious effects of erosion include: a reduced lifetime for the plasma-facing material, contamination of the fusion plasma, and tritium uptake due to codeposition of eroded material with the hydrogen fuel. Indeed, these issues are among the critical research and development challenges that need to be resolved for next-generation fusion devices such as the International Thermonuclear Experimental Reactor, ITER.

The preparation of this compendium results from an IAEA Coordinated Research Program on "Plasma-Interaction Induced Erosion of Fusion Reactor Materials." The objective of the program was to focus and coordinate the research activities of the participating institutions on the understanding of physical mechanisms of erosion processes and to undertake the compilation and critical assessment of a comprehensive erosion database for fusion research. We anticipate that the information so generated will be useful for the design of plasma-facing components, and also for modeling the transport of eroded particles in the fusion plasma, which in most cases leads to the redeposition of such particles on wall surfaces.

Due to the multifaceted nature of erosion and the broad spectrum of elements and compounds for which erosion data are available, an all-inclusive compendium would not only entail an immense task, but would also be cumbersome for the user community. Hence, in this document we focus on erosion due to **physical sputtering, chemical erosion** and **radiation-enhanced sublimation** induced by fusion plasma particle impact. Thermal sublimation is well understood and has been documented in standard handbooks.

Regarding target materials, we have selected Be, C and W, the three primary candidate materials being considered for ITER. Some relevant compounds of these elements (e.g., B_4C, TiC, SiC, etc.), as well as dopants used in conjunction with carbon, are also included. The impacting plasma species have also been selected on the basis of their fusion relevance. Here we included the hydrogenic species H, D, T, the He ash, O impurity, and elements that either result from the erosion process (such as C, Be, W, etc.) or are injected into the plasma for their effectiveness in dispersing power loading via enhanced radiation (e.g., Ne, Ar, N_2, etc.).

1.2 Basic Features of Particle-Induced Erosion Processes

Physical sputtering occurs via collisional interactions between impacting projectile atoms and atoms in the target, leading to the ejection of some of the target atoms. This process occurs for all materials for incident particle energies above a certain threshold, which is characteristic of the target-projectile combination; the

physical sputtering yield is not a function of temperature. The mechanisms associated with physical sputtering are well understood and are well-documented [1-5].

The occurrence of **chemical erosion** depends on the projectile-target combination and its mutual chemical reactivity. Chemical erosion can occur at all incident particle energies. For example, in the case of carbon, H impact leads to the formation of hydrocarbons, with yields peaking in the 500-1000 K temperature range; reactions occur even at sub-eV impact energies, with no evidence of an energy threshold. At present, the mechanisms associated with chemical erosion of carbon due to hydrogen impact are not fully understood. Recent modeling advances [6-10], however, have provided new insights into the complex physical/chemical interactions. Oxygen impact on carbon produces CO_2 and CO. Combined H and O also leads to the formation of some water. For Be and W, chemical erosion is also possible; e.g., O impact on W produces a variety of tungsten oxides, W_xO_y. An assessment and presentation on the chemical erosion of carbon and carbon-based materials has been reported in Volume 7A of this series.

Radiation-enhanced sublimation (RES) has only been observed in carbon-based materials, and is induced by energetic particle impact at temperatures above ~1200 K. The present understanding of RES is based on the formation of interstitial-vacancy pairs in the implantation zone by energetic incident atoms (chemically inert or otherwise). At sufficiently high temperatures the interstitial C atoms diffuse to the surface, and subsequently leave the surface with 'thermal' energy [11-14]. This model of RES agrees well with experimental observations, with the exception of flux-dependence predictions. The model predicts a decrease of RES yield with increasing incident particle flux to the power of (-0.25). Experimental results generally show a power of ~(-0.1) [15-18]. Since RES results from atom displacements, this process (like physical sputtering) only occurs above an incident particle energy threshold.

The contribution of these erosion processes to the total erosion yield depends on both target and projectile characteristics. For example, in Fig. 1.1 we show the relative role of physical sputtering [5], chemical erosion [19-22] and RES [13, 15] for protium and deuterium impact on carbon for different H [Fig. 1.1a] and D [Fig. 1.1b] energies, as a function of carbon temperature. For both H and D, we note that physical sputtering yields are only applicable for energies above the sputtering threshold (~40 eV for H and ~33 eV for D). Physical sputtering is a function of energy, and the yield for 1000 eV H and D are relatively higher than those at 100 eV. Chemical erosion becomes significant for temperatures below ~1000 K, with the chemical erosion yield being dependent on both the target temperature and projectile energy. The chemical erosion yield vs temperature curves are characterized by a maximum whose level (Y_m) and the temperature at which it occurs (T_m) also depend on the projectile energy. The monotonically increasing yield for temperatures above ~1000 K for the 100 and 1000 eV cases is due to radiation-enhanced sublimation. For the sub-eV and 10 eV cases only chemical erosion occurs, as these energies are below the thresholds for both physical sputtering and RES. We note that the physical sputtering and RES yields for D are relatively higher than for H. On the other hand, the chemical erosion yields for the two isotopes of hydrogen are not significantly different. In addition to the parameters noted above, the incident projectile flux density is also an important parameter. Unfortunately, the flux density range available with mass-

analyzed accelerators is limited to $\sim 10^{16}/cm^2s$ which is 2 or 3 orders of magnitude lower than the fluxes existing in the divertor and limiter regions of tokamaks. To explore the high tokamak-relevant fluxes, erosion yield measurements are also being performed in laboratory plasma devices and tokamaks.

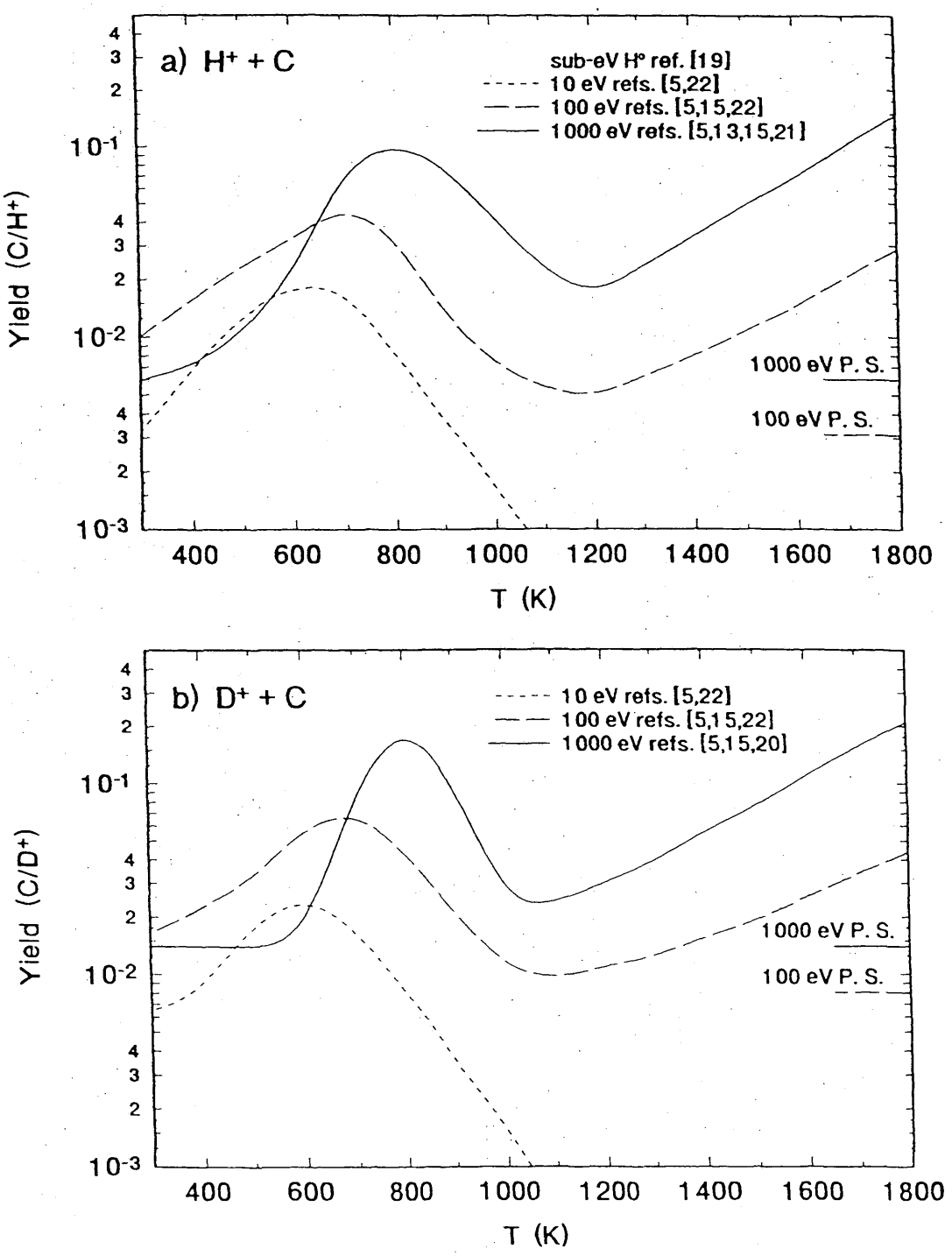

Figure 1.1: Erosion yields due to hydrogen and deuterium impact of carbon are presented at various energies, illustrating the characteristics of physical sputtering, radiation-enhanced sublimation and chemical erosion.

1.3 Organization and Presentation of the Compiled Erosion Data

The information in this compendium has been organized with two objectives in mind. First, selected collections of data obtained by various laboratories under specified parameter groupings have been compiled. In this process, the authors of the compendium exercised a degree of critical assessment. The second objective was to present the data in a form that is transparent to the user community – for the design of plasma-facing components and the modeling of impurity transport and redeposition processes in tokamaks.

For the most part, the experimental erosion data presented in this compendium were obtained from controlled laboratory experiments with mass-analyzed ion beams. Furthermore, only steady-state measurements are included. In the case of physical sputtering, the process is well understood and reliable model calculations are also available, and the experimental data have been fitted to the model. In cases where no experimental data are available, especially at low energies, only model calculations are given. Attempts at modeling chemical erosion and radiation-enhanced sublimation have also been made, with varying success, and work in this area is still continuing. Where applicable, models are fitted to the experimental data. However, for the most part, the chemical and RES data are fitted to polynomial or other appropriate analytic expressions. Therefore, users of the data presented here are cautioned that the **fitting equations only apply in the experimental parameter ranges indicated**.

The individual data sheets in Sections 2 and 3 include the data source, accuracy when known, analytic fitting functions and coefficients used to parameterize the data, and brief comments on the relevant experimental conditions or parameters. The accuracies indicated are absolute unless otherwise noted. A list of abbreviations used in the comments on the data sheets (and on some graphs) is given in Appendix A. This includes abbreviations for the 'ALADDIN' hierarchical labels appearing on the data sheets, which specify a particular reactant, material, or type of erosion process. A list of the analytic functions used for fitting (ALADDIN evaluation functions) are given in Appendix B. This information will be used in (web accessible) computer databasing of the erosion data included in this compendium. ALADDIN (**A** **L**abelled **A**tomic **D**ata **IN**terface) is the data format and database system currently utilized by the Atomic and Molecular Data Unit, IAEA, to provide web retrievals of numerical atomic, molecular and plasma-surface interaction data for fusion research.

The compendium is presented in two Volumes of *Atomic and Plasma-Material Interaction Data for Fusion.* In this Volume, Part B, we present physical sputtering and RES data for C, Be, W, and carbon-based materials. In the previous Volume, Part A, chemical erosion data for carbon based materials are presented.

References for Section 1

[1] ECKSTEIN, W., PHILIPPS, V., "Physical Sputtering and Radiation Enhanced Sublimation", in *Physical Processes of the Interaction of Fusion Plasmas with Solids* (HOFER, W. O., J. ROTH, Eds.), Academic Press, San Diego (1996) 93.

[2] BEHRISCH, R. (Ed.), *Sputtering by Particle Bombardment I*, Topics in Applied Physics, Vol. **47**, Springer, Berlin (1981).

[3] BEHRISCH, R., (Ed.), *Sputtering by Particle Bombardment II*, Topics in Applied Physics, Vol. **52**, Springer, Berlin (1983).

[4] BEHRISCH, R., WITTMAACK, K. (Eds.), *Sputtering by Particle Bombardment III*, Topics in Applied Physics, Vol. **64**, Springer, Berlin (1991).

[5] ECKSTEIN, W., C. GARCIA-ROSALES, C., ROTH, J., OTTENBERGER, W., "Sputtering Data", Max-Planck-Institut für Plasmaphysik Report IPP 9/82 (1993).

[6] HORN, A., SCHENK, A., BEINER, J., WINTER, B., LUTTERLOH, C., WITTMANN, M., KÜPPERS, J., Chemical Physics Lett. **231** (1994) 193.

[7] WITTMANN, M., KÜPPERS, J., J. Nucl. Mater. **227** (1996) 186.

[8] ROTH, J., GARCIA-ROSALES, C., Nucl. Fusion **36** (1996) 1647.

[9] MECH, B. V., HAASZ, A. A., DAVIS, J. W., "A Model for Graphite Erosion Due to Low-energy H^+ and D^+", J. Appl. Phys., submitted.

[10] VIETZKE, E., HAASZ, A. A. "Chemical Erosion", in *Physical Processes of the Interaction of Fusion Plasmas with Solids* (HOFER, W. O., ROTH, J., Eds.), Academic Press, San Diego (1996) 135.

[11] ROTH, J., MÖLLER, W., Nucl. Instrum. and Meth. B **7/8** (1985) 788.

[12] VIETZKE, E., FLASKAMP, K., HENNES, M., PHILIPPS, V., Nucl. Instrum. and Meth. B **2** (1984) 617.

[13] FRANZEN, P., DAVIS, J. W., HAASZ, A. A., J. Appl. Phys. **78** (1995) 817.

[14] UEDA, Y., NAKANO, K., OHTSUKA, Y., ISOBE, M., GOTO, S., NISHIKAWA, M., J. Nucl. Mater. **227** (1996) 251.

[15] HAASZ, A. A., DAVIS, J. W., J. Nucl. Mater. **151** (1987) 77.

[16] PHILIPPS, V., VIETZKE, E., SCHORN, R. P., TRINKAUS, H., J. Nucl. Mater. **155-157** (1987) 319.

[17] HAASZ, A. A., DAVIS, J. W., CROESSMANN, C. D., DOYLE, B. L., NYGREN, R. E., WALSH, D. S., WATKINS, J. G., WHITLEY, J. B., J. Nucl. Mater. **173** (1990) 108.

[18] HAASZ, A. A., DAVIS, J. W., J. Nucl. Mater. **224** (1995) 141.

[19] DAVIS, J. W., HAASZ, A. A., STANGEBY, P. C., J. Nucl. Mater. **155-157** (1988) 234.

[20] ROTH, J., BOHDANSKY, J., Nucl. Instr. Meth. **B23** (1987) 549.

[21] HAASZ, A. A., DAVIS, J. W., J. Nucl. Mater. **175** (1990) 84.

[22] MECH, B. V., HAASZ, A. A., DAVIS, J. W., J. Nucl. Mater. **255** (1998) 153.

2 Physical Sputtering of Elemental Targets and Compounds: Data Collection

Physical Sputtering is defined as a kinetic process by which energy is transferred from an energetic incident atom or ion (projectile) on target atoms. The developing collision cascade leads to the emission of target atoms. The characteristic value of importance is the sputter yield defined as the number of sputtered atoms divided by the number of projectiles. The sputter yield exhibits a threshold below which the amount of energy transferred to the target atoms is too small for them to overcome the surface barrier. With increasing energy of the projectiles the sputter yield increases, reaches a maximum and decreases again. This decrease at higher energies is caused by the increasing depth of the collision cascade, moving away from the surface. Whereas the collision kinetics is governed by the mass ratio of target atom mass to projectile mass, each element has its specific surface binding energy (usually the heat of sublimation is assumed).

In addition to the dependence of the sputter yield on the collision partners and projectile energy, the yield depends also on the angle of incidence, measured from the surface normal. The sputter yield increases with increasing angle of incidence (as the collision cascade moves closer to the surface), reaches a maximum (typically between 55° and 80°, depending on the projectile target system), and decreases for glancing angles of incidence due to the increase of the particle reflection coefficient.

Most experimental data have been obtained with the weight loss method. The errors are typically in the 10% to 20% range, but sometimes the reproducibility can be as much as a factor of two, which is attributed to surface structure changes with bombarding fluence. In general, the surfaces in the experiments are not well characterized regarding surface roughness, and to a lesser extent, surface impurities (depending on residual gas pressure, flux and fluence of the incident beam). Usually, yields measured with the weight loss method are determined for large fluences, which are needed to get a reasonable weight loss.

Sputter yields calculated by computer simulation depend on mean repulsive interaction potentials which may be better known for some projectile-target combinations than for others. Uncertainties due to this effect should be less than a factor of two in most cases. The statistical errors of the calculated sputtering yields are better than 3% (1σ) in nearly all cases; for very low yields (below 10^{-5}), however, the statistical error can be of the order of 20% .

Nearly all simulations consider a flat surface (roughness of the order of half a monolayer thickness is often taken into account). The calculated values are valid for nearly flat surfaces. To check the sensitivity of plasma edge simulation results on surface roughness a sputter yield of twice the yield at normal incidence and independent on the angle of incidence can be tried (an assumption used in DIVIMP [1, 2] for rough surfaces). A more accurate method, described in [33], has been applied to C [33] and to Be [34].

Static programs, like TRIM.SP and ACAT for example, provide yields only at low fluence ('zero' fluence case). Sputtering of compounds or mixtures of elements usually leads to a preferential sputtering of the lighter species, and therefore to a composition change in the implantation range. Bombardment of targets with non-

volatile species can also lead to composition changes and to deposited layers of this species on the substrate. These processes depend on the incident fluence and have to be determined in each case. These processes are not discussed here, but information on relevant systems can be found in [35].

In contrast to earlier fitting formulae, a new approximation is used here. In [15] the revised Bohdansky formula was applied to describe the energy dependence of the sputter yield at normal incidence

$$Y(E_0) = Q s_n^{KrC}(\varepsilon) \left[1 - \left(\frac{E_{th}}{E_0}\right)^{2/3}\right] \left(1 - \frac{E_{th}}{E_0}\right)^2$$

where $s_n^{KrC}(\varepsilon)$ is the nuclear stopping based on the Kr-C interaction potential, which is a good mean potential for many species.

$$s_n^{KrC}(\varepsilon) = \frac{0.5 \ln(1 + 1.2288\varepsilon)}{\varepsilon + 0.1728\sqrt{\varepsilon} + 0.008\varepsilon^{0.1504}}$$

$$\text{with} \qquad \varepsilon = E_0 \frac{M_2}{M_1 + M_2} \frac{a_L}{Z_1 Z_2 e^2} = E_0 \varepsilon_L \quad .$$

Z_1 and Z_2 are the atomic numbers, and M_1 and M_2 the masses of the projectile and the target atoms, respectively. The Lindhard screening length, a_L, is given by

$$a_L = \left(\frac{9\pi^2}{128}\right)^{1/3} a_B \left(Z_1^{2/3} + Z_2^{2/3}\right)^{-1/2}$$

where a_B is the Bohr radius. E_{th} is the threshold energy for sputtering, and E_0 is the incident energy of the projectile. Q and E_{th} are used as parameters. Some discrepancies in calculated values originate from the fact that TRIM.SP uses the Lindhard screening length, whereas ACAT applies the Firsov screening length (the exponents of the charge term are exchanged), which can differ for the same system by 4 to 12 percent. Yamamura and coworkers [62,63,66] applied a small correction to the screening length in many cases, to get better agreement with experimental data, which was not done in the TRIM.SP calculations.

Newer calculated sputter yields [15, 16] give a lower sputtering threshold than the fit with the revised Bohdansky formula. For this reason a new fit formula was developed in the present study,

$$Y(E_0) = 0.5Q \frac{\left(\frac{E_0}{E_{th}} - 1\right)^{\mu} \ln(1 + 1.2288\varepsilon)}{\lambda + \left(\frac{E_0}{E_{th}} - 1\right)^{\mu} [\varepsilon + 0.1728\sqrt{\varepsilon} + 0.008\varepsilon^{0.1504}]} \quad .$$

Comparison with the Bohdansky formula shows that the exponent of the threshold terms is now the parameter μ. The threshold term appears in both the numerator and the denominator to ensure that the high energy is not affected by the threshold term. The additional third parameter λ is introduced to ensure that the denominator does not become too small.

The assigned accuracy of the data points is 10% for the experimental points and 5% for the calculated points. These accuracies have been changed in some cases to produce a better fit to the data points.

The reason for also changing the formula for the angular dependence of the sputter yield is that the often used Yamamura formula does not agree with the available data for all cases, especially for low incident energies and for selfbombardment, see [15]. The Yamamura formula is given by

$$Y(E_0,\alpha) = Y(E_0,0)\,[\cos(\alpha)]^{-f} \exp\left\{f\left[1-\frac{1}{\cos\alpha}\right]\sin(\eta)\right\}$$

$$\text{with} \qquad \eta = \pi/2 - \alpha_{opt} \qquad ,$$

where the angle of incidence α is measured from the surface normal, and α_{opt} is the angle of incidence for which the sputter yield has a maximum. f and η are used as fit parameters. The new fit formula

$$Y(E_0,\alpha) = Y(E_0,0)\left\{\cos\left[\left(\frac{\alpha}{\alpha_0}\frac{\pi}{2}\right)^c\right]\right\}^{-f} \exp\left\{b\left(1-\frac{1}{\cos\left[\left(\frac{\alpha}{\alpha_0}\frac{\pi}{2}\right)^c\right]}\right)\right\}$$

keeps most of the original Yamamura formula, but introduces additional physical information. Namely, incident atoms (projectiles) may experience a binding energy E_{sp}, which creates an acceleration and a refraction towards the surface normal [14], so that an incidence angle of 90° is never reached. The parameter η is not used anymore, but a new parameter c is chosen. The new value α_0 is given by

$$\alpha_0 = \pi - \arccos\sqrt{\frac{1}{1+E_0/E_{sp}}} \geq \frac{\pi}{2}$$

where the binding energy of projectiles, E_{sp}, has to be provided. It is assumed that for selfbombardment, E_{sp} is equal to the surface binding energy of target atoms; for noble gas projectiles, $E_{sp} = 0$; for hydrogen isotopes, $E_{sp} = 1$ eV.

The data sets presented here have been separated into two categories. The first category contains data with correct calibration, while the second category are suspected to possess an offset to the true calibration but possess the correct information about the form of the fitting curve. These latter data were assigned scale factors, which together with the model parameters, were determined by employing Bayesian probability theory.

The new formula has been successful in describing sputtering, especially at low energies near the sputtering threshold. Other approaches in the present study have been tested but with no better success. For the fitting two approaches have been tried. For the target charges and masses the mean values are used or ε_L has been used as a free parameter. As mentioned above, the second procedure sometimes provides a better fit, although it is not justified on physical grounds. In some cases the fit was significantly better if ε_L is was used as a free fitting parameter. Although

there is no physical justification for doing this it has been used in some cases for a better fitting of the available data. This implies that the fit formula with the given parameters should be only used in the energy range where data are available.

In the section on the angular dependence of the sputtering yield, calculated data points have been fitted separately from the experimental points, because the calculations assume a flat surface (roughness smaller than the mean atomic distance in the solid) and experimental surfaces have larger, mostly unknown, roughness. Due to the fact that targets can be polished by ion bombardment, if the data was available, a fit for the calculated and measured points were performed separately. For a reasonable fit, the yield at normal incidence, $Y(E_0, 0)$, was used as a fit parameter.

For more detailed information on the sputtered atoms, the following procedures are recommended [16]. The energy distribution of the sputtered atoms can be described by a Thompson distribution [57]:

$$f(E)dE = \frac{E}{(E+E_s)^3}dE \quad . \tag{1}$$

Applying this distribution, an energy E can be determined by a pseudo-random number r according to the formula [16]

$$\frac{E}{E_s} = \frac{1}{(1+1/E_m)\sqrt{1/r-1}} \quad , \tag{2}$$

where E_s is the surface binding energy and E_m the maximum transferable energy divided by the surface binding energy:

$$E_m = \gamma\frac{E_0}{E_s} \qquad \text{with} \qquad \gamma = \frac{4M_1M_2}{(M_1+M_2)^2} \quad . \tag{3}$$

E_0 is the incident energy. Another possibility is to use the mean energy $< E >$ of sputtered atoms given by

$$< E(E_0,\alpha) >= E_0\frac{Y_E(E_0,\alpha)}{Y(E_0,\alpha)} \quad . \tag{4}$$

The angular distribution of sputtered atoms can be approximated by a cosine distribution. An exit angle θ can again be determined by a random number r, i.e.,

$$\theta = \arcsin r \quad . \tag{5}$$

Due to ion bombardment, the composition of Be- and C- containing compounds in the implantation region will change with the incident fluence until some steady state is reached [49]. For volatile projectiles and compounds like Be_4B or B_4C [70], where the masses of the compound constituents are very close, this effect is small; but the effect can be rather large for constituents with very different masses (like WC), especially close to the sputtering threshold. As mentioned above, experimental are usually made after fluences, whereas results from calculations with static programs represent values at 'zero' fluence. Deviations between experimental data and calculated results are, therefore, reasonable, especially at low energies.

References for Section 2

[1] STANGEBY, P. C., FARRELL, C., HOSKINS, S., WOOD, L., Nucl. Fusion **28** (1988) 1945.

[2] STANGEBY, P. C., ELDER, J. D., J. Nucl. Mater. **196-198** (1992) 258.

[3] ALMÉN, O., BRUCE, G., Nucl. Instrum. Methods **11** (1961) 257.

[4] ALMÉN, O., BRUCE, G., Nucl. Instrum. Methods **11** (1961) 279.

[5] BALDEN, M., ROTH, J., WU, C. H., J. Nucl. Mater. **258-263** (1998) 740.

[6] BAY, H. L., BOHDANSKY, J., HOFER, W. O., ROTH, J., Appl. Phys. **21** (1980) 327.

[7] BETZ, G., DOBROZEMSKY, R., VIEHBÖCK, F. P., WOTTKE, H., Proc. 9th Int. Conf. Phenomenon Ionized Gases (1969) 91.

[8] BOHDANSKY, J., ROTH, J., SINHA, M. K., proc. 9th Symp. Fusion Technol. (1976) 541.

[9] BOHDANSKY, J., BAY, H. L., OTTENBERGER, W., J. Nucl. Mater. **76 & 77** (1978) 163.

[10] BOHDANSKY, J., CHEN, G. L., ECKSTEIN, W., ROTH, J., SCHERZER, B. M. U., BEHRISCH, R., J. Nucl. Mater. **111 & 112** (1982) 717.

[11] BOHDANSKY, J., ROTH, J., OTTENBERGER, W., IPP-JET No. 31, Garching (1985).

[12] BORDERS, J. A., LANGLEY, R. A., WILSON, K. L., J. Nucl. Mater. **76 & 77** (1978) 168.

[13] ECKSTEIN, W., LÁSZLÓ, J., J. Nucl. Mater. **183** (1991) 19.

[14] ECKSTEIN, W., Computer Simulation of Ion-Solid Interactions, Springer Series in Materials Science, Vol. 10, Springe, Berlin, Heidelberg, New York (1991).

[15] ECKSTEIN, W., GARCIA-ROSALES, C., ROTH, J., OTTENBERGER, W., Report IPP 9/82, Garching (1993).

[16] ECKSTEIN, W., Report IPP 9/117, Garching (1998).

[17] FETZ H., OECHSNER, H., Proc. 6th Int. Conf. Ionization Phenomena in Gases Vol. II, Paris, (1963) 39.

[18] GARCÍA-ROSALES, C., GAUTHIER, E., ROTH, J., R. Schwörer and W.Eckstein, J. Nucl. Mater. **189** (1992) 1.

[19] GAUTHIER, E., ECKSTEIN, W., LÁSZLÓ, J., ROTH, J., J. Nucl. Mater. **176 & 177** (1990) 438.

[20] GURMIN, B. M., MARTYNENKO, T. P., RYZHOV, YU. A., Sov. Phys. - Solid State **10** (1968) 324.

[21] GUSEVA, M., GUREEV, V. M., KORSHUNOV, S. N., NEUMOIN, V. E., SOKOLOV, YU. A., STOLYAROVA, V. G., VASILIEV, V. I., RYLOV, S. V., J. Nucl. Mater. **220-222** (1995) 957.

[22] GUSEVA, M., BIRUKOV, A. YU., GUREEV, V. M., DANELJAN, L. S., KORSHUNOV, S. N., MARTYNENKO, YU. V., MOSKOVIN, P. S., SOKOLOV, YU. A., STOLYAROVA, V. G., KALIKAUSKAS, V. S., J. Nucl. Mater. **233-237** (1996) 681.

[23] HAASZ, A. A., DAVIS, J. W., WU, C. H., J. Nucl. Mater. **162-164** (1989) 915.

[24] HECHTL, E., BOHDANSKY, J., ROTH, J., Proc. Symp. on Sputtering, ed. P. Varga, G. Betz and F. P. Viehböck, Inst. für Allg. Physik, Techn. Univ. Vienna (1980) 834.

[25] HECHTL, E., BOHDANSKY, J., ROTH, J., J. Nucl. Mater. **103 & 104** (1981) 333.

[26] HECHTL, E., BOHDANSKY, J., J. Nucl. Mater. **122 & 123** (1984) 1431.

[27] HECHTL, E., YANG, H. R., WU, C. H., ECKSTEIN, W., J. Nucl. Mater. **176 & 177** (1990) 874.

[28] HECHTL, E., ECKSTEIN, W., ROTH, J., LÁSZLÓ, J., J. Nucl. Mater. **179 - 181** (1991) 290.

[29] HECHTL, E., ROTH, J., ECKSTEIN, W., WU, C. H., J. Nucl. Mater. **220 - 222** (1995) 883.

[30] HIROOKA, Y., WON, J., BOIVIN, R., SZE, D., NEUMOIN, V., J. Nucl. Mater. **228** (1996) 148.

[31] HIROOKA, Y., WON, J., BOIVIN, R., SZE, D., NEUMOIN, V., J. Nucl. Mater. **230** (1996) 173.

[32] KOSHKIN, V. K., RYSOV, J. A., SHKARBAN, I. I., GOURMIN, B. M., Proc. 9th Int. Conf. Phenomenon Ionized Gases (1969) 92.

[33] KÜSTNER, M., ECKSTEIN, W., DOSE, V., ROTH, J., Nucl. Instrum. Meth. B **145** (1998) 320.

[34] KÜSTNER, M., ECKSTEIN, W., HECHTL, E., ROTH, J., J. Nucl. Mater. **265** (1999) 22.

[35] ECKSTEIN, W., J. Nucl. Mater. **xxx** (2000) in press.

[36] LAEGREID, N., WEHNER, G. K., J. Appl. Phys. **32** (1961) 365.

[37] NAVINSEK, B., CARTER, G., SPIG, Hercegnovi (1970) 65.

[38] OECHSNER, H., Z. Physik **261** (1973) 37.

[39] PLANK, H., SCHWÖRER, R., ROTH, J., Nucl. Instrum. Meth. B **111** (1996) 63.

[40] PLANK, H., SCHWÖRER, R., ROTH, J., Surf. Coat. Technol. **83** (1996) 93.

[41] ROSENBERG, D., WEHNER, G. K., J. Appl. Phys. **33** (1962) 1842.

[42] ROTH, J., BOHDANSKY, J., POSCHENRIEDER, W., SINHA, M. K., J. Nucl. Mater. **63** (1976) 222.

[43] ROTH, J., BOHDANSKY, J., OTTENBERGER, W., Report IPP 9/26, Garching (1979).

[44] ROTH, J., BOHDANSKY, J., BLEWER, R. S., OTTENBERGER, W., J. Nucl. Mater. **85 & 86** (1979) 1077.

[45] ROTH, J., BOHDANSKY, J., MARTINELLI, A. P., Radiat. Eff. **48** (1980) 213.

[46] ROTH, J., J. Nucl. Mater. **145 - 147** (1987) 87.

[47] ROTH, J., BOHDANSKY, J., OTTENBERGER, W., J. Nucl. Mater. **165** (1989) 193.

[48] ROTH, J., ECKSTEIN, W., BOHDANSKY, J., J. Nucl. Mater. **165** (1989) 199.

[49] ROTH, J., ECKSTEIN, W., GUSEVA, M., Fusion Engineering and Design **37** (1997) 465.

[50] RUZIC, D. N., SMITH, P. C., TURKOT, JR., R. B., J. Nucl. Mater. **241-243** (1997) 1170.

[51] SAIDOH, M. SONE, K., Jap. J. Appl. Phys. **22** (1983) 1361.

[52] SCHIRRWITZ, H., Beiträge aus der Plasmaphysik **2** (1962) 188.

[53] SMITH, JR., J. N., MAYER, JR., C. H., LAYTON, J. K., Trans. Am. Nucl. Soc. **22** (1975) 29.

[54] SMITH, JR., J. N., MAYER, JR., C. H., LAYTON, J. K., Nucl. Technol. **29** (1976) 318.

[55] SMITH, JR., J. N., MAYER, JR., C. H., LAYTON, J. K., J. Nucl. Mater. **67** (1977) 234.

[56] STUART, R. V., WEHNER, G. K., J. Appl. Phys. **33** (1962) 2345.

[57] THOMPSON, M. W., Philos. Mag. **18** (1968) 377.

[58] UEDA, S., OHSAKA, T., KUWAJIMA, S., J. Nucl. Mater. **258 - 263** (1998) 713.

[59] WINTERS, H. F., HORNE, D., Phys. Rev. B **10** (1974) 55.

[60] WU, C. H., E. HECHTL, E., YANG, H. R., ECKSTEIN, W., J. Nucl. Mater. **176 & 177** (1990) 845.

[61] WU, C. H., E. HECHTL, E., J. Nucl. Mater. **196 - 198** (1992) 569.

[62] YAMAMURA, Y., SAKAOKA, K., TAWARA, H., Report NIFS-DATA-31, Nagoya (1995).

[63] YAMAMURA, Y., TAWARA, H., Atomic Data and Nuclear Data Tables **62** (1995) 149.

[64] ZIEGLER, J. F., CUOMO, J. J., ROTH, J., Appl. Phys. Lett. **30** (1977) 268.

[65] S. N. Korshunov, M. I. Guseva, V. G. Stoljarova, Proc. 2nd IEA Int. Workshop on Beryllium Technology for Fusion, G. R. Longhurst (ed.), Lockheed Idaho Technologies CONF-9509218, (1995) 285.

[66] YAMAMURA, Y., TAWARA, H. Report NIFS-DATA-23, Nagoya (1995).

[67] BOHDANSKY, J., ROTH, J., SINHA, M. K., Proc. 9th Symposium Fusion Technology, Pergamon (1976) 541.

[68] BOHDANSKY, J., BAY, H. L., ROTH, J., Proc. 7th Int. Vac. Congr. & 3rd Conf. Solid Surfaces, Vienna (1978) 1509.

[69] ROTH, J., BOHDANSKY, J., WILSON, K. L., J. Nucl. Mater. **111 & 112** (1982) 775.

[70] ONO, T., KAWAMURA, T., ISHII, K., YAMAMURA, Y., Report NIFS-DATA-34, Nagoya (1996).

List of Reactions for Section 2

2 Physical sputtering of Be, C, W, and selected compounds

2.1 Energy dependence

2.1.1 Be

2.1.1.1 $H^+ + Be \rightarrow Be$

2.1.1.2 $D^+ + Be \rightarrow Be$

2.1.1.3 $T^+ + Be \rightarrow Be$

2.1.1.4 $He^+ + Be \rightarrow Be$

2.1.1.5 $Be^+ + Be \rightarrow Be$

2.1.1.6 $N^+ + Be \rightarrow Be$

2.1.1.7 $O^+ + Be \rightarrow Be$

2.1.1.8 $Ne^+ + Be \rightarrow Be$

2.1.1.9 $Ar^+ + Be \rightarrow Be$

2.1.2 C

2.1.2.1 $H^+ + C \rightarrow C$

2.1.2.2 $D^+ + C \rightarrow C$

2.1.2.3 $T^+ + C \rightarrow C$

2.1.2.4 $He^+ + C \rightarrow C$

2.1.2.5 $C^+ + C \rightarrow C$

2.1.2.6 $N^+ + C \rightarrow C$

2.1.2.7 $O^+, H_2O^+ + C \rightarrow C$

2.1.2.8 $Ne^+ + C \rightarrow C$

2.1.2.9 $Ar^+ + C \rightarrow C$

2.1.3 W

2.1.3.1 $H^+ + W \rightarrow W$

2.1.3.2 $D^+ + W \rightarrow W$

2.1.3.3 $T^+ + W \rightarrow W$

2.1.3.4 $He^+ + W \rightarrow W$

2.1.3.5 $C^+ + W \rightarrow W$

2.1.3.6 $N^+ + W \rightarrow W$

2.1.3.7 $O^+ + W \rightarrow W$

2.1.3.8 $Ne^+ + W \rightarrow W$

2.1.3.9 $Ar^+ + W \rightarrow W$

2.1.3.10 $W^+ + W \rightarrow W$

2.1.4 Selected Compounds

2.1.4.1 H^+, D^+, He^+ + Be_4B → total
2.1.4.2 H^+ + B_4C → total
2.1.4.3 D^+ + B_4C → total
2.1.4.4 T^+ + B_4C → total
2.1.4.5 He^+ + B_4C → total
2.1.4.6 B^+ + B_4C → total
2.1.4.7 C^+ + B_4C → total
2.1.4.8 H_2O^+ + B_4C → total
2.1.4.9 Ne^+ + B_4C → total
2.1.4.10 Ar^+ + B_4C → total
2.1.4.11 D^+ + Be_2C → total
2.1.4.12 H^+ + BeO → total
2.1.4.13 D^+ + BeO → total
2.1.4.14 He^+ + BeO → total
2.1.4.15 O^+ + BeO → total
2.1.4.16 H^+, D^+, He^+ + SiC → total
2.1.4.17 O^+, Ne^+ + SiC → total
2.1.4.18 H^+, D^+, He^+ + TiC → total
2.1.4.19 O^+, Ne^+ + TiC → total
2.1.4.20 H^+, D^+, He^+ + WC → total
2.1.4.21 D^+ + NS31 → total
2.1.4.22 D^+ + C (C-SiC matrix, Ti doped) → total
2.1.4.23 D^+ + C (Si doped) → total
2.1.4.24 D^+ + C (B doped) → total
2.1.4.25 D^+ + C (Ti doped) → total
2.1.4.26 D^+ + N112 → total

2.2 Angular dependence

2.2.1 Be

2.2.1.1 D^+ + Be → Be
2.2.1.2 T^+ + Be → Be
2.2.1.3 He^+ + Be → Be
2.2.1.4 He^+ + Be → Be
2.2.1.5 Be^+ + Be → Be
2.2.1.6 Be^+ + Be → Be
2.2.1.7 Be^+ + Be → Be
2.2.1.8 C^+ + Be → Be

2.2.2 C

2.2.2.1 $H^+ + C \rightarrow C$

2.2.2.2 $H^+ + C(HOPG) \rightarrow C$

2.2.2.3 $D^+ + C \rightarrow C$

2.2.2.4 $D^+ + C \rightarrow C$

2.2.2.5 $T^+ + C \rightarrow C$

2.2.2.6 $He^+ + C \rightarrow C$

2.2.2.7 $He^+ + C \rightarrow C$

2.2.2.8 $C^+ + C \rightarrow C$

2.2.2.9 $C^+ + C \rightarrow C$

2.2.3 W

2.2.3.1 $H^+ + W \rightarrow W$

2.2.3.2 $OH^+ + W \rightarrow W$

2.2.3.3 $Ar^+ + W \rightarrow W$

2.2.3.4 $W^+ + W \rightarrow W$

2.2.3.5 $W^+ + W \rightarrow W$

2.2.4 Selected Compounds

2.2.4.1 $D^+ + B_4C \rightarrow$ total

2.2.4.2 He^+, $C^+ + B_4C \rightarrow$ total

2.2.4.3 H^+, D^+, $He^+ + SiC \rightarrow$ total

2.2.4.4 $H^+ + TiC \rightarrow$ total

2.2.4.5 $D^+ + TiC \rightarrow$ total

2.2.4.6 $He^+ + TiC \rightarrow$ total

2.1.1.1 H^+ + Be

Comments: (1) Fit valid between E_{min}=E_{th} and E_{max}= 3.0000E+03 eV.
(2) Be (20°) is probably BeO (15Å) on Be.
(3) Be (650°) is probably Be layers on BeO.

Fitting parameters:

Parameter:	λ	q	μ	ϵ_L(eV^{-1})	E_{th}(eV)	Avg. Error (%)
	5.1192E-01	5.1960E-02	1.4954E+00	2.7931E-03	1.4425E+01	15.3

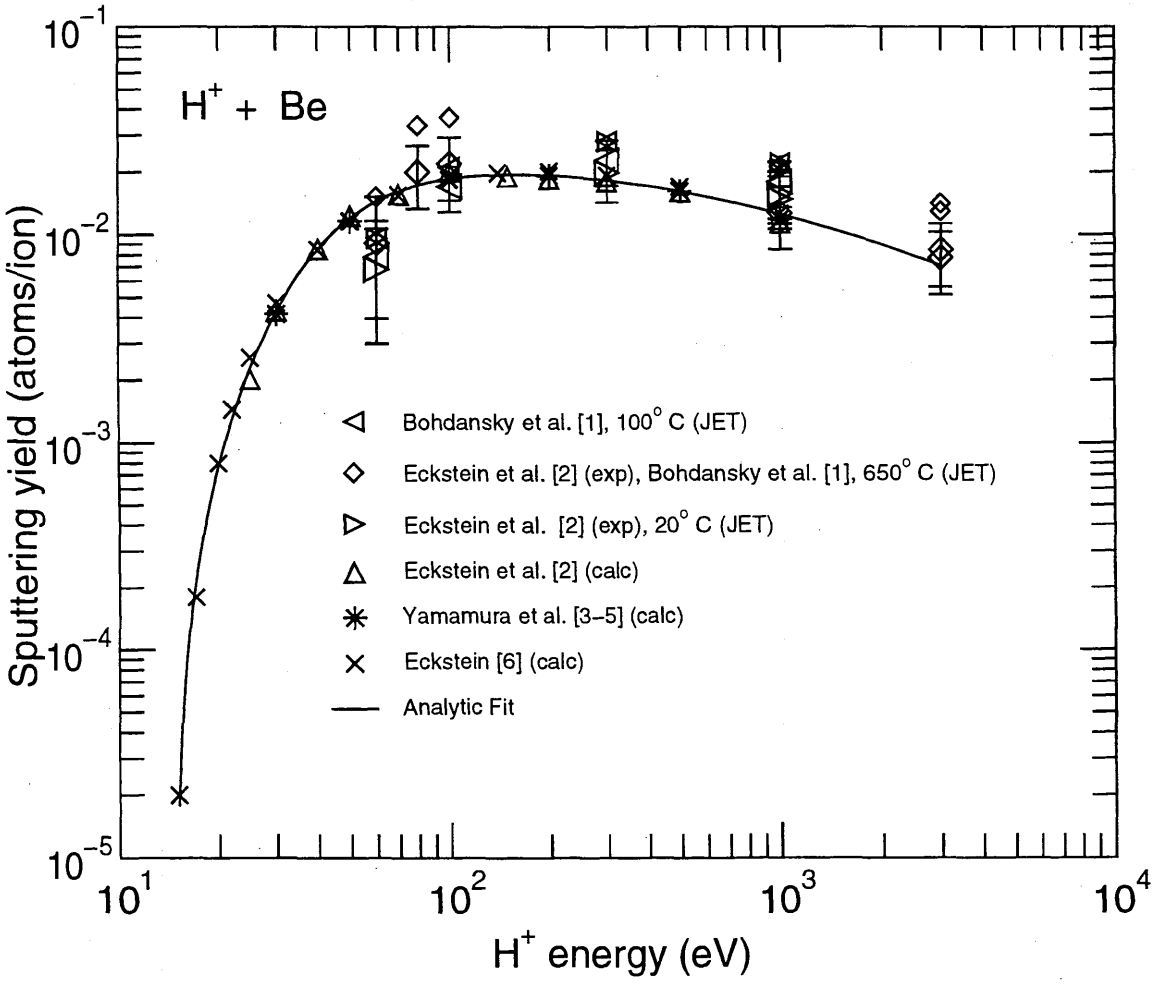

2.1.1.2 D^+ + Be

Comments: (1) Fit valid between E_{min}=E_{th} and E_{max}= 5.0000E+03 eV.
(2) Be (20°) is probably BeO (15Å) on Be.
(3) Be (650°) is probably Be layers on BeO.

Fitting parameters:

Parameter:	λ	q	μ	$\epsilon_L(eV^{-1})$	E_{th}(eV)	Avg. Error (%)
	4.7919E-01	9.0528E-02	1.4496E+00	1.8624E-03	1.0688E+01	33.7

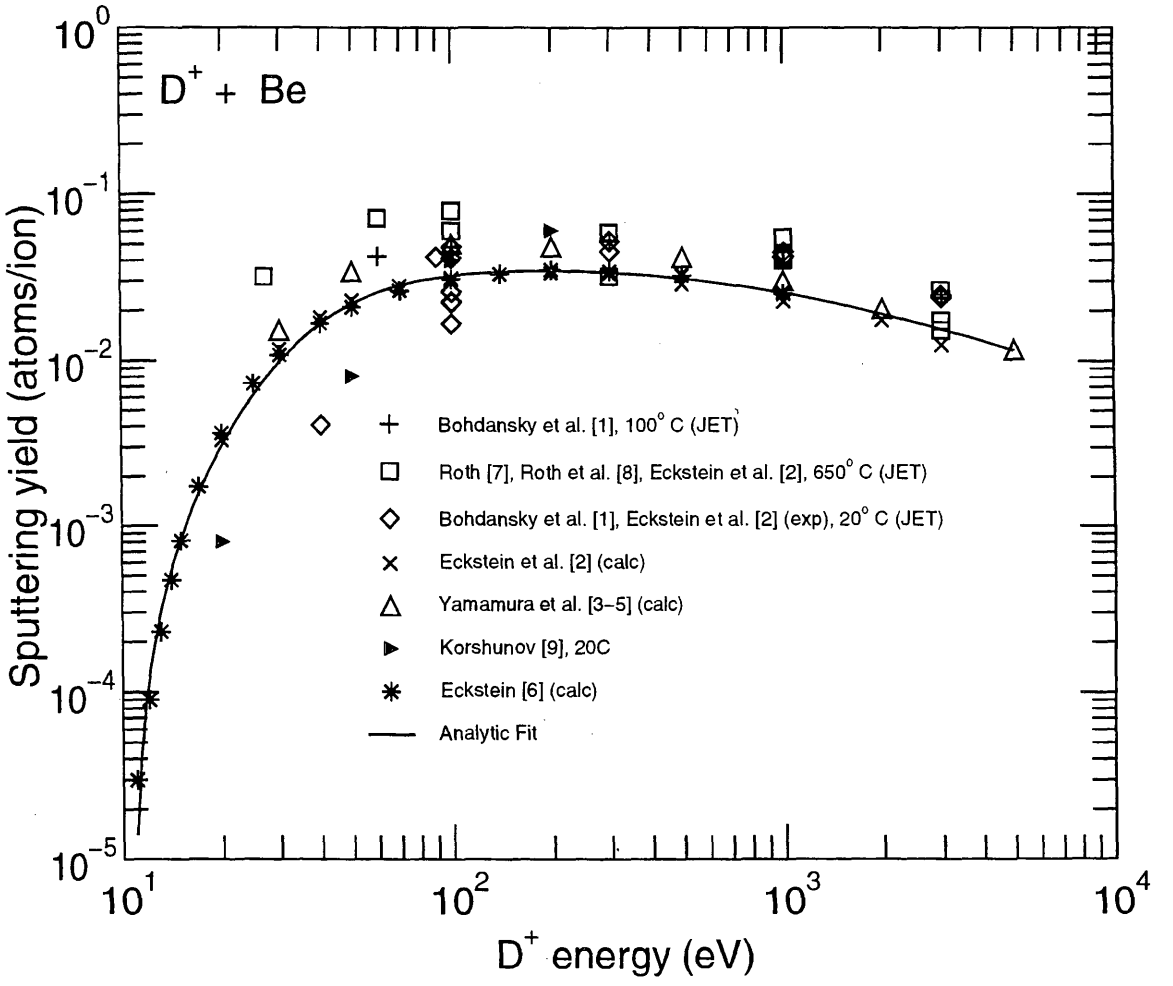

2.1.1.3 T^+ + Be

Comments: (1) Fit valid between E_{min}=E_{th} and E_{max}= 5.0000E+03 eV.
(2) Only calculated values.

Fitting parameters:

Parameter:	λ	q	μ	$\epsilon_L(eV^{-1})$	E_{th}(eV)	Avg. Error (%)
	4.0502E-01	1.1422E-01	1.5069E+00	1.1094E-03	9.7584E+00	15.2

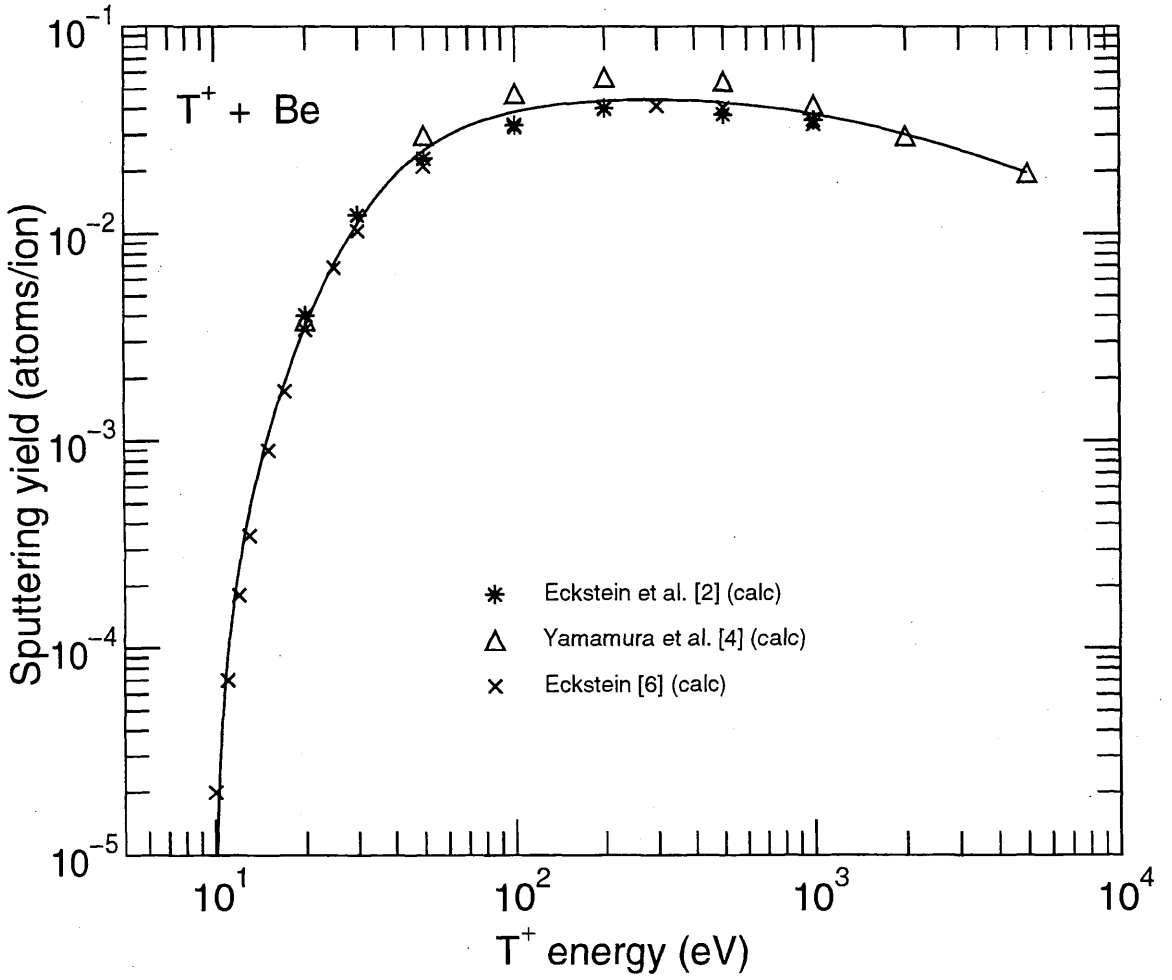

2.1.1.4 He^+ + Be

Comments: (1) Fit valid between E_{min}=E_{th} and E_{max}= 1.0000E+04 eV.
(2) Be (20°) is probably BeO (15Å) on Be.
(3) Be (650°) is probably Be layers on BeO.

Fitting parameters:

Parameter:	λ	q	μ	$\epsilon_L(eV^{-1})$	E_{th}(eV)	Avg. Error (%)
	5.6114E-01	2.7200E-01	1.7795E+00	5.0405E-04	1.0945E+01	26.2

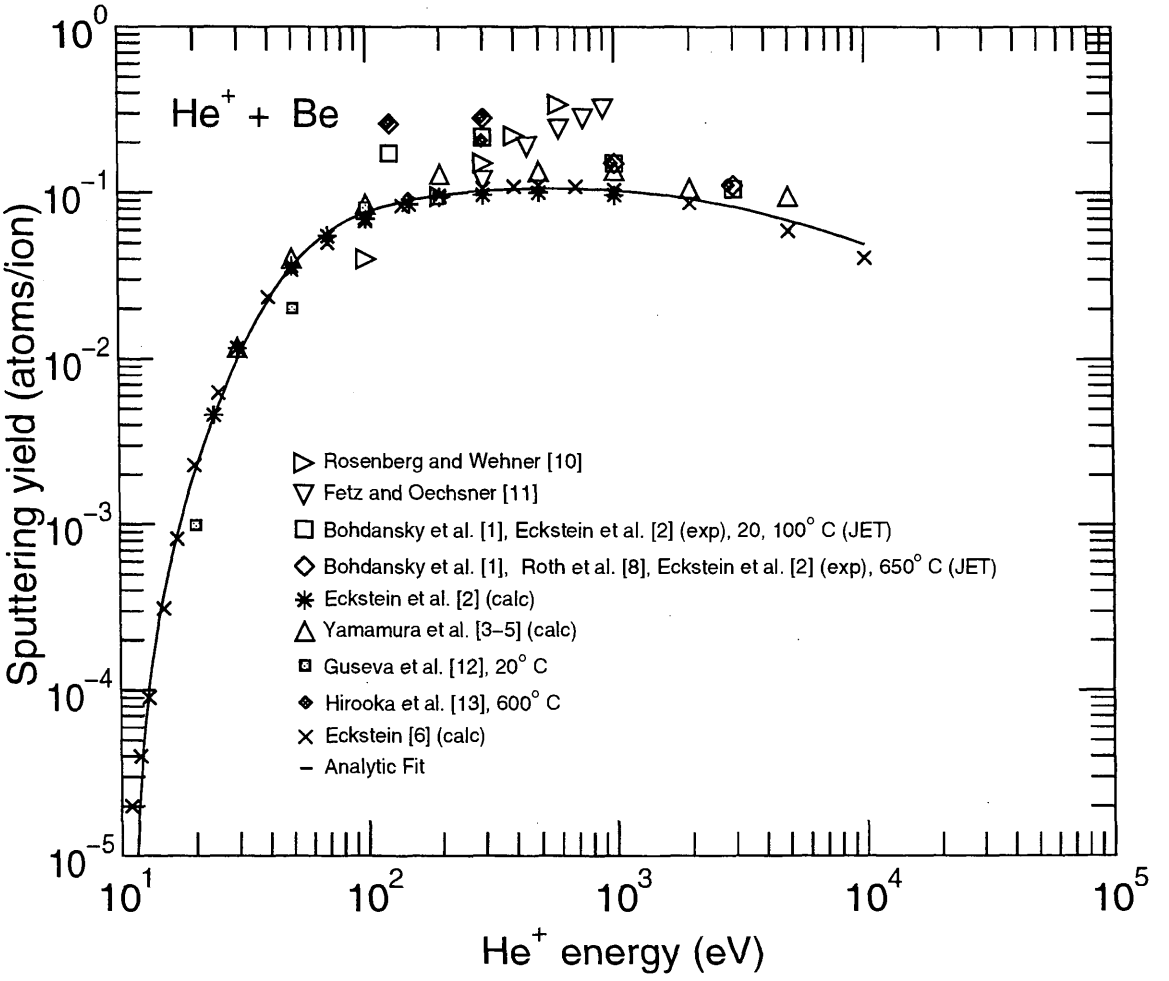

2.1.1.5 Be^+ + Be

Comments: (1) Fit valid between E_{min}=E_{th} and E_{max}= 1.0000E+04 eV.

Fitting parameters:

Parameter:	λ	q	μ	$\epsilon_L(eV^{-1})$	E_{th}(eV)	Avg. Error (%)
	2.2324E+00	6.8078E-01	2.2490E+00	9.3490E-05	1.0025E+01	15.5

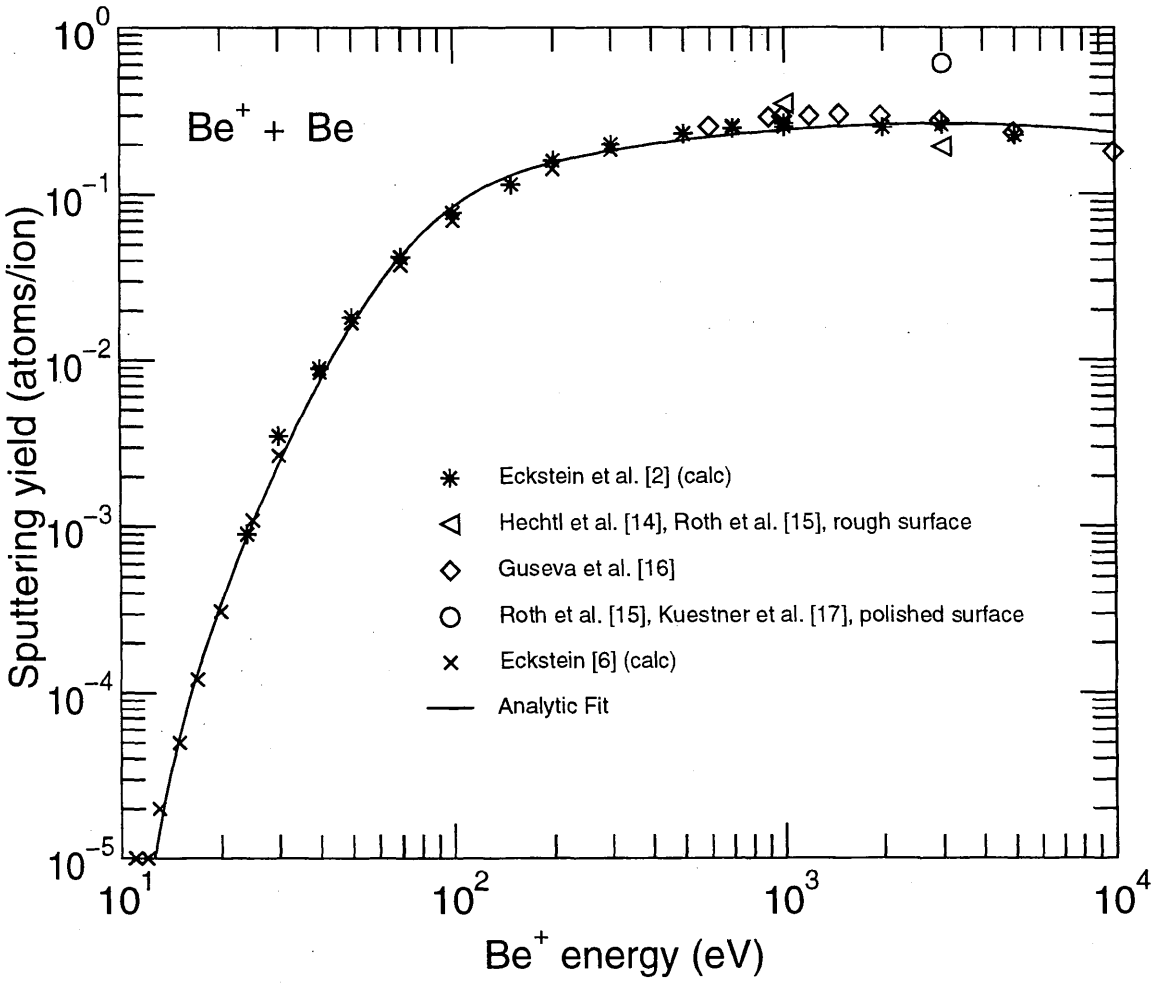

2.1.1.6 N^+ + Be

Comments: (1) Fit valid between E_{min}=E_{th} and E_{max}= 1.0000E+03 eV.
(2) Only calculated values.

Fitting parameters:

Parameter:	λ	q	μ	$\epsilon_L(eV^{-1})$	E_{th}(eV)	Avg. Error (%)
	1.0603E-01	3.9794E+00	2.0479E+00	3.0250E-06	1.9900E+01	11.9

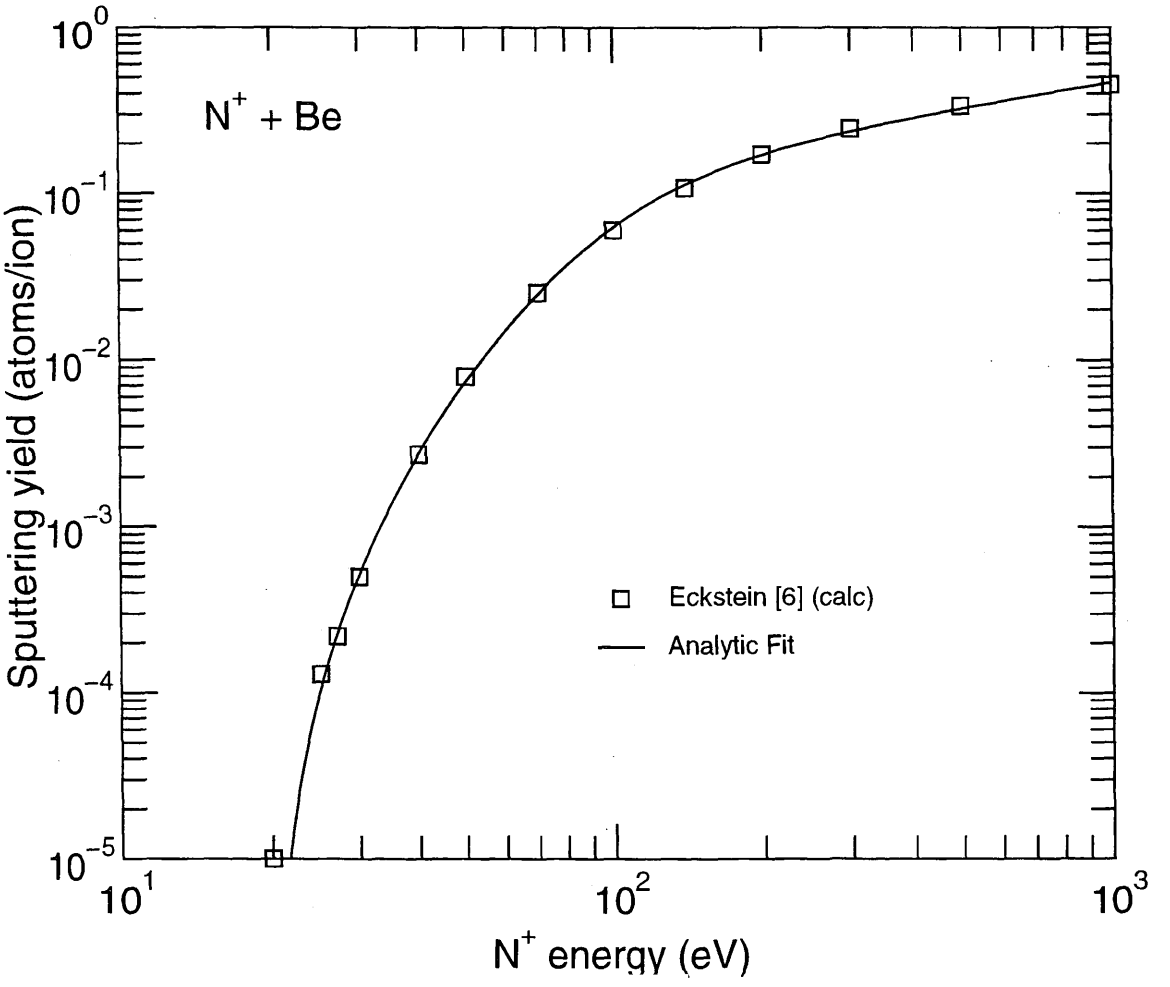

2.1.1.7 O^+ + Be

Comments: (1) Fit valid between E_{min}=E_{th} and E_{max}= 1.0000E+04 eV.
(2) Only calculated values.
(3) Only valid for low fluences due to oxide formation.

Fitting parameters:

Parameter:	λ	q	μ	$\epsilon_L(eV^{-1})$	E_{th}(eV)	Avg. Error (%)
	4.6278E-01	1.5308E+00	1.9851E+00	2.6664E-05	1.9633E+01	11.7

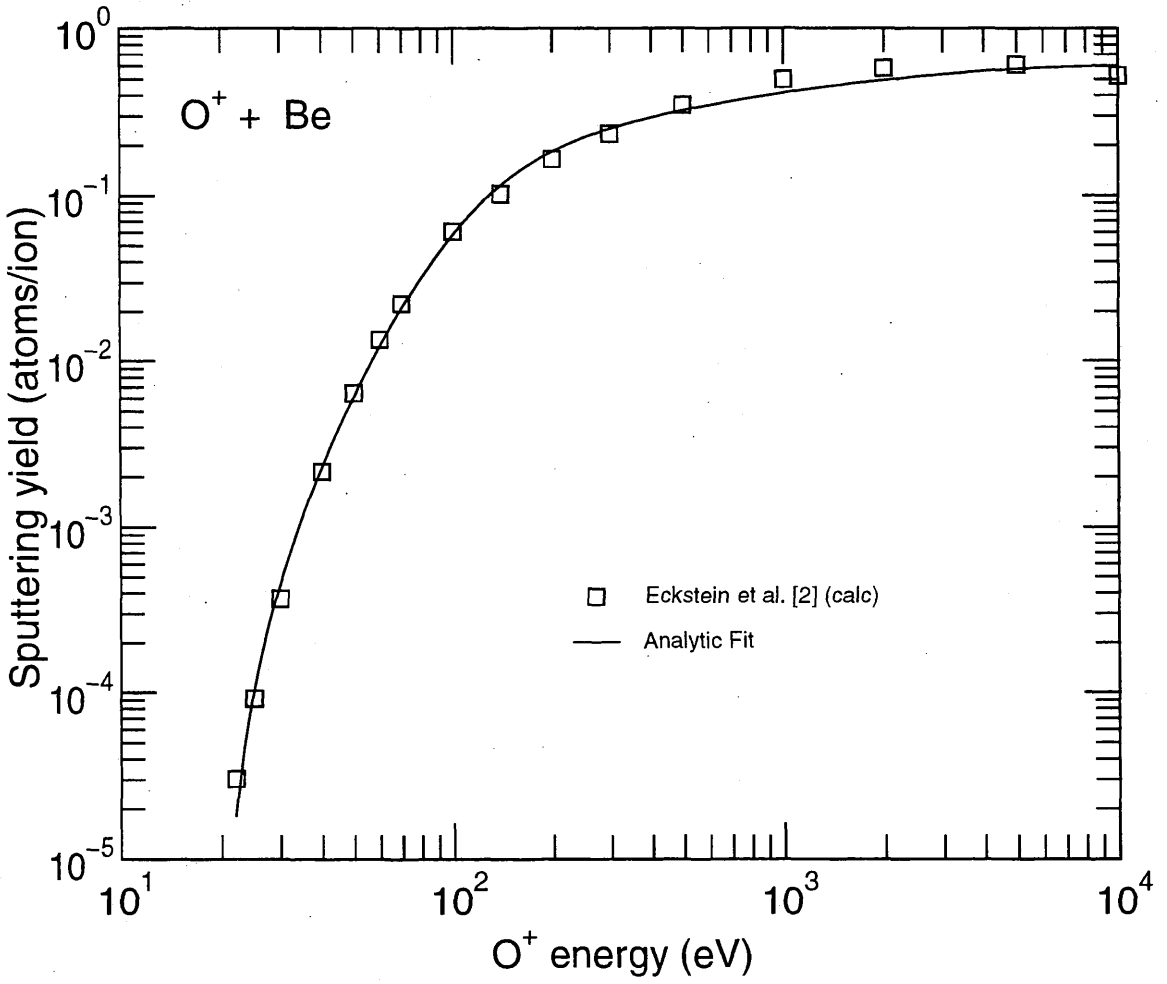

2.1.1.8 Ne^+ + Be

Comments: (1) Fit valid between E_{min}=E_{th} and E_{max}= 1.0000E+04 eV.

Fitting parameters:

Parameter:	λ	q	μ	$\epsilon_L(eV^{-1})$	E_{th}(eV)	Avg. Error (%)
	3.2343E+00	1.7612E+00	1.7824E+00	9.4315E-05	1.9900E+01	27.7

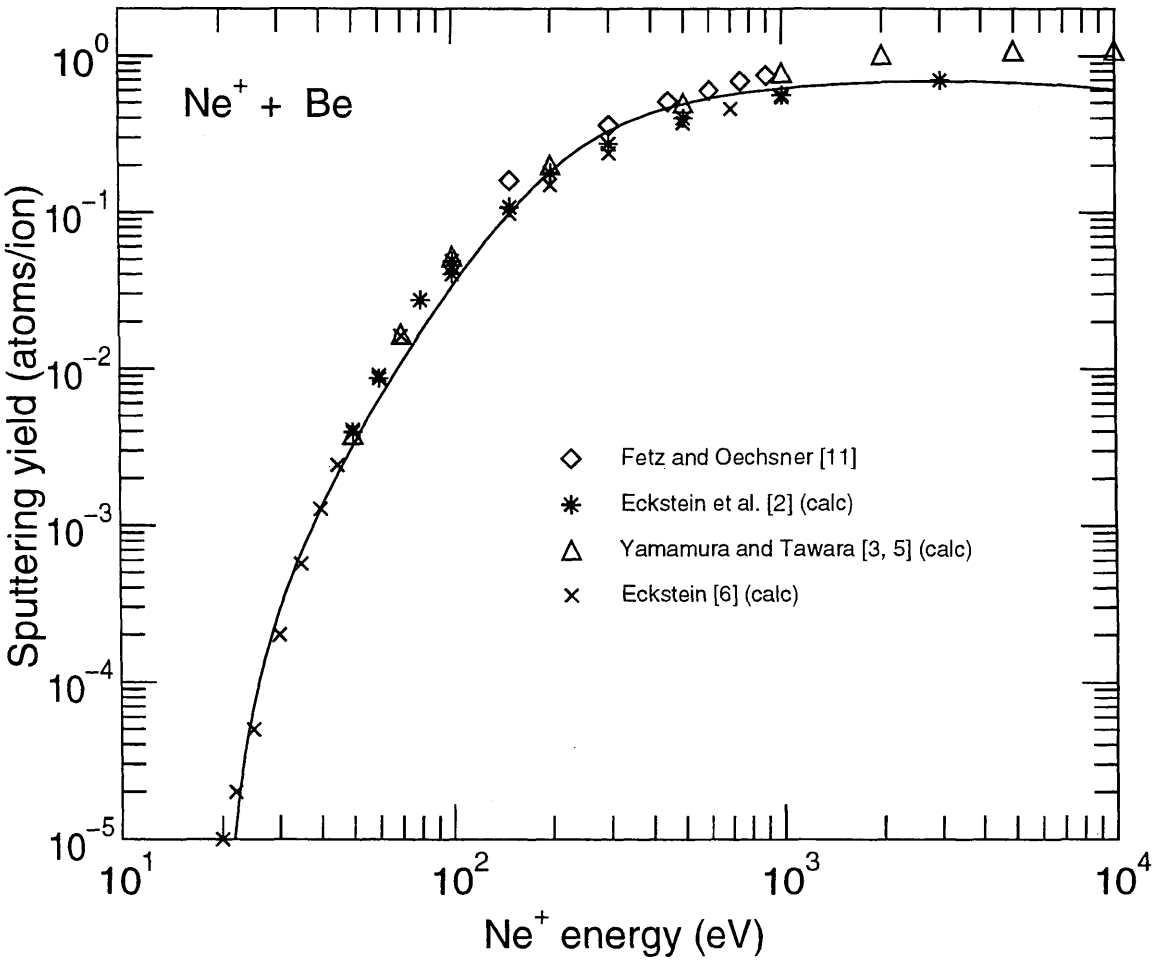

2.1.1.9 Ar^+ + Be

Comments: (1) Fit valid between E_{min}=E_{th} and E_{max}= 1.0000E+05 eV.

Fitting parameters:

Parameter:	λ	q	μ	$\epsilon_L(eV^{-1})$	E_{th}(eV)	Avg. Error (%)
	1.8074E+00	3.0089E+00	1.8061E+00	2.7649E-05	2.9850E+01	28.9

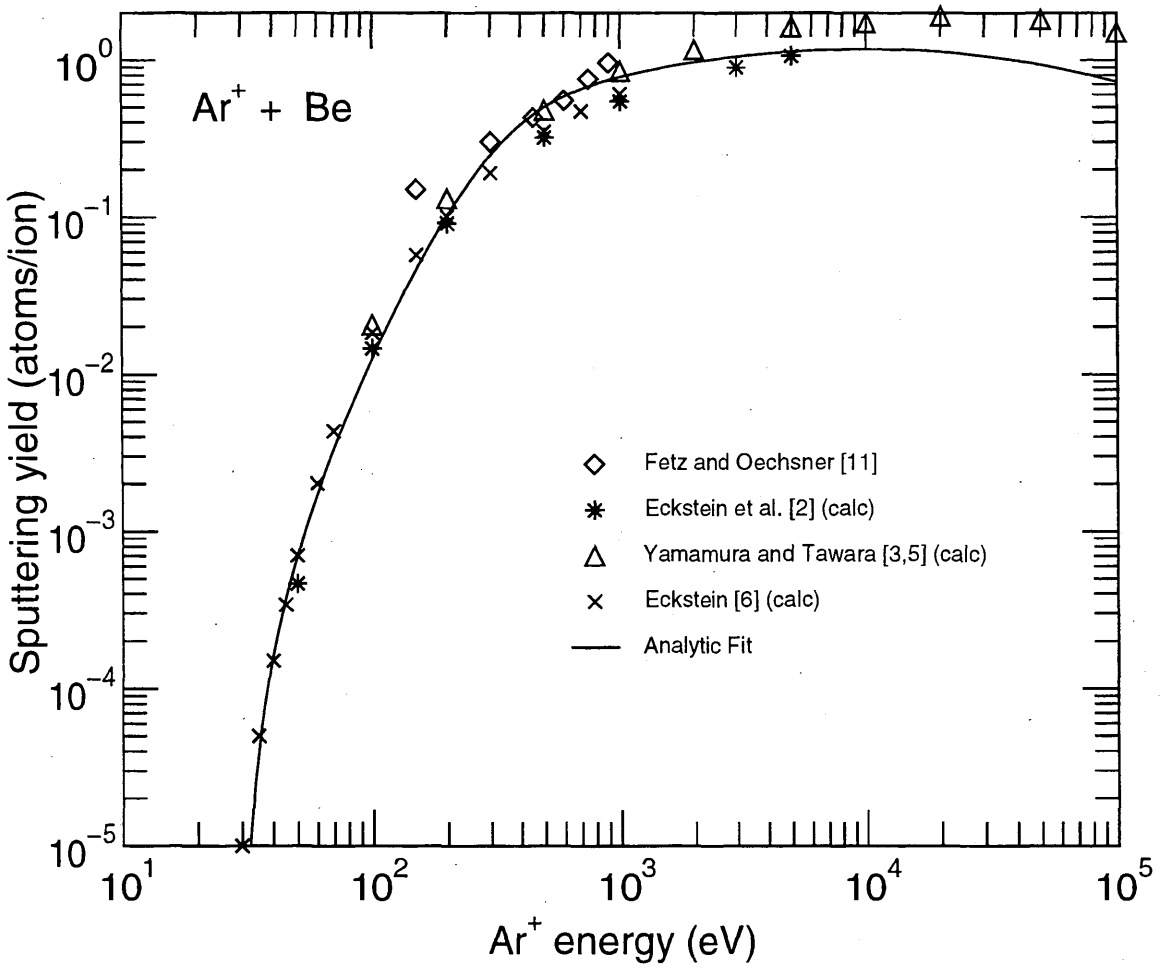

2.1.2.1 $H^+ + C$

Comments: (1) Fit valid between E_{min}=E_{th} and E_{max}= 2.0000E+03 eV.
(2) Only calculated points used for fit because experimental data are affected by chemical erosion.
(3) Different experimental targets. See references.

Fitting parameters:

Parameter:	λ	q	μ	$\epsilon_L(eV^{-1})$	E_{th}(eV)	Avg. Error (%)
	6.0314E-01	1.9814E-02	1.3279E+00	1.5744E-03	3.8954E+01	9.8

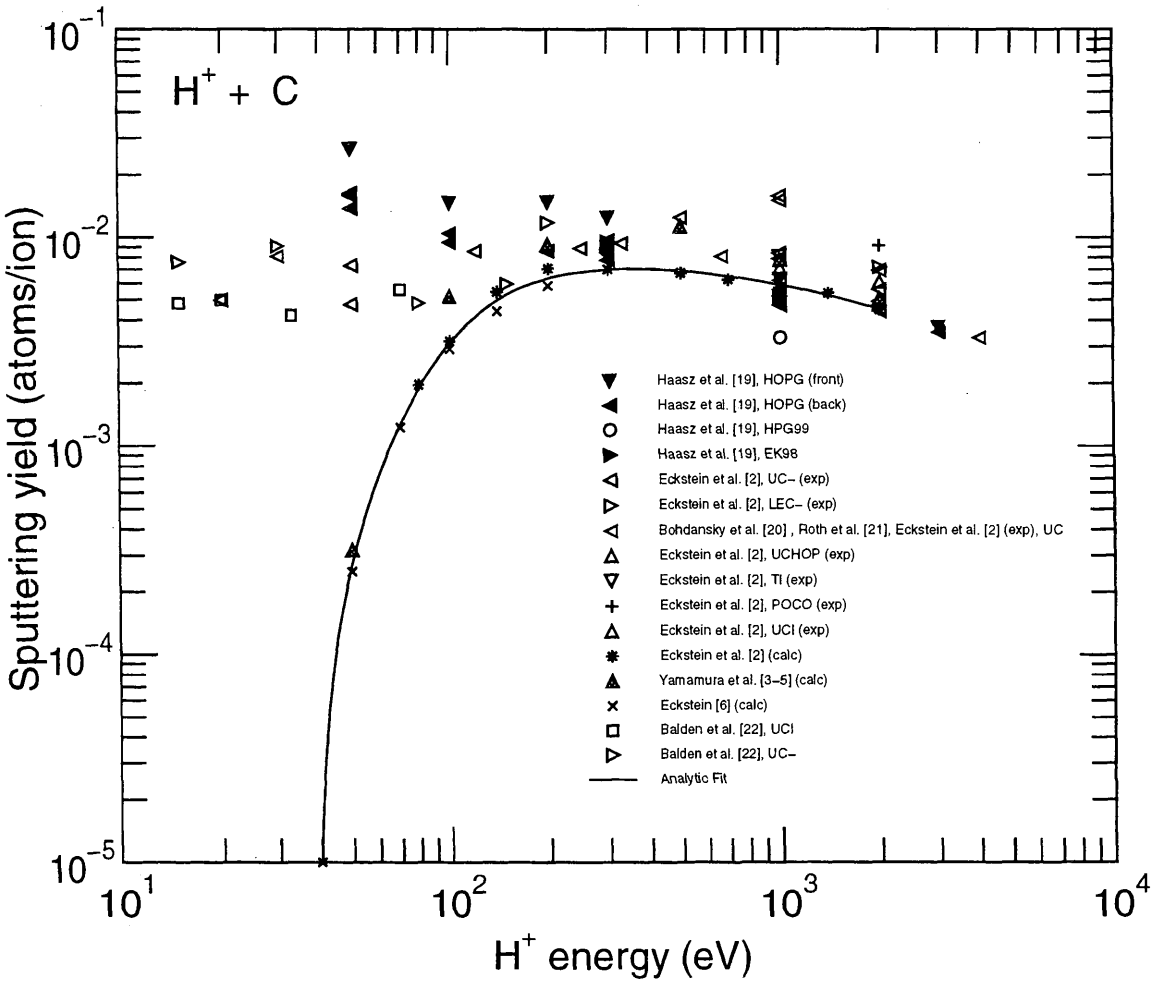

2.1.2.2 $D^+ + C$

Comments: (1) Fit valid between E_{min}=E_{th} and E_{max}= 5.0000E+03 eV.
(2) Only calculated points used for fit because experimental data are affected by chemical erosion.
(3) Different experimental targets. See references.

Fitting parameters:

Parameter:	λ	q	μ	$\epsilon_L(eV^{-1})$	E_{th}(eV)	Avg. Error (%)
	2.6122E+00	3.6781E-02	2.4637E+00	8.8905E-04	1.7624E+01	22.9

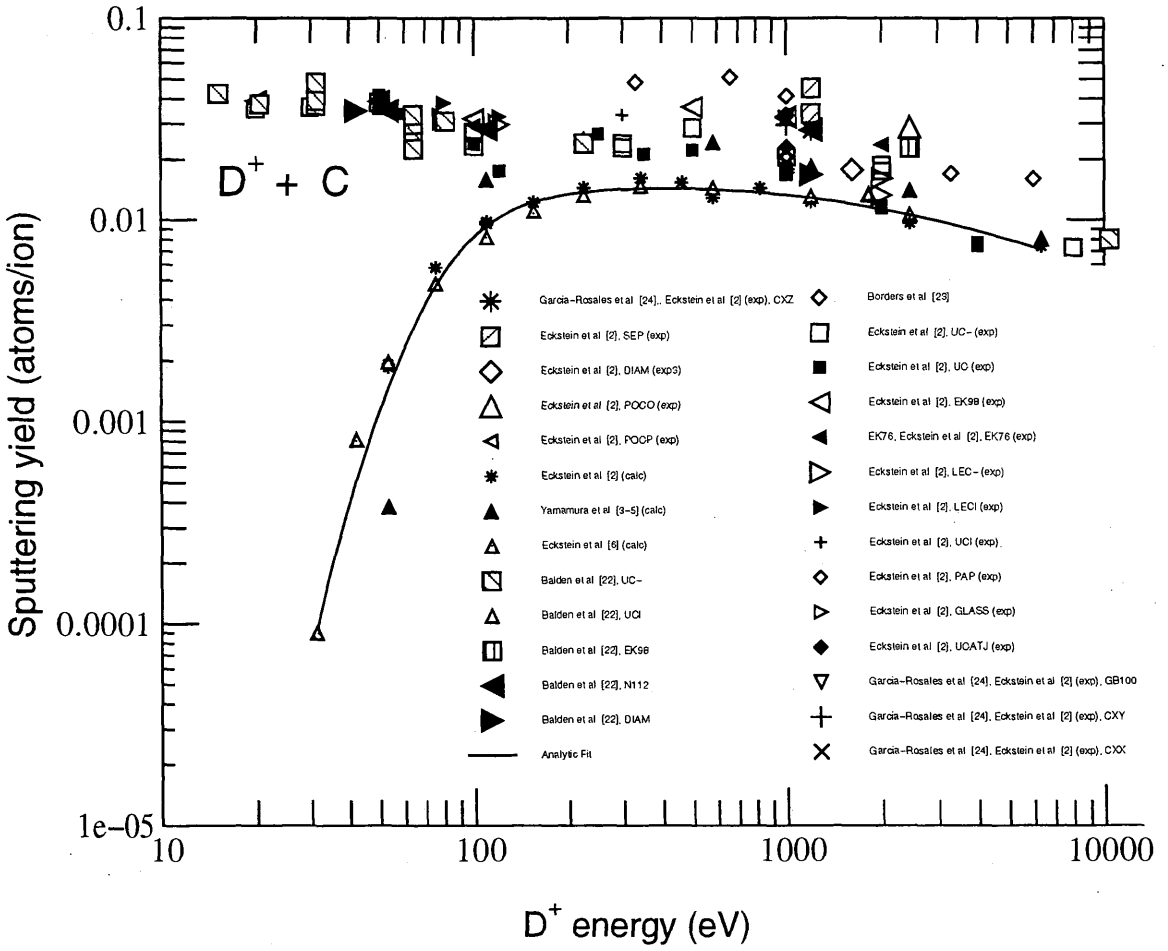

2.1.2.3 $T^+ + C$

Comments: (1) Fit valid between E_{min}=E_{th} and E_{max}= 1.0000E+04 eV.
(2) Only calculated values.

Fitting parameters:

Parameter:	λ	q	μ	$\epsilon_L(eV^{-1})$	E_{th}(eV)	Avg. Error (%)
	1.4855E+00	7.8525E-02	9.2171E-01	2.0912E-03	2.4797E+01	28.7

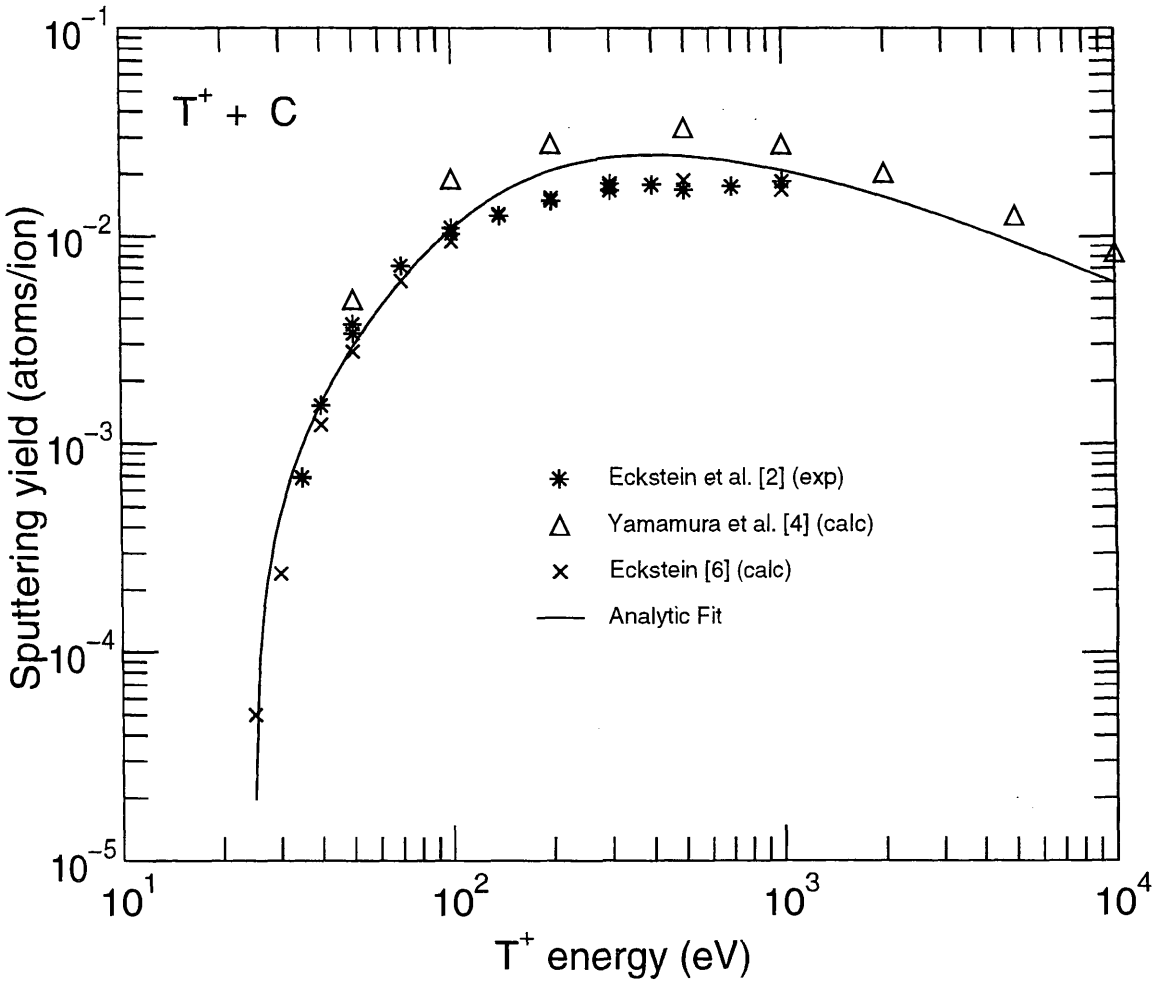

2.1.2.4 $He^+ + C$

Comments: (1) Fit valid between E_{min}=E_{th} and E_{max}= 2.0000E+04 eV.

Fitting parameters:

Parameter:	λ	q	μ	$\epsilon_L(eV^{-1})$	E_{th}(eV)	Avg. Error (%)
	4.5419E-01	1.5368E-01	1.3054E+00	3.7682E-04	2.4875E+01	35.6

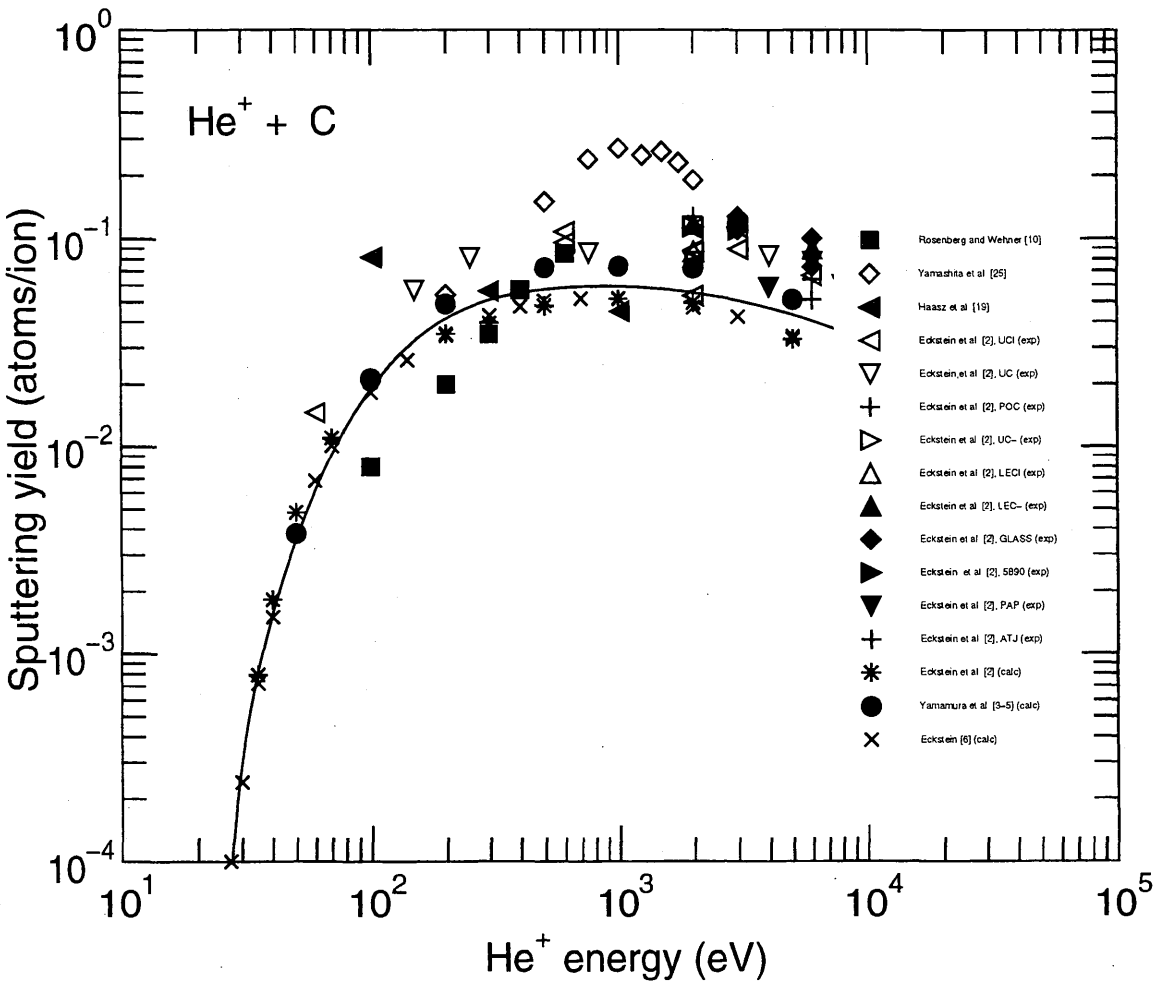

2.1.2.5 $C^+ + C$

Comments: (1) Fit valid between E_{min}=E_{th} and E_{max}= 1.0000E+04 eV.

Fitting parameters:

Parameter:	λ	q	μ	$\epsilon_L(eV^{-1})$	E_{th}(eV)	Avg. Error (%)
	3.2678E+00	7.4551E-01	1.5411E+00	1.7582E-04	2.9850E+01	35.7

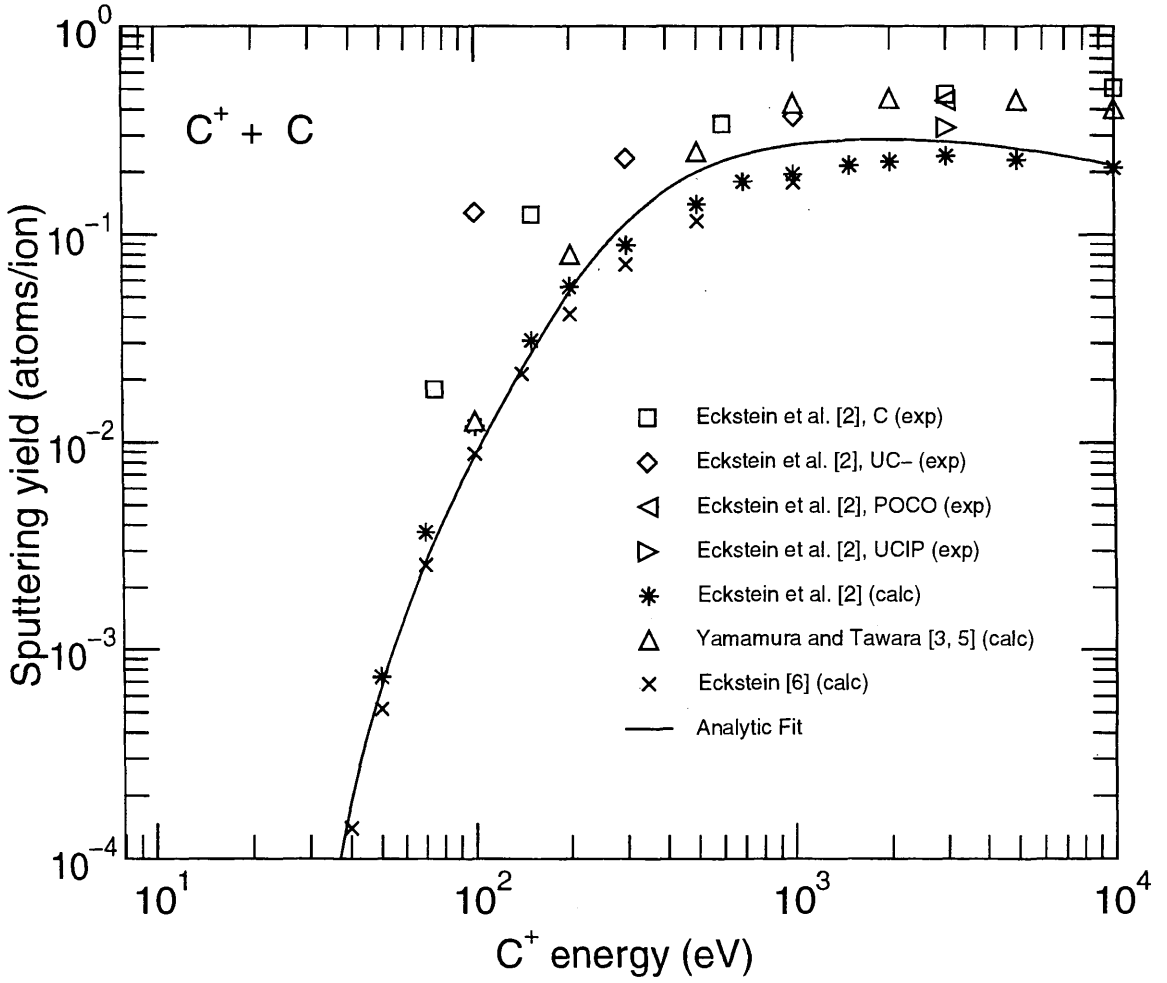

2.1.2.6 $N^+ + C$

Comments: (1) Fit valid between E_{min}=E_{th} and E_{max}= 1.0000E+03 eV.
(2) Only calculated values.
(3) Fit valid only for low fluence due to chemical reaction with nitrogen and nitrogen implantation.

Fitting parameters:

Parameter:	λ	q	μ	$\epsilon_L(eV^{-1})$	E_{th}(eV)	Avg. Error (%)
	1.9555E+00	4.5004E-01	1.7579E+00	1.3549E-04	3.6130E+01	15.2

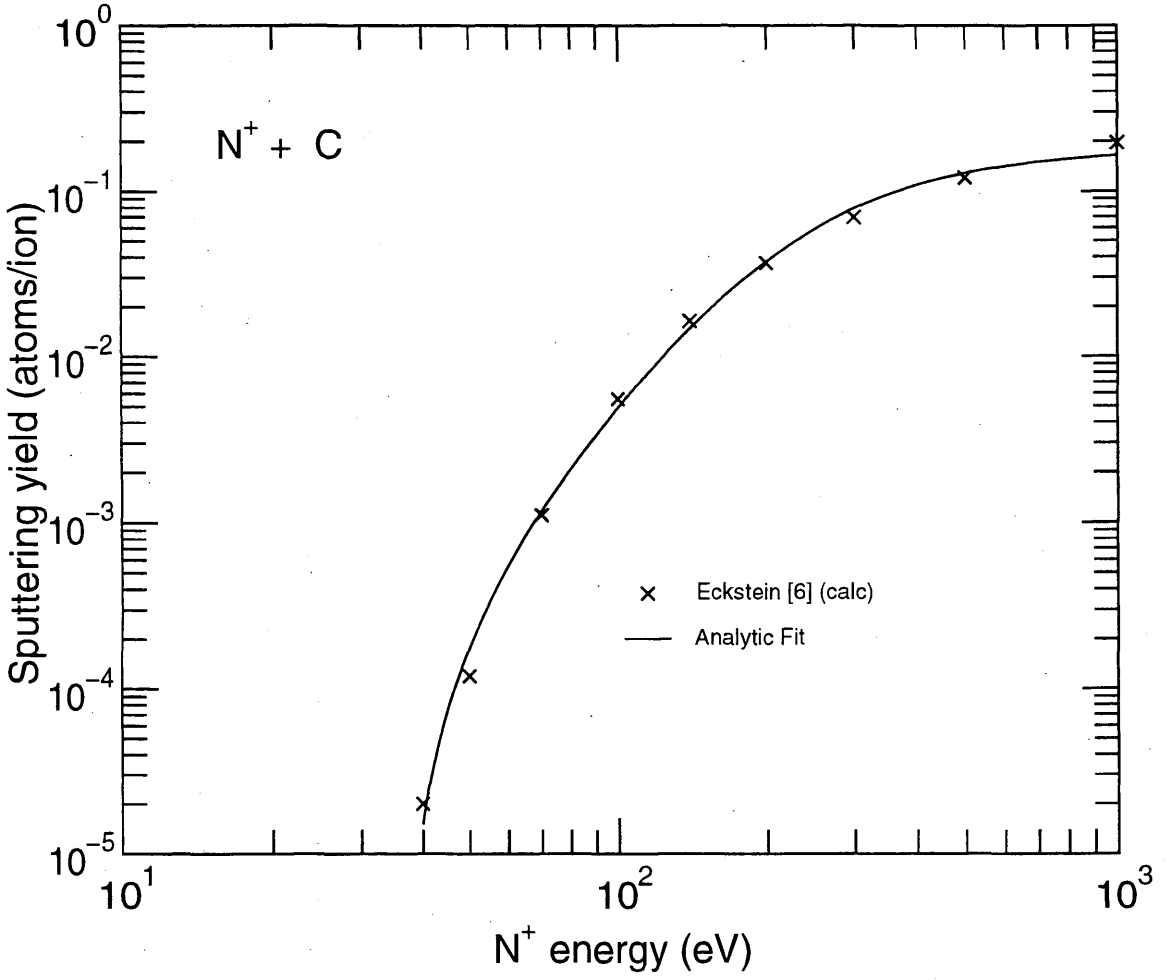

2.1.2.7 $O^+ + C$

Comments: (1) Fit valid between E_{min}=E_{th} and E_{max}= 6.0000E+03 eV.
(2) Only calculated points used for fit because experimental data are dominated by chemical erosion.
(3) Fit only valid for low fluence due to chemical reaction of O with C (oxide formation).

Fitting parameters:

Parameter:	λ	q	μ	$\epsilon_L(eV^{-1})$	E_{th}(eV)	Avg. Error (%)
	2.8214E-01	1.0579E+00	1.7248E+00	1.1109E-05	4.2683E+01	7.3

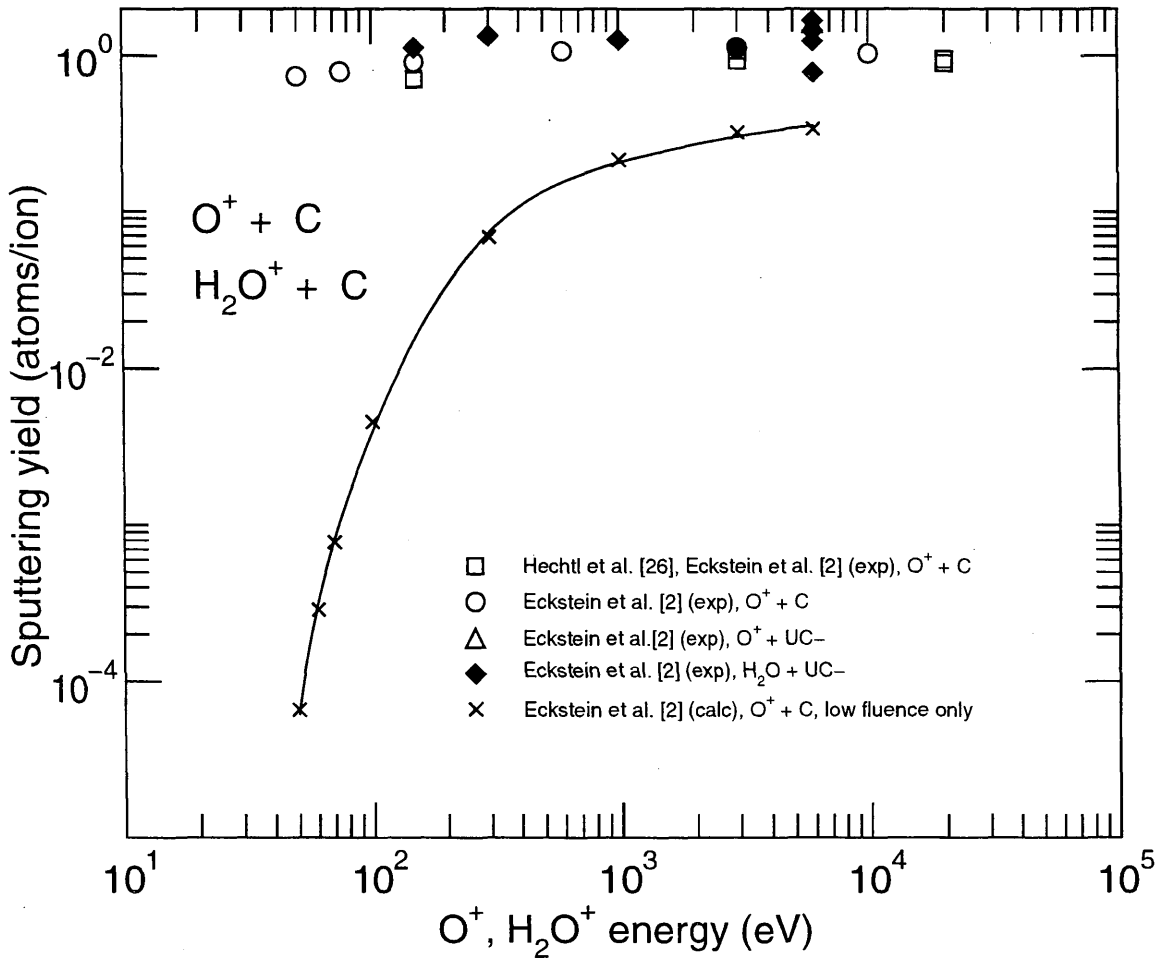

2.1.2.8 $Ne^+ + C$

Comments: (1) Fit valid between E_{min}=E_{th} and E_{max}= 2.0000E+04 eV.

Fitting parameters:

Parameter:	λ	q	μ	$\epsilon_L(eV^{-1})$	E_{th}(eV)	Avg. Error (%)
	2.0335E-01	1.4151E+00	1.5379E+00	8.3896E-06	4.9750E+01	28.5

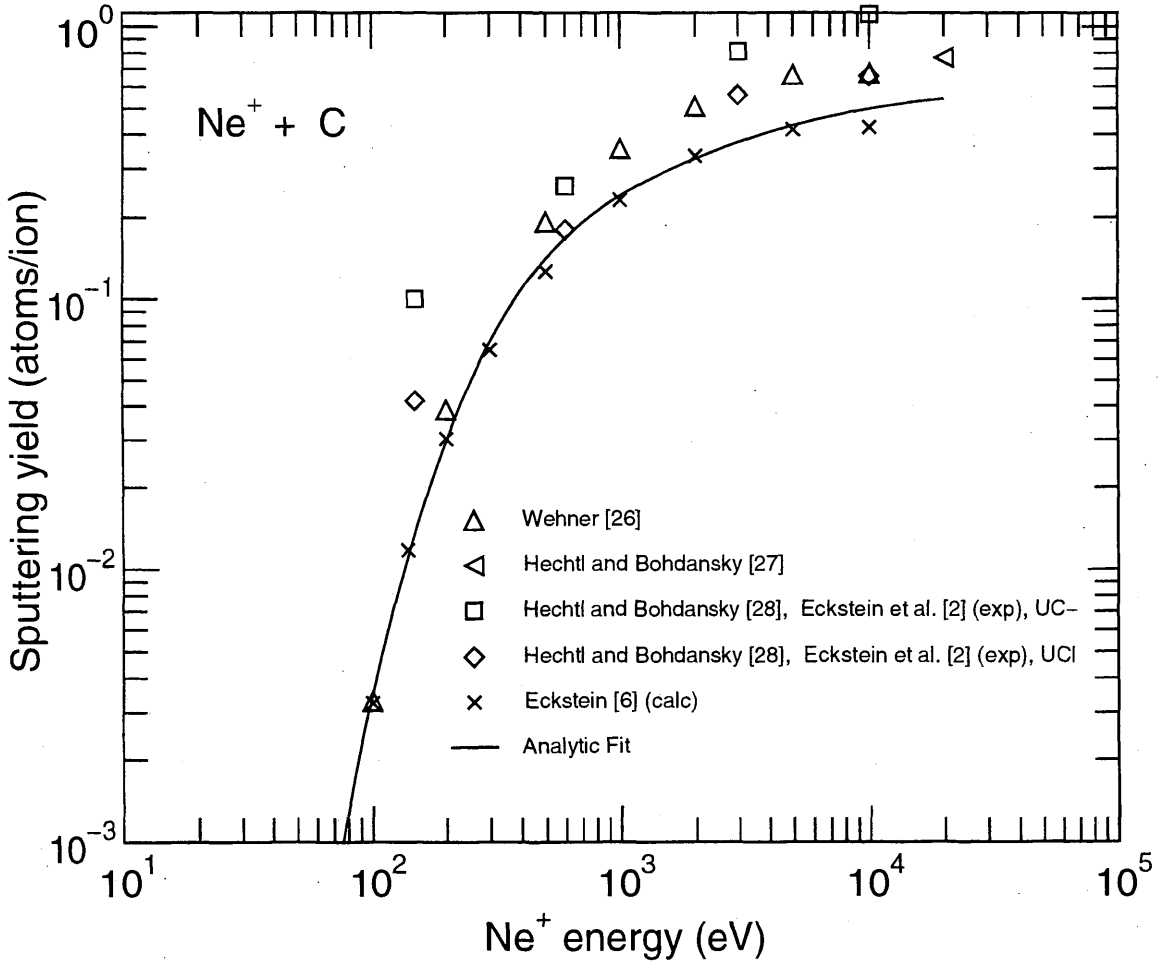

2.1.2.9 $Ar^+ + C$

Comments: (1) Fit valid between E_{min}=E_{th} and E_{max}= 4.0000E+04 eV.

Fitting parameters:

Parameter:	λ	q	μ	$\epsilon_L(eV^{-1})$	E_{th}(eV)	Avg. Error (%)
	1.1820E-01	1.0427E+01	1.9802E+00	2.6164E-07	5.6270E+01	29.2

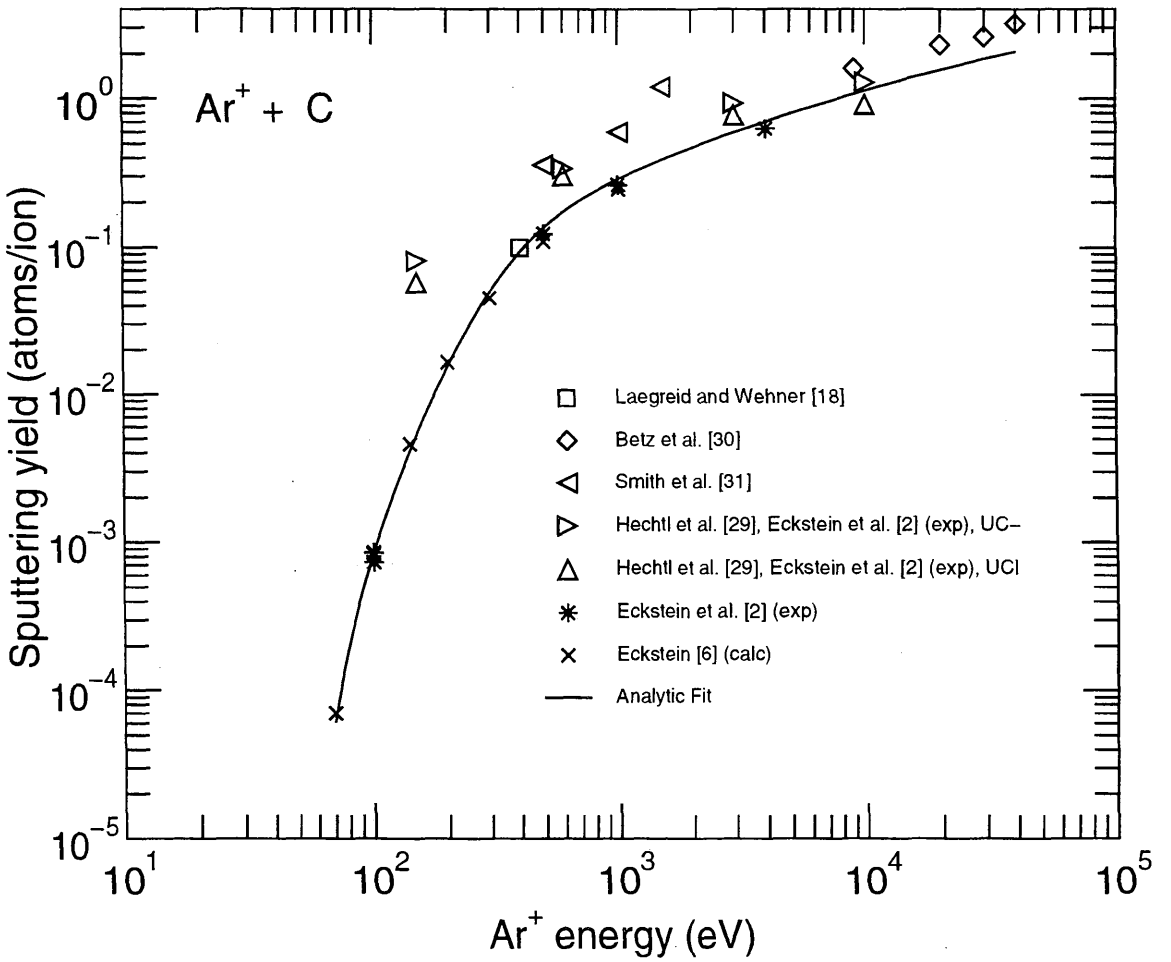

2.1.3.1 $H^+ + W$

Comments: (1) Fit valid between E_{min}=E_{th} and E_{max}= 2.0000E+04 eV.

Fitting parameters:

Parameter:	λ	q	μ	$\epsilon_L(eV^{-1})$	E_{th}(eV)	Avg. Error (%)
	1.3849E+00	7.1574E-03	8.5638E-01	1.5136E-04	4.8731E+02	26.4

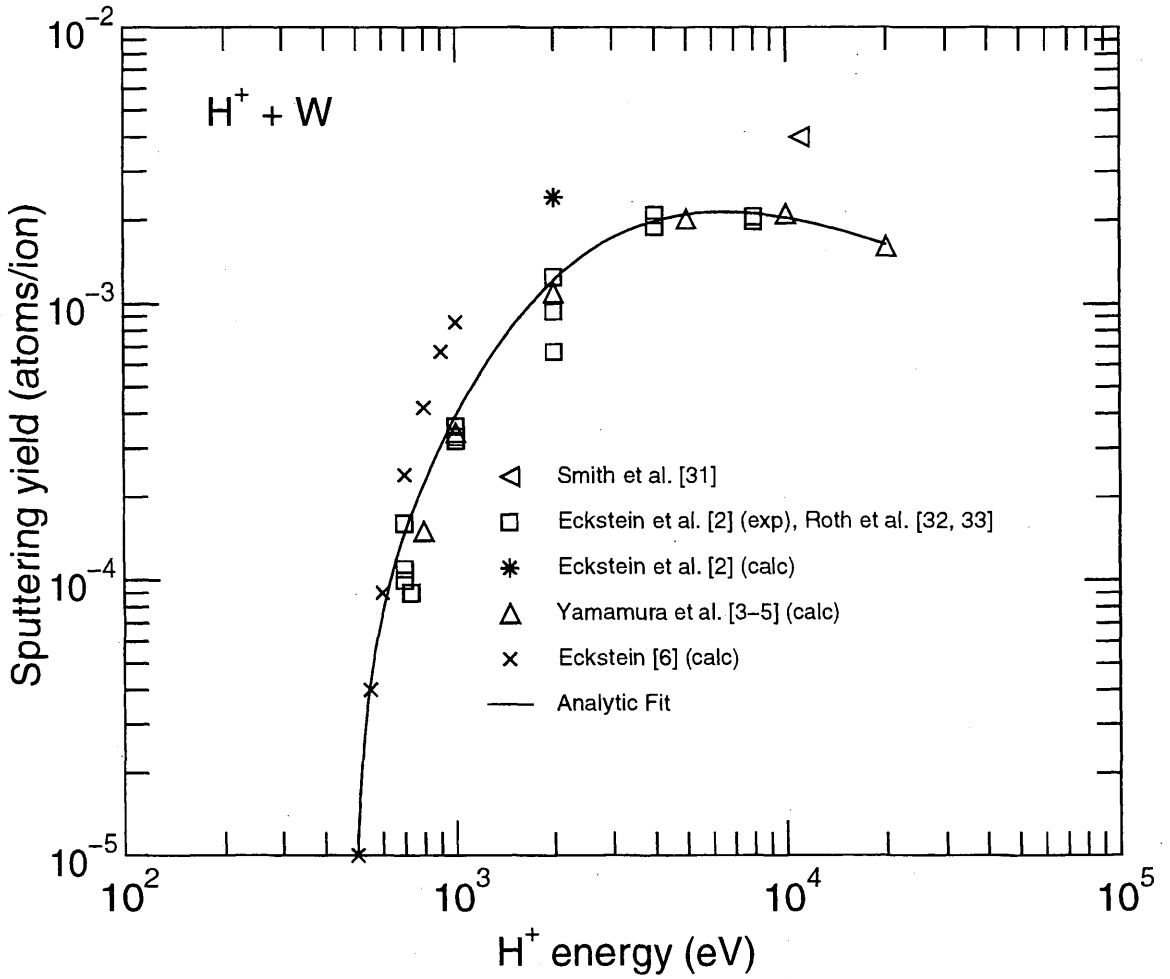

2.1.3.2 $D^+ + W$

Comments: (1) Fit valid between E_{min}=E_{th} and E_{max}= 1.0000E+05 eV.

Fitting parameters:

Parameter:	λ	q	μ	$\epsilon_L(eV^{-1})$	E_{th}(eV)	Avg. Error (%)
	4.2193E-01	1.9086E-02	9.8997E-01	1.2679E-04	2.4471E+02	29.4

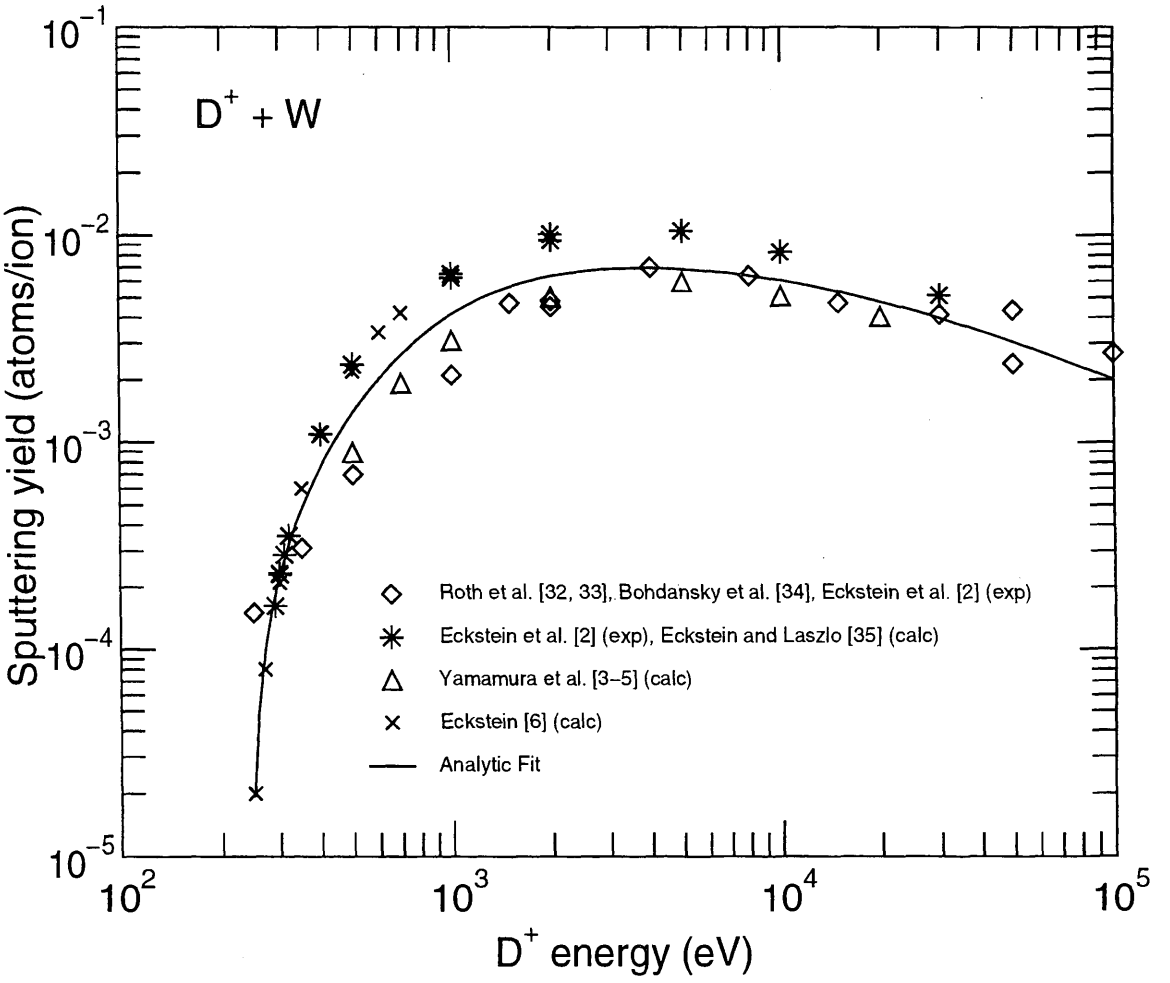

2.1.3.3 $T^+ + W$

Comments: (1) Fit valid between E_{min}=E_{th} and E_{max}= 1.0000E+04 eV.
(2) Only calculated values.

Fitting parameters:

Parameter:	λ	q	μ	$\epsilon_L(eV^{-1})$	E_{th}(eV)	Avg. Error (%)
	1.3563E-01	4.3625E-02	1.5398E+00	5.4067E-05	1.5599E+02	17.7

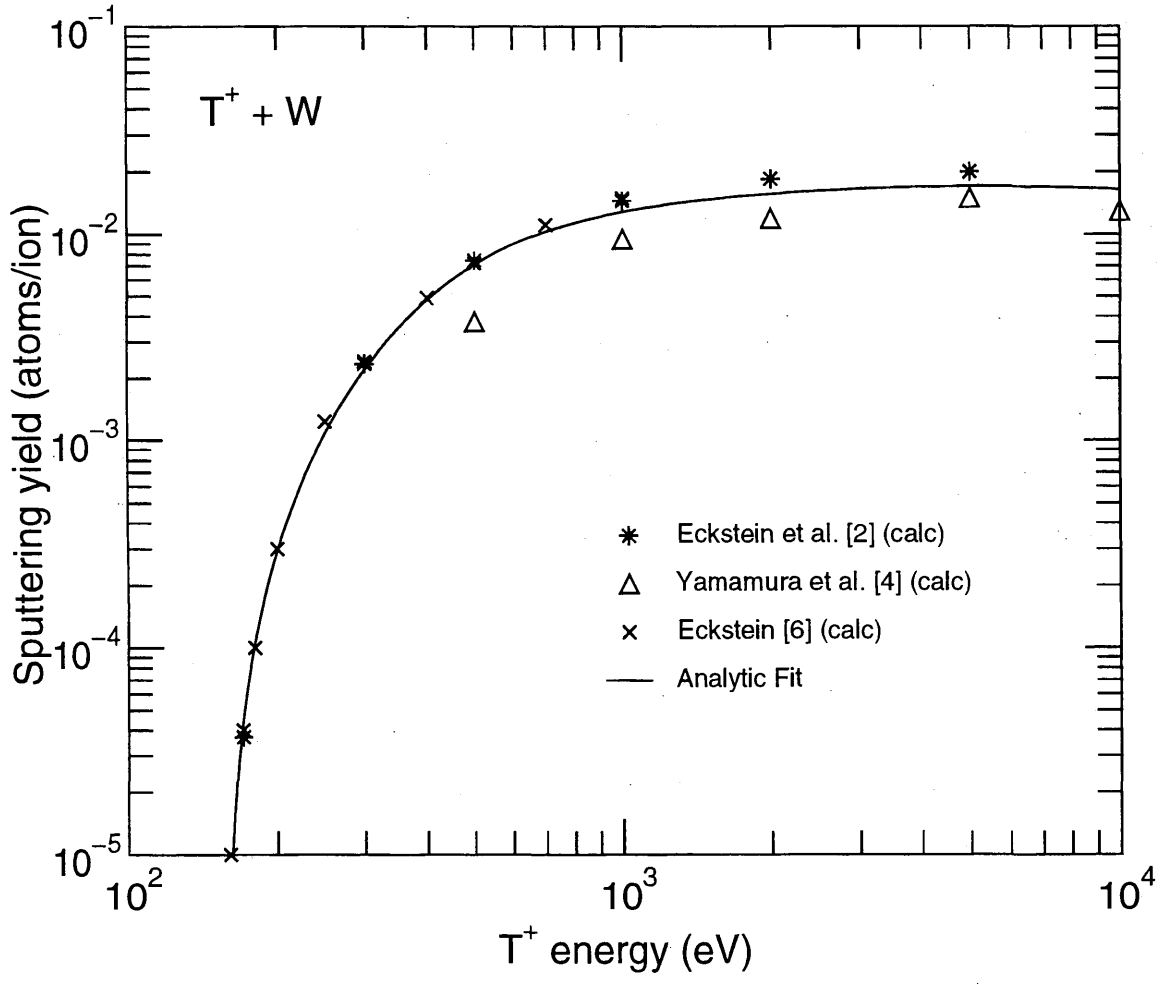

2.1.3.4 $He^+ + W$

Comments: (1) Fit valid between E_{min}=E_{th} and E_{max}= 5.0000E+04 eV.

Fitting parameters:

Parameter:	λ	q	μ	$\epsilon_L(eV^{-1})$	E_{th}(eV)	Avg. Error (%)
	1.0050E-01	9.7767E-02	1.2431E+00	2.9415E-05	1.2621E+02	30.4

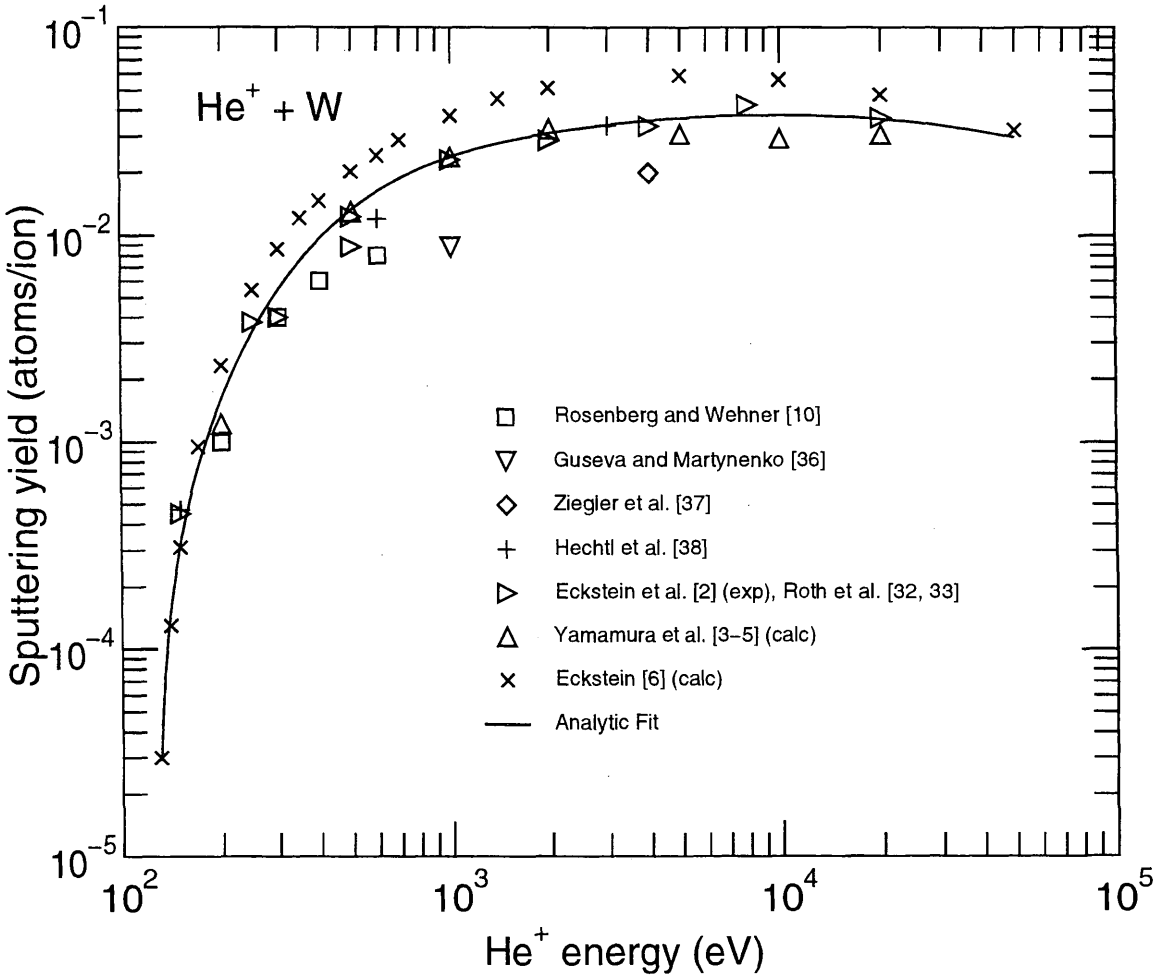

2.1.3.5 $C^+ + W$

Comments: (1) Fit valid between E_{min}=E_{th} and E_{max}= 1.0000E+04 eV.
(2) The calculated values are only valid for low fluences due to C layer formation on W.

Fitting parameters:

Parameter:	λ	q	μ	$\epsilon_L(eV^{-1})$	E_{th}(eV)	Avg. Error (%)
	1.8984E-02	1.9221E+00	1.8857E+00	2.8775E-06	5.1992E+01	25.6

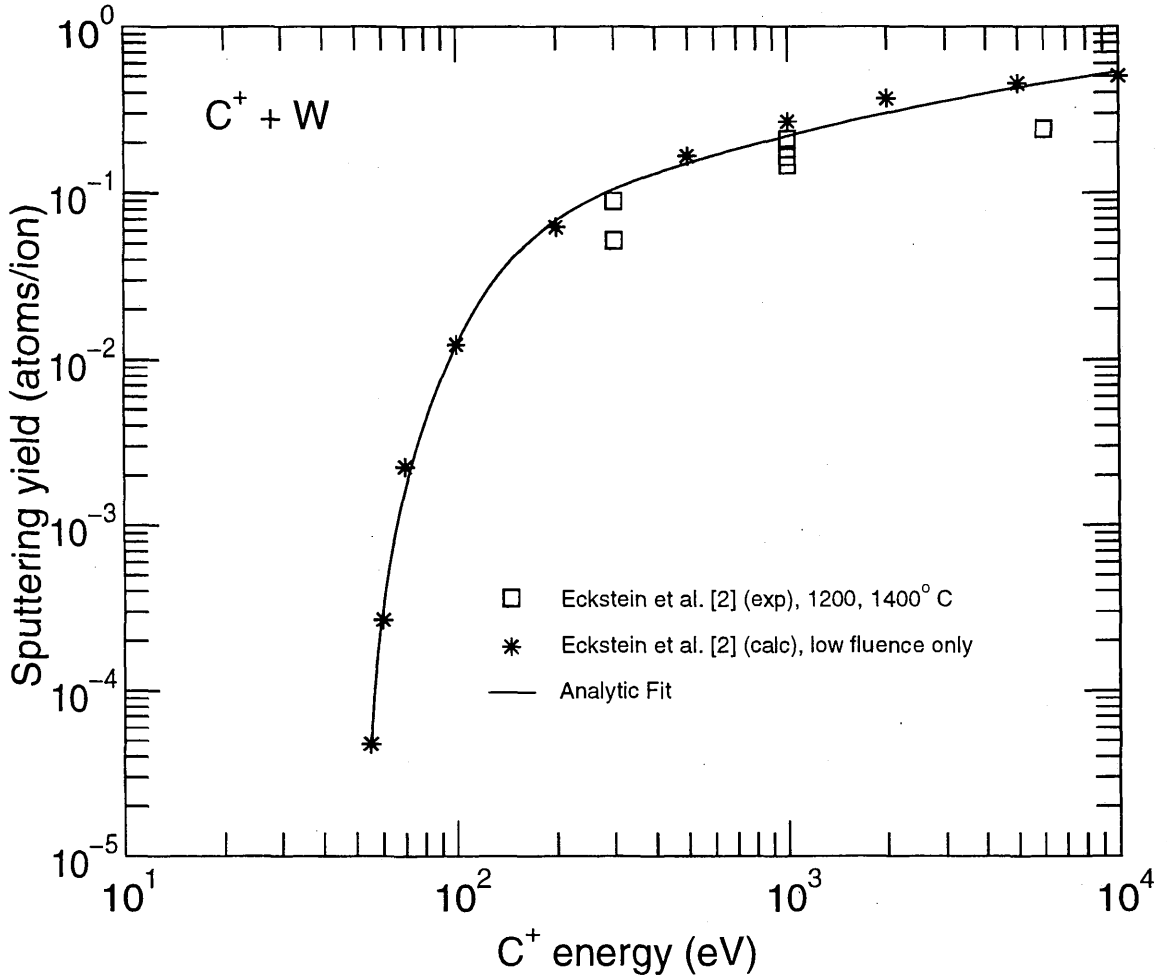

2.1.3.6 $N^+ + W$

Comments: (1) Fit valid between E_{min}=E_{th} and E_{max}= 5.0000E+03 eV.
(2) Only calculated values are used for the fit because of chemical interactions and old data.

Fitting parameters:

Parameter:	λ	q	μ	$\epsilon_L(eV^{-1})$	E_{th}(eV)	Avg. Error (%)
	1.6012E-02	4.9256E+00	1.8338E+00	8.8820E-07	4.6767E+01	9.8

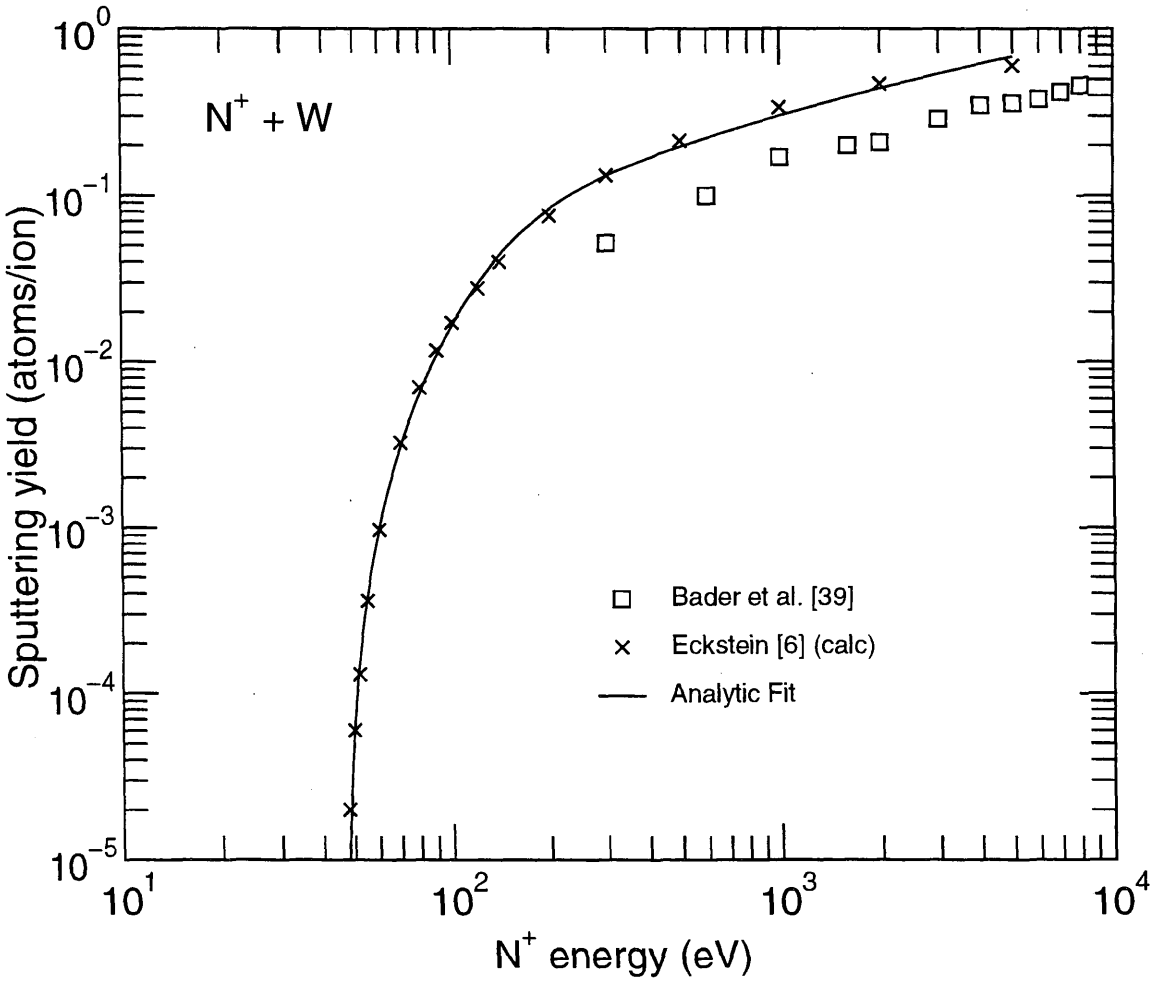

2.1.3.7 $O^+ + W$

Comments: (1) Fit valid between E_{min}=E_{th} and E_{max}= 1.0000E+04 eV.
(2) Only calculated values are used for the fit because of chemical interactions.
(3) Low temperature data are probably due to tungsten oxide at the surface (25Å).

Fitting parameters:

Parameter:	λ	q	μ	$\epsilon_L(eV^{-1})$	E_{th}(eV)	Avg. Error (%)
	1.1730E-01	1.7372E+00	8.1924E-01	2.7649E-05	4.9347E+01	14.7

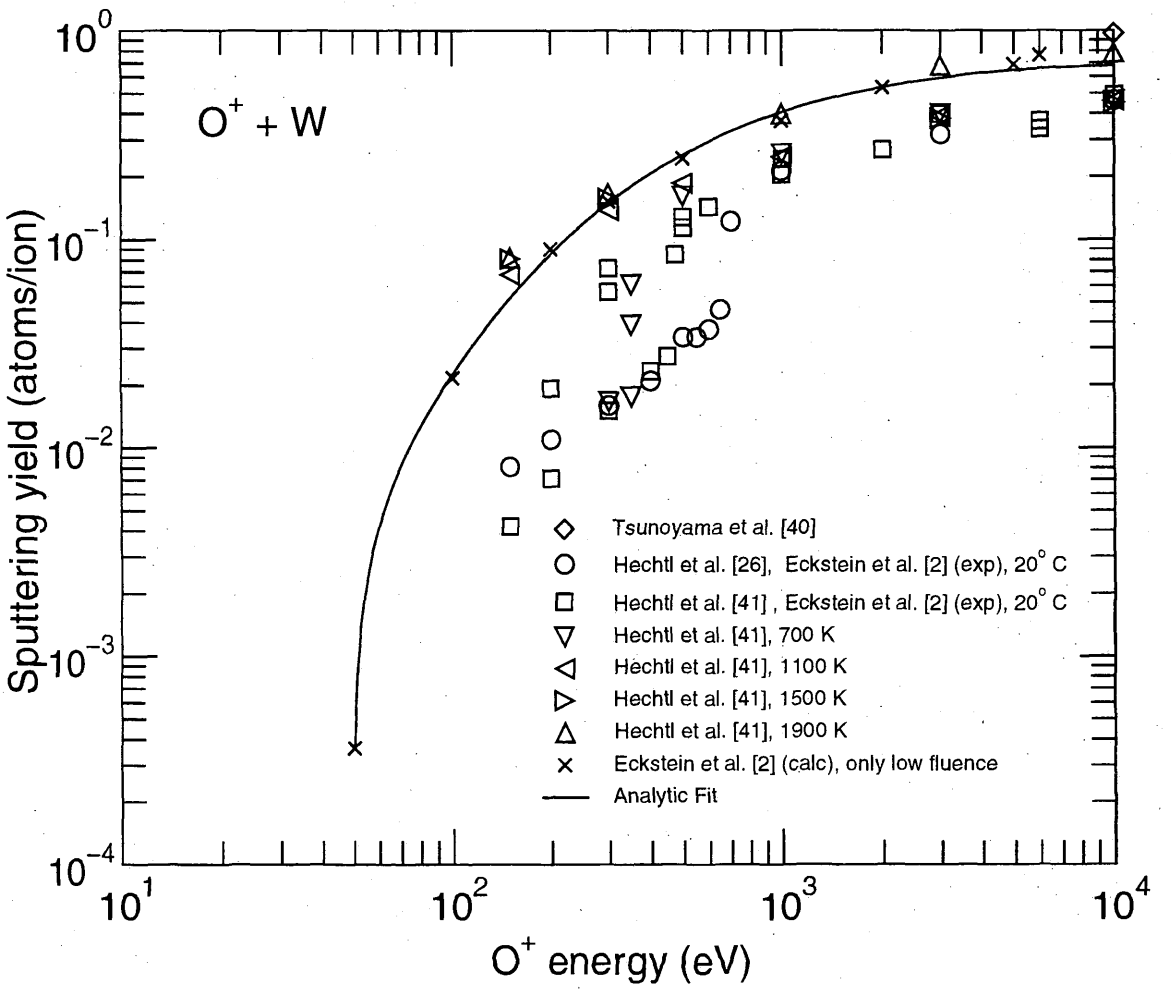

2.1.3.8 $Ne^+ + W$

Comments: (1) Fit valid between E_{min}=E_{th} and E_{max}= 1.0000E+04 eV.

Fitting parameters:

Parameter:	λ	q	μ	$\epsilon_L(eV^{-1})$	E_{th}(eV)	Avg. Error (%)
	1.9073E-02	1.3040E+01	2.5470E+00	3.2350E-07	3.5820E+01	27.4

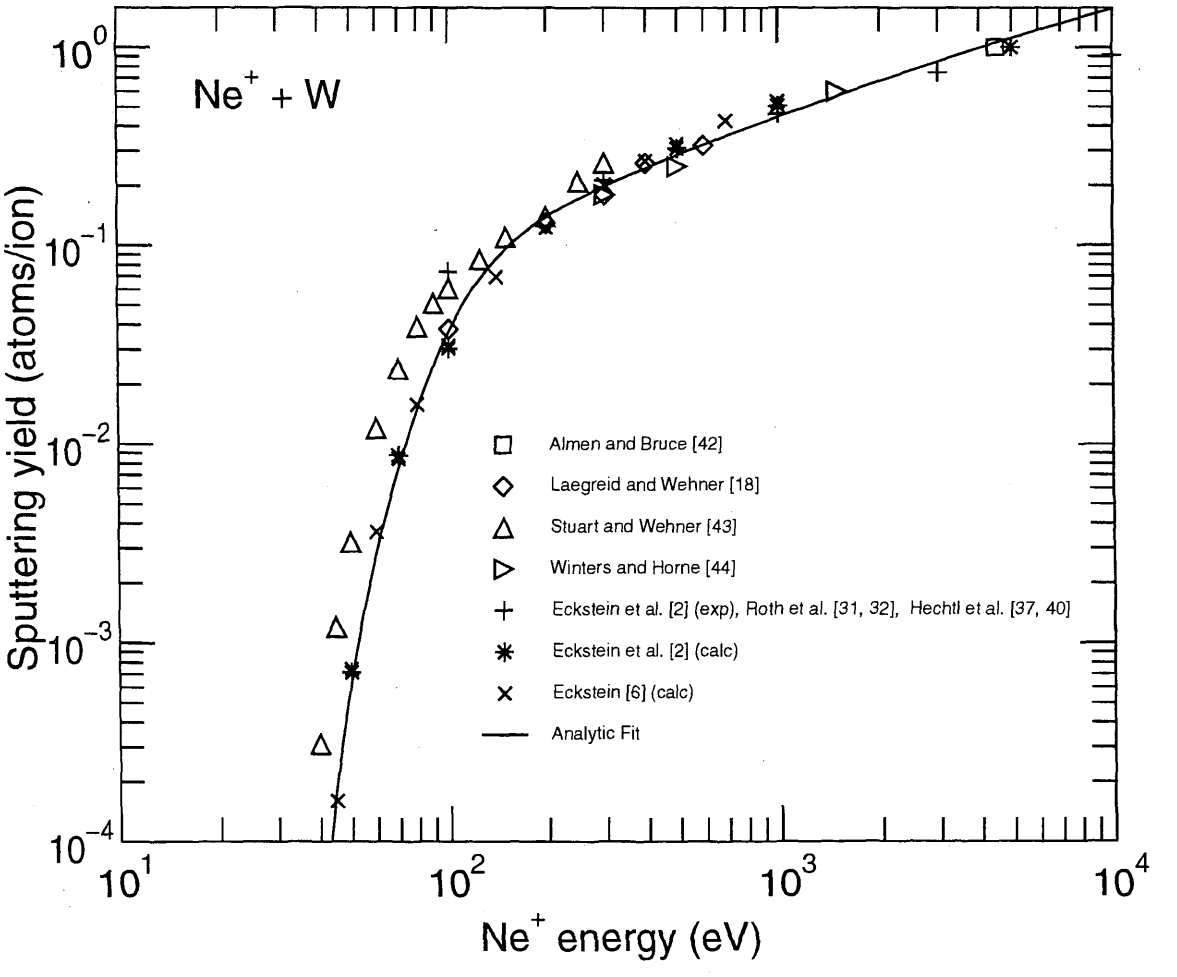

2.1.3.9 $Ar^+ + W$

Comments: (1) Fit valid between E_{min}=E_{th} and E_{max}= 2.0500E+04 eV.

Fitting parameters:

Parameter:	λ	q	μ	$\epsilon_L(eV^{-1})$	E_{th}(eV)	Avg. Error (%)
	6.0743E-02	1.1639E+01	2.1198E+00	1.0902E-06	2.9850E+01	14.8

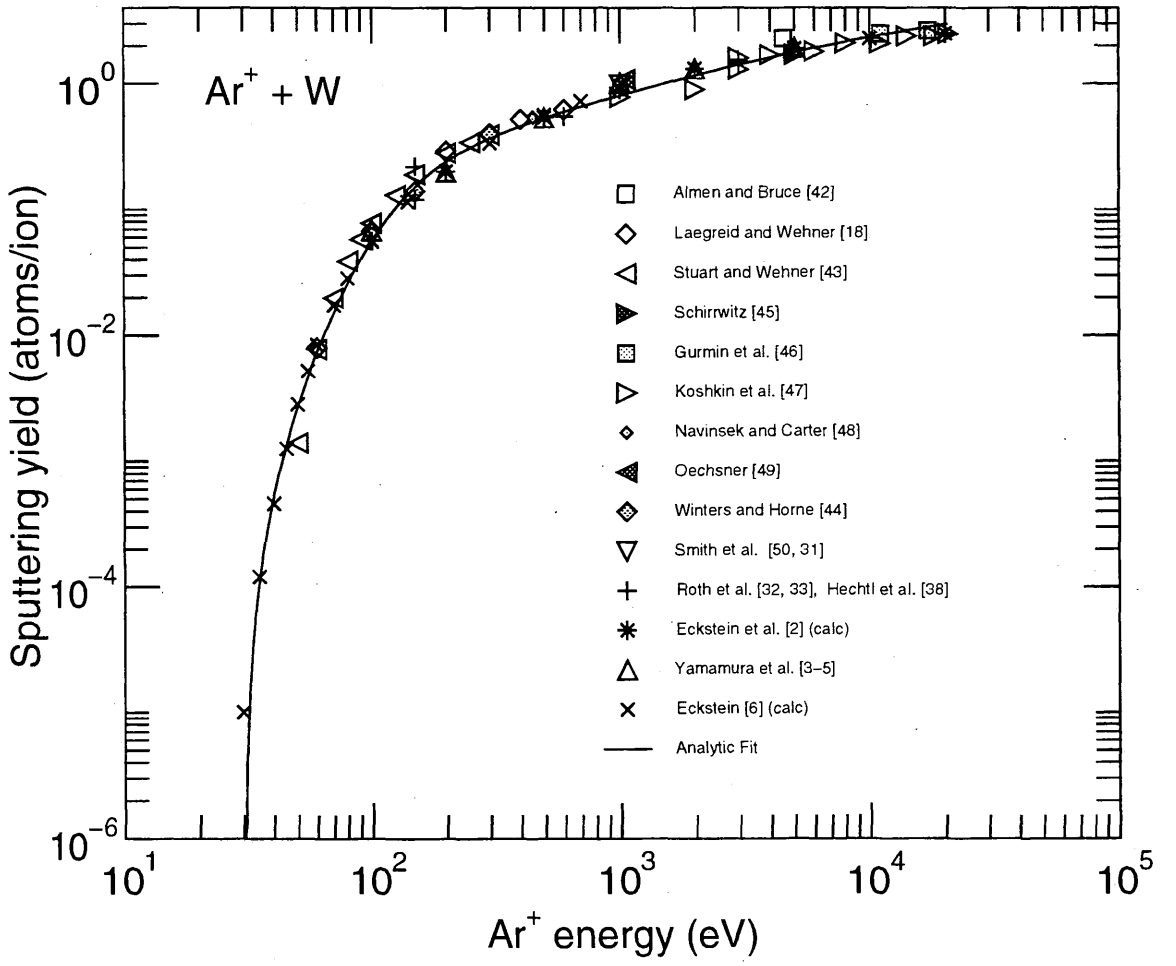

2.1.3.10 $W^+ + W$

Comments: (1) Fit valid between E_{min}=E_{th} and E_{max}= 1.0000E+05 eV.

Fitting parameters:

Parameter:	λ	q	μ	$\epsilon_L(eV^{-1})$	E_{th}(eV)	Avg. Error (%)
	1.3707E+00	3.8011E+01	2.6794E+00	1.9358E-07	2.3462E+01	18.0

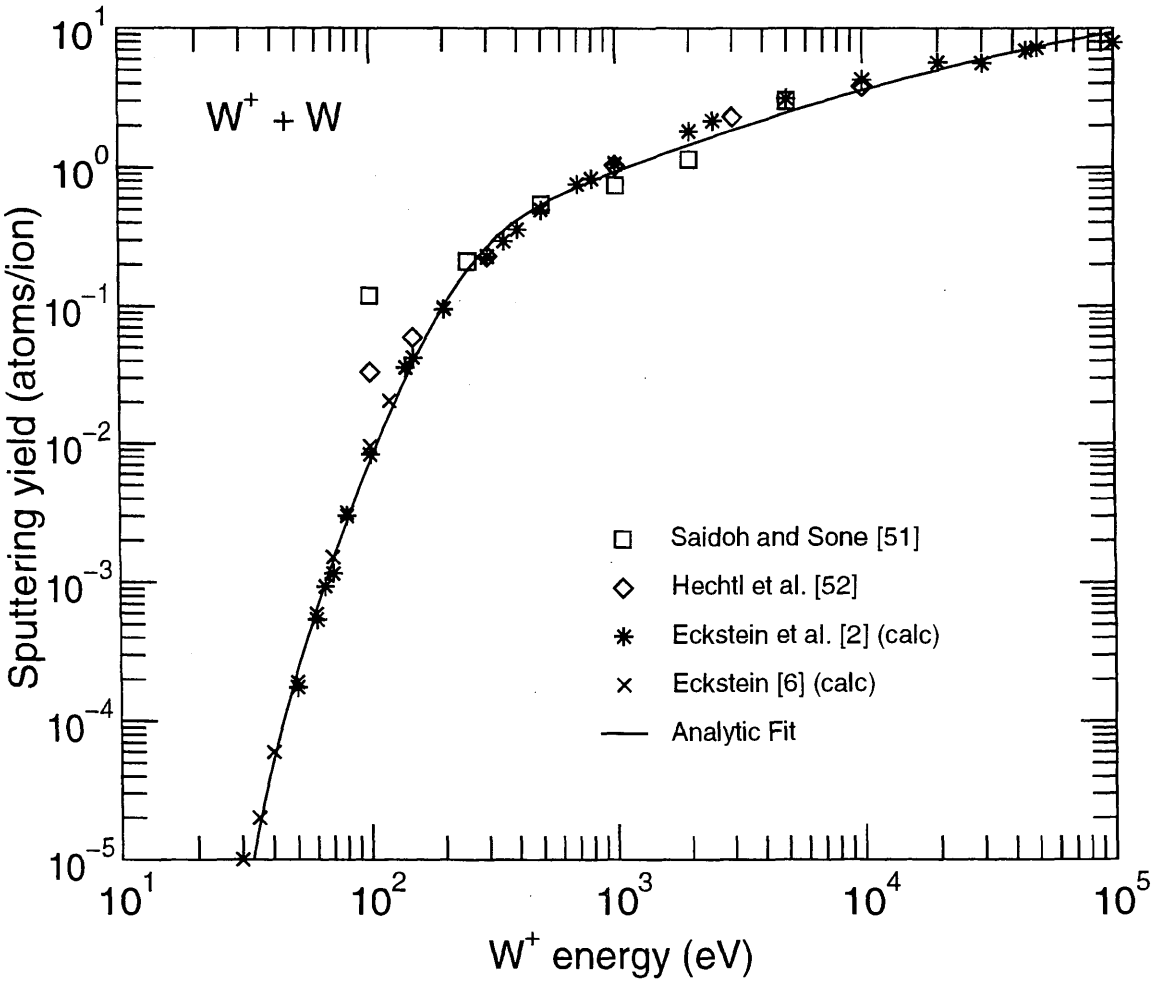

2.1.4.1 H^+, D^+, He^+ + Be_4B

Comments: (1) H^+: fit valid between E_{min}=E_{th} and E_{max}= 3.0000E+03 eV.
(2) D^+: fit valid between E_{min}=E_{th} and E_{max}= 4.0000E+03 eV.
(3) He^+: fit valid between E_{min}=E_{th} and E_{max}= 4.0000E+03 eV.
(4) Threshold energies probably too high due to missing low energy points.

Fitting parameters:

Parameter:	λ	q	μ	ϵ_L(eV^{-1})	E_{th}(eV)	Avg. Error (%)
H	-1.7002E-01	6.9894E-02	-7.2090E-01	3.3646E-03	9.9500E+01	0.0
D	2.4530E-01	2.2629E-01	1.8987E-02	3.3646E-03	4.9750E+01	10.6
He	-3.0663E-02	5.1983E-01	-9.0982E-01	1.3271E-03	1.4925E+02	7.6

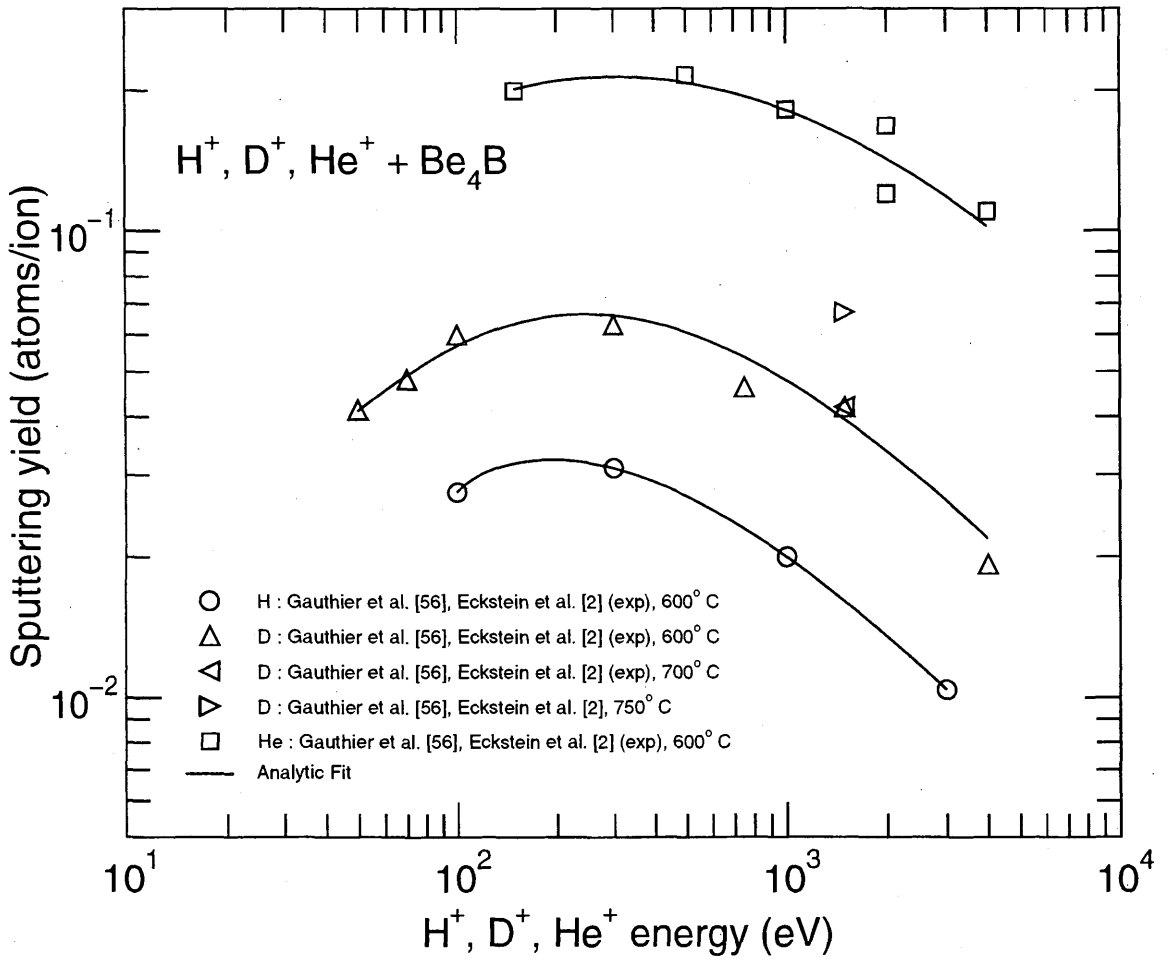

2.1.4.2 $H^+ + B_4C$

Comments: (1) Fit valid between E_{min}=E_{th} and E_{max}= 1.0000E+04 eV.
(2) The calculated data points are only valid at low fluences due to preferential sputtering particularly near the threshold energy.

Fitting parameters:

Parameter:	λ	q	μ	$\epsilon_L(eV^{-1})$	E_{th}(eV)	Avg. Error (%)
	8.1070E-01	4.1957E-02	1.1437E+00	2.6760E-03	3.1538E+01	21.3

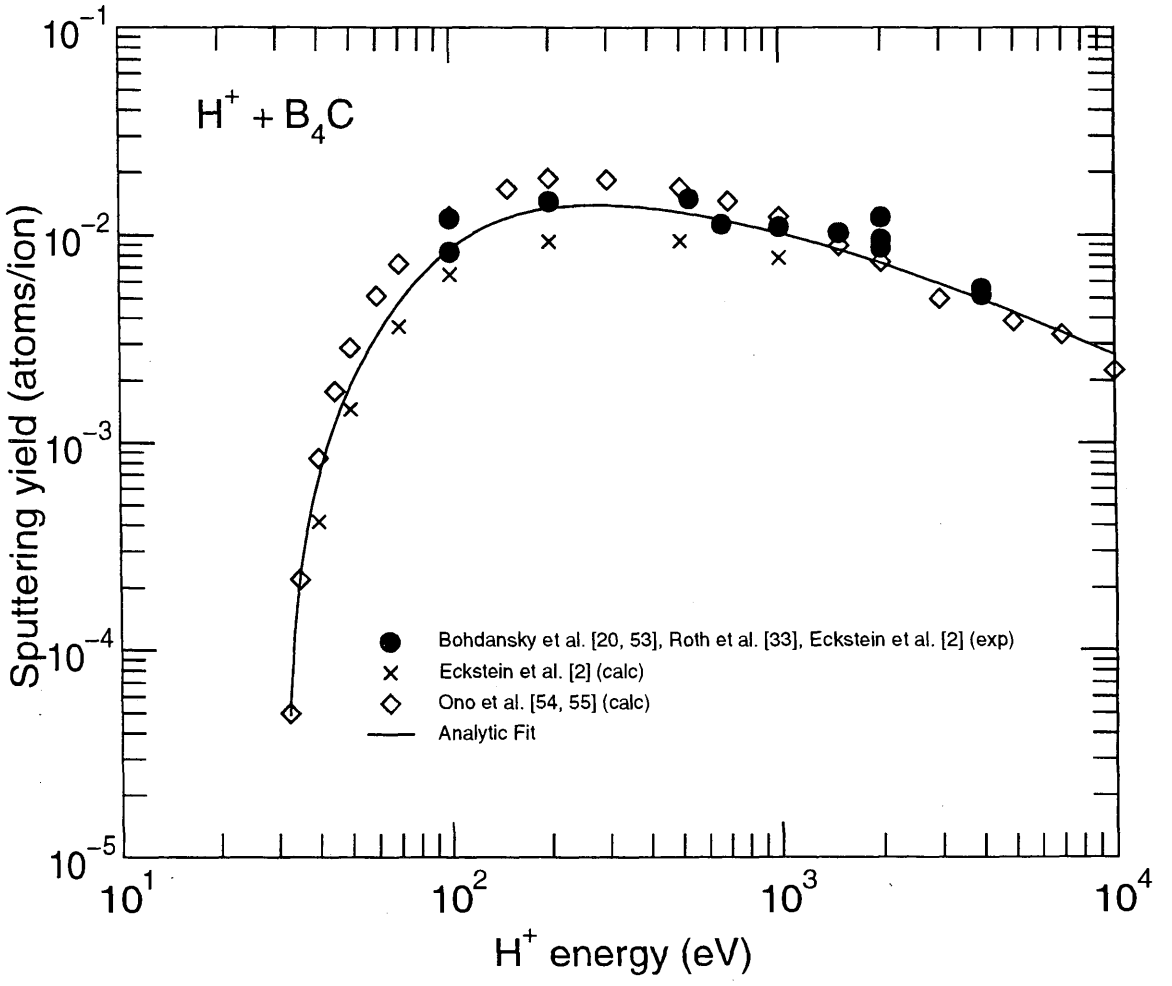

2.1.4.3 $D^+ + B_4C$

Comments: (1) Fit valid between E_{min}=E_{th} and E_{max}= 1.0000E+04 eV.
(2) The calculated data points are only valid at low fluences due to preferential sputtering particularly near the threshold energy.

Fitting parameters:

Parameter:	λ	q	μ	$\epsilon_L(eV^{-1})$	E_{th}(eV)	Avg. Error (%)
	6.0340E-01	7.5073E-02	1.5094E+00	1.6858E-03	2.1157E+01	20.0

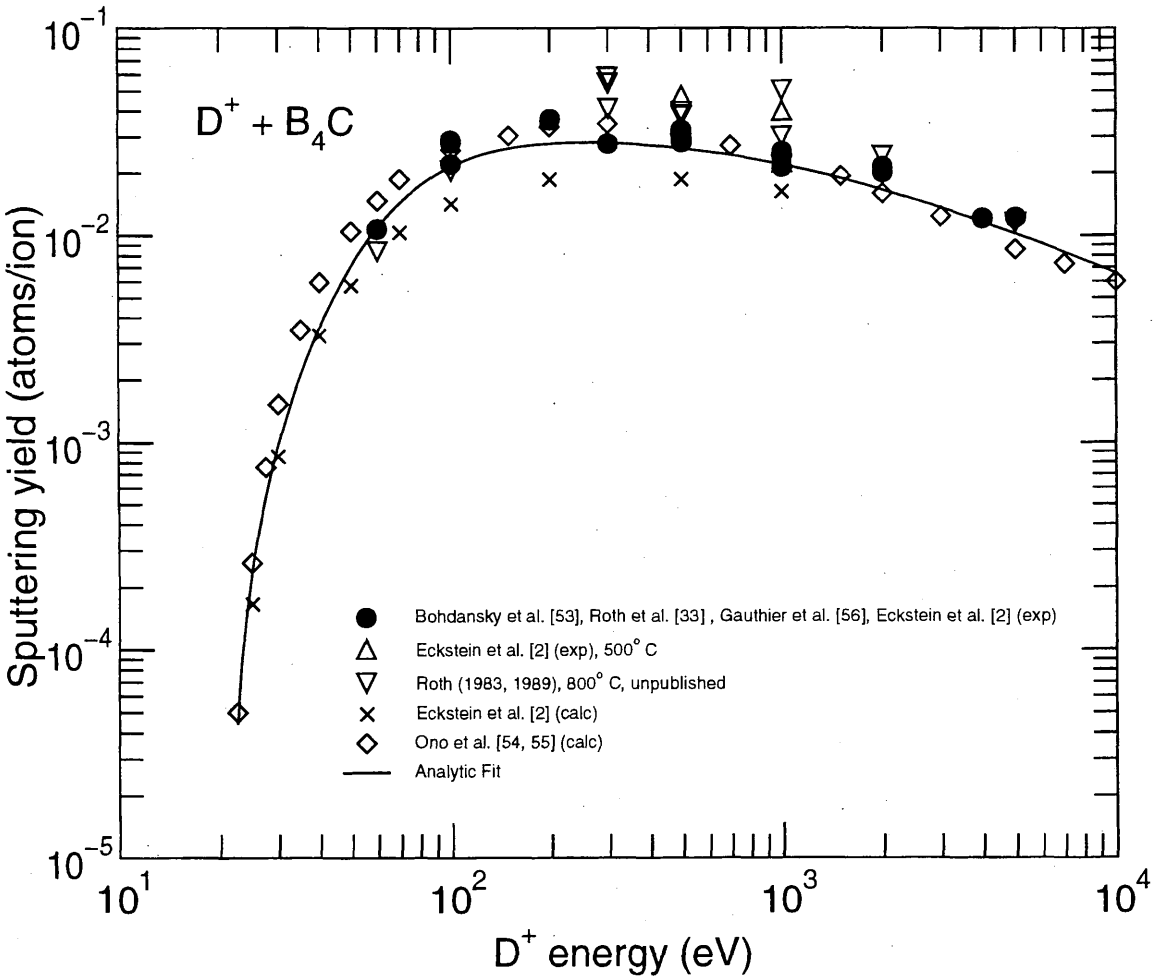

2.1.4.4 $T^+ + B_4C$

Comments: (1) Fit valid between E_{min}=E_{th} and E_{max}= 1.0000E+04 eV.
(2) Only calculated values.
(3) The calculated data points are only valid at low fluences due to preferential sputtering particularly near the threshold energy.

Fitting parameters:

Parameter:	λ	q	μ	ϵ_L(eV^{-1})	E_{th}(eV)	Avg. Error (%)
	4.8332E-01	1.0080E-01	1.5626E+00	1.6920E-03	2.0399E+01	5.9

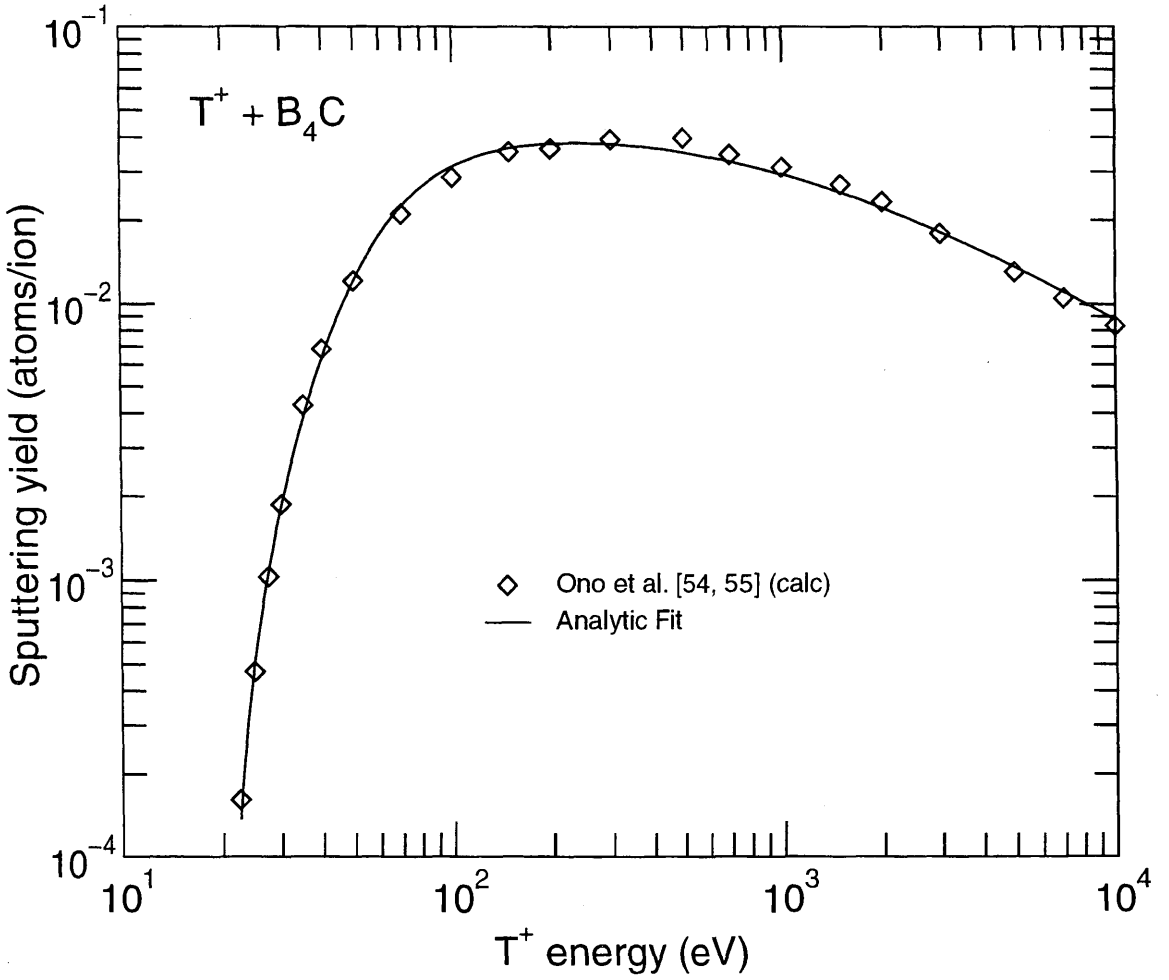

2.1.4.5 $He^+ + B_4C$

Comments: (1) Fit valid between E_{min}=E_{th} and E_{max}= 1.0000E+04 eV.
(2) The calculated data points are only valid at low fluences due to preferential sputtering particularly near the threshold energy.

Fitting parameters:

Parameter:	λ	q	μ	$\epsilon_L(eV^{-1})$	E_{th}(eV)	Avg. Error (%)
	1.9055E-01	1.9321E-01	1.4557E+00	4.2854E-04	2.5971E+01	16.2

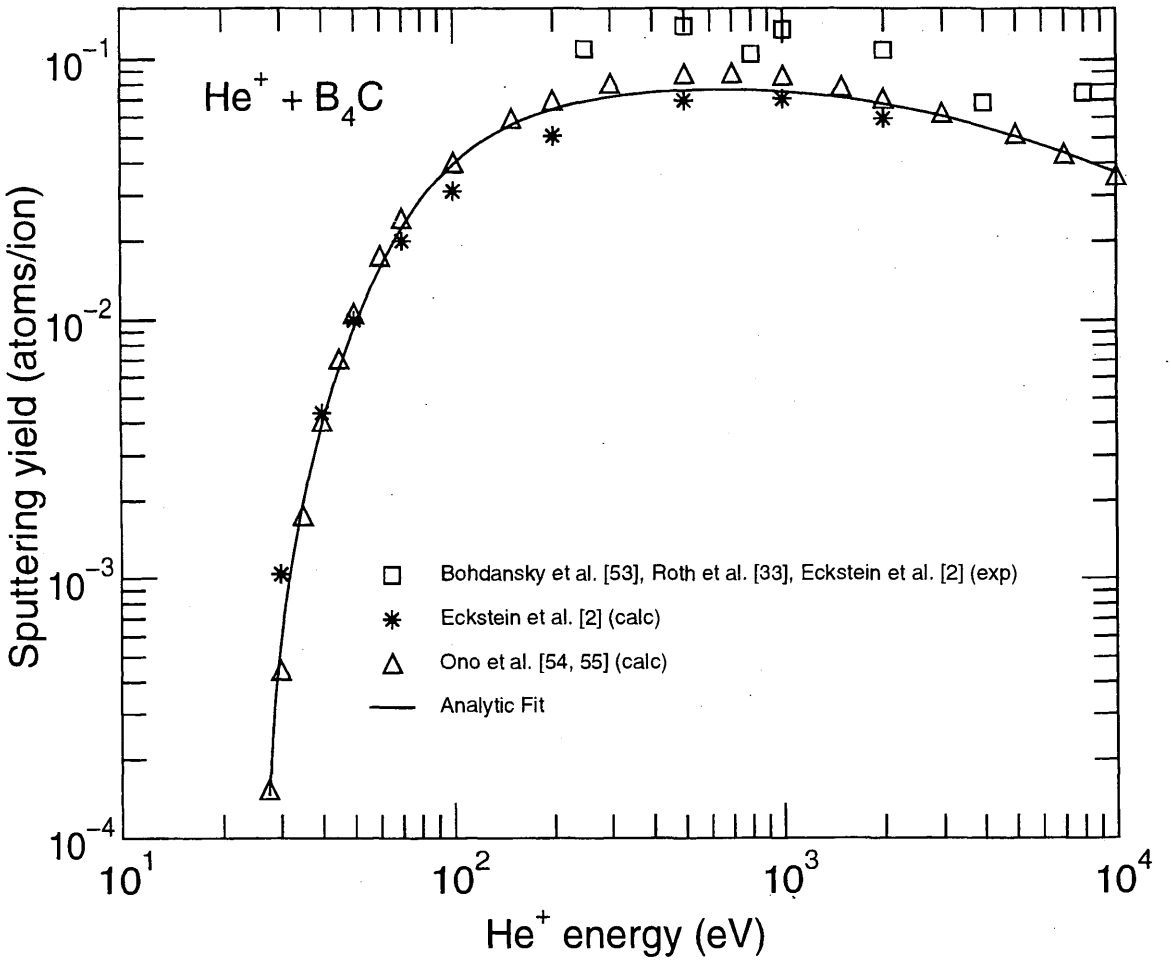

2.1.4.6 $B^+ + B_4C$

Comments: (1) Fit valid between E_{min}=E_{th} and E_{max}= 1.0000E+05 eV.
(2) Only calculated values.
(3) The calculated data points are only valid at low fluences due to preferential sputtering and possible compositional changes particularly near the threshold energy.

Fitting parameters:

Parameter:	λ	q	μ	$\epsilon_L(eV^{-1})$	E_{th}(eV)	Avg. Error (%)
	4.7196E-01	7.1342E-01	1.4376E+00	1.0628E-04	4.5420E+01	5.9

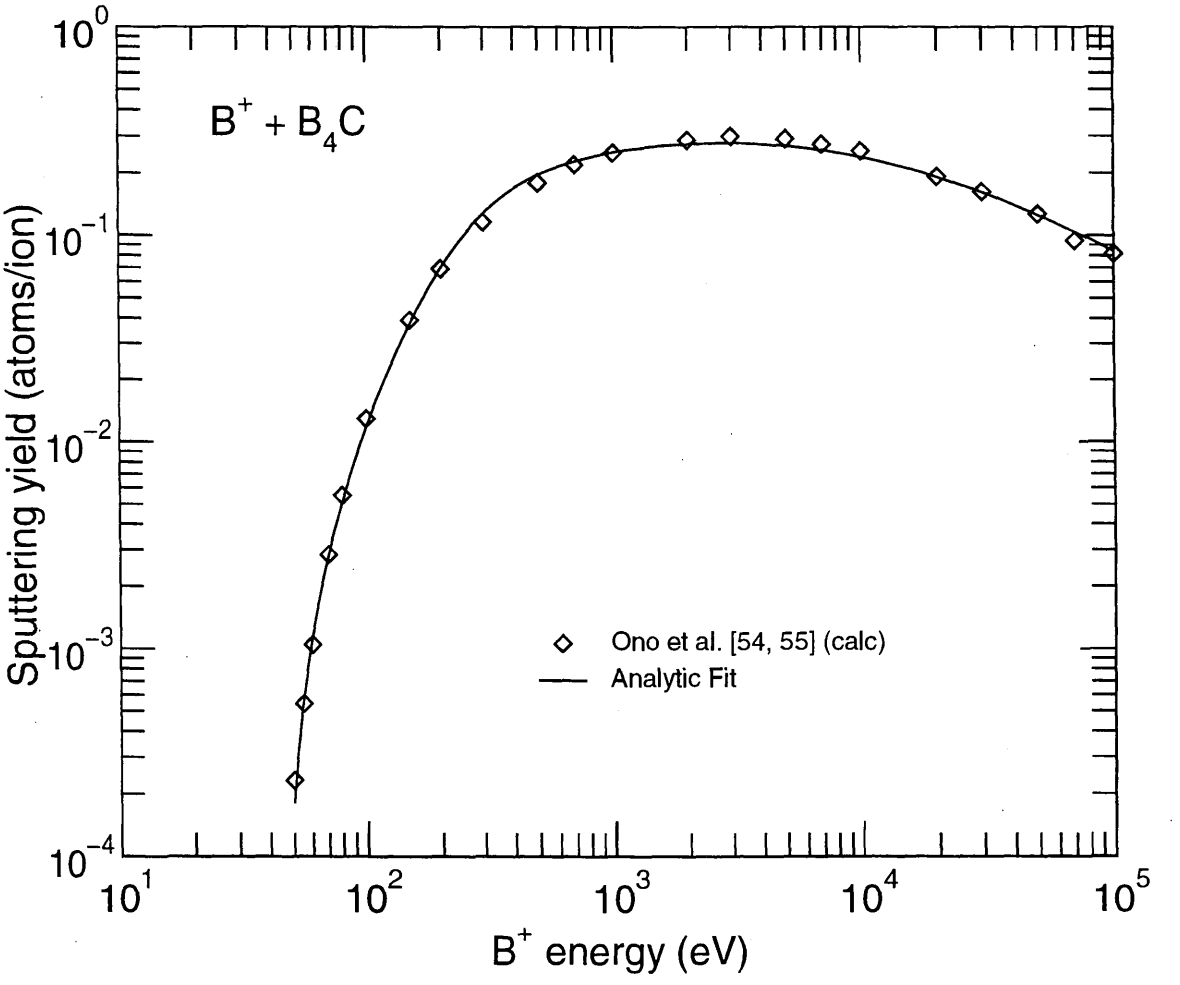

2.1.4.7 $C^+ + B_4C$

Comments: (1) Fit valid between E_{min}=E_{th} and E_{max}= 1.0000E+05 eV.
(2) Points are valid only for low fluence due to possible compositional changes.

Fitting parameters:

Parameter:	λ	q	μ	$\epsilon_L(eV^{-1})$	E_{th}(eV)	Avg. Error (%)
	5.1380E-01	8.7393E-01	1.5131E+00	8.0728E-05	4.6233E+01	7.3

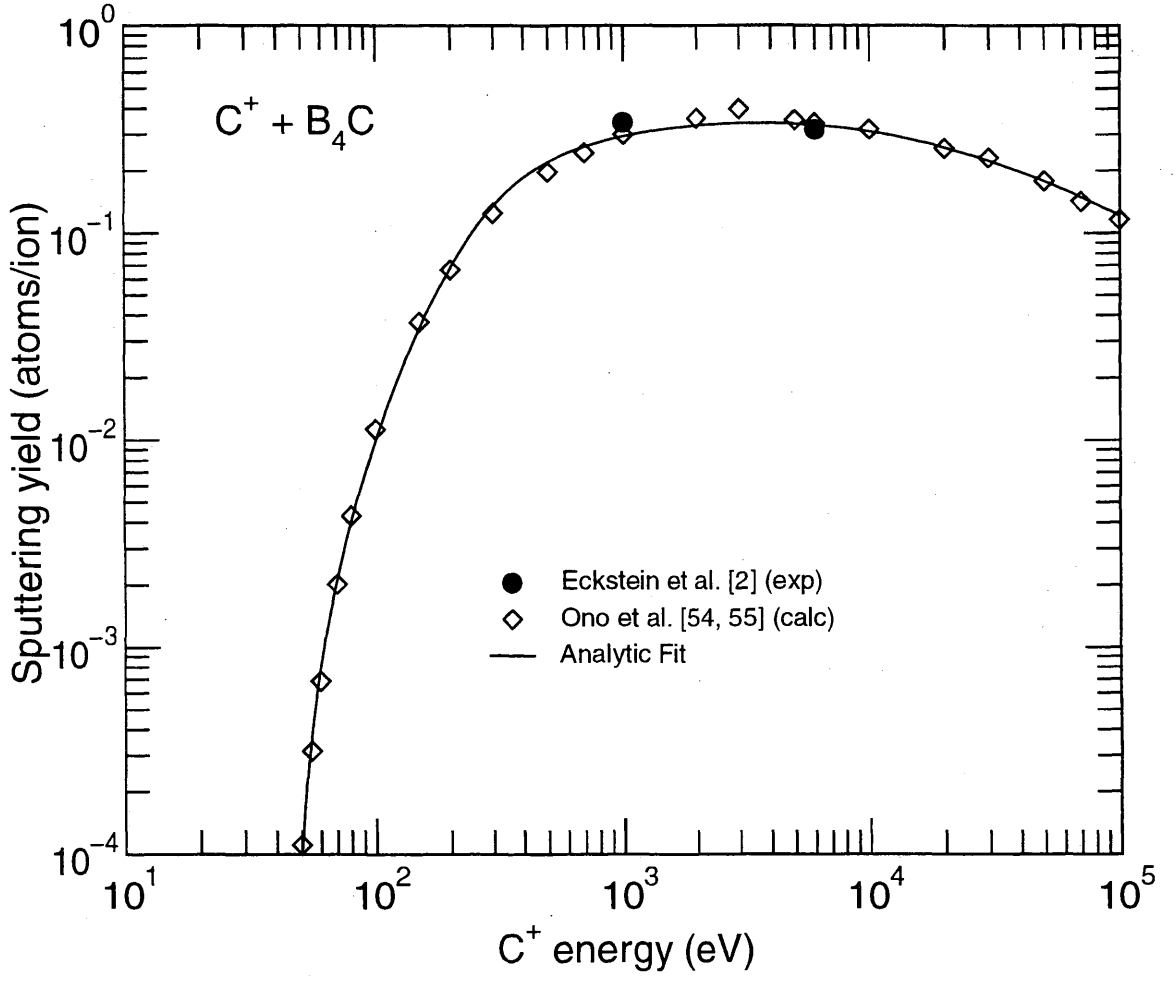

2.1.4.8 $H_20^+ + B_4C$

Comments: (1) Fit valid between E_{min}=E_{th} and E_{max}= 6.0000E+03 eV.
(2) Threshold probably too high due to lack of low energy data.

Fitting parameters:

Parameter:	λ	q	μ	$\epsilon_L(eV^{-1})$	E_{th}(eV)	Avg. Error (%)
	1.5054E-01	1.8538E+00	1.0000E-04	6.9062E-04	1.4925E+02	13.8

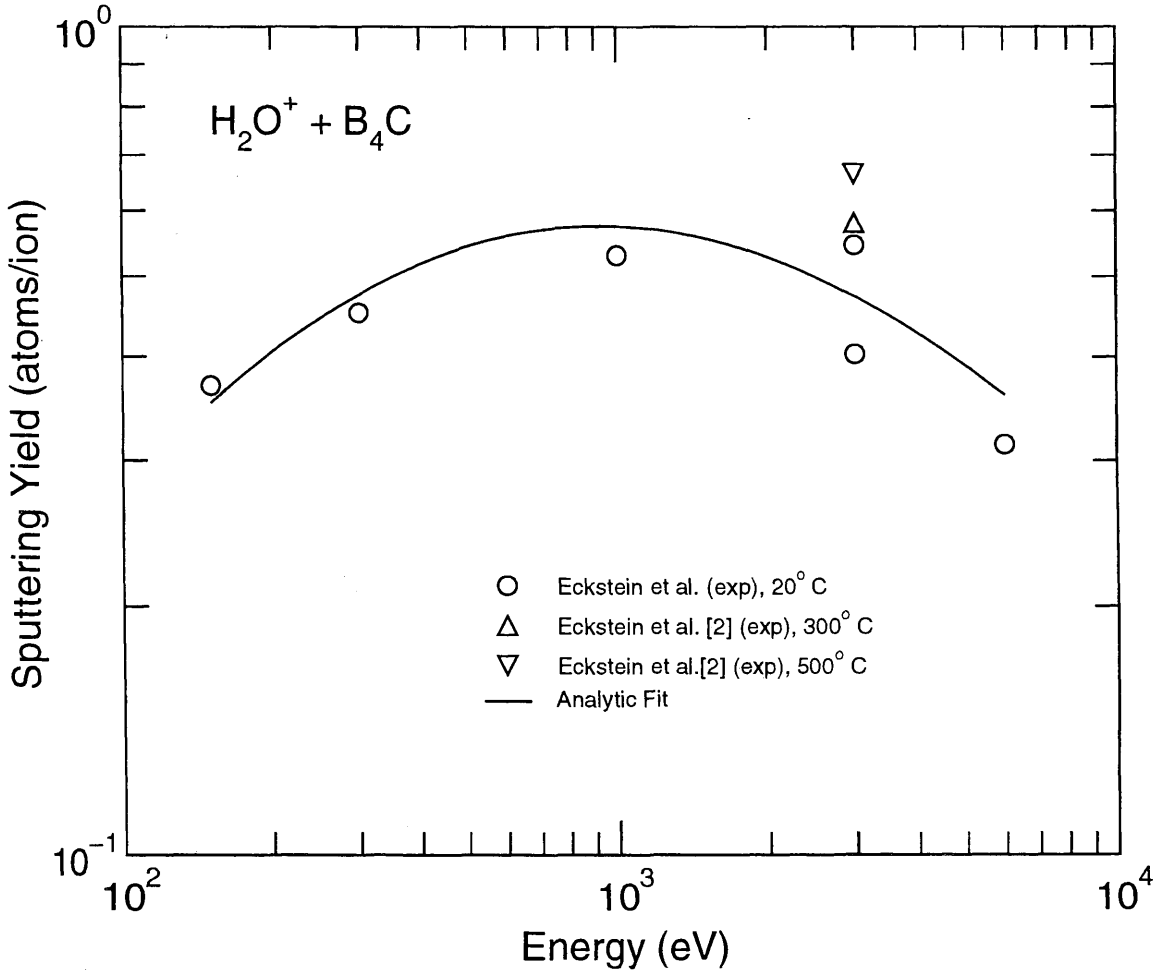

2.1.4.9 $Ne^+ + B_4C$

Comments: (1) Fit valid between E_{min}=E_{th} and E_{max}= 1.0000E+05 eV.
(2) Threshold energy probably too high due to missing low energy points.
(3) The calculated points are only valid at low fluence due to preferential sputtering.

Fitting parameters:

Parameter:	λ	q	μ	$\epsilon_L(eV^{-1})$	E_{th}(eV)	Avg. Error (%)
	3.3462E-01	1.5502E+00	1.5123E+00	2.8787E-05	5.8822E+01	10.3

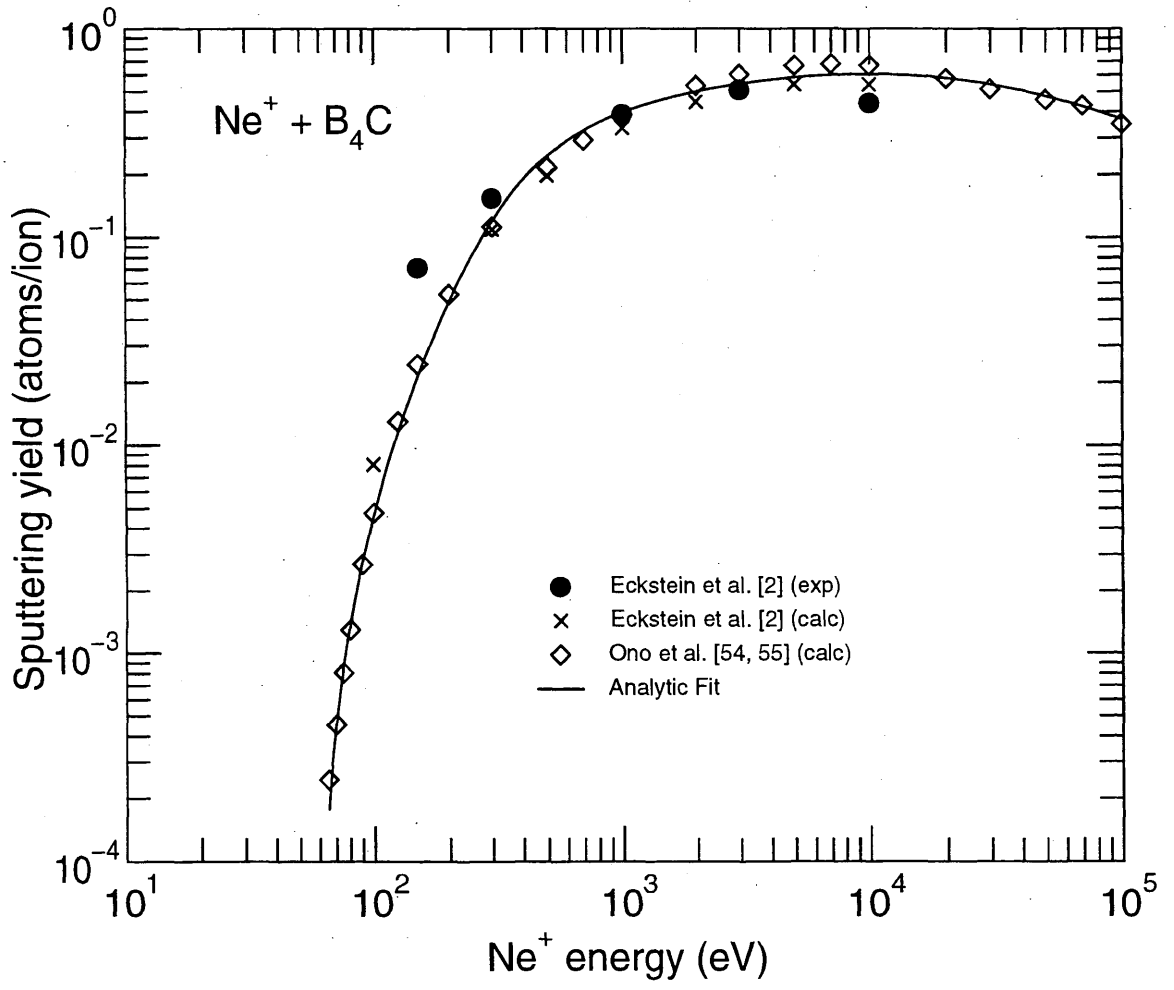

2.1.4.10 $Ar^+ + B_4C$

Comments: (1) Fit valid between E_{min}=E_{th} and E_{max}= 5.0000E+05 eV.
(2) Only calculated values.
(3) Threshold energy probably too high due to missing low energy points.
(4) The calculated points are only valid at low fluence due to preferential sputtering.

Fitting parameters:

Parameter:	λ	q	μ	$\epsilon_L(eV^{-1})$	E_{th}(eV)	Avg. Error (%)
	2.0734E-01	2.8560E+00	1.0931E+00	1.3925E-05	9.5910E+01	7.5

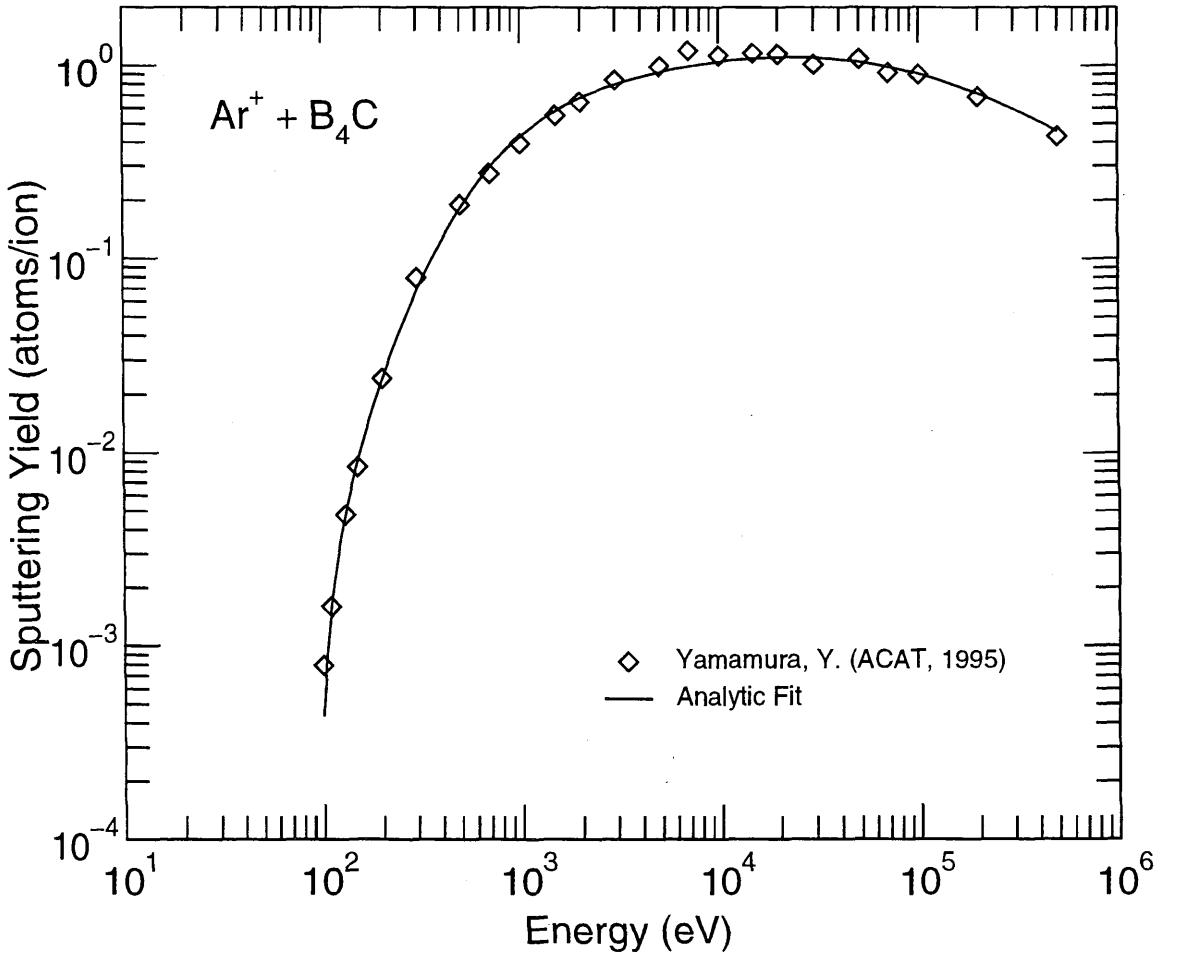

2.1.4.11 $D^+ + Be_2C$

Comments: (1) Fit valid between E_{min}=E_{th} and E_{max}= 2.0000E+03 eV.
(2) Calculated values only valid for low fluences due to composition changes by bombardment due to preferential sputtering.

Fitting parameters:

Parameter:	λ	q	μ	$\epsilon_L(eV^{-1})$	E_{th}(eV)	Avg. Error (%)
total	9.3013E-01	8.7529E-02	9.3542E-01	3.2271E-03	1.8002E+01	14.5
Be	3.3424E-01	4.4858E-02	1.0264E+00	1.8599E-03	1.7358E+01	2.3
C	3.7038E-01	1.8592E-02	1.3901E+00	1.4674E-03	1.8196E+01	2.5

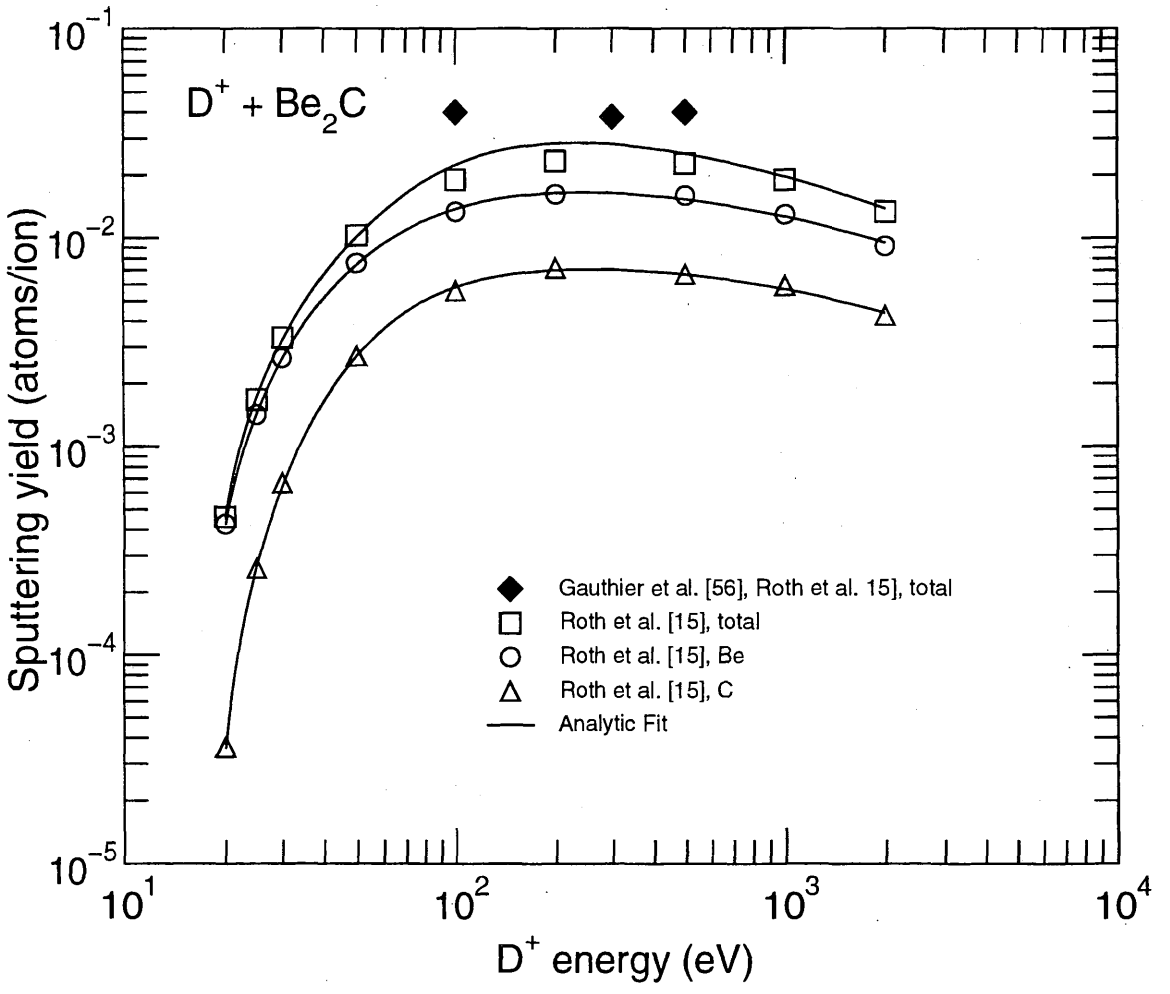

2.1.4.12 H^+ + BeO

Comments: (1) Fit valid between E_{min}=E_{th} and E_{max}= 4.0000E+03 eV.
(2) Threshold energy probably too high due to missing low energy points.

Fitting parameters:

Parameter:	λ	q	μ	ϵ_L(eV^{-1})	E_{th}(eV)	Avg. Error (%)
	2.5955E+00	1.0117E-01	1.7952E-01	1.6124E-03	6.9650E+01	28.5

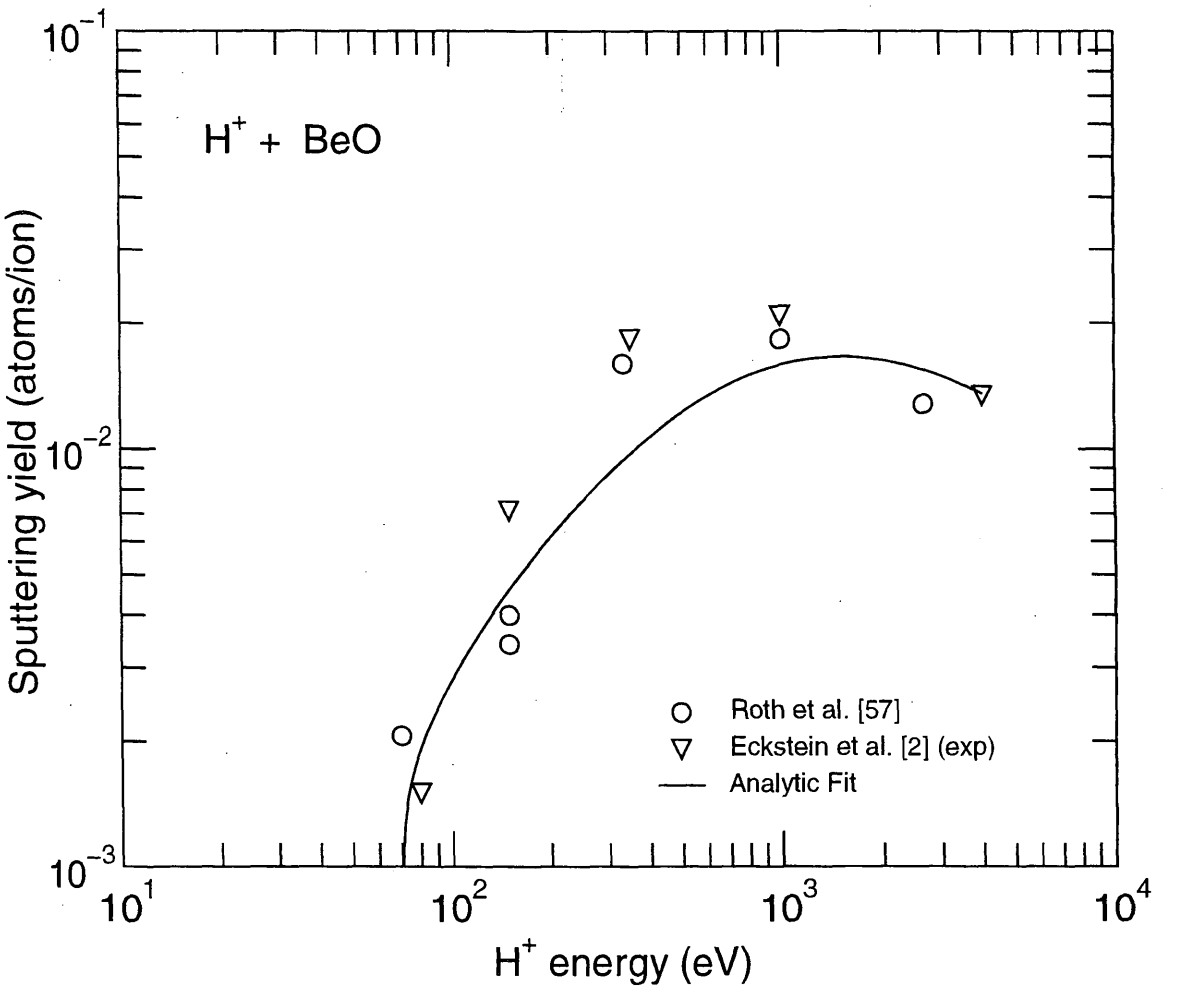

2.1.4.13 D^+ + BeO

Comments: (1) Fit valid between E_{min}=E_{th} and E_{max}= 3.3330E+03 eV.
(2) Threshold energy probably too high due to missing low energy points.

Fitting parameters:

Parameter:	λ	q	μ	$\epsilon_L(eV^{-1})$	E_{th}(eV)	Avg. Error (%)
	1.7507E+00	1.9070E-01	4.6536E-02	1.5134E-03	4.9750E+01	29.8

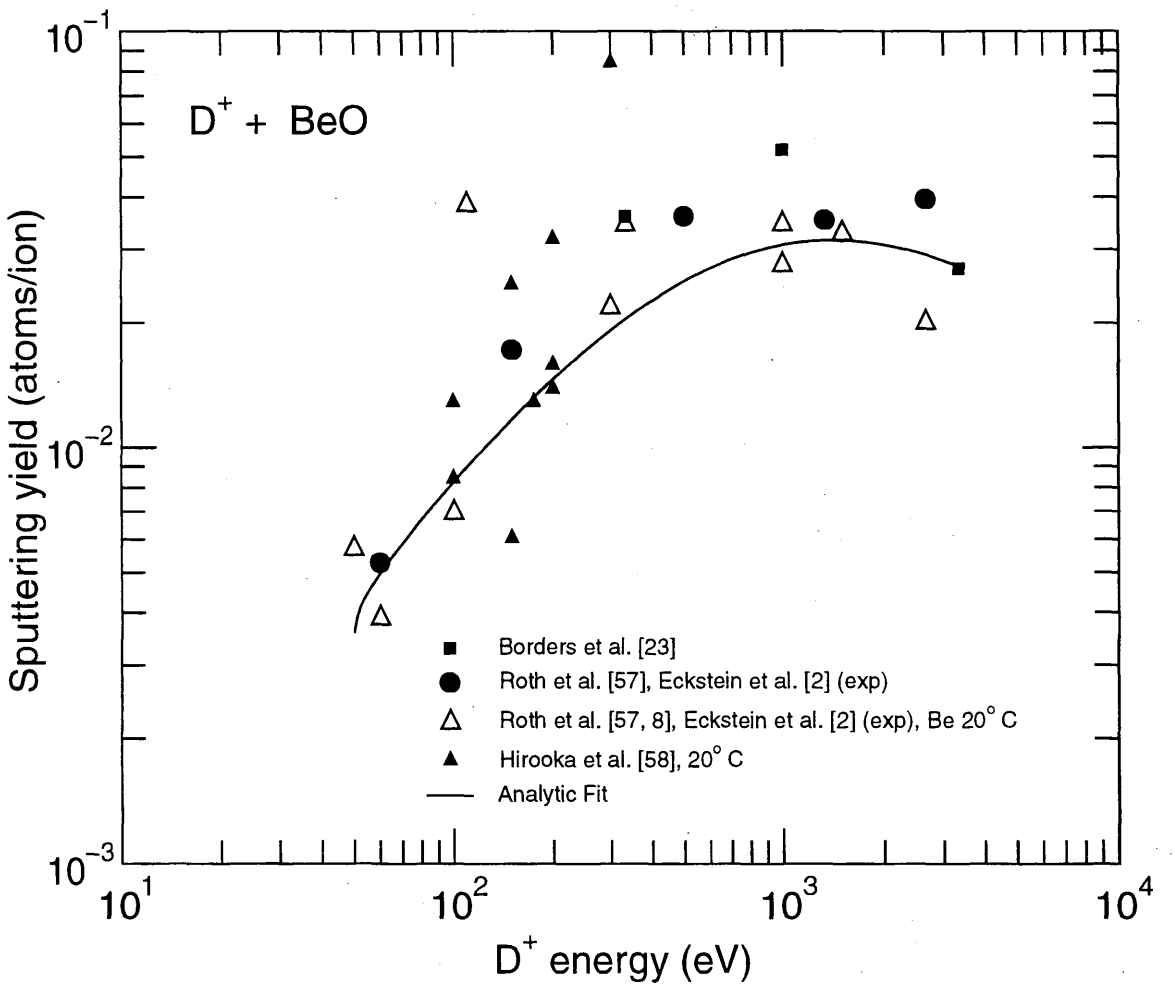

2.1.4.14 He^+ + BeO

Comments: (1) Fit valid between E_{min}=E_{th} and E_{max}= 4.5000E+03 eV.
(2) Threshold energy probably too high due to missing low energy points.

Fitting parameters:

Parameter:	λ	q	μ	$\epsilon_L(eV^{-1})$	E_{th}(eV)	Avg. Error (%)
	1.2356E+00	6.5513E-01	2.7535E-02	8.9986E-04	1.2935E+02	22.8

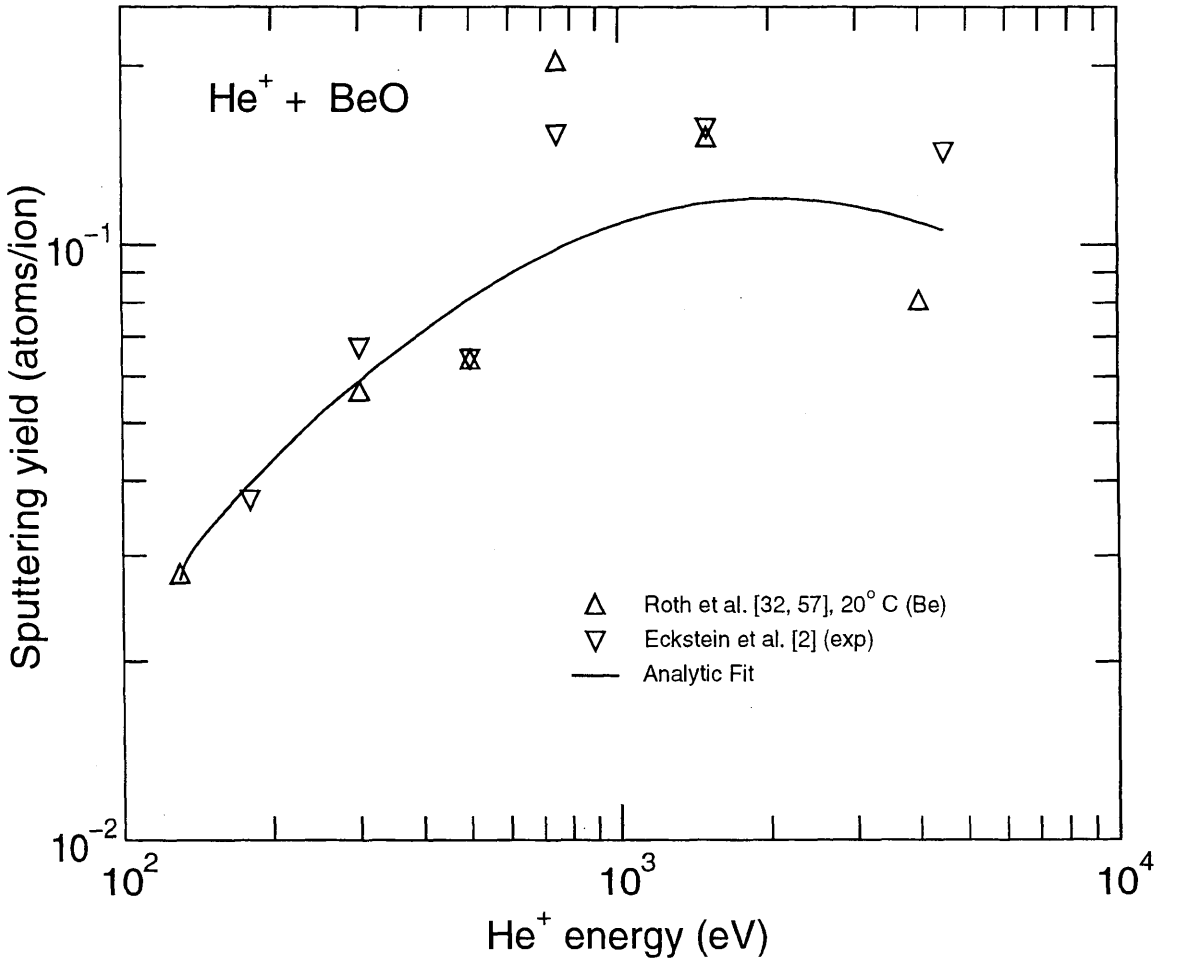

2.1.4.15 O^+ + BeO

Comments: (1) Fit valid between E_{min}=E_{th} and E_{max}= 1.0000E+04 eV.
(2) Threshold energy probably too high due to missing low energy points.

Fitting parameters:

Parameter:	λ	q	μ	$\epsilon_L(eV^{-1})$	E_{th}(eV)	Avg. Error (%)
	6.4928E-02	1.1747E+00	3.9558E-01	4.9738E-05	9.8142E+01	12.4

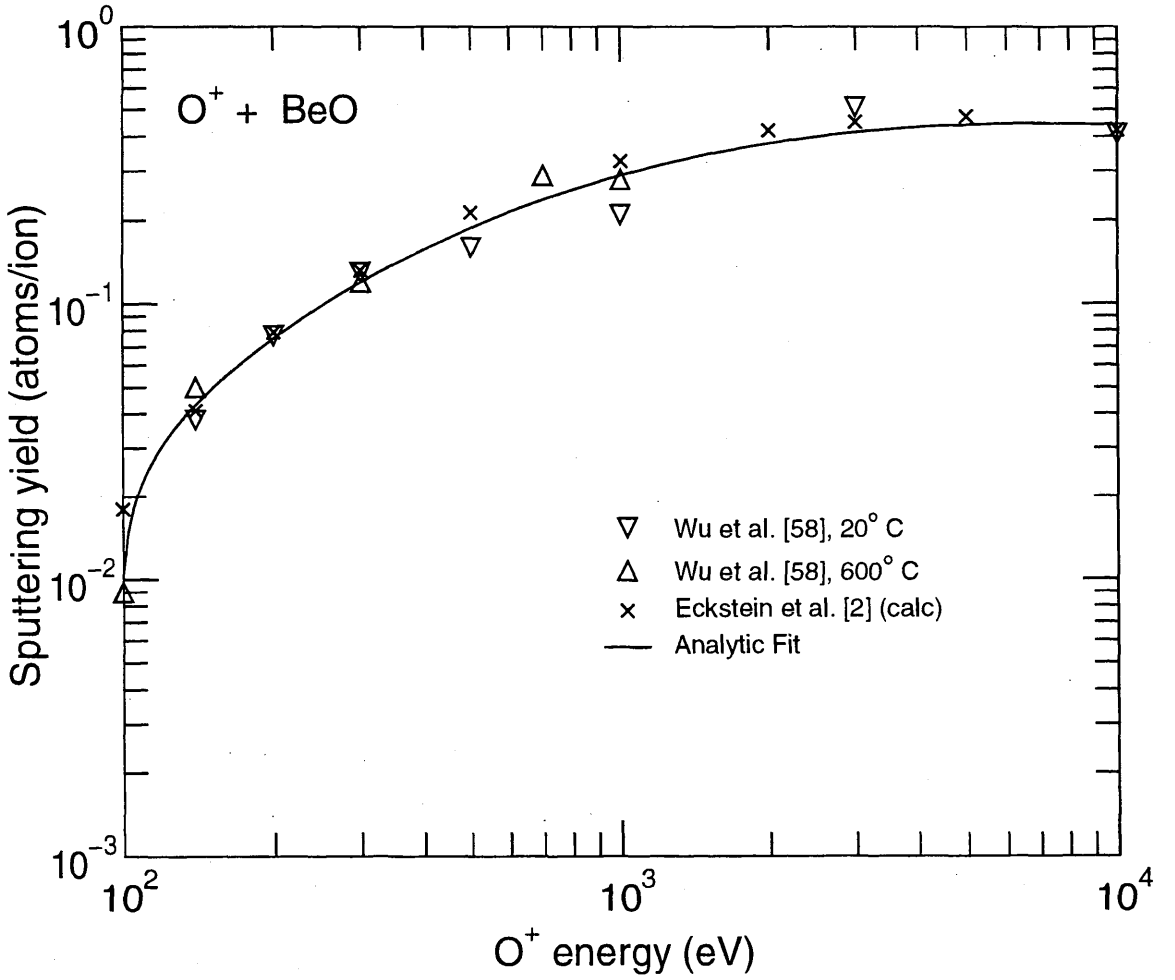

2.1.4.16 H^+, D^+, He^+ + SiC

Comments: (1) H^+: fit valid between $E_{min} = E_{th}$ and E_{max} = 4.0000E+03 eV.
(2) D^+: fit valid between $E_{min} = E_{th}$ and E_{max} = 5.0000E+03 eV.
(3) He^+: fit valid between $E_{min} = E_{th}$ and E_{max} = 8.0000E+03 eV.
(4) Threshold energies probably too high due to missing low energy points.

Fitting parameters:

Parameter:	λ	q	μ	$\epsilon_L(eV^{-1})$	E_{th}(eV)	Avg. Error (%)
H	2.4391E+00	6.8841E-02	6.7093E-02	3.4004E-03	9.9500E+01	25.2
D	3.0157E+00	2.6034E-01	1.4113E-02	3.4960E-03	9.9500E+01	6.7
He	3.7228E-02	2.7707E-01	1.0000E-04	2.7916E-04	2.4875E+02	24.2

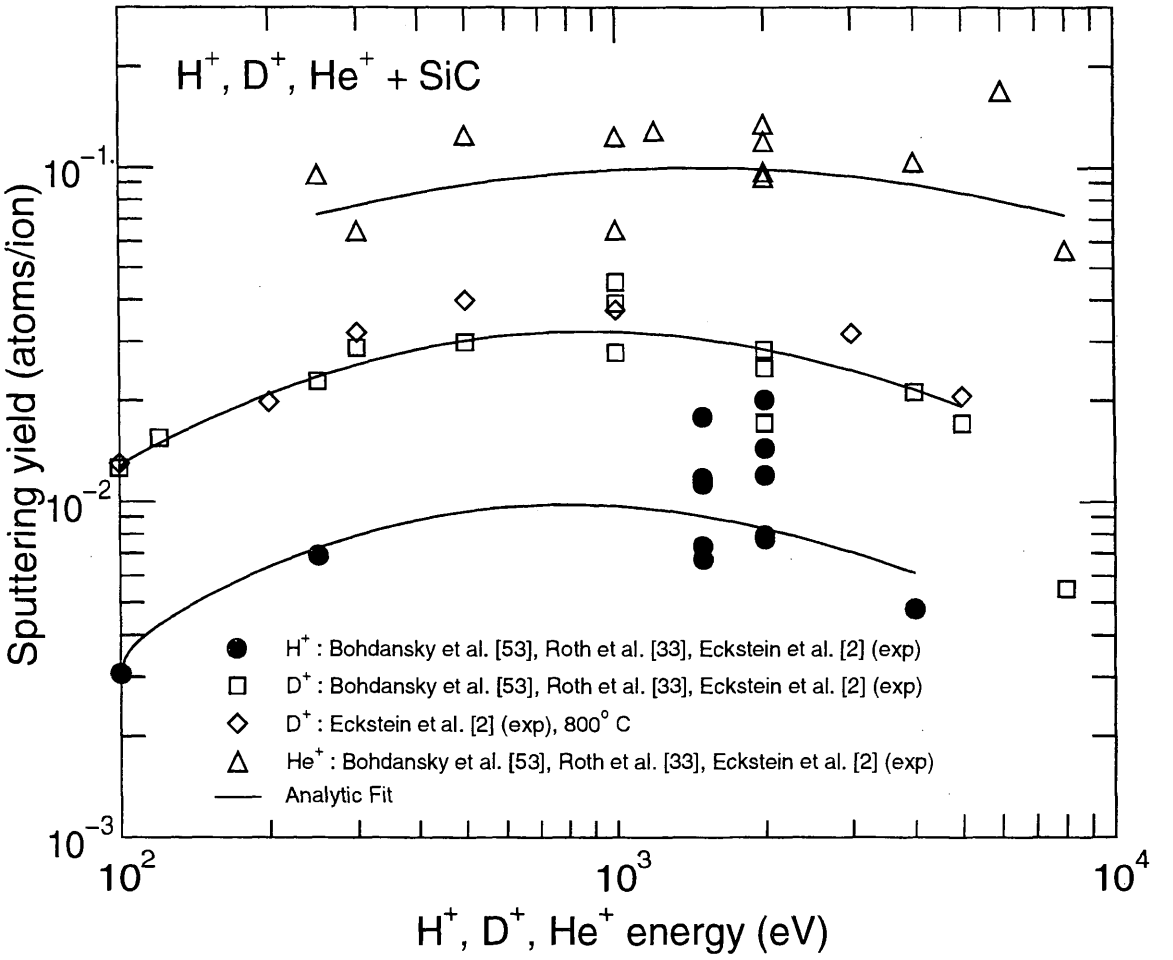

2.1.4.17 O^+, Ne^+ + SiC

Comments: (1) Fits valid between $E_{min} = E_{th}$ and E_{max} = 1.0000E+04 eV.
(2) Threshold energies probably too high due to missing low energy points.

Fitting parameters:

Parameter:	λ	q	μ	$\epsilon_L(eV^{-1})$	E_{th}(eV)	Avg. Error (%)
O	8.6409E-03	2.1072E+00	5.0526E-01	4.3707E-06	1.4455E+02	0.0
Ne	1.5948E-02	2.0503E+00	2.0950E-03	4.0329E-05	9.9500E+02	1.9

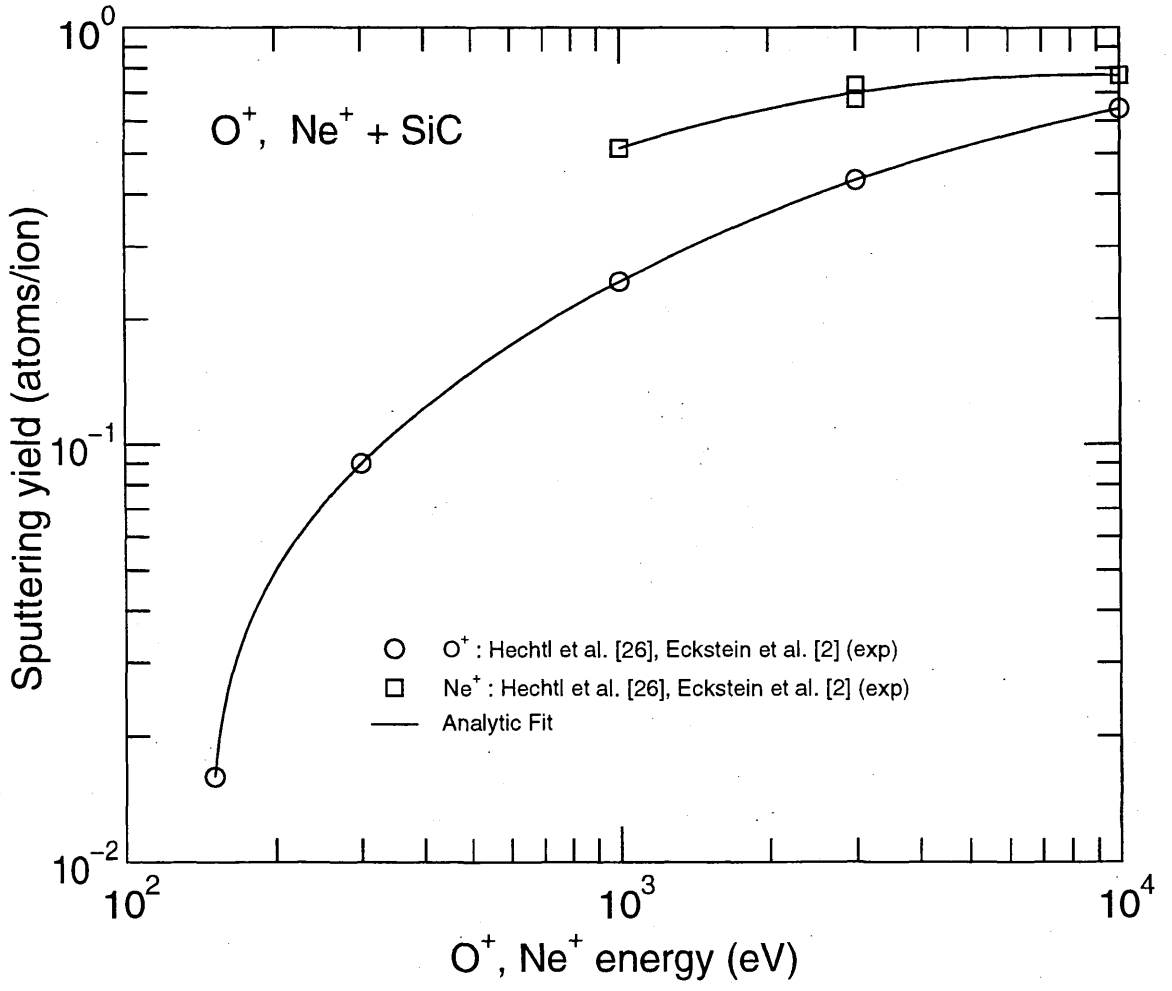

2.1.4.18 H^+, D^+, He^+ + TiC

Comments: (1) H^+: fit valid between $E_{min} = E_{th}$ and E_{max} = 4.0000E+03 eV.
(2) D^+: fit valid between $E_{min} = E_{th}$ and E_{max} = 8.0000E+03 eV.
(3) He^+: fit valid between $E_{min} = E_{th}$ and E_{max} = 8.0000E+03 eV.
(4) Threshold energies probably too high due to missing low energy points.

Fitting parameters:

Parameter:	λ	q	μ	$\epsilon_L(eV^{-1})$	E_{th}(eV)	Avg. Error (%)
H	4.5573E-01	2.4257E-02	1.8780E-01	8.6177E-04	2.4875E+02	15.8
D	7.1466E-01	5.7766E-02	3.7505E-01	8.3484E-04	9.9500E+01	23.1
He	1.7489E-01	2.3376E-01	1.0000E-04	3.7694E-04	1.9900E+02	27.4

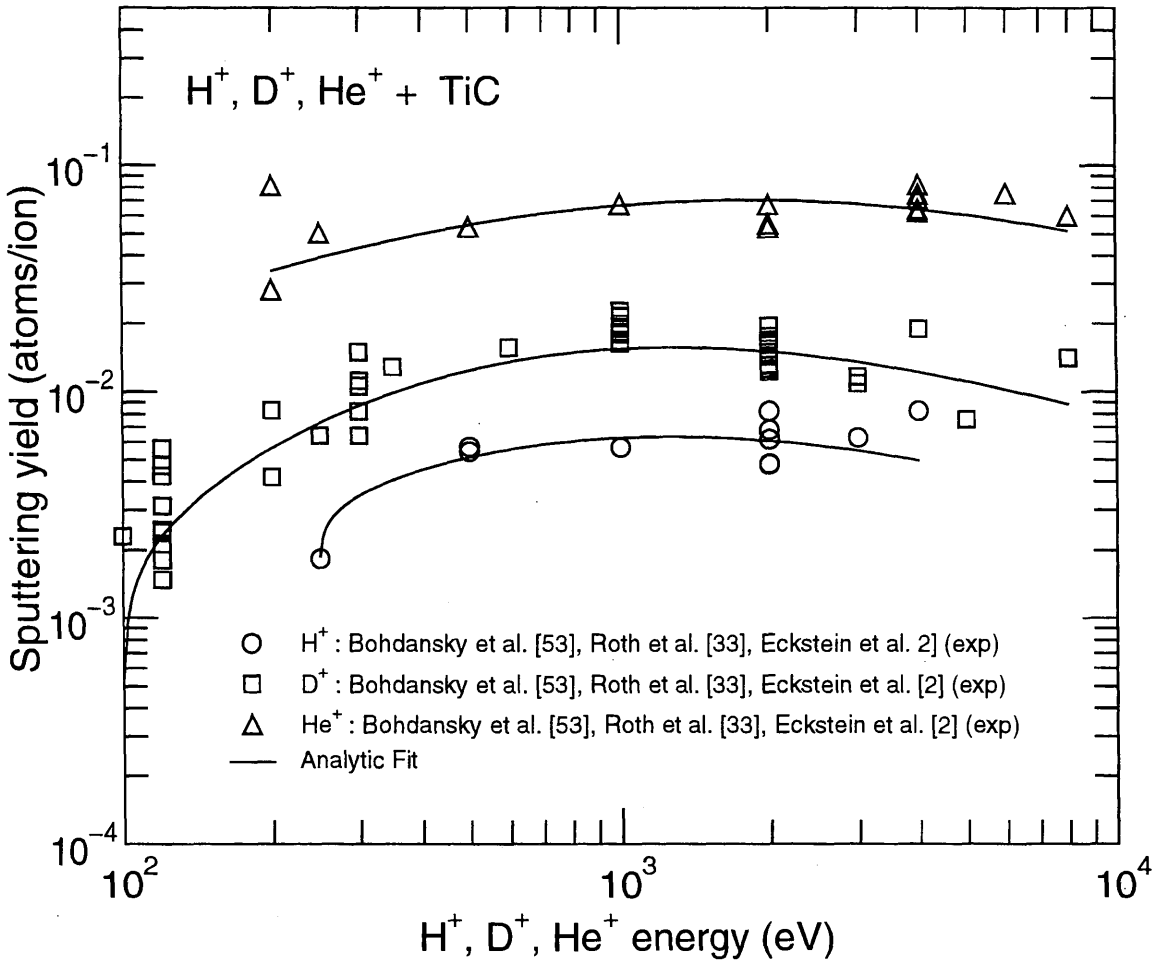

2.1.4.19 Ne^+, O^+ + TiC

Comments: (1) Fits valid between $E_{min} = E_{th}$ and E_{max} = 5.0000E+03 eV.
(2) Threshold energies probably too high due to missing low energy points.

Fitting parameters:

Parameter:	λ	q	μ	$\epsilon_L(eV^{-1})$	E_{th}(eV)	Avg. Error (%)
O	1.2476E-02	3.3307E+00	5.0532E-01	1.8800E-06	1.3984E+02	0.0
Ne	1.0000E-04	2.4086E+00	1.0000E-04	8.6823E-06	1.4925E+02	7.0

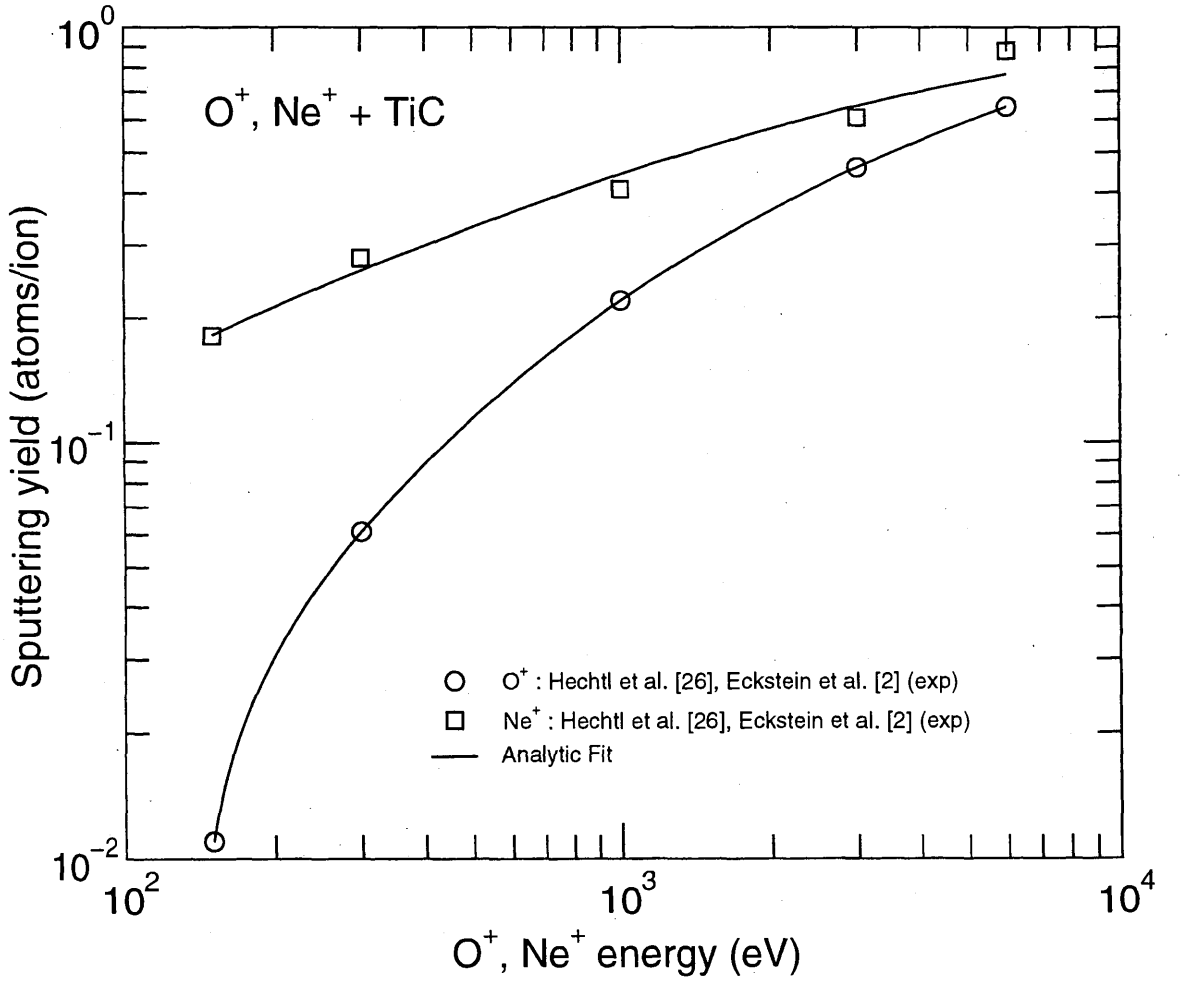

2.1.4.20 H^+, D^+, He^+ + WC

Comments: (1) H^+: fit valid between $E_{min} = E_{th}$ and E_{max} = 8.0000E+03 eV.
(2) D^+: fit valid between $E_{min} = E_{th}$ and E_{max} = 8.0000E+03 eV.
(3) He^+: fit valid between $E_{min} = E_{th}$ and E_{max} = 1.5000E+04 eV.
(4) Threshold energies probably too high due to missing low energy points.

Fitting parameters:

Parameter:	λ	q	μ	$\epsilon_L(eV^{-1})$	E_{th}(eV)	Avg. Error (%)
H	1.1437E+00	3.1271E-02	1.2796E-01	1.0452E-04	9.9500E+02	7.9
D	2.5561E+00	9.6543E-02	2.2644E-01	2.2334E-04	2.4875E+02	7.2
He	1.7195E-01	2.0080E-01	9.9747E-01	1.0720E-04	1.6546E+02	9.8

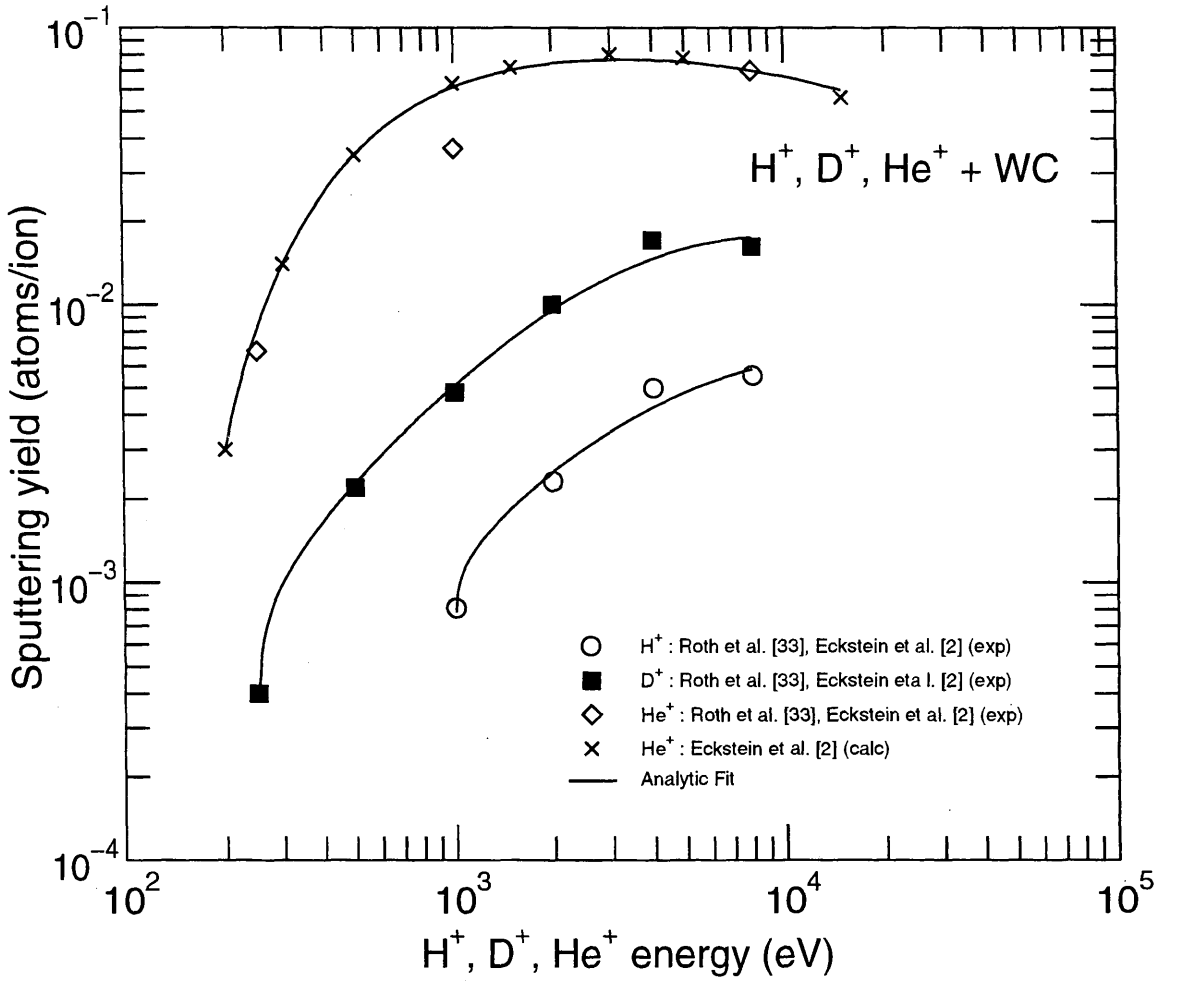

2.1.4.21 D^+ + NS31

Comments: (1) Fits valid between E_{min}=E_{th} and E_{max}= 3.0000E+03 eV.
(2) Threshold energies probably too high due to chemical erosion.

Fitting parameters:

Parameter:	λ	q	μ	$\epsilon_L(eV^{-1})$	E_{th}(eV)	Avg. Error (%)
300 K	2.1105E-01	1.0743E-01	1.0000E-04	3.9113E-03	1.9900E+01	14.9
800 K	1.4710E-02	2.1014E-01	1.0000E-04	7.9943E-04	1.9900E+01	20.4

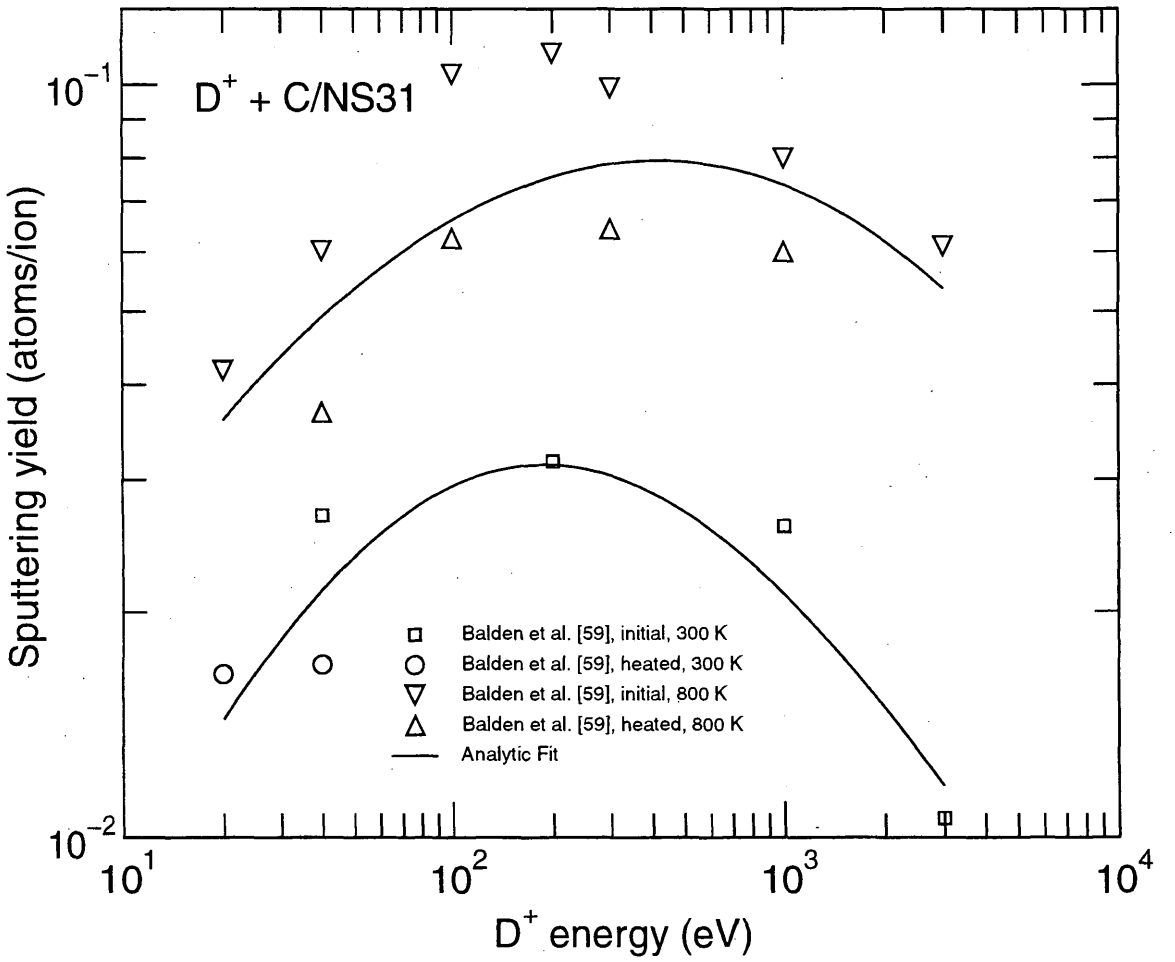

2.1.4.22 D^+ + C (C-SiC matrix, Ti doped)

Comments: (1) Fit valid between E_{min}=E_{th} and E_{max}= 1.0000E+03 eV.
(2) Threshold energies probably too high due to chemical erosion.

Fitting parameters:

Parameter:	λ	q	μ	$\epsilon_L(eV^{-1})$	E_{th}(eV)	Avg. Error (%)
	1.6841E+00	1.1203E-01	6.2717E-01	1.3119E-03	3.9437E+00	27.7

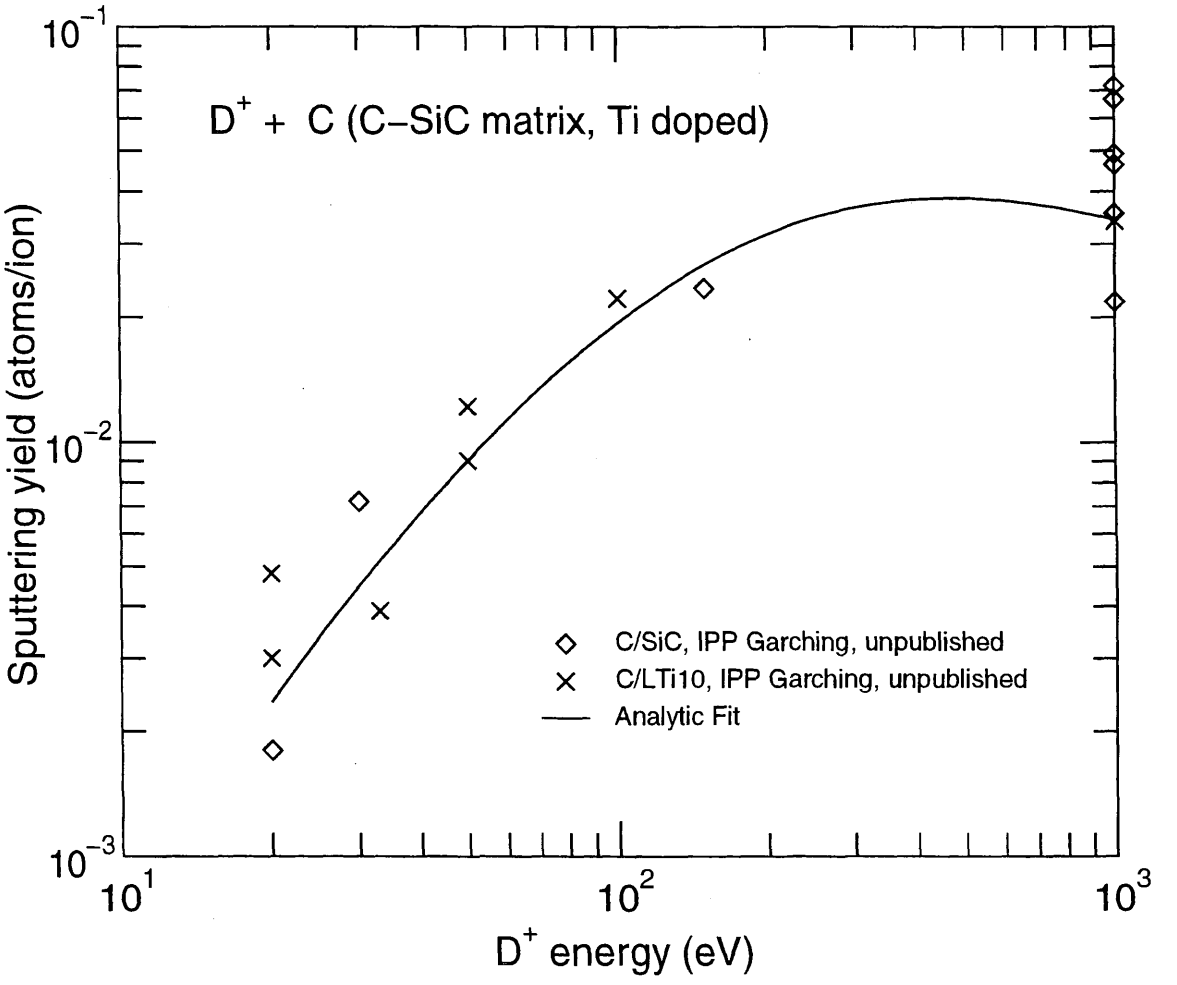

2.1.4.23 D^+ + C (Si doped)

Comments: (1) No fit to the data points because they are dominated by chemical erosion.
(2) The D^+ + C curve for physical sputtering (2.1.2.2) has been included for comparison.

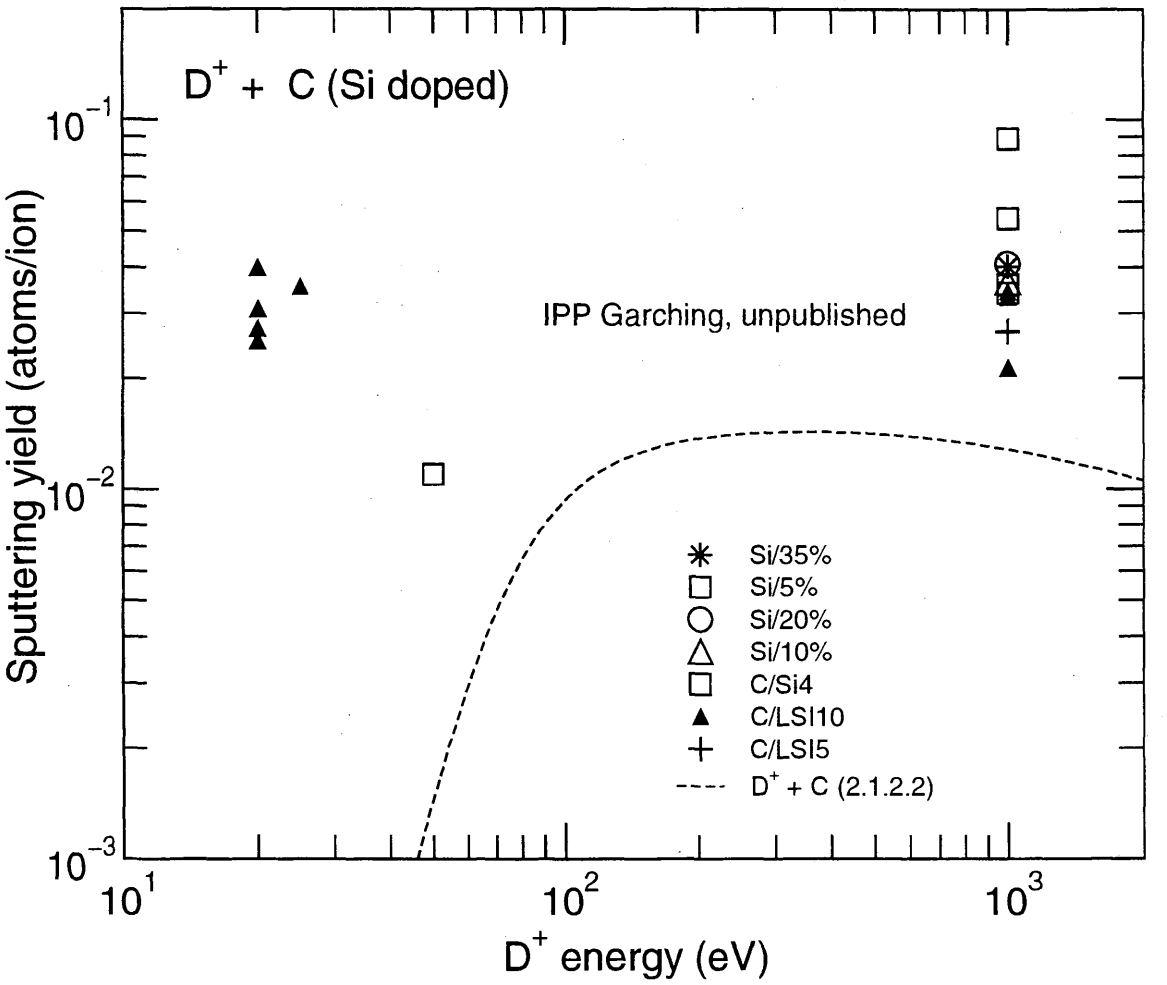

2.1.4.24 D^+ + C (B doped)

Comments: (1) No fit to the data points because they are dominated by chemical erosion.
(2) The D^+ + C curve for physical sputtering (2.1.2.2) has been included for comparison.

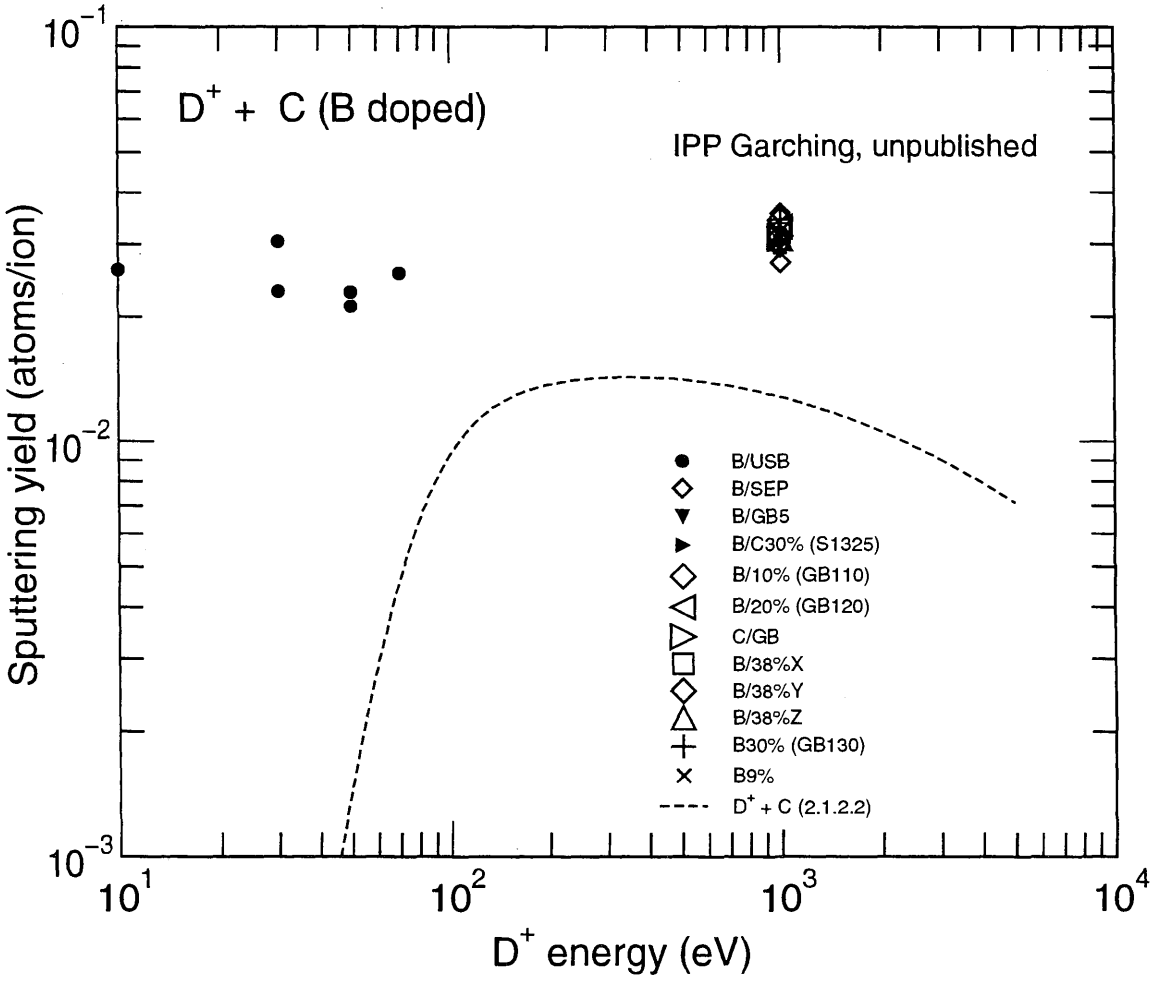

2.1.4.25 D^+ + C (Ti doped)

Comments: (1) No fit to the data points because they are dominated by chemical erosion.
(2) The D^+ + C curve for physical sputtering (2.1.2.2) has been included for comparison.

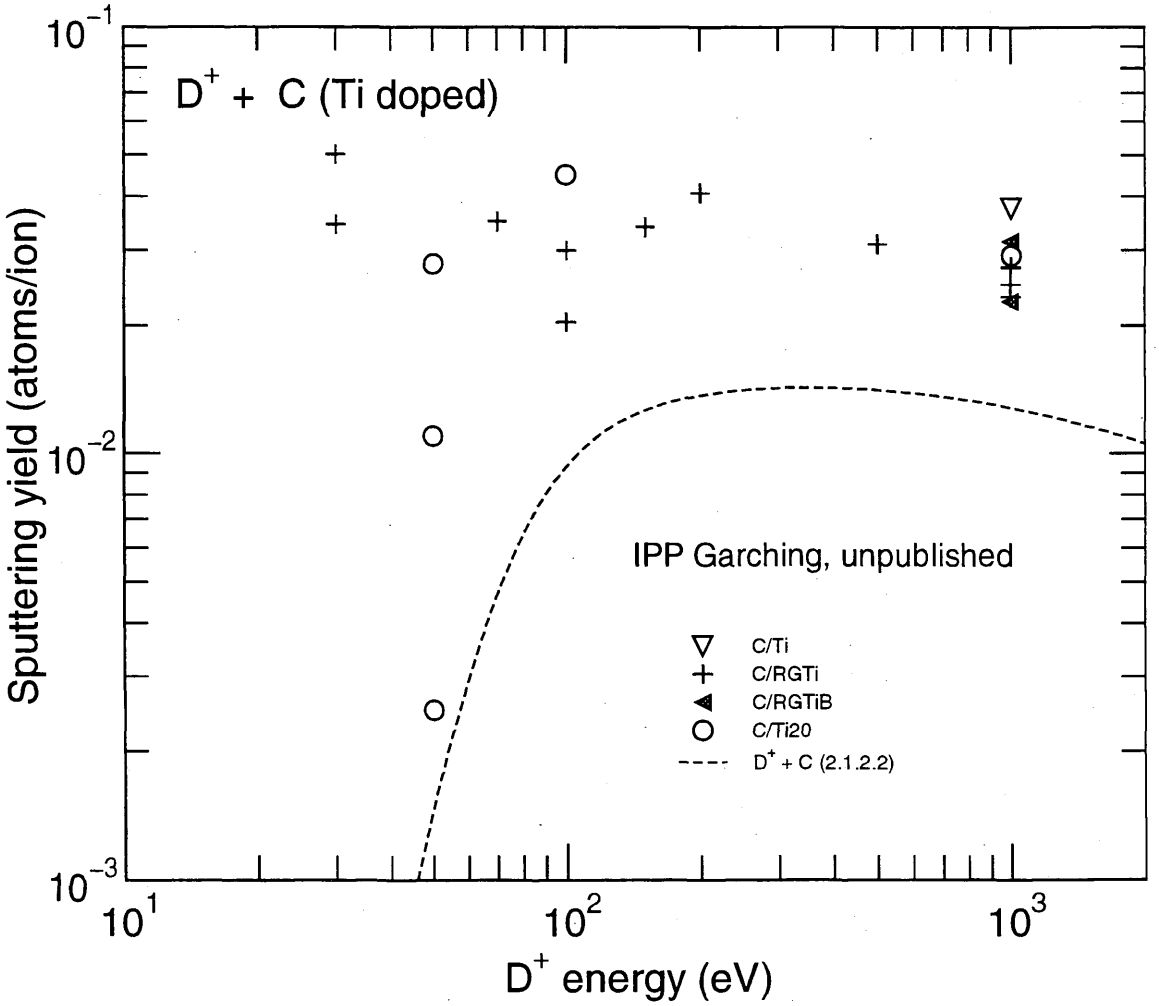

2.1.4.26 D^+ + N112

Comments: (1) Fit valid between E_{min}=E_{th} and E_{max}= 1.0000E+03 eV.
(2) Threshold energies probably too high due to chemical erosion.

Fitting parameters:

Parameter:	λ	q	μ	$\epsilon_L(eV^{-1})$	E_{th}(eV)	Avg. Error (%)
20 C	1.0000E-04	8.3187E-02	1.0000E-04	1.2128E-03	4.9750E+01	10.8
530 C	4.8975E-02	4.2769E-01	1.2207E-01	2.2406E-03	4.9750E+01	4.4

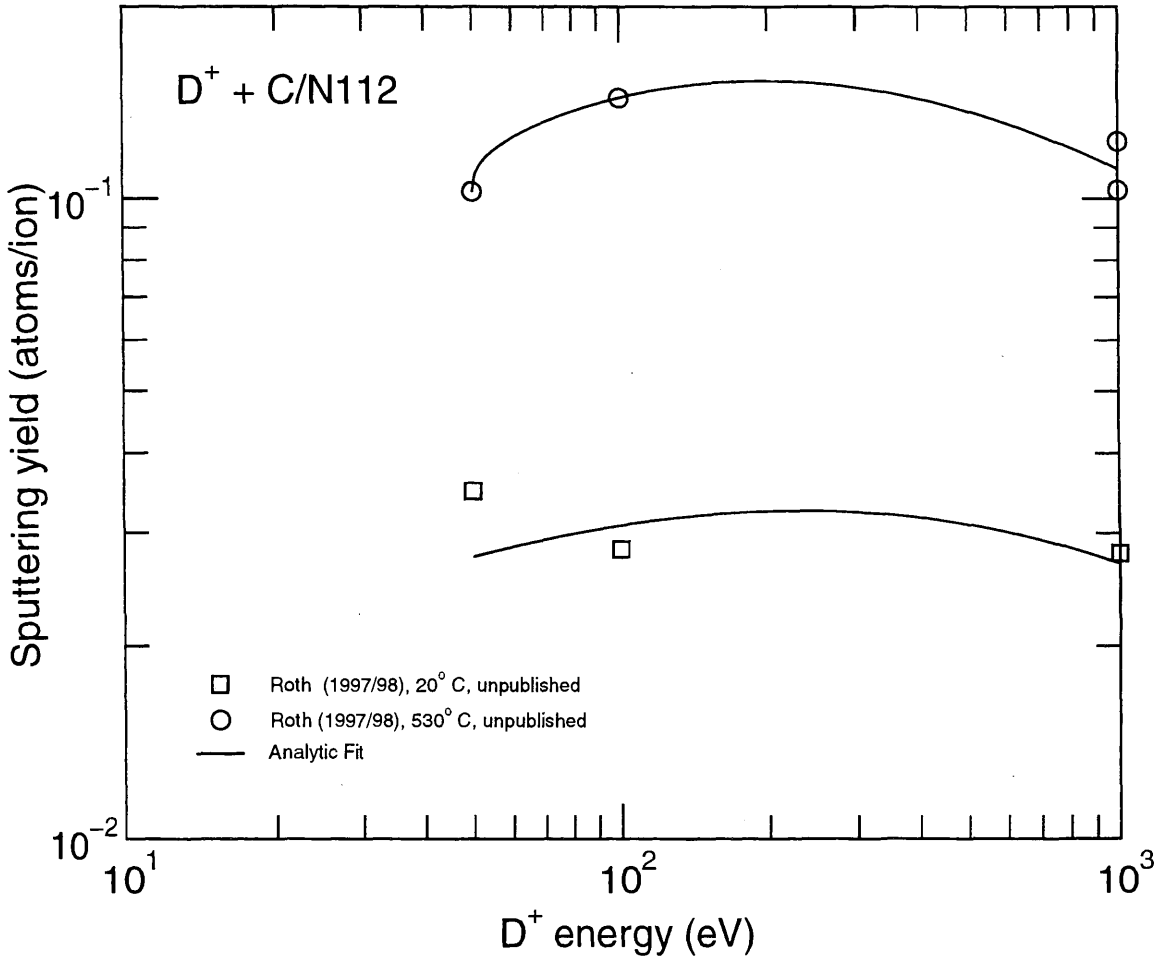

2.2.1.1 D^+ + Be

Comments: (1) Be (20°) is probably BeO, and the oxide layer is 15$\AA$ thick.
(2) Be (650°) is probably Be layers on BeO.

Fitting parameters:

Parameter:	f	b	c	Y(E_0,0)	α_0	E_0 (eV)	Avg. Error (%)
calc	4.9595E+00	1.5116E+00	9.9500E-01	3.5609E-02	1.6285E+00	3.00E+02	7.5
exp	1.9070E+00	2.4855E-01	9.2539E-01	1.7849E-02	1.5891E+00	3.00E+03	18.1
calc	3.0357E+00	4.1951E-01	9.4887E-01	1.3326E-02	1.5891E+00	3.00E+03	6.8

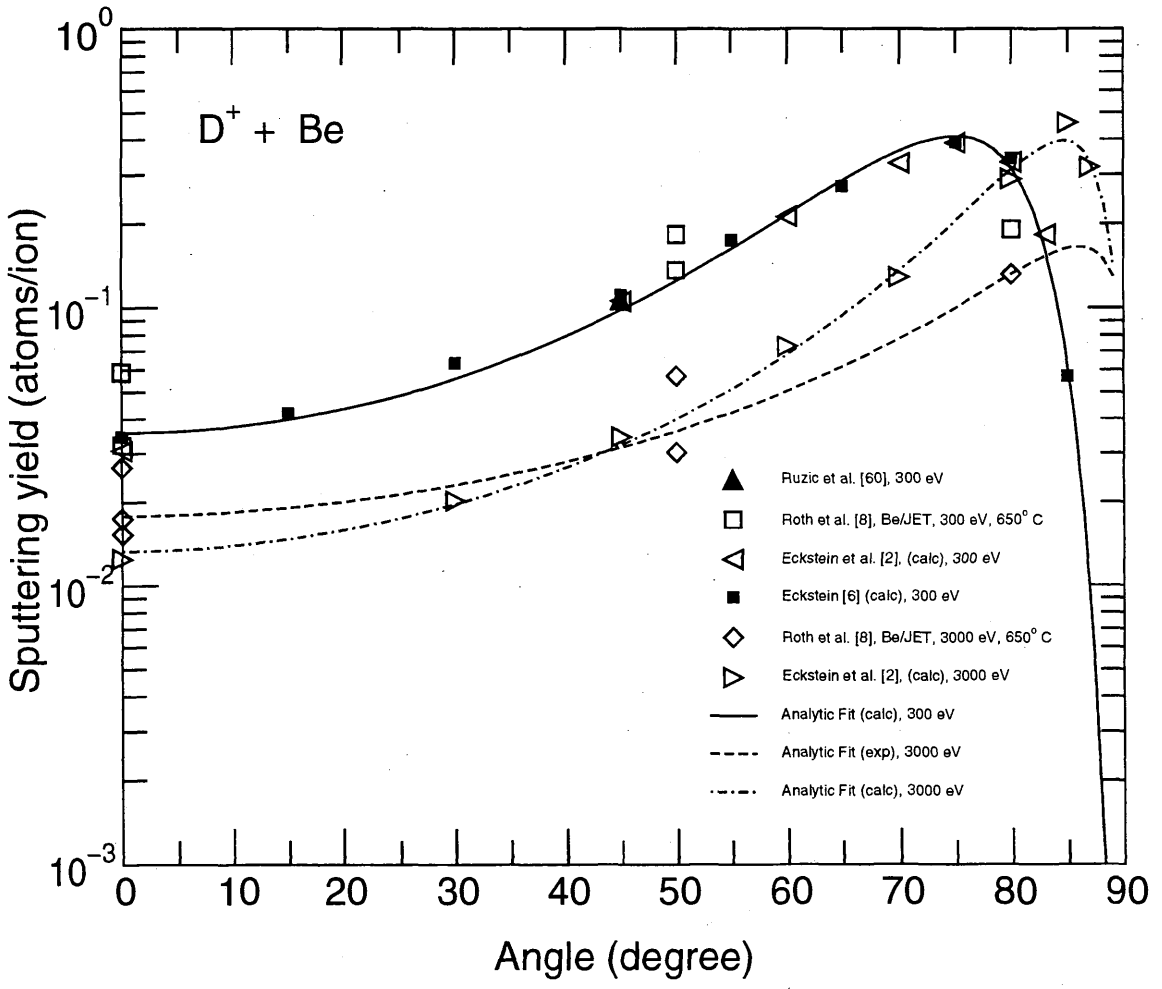

2.2.1.2 T^+ + Be

Comments: (1) Only calculated values.

Fitting parameters:

Parameter:	f	b	c	$Y(E_0,0)$	α_0	E_0 (eV)	Avg. Error (%)
	1.2452E+01	7.1330E+00	7.2087E-01	3.4374E-03	1.7908E+00	2.00E+01	7.6
	1.2081E+01	6.6200E+00	7.7877E-01	1.0263E-02	1.7514E+00	3.00E+01	6.8
	1.0978E+01	5.5587E+00	8.4341E-01	2.0885E-02	1.7113E+00	5.00E+01	3.7
	8.5922E+00	3.7407E+00	9.2231E-01	3.4401E-02	1.6705E+00	1.00E+02	3.6
	6.3797E+00	2.2856E+00	9.7030E-01	4.2873E-02	1.6414E+00	2.00E+02	6.4
	4.8164E+00	1.3482E+00	9.5686E-01	4.2091E-02	1.6155E+00	5.00E+02	7.0
	4.1554E+00	9.8292E-01	8.9781E-01	3.5386E-02	1.6024E+00	1.00E+03	4.1

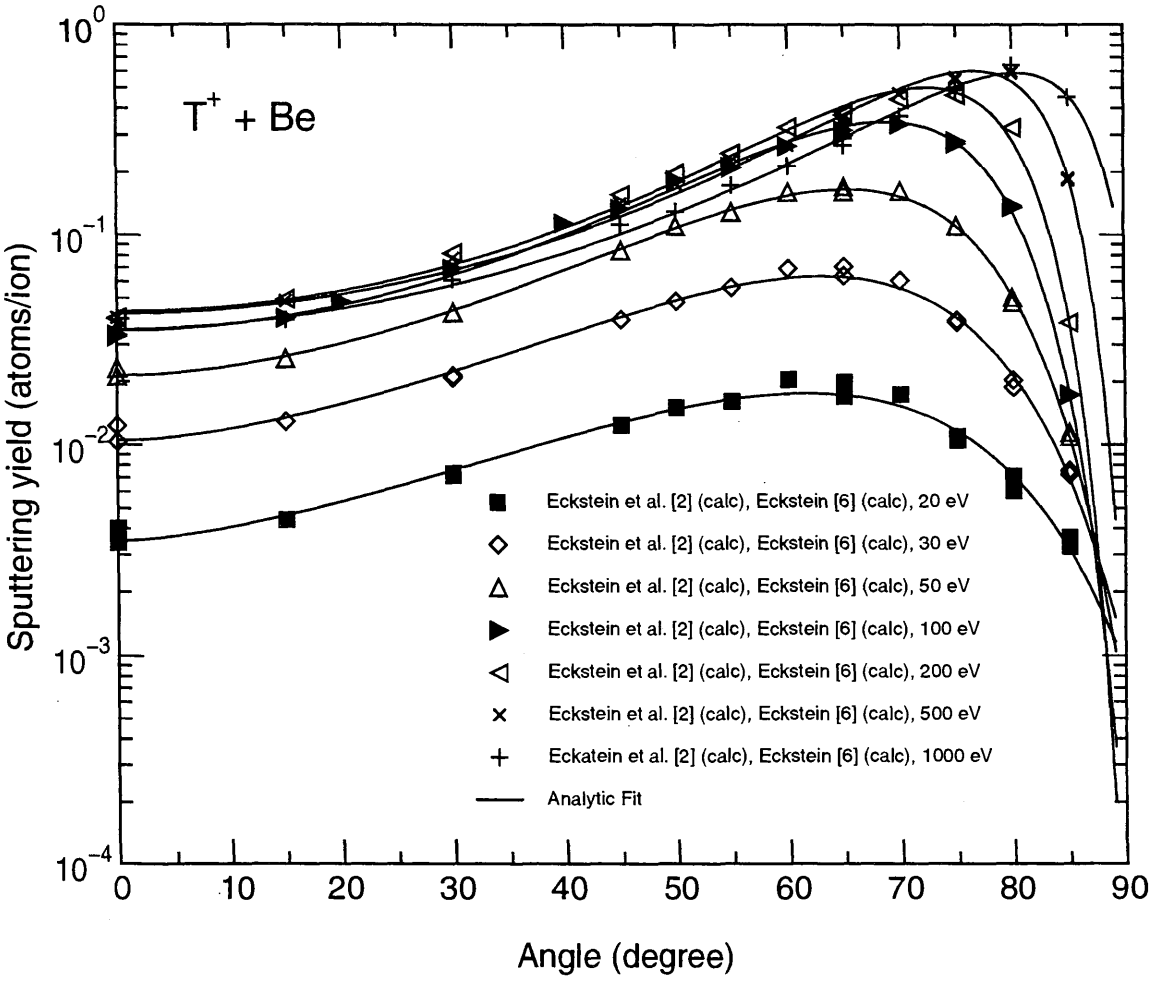

2.2.1.3 He^+ + Be

Comments: (1) Be (20°) is probably BeO, and the oxide layer is 15$\AA$ thick.
(2) Be (650°) is probably Be layers on BeO.

Fitting parameters:

Parameter:	f	b	c	Y(E_0,0)	α_0	E_0 (eV)	Avg. Error (%)
exp	5.1937E+00	1.9660E+00	6.3364E-01	6.6994E-02	1.5708E+00	3.00E+02	21.7
calc	2.8242E+00	8.0455E-01	7.1305E-01	1.4347E-01	1.5708E+00	3.00E+02	3.2
calc, rough	5.0170E+00	1.6681E+00	9.6797E-01	1.1720E-01	1.5708E+00	3.00E+02	8.2

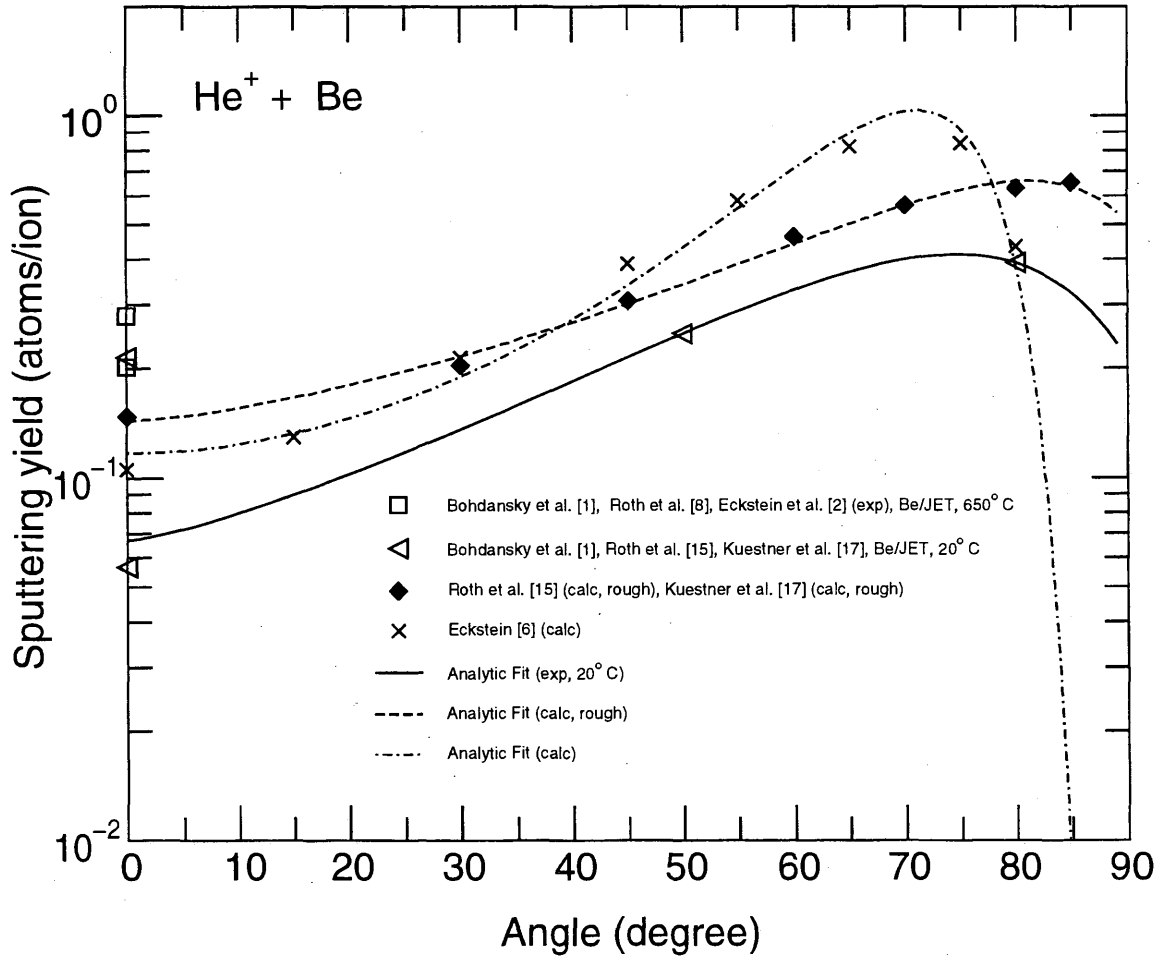

2.2.1.4 He^+ + Be

Comments: (1) Be (20°) is probably BeO, and the oxide layer is 15Å thick.
(2) Be (650°) is probably Be layers on BeO.

Fitting parameters:

Parameter:	f	b	c	Y(E_0,0)	α_0	E_0 (eV)	Avg. Error (%)
exp	2.1005E+00	4.6446E-01	1.0495E+00	1.0500E-01	1.5708E+00	3.00E+03	5.6
calc	2.6592E+00	3.7404E-01	9.9824E-01	7.7403E-02	1.5708E+00	3.00E+03	8.5
calc, rough	2.9898E+00	6.9857E-01	8.1879E-01	8.8449E-02	1.5708E+00	3.00E+03	4.3

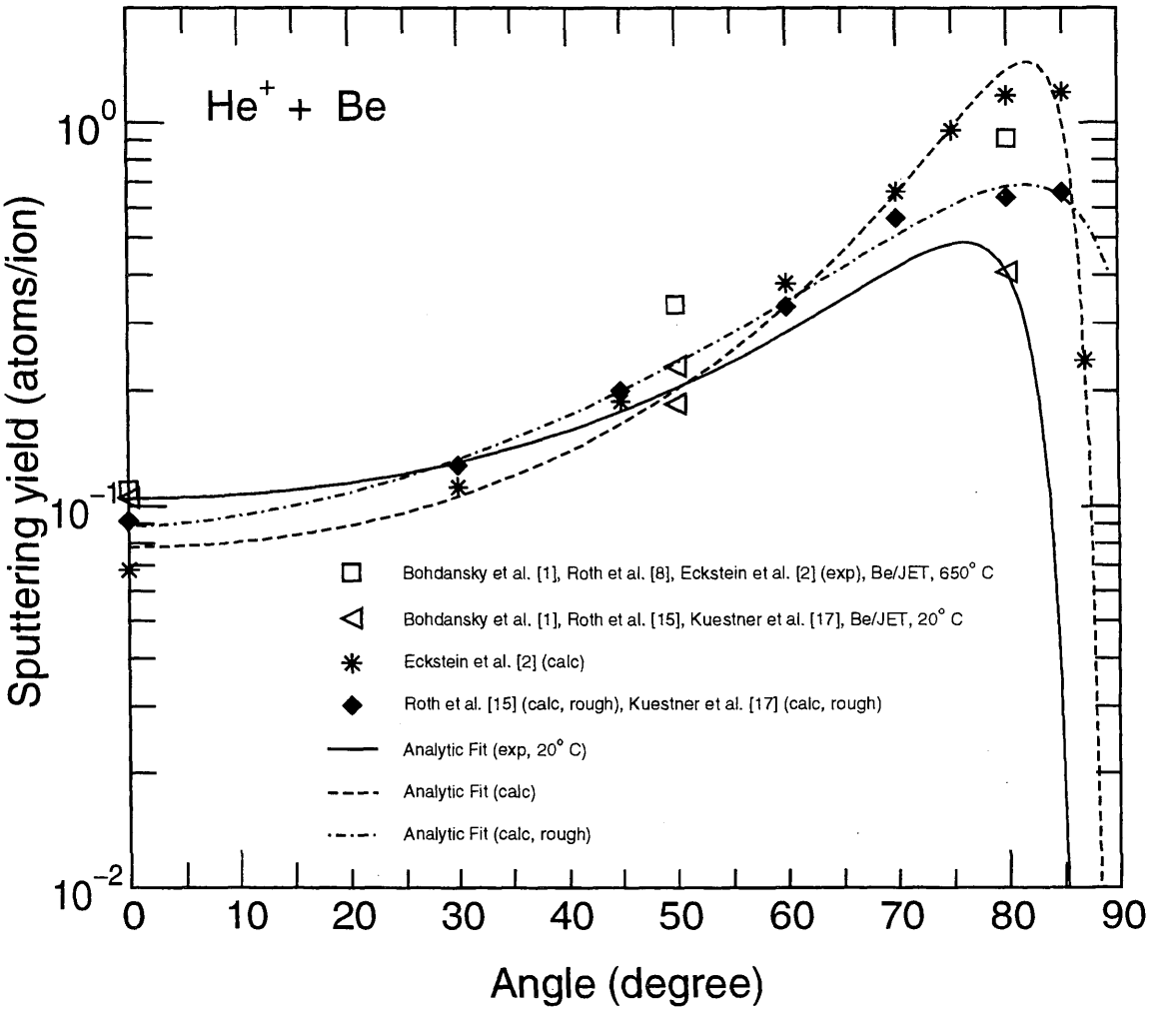

2.2.1.5 $Be^+ + Be$

Comments: (1) None.

Fitting parameters:

Parameter:	f	b	c	Y(E_0,0)	α_0 (rad)	E_0 (eV)	Avg. Error (%)
exp	3.6145E+00	1.2790E+00	8.0975E-01	3.0407E-01	1.6289E+00	1.00E+03	10.9
calc	5.3590E+00	1.8039E+00	9.4602E-01	2.8510E-01	1.6289E+00	1.00E+03	6.7

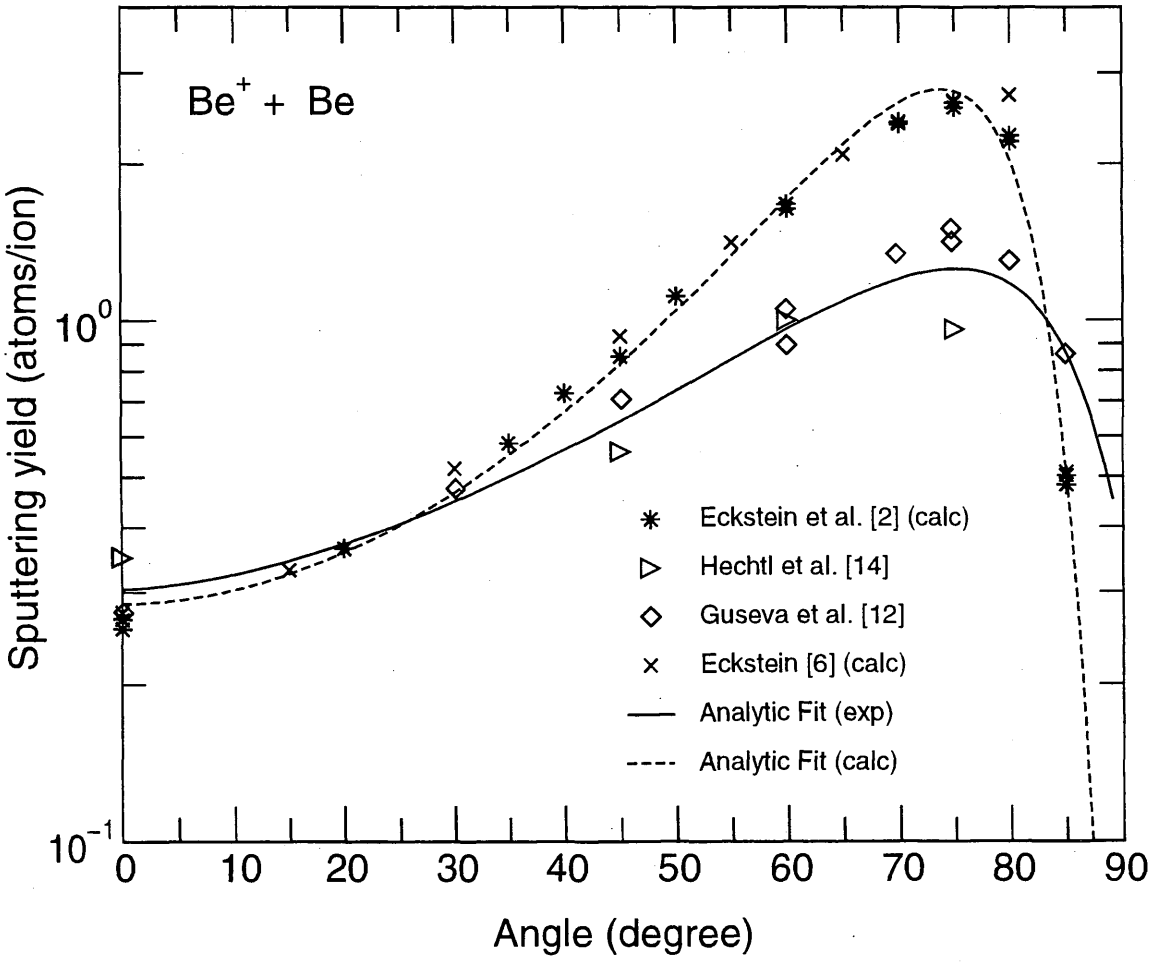

2.2.1.6 Be^+ + Be

Comments: (1) The calculated points of Kuestner et al. [17] are based on the experimentally determined roughness of the target.

Fitting parameters:

Parameter:	f	b	c	Y(E_0,0)	α_0 (rad)	E_0 (eV)	Avg. Error (%)
rough	9.3403E-01	6.7068E-02	7.6656E-01	4.2625E-01	1.6043E+00	3.00E+03	15.9
polished	1.1304E+00	1.9838E-01	6.2699E-01	6.9032E-01	1.6043E+00	3.00E+03	5.6
calc [2]	4.0477E+00	1.0281E+00	9.0356E-01	2.6577E-01	1.6043E+00	3.00E+03	2.5

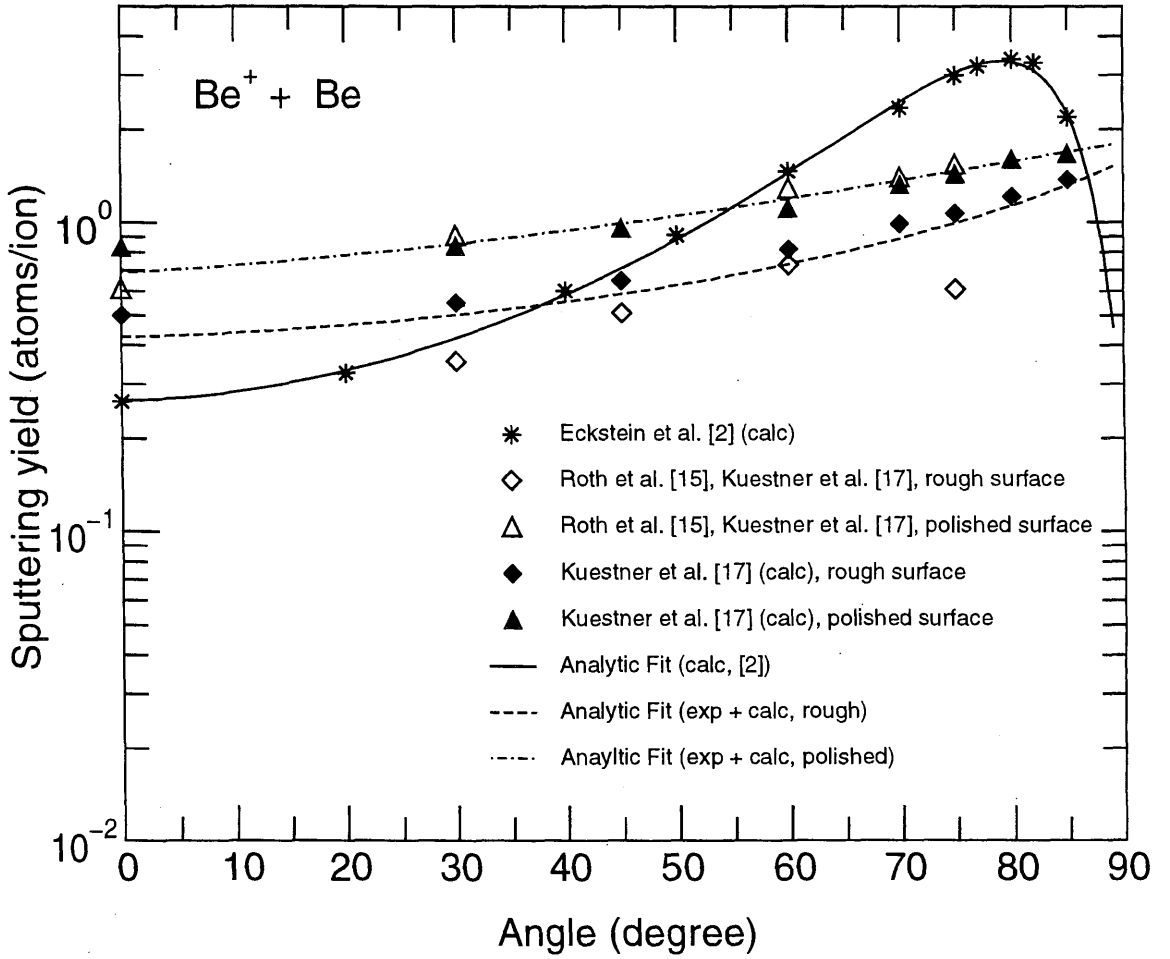

2.2.1.7 Be^+ + Be

Comments: (1) The strong decrease in the single crystal data [61] is not understood.

Fitting parameters:

Parameter:	f	b	c	Y(E_0,0)	α_0 (rad)	E_0 (eV)	Avg. Error (%)
calc	2.2783E+01	1.3082E+01	5.3852E-01	1.6284E-02	1.8252E+00	5.00E+01	8.0
Ueda 001/010	6.1212E+01	4.7345E+01	6.9029E-01	1.7592E-02	1.8252E+00	5.00E+01	43.3
calc	1.6911E+01	9.5574E+00	6.3938E-01	7.0379E-02	1.7526E+00	1.00E+02	3.9
calc	1.1845E+01	6.0865E+00	7.7693E-01	1.5101E-01	1.7001E+00	2.00E+02	3.2
calc	3.7404E+00	8.4387E-01	8.6605E-01	2.2814E-01	1.5968E+00	5.00E+03	1.2

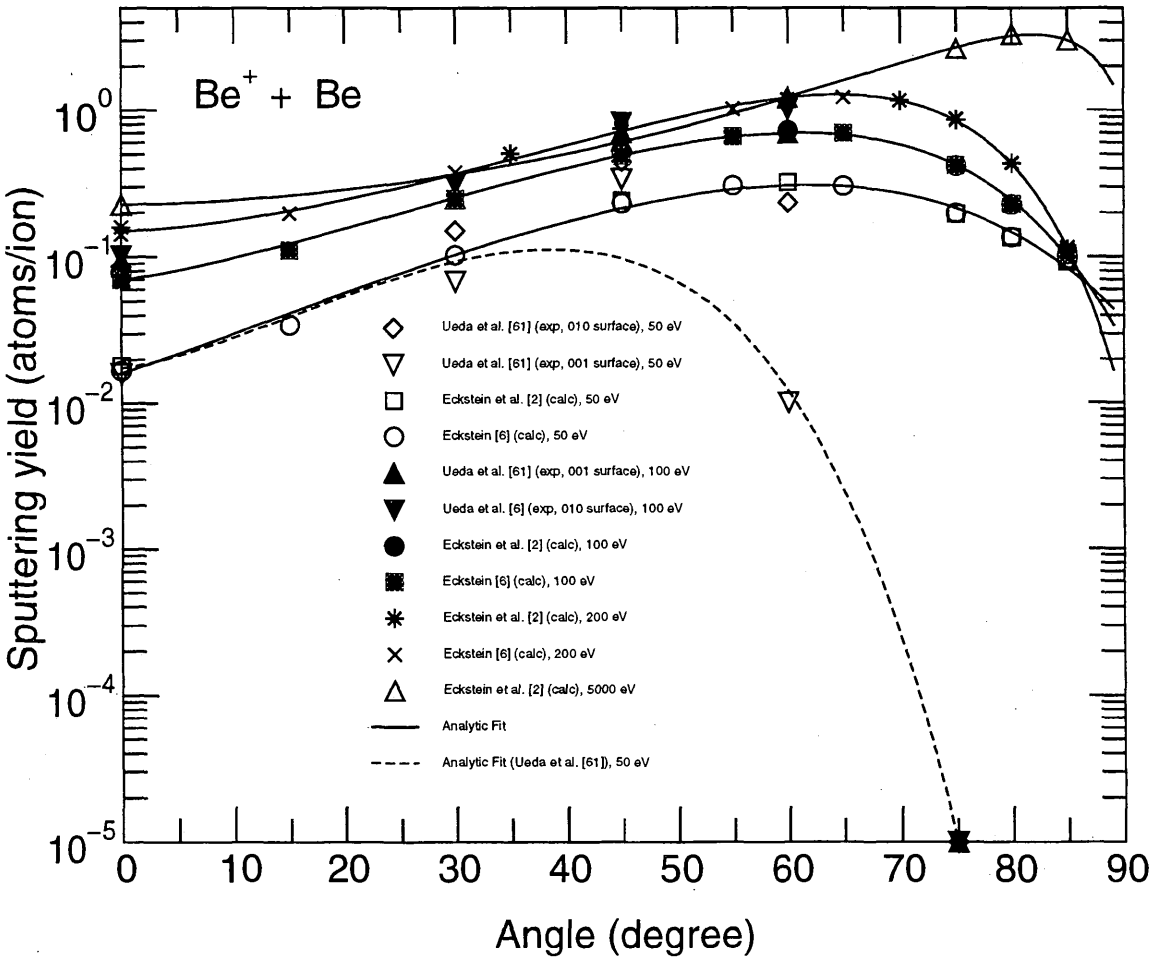

2.2.1.8 C^+ + Be

Comments: (1) Only calculated values.
(2) Calculated points are only valid at low fluence due to composition changes by C implantation.

Fitting parameters:

Parameter:	f	b	c	$Y(E_0,0)$	α_0 (rad)	E_0 (eV)	Avg. Error (%)
	9.7662E+00	4.7360E+00	7.6017E-01	2.3194E-01	1.6285E+00	3.00E+02	3.1
	6.1673E+00	2.3670E+00	7.8800E-01	3.8103E-01	1.6024E+00	1.00E+03	1.6

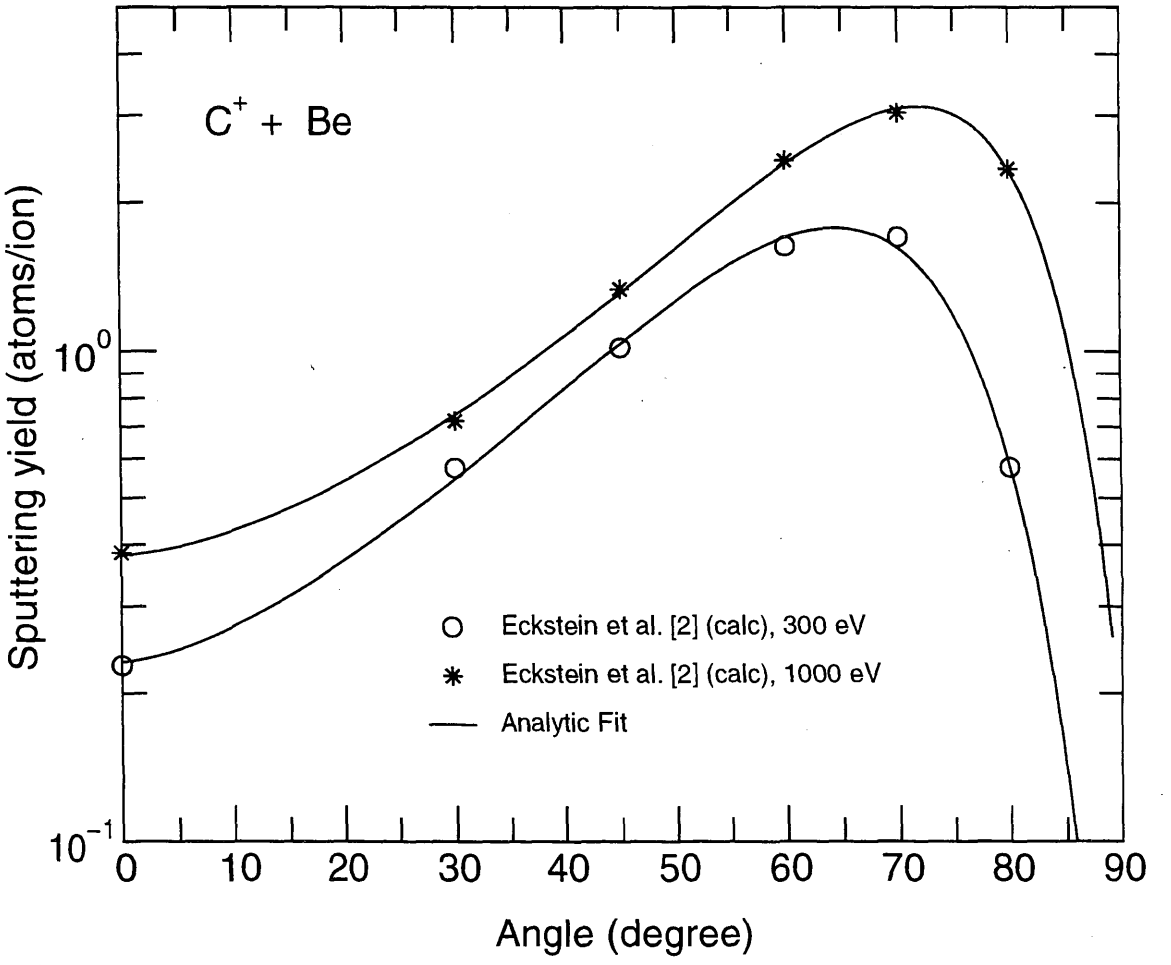

2.2.2.1 $H^+ + C$

Comments: (1) None.

Fitting parameters:

Parameter:	f	b	c	Y(E_0,0)	α_0 (rad)	E_0 (eV)	Avg. Error (%)
calc	4.1978E+00	1.7265E+00	1.0405E+00	2.9675E-03	1.6705E+00	1.00E+02	6.4
exp	4.9187E+00	1.6403E+00	5.6024E-01	7.1371E-03	1.6024E+00	1.00E+03	1.7
calc	4.6671E+00	1.1533E+00	8.4728E-01	5.2988E-03	1.6024E+00	1.00E+03	5.8
exp	3.6906E+00	9.5906E-01	8.7602E-01	5.6222E-03	1.5932E+00	2.00E+03	13.3

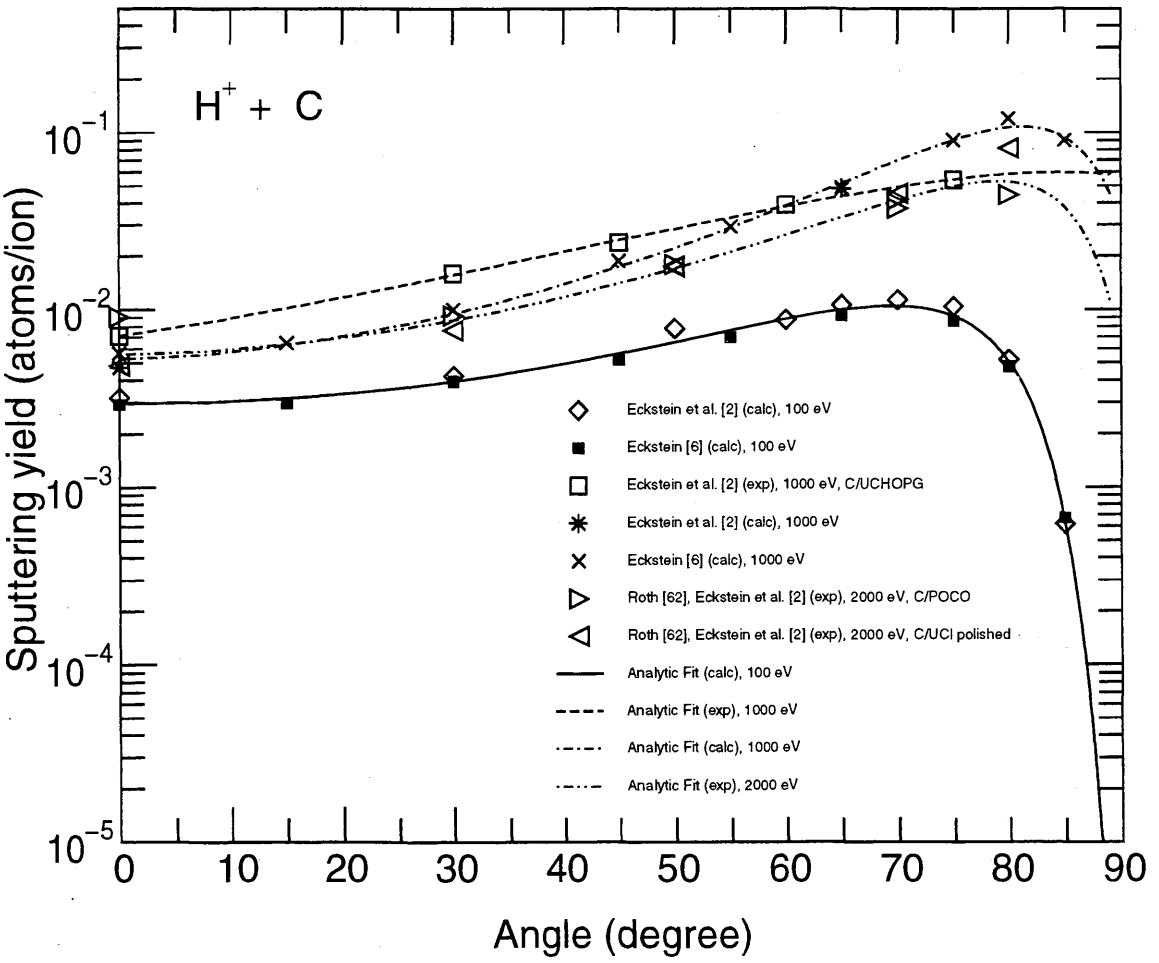

2.2.2.2 H^+ + C(HOPG)

Comments: (1) Experimental data by Haasz et al. [19] may be dominated by chemical erosion.

Fitting parameters:

Parameter:	f	b	c	$Y(E_0,0)$	α_0 (rad)	E_0 (eV)	Avg. Error (%)
	2.5008E+00	6.6075E-01	8.3530E-01	1.5123E-02	1.6414E+00	2.00E+02	3.3
	3.7154E+00	1.0400E+00	1.0698E+00	5.9770E-03	1.6414E+00	2.00E+02	1.6
	3.4850E+00	8.5179E-01	8.7310E-01	3.7628E-03	1.5891E+00	3.00E+03	1.8
	2.3129E+00	5.4550E-01	9.0198E-01	1.1181E-02	1.6285E+00	3.00E+02	1.2
	2.8123E+00	1.0801E+00	5.4571E-01	1.0995E-02	1.6285E+00	3.00E+02	.9

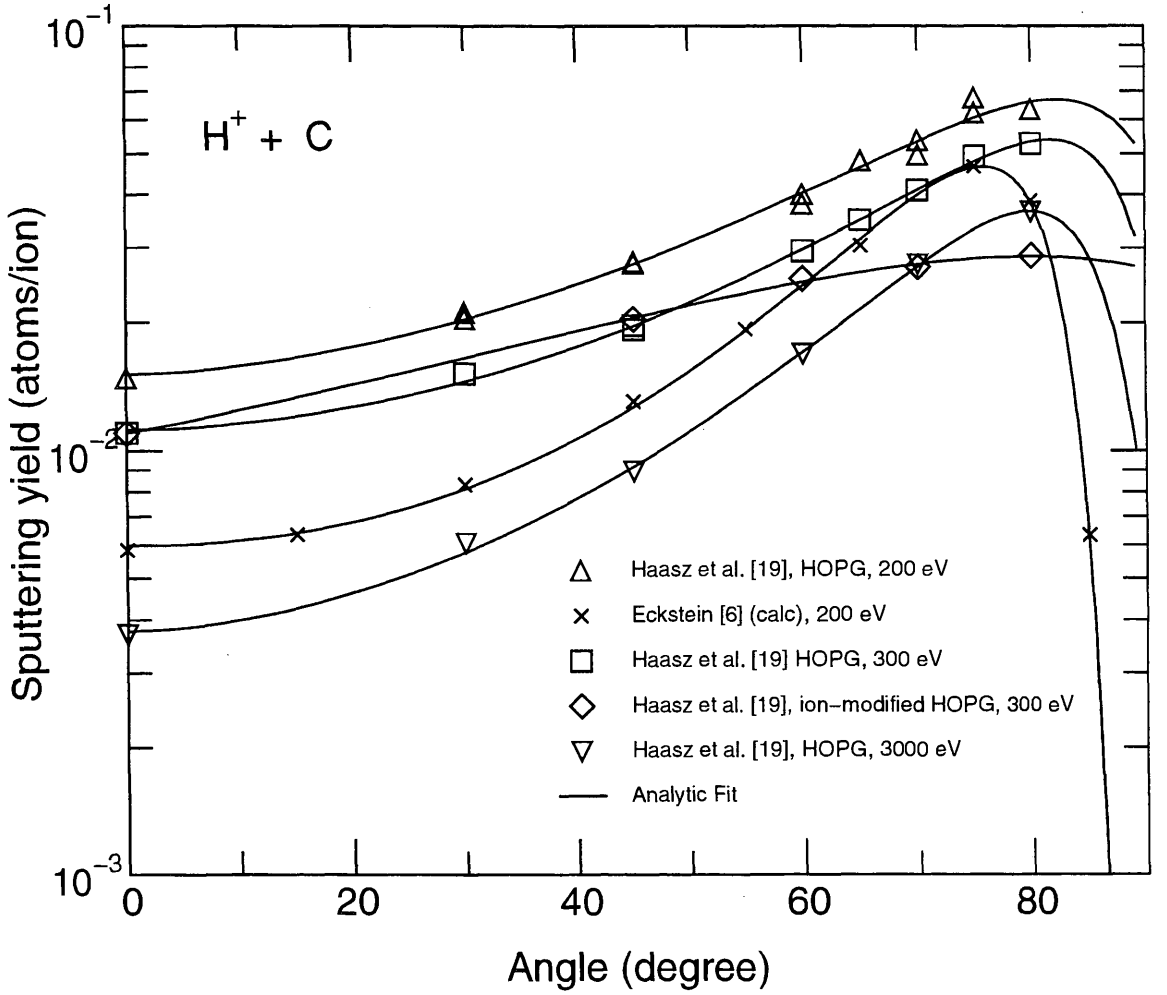

2.2.2.3 $D^+ + C$

Comments: (1) None.

Fitting parameters:

Parameter:	f	b	c	Y(E_0,0)	α_0 (rad)	E_0 (eV)	Avg. Error (%)
	8.1753E+00	4.4733E+00	8.5569E-01	1.9959E-03	1.7113E+00	5.00E+01	6.7
	5.2975E+00	2.0315E+00	1.0316E+00	8.7926E-03	1.6705E+00	1.00E+02	6.1
	4.7402E+00	1.4023E+00	1.0004E+00	1.5178E-02	1.6285E+00	3.00E+02	3.8
	4.2714E+00	1.0295E+00	9.0505E-01	1.3272E-02	1.6024E+00	1.00E+03	5.2

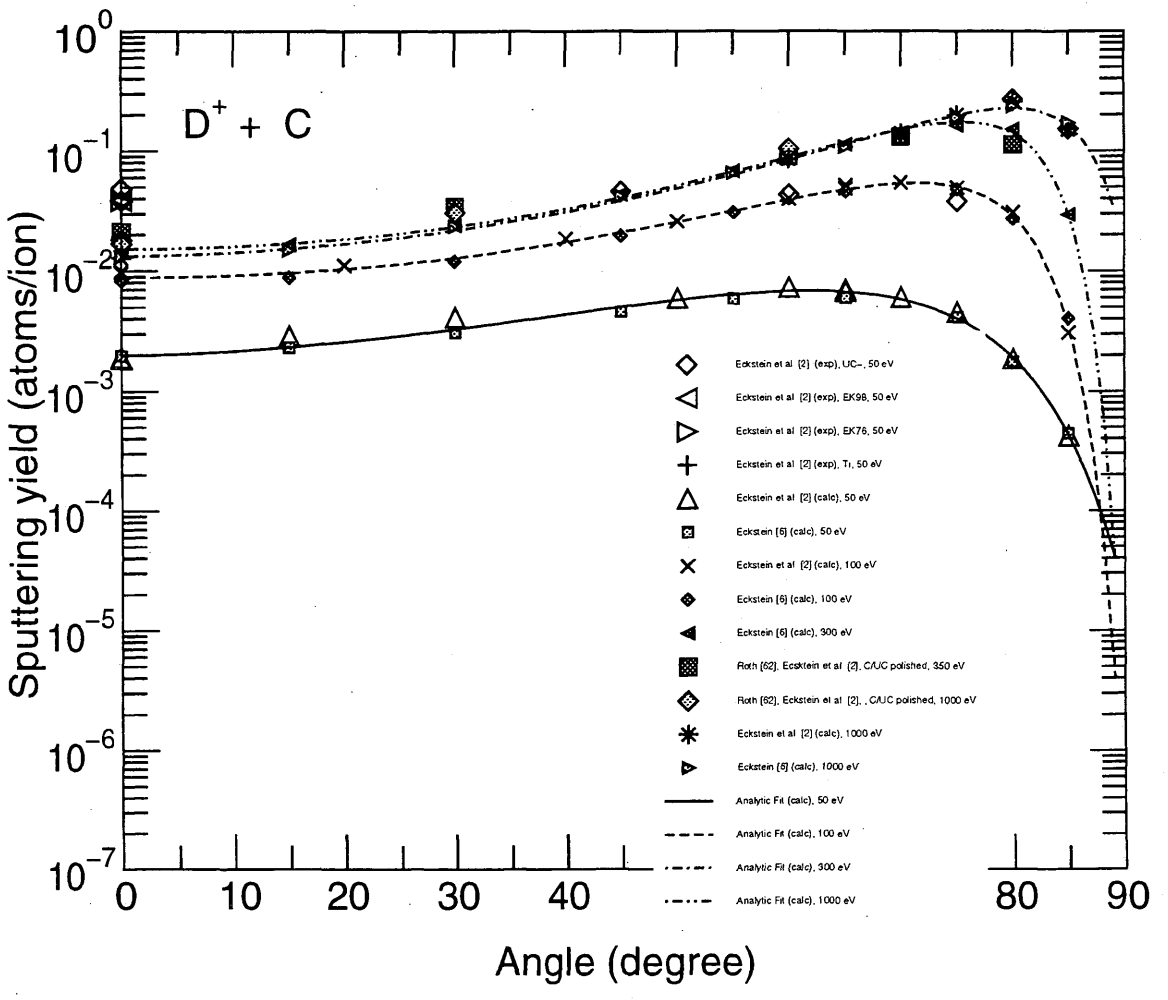

2.2.2.4 $D^+ + C$

Comments: (1) None.

Fitting parameters:

Parameter:	f	b	c	$Y(E_0,0)$	α_0 (rad)	E_0 (eV)	Avg. Error (%)
calc	4.0296E+00	8.2449E-01	8.9377E-01	1.0228E-02	1.5932E+00	2.00E+03	5.6
exp+calc, UCI	3.0166E+00	3.9687E-01	7.0437E-01	1.1839E-02	1.5932E+00	2.00E+03	14.6
exp+calc, EK98	1.2681E+00	3.5658E-02	2.8526E-01	2.2895E-02	1.5932E+00	2.00E+03	5.2

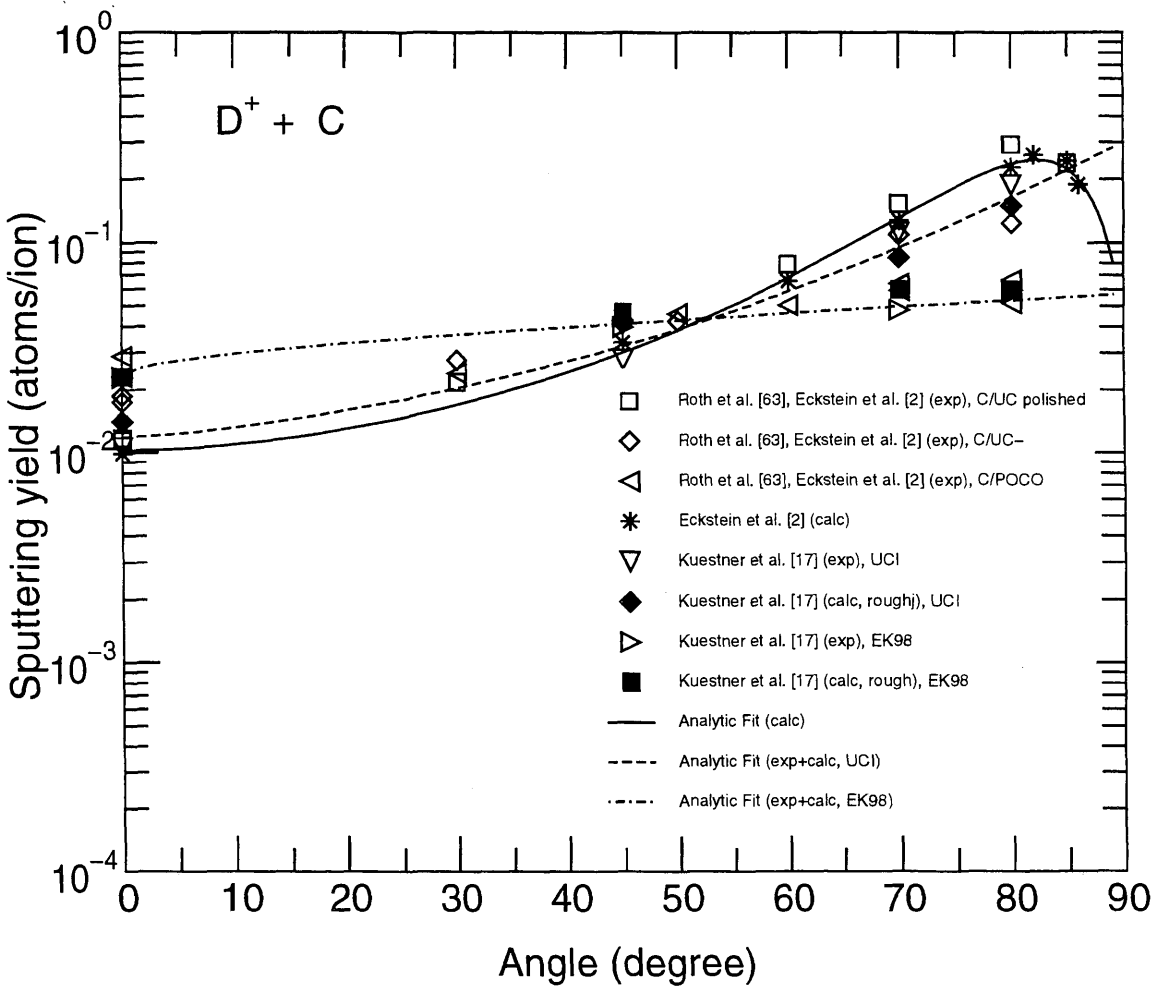

2.2.2.5 $T^+ + C$

Comments: (1) Only calculated values.

Fitting parameters:

Parameter:	f	b	c	Y(E_0,0)	α_0 (rad)	E_0 (eV)	Avg. Error (%)
	1.2880E+01	7.3765E+00	7.2693E-01	6.8951E-04	1.7382E+00	3.50E+01	2.8
	7.0779E+00	2.8300E+00	9.7374E-01	1.0202E-02	1.6705E+00	1.00E+02	3.2
	5.4157E+00	1.6858E+00	9.7219E-01	1.8346E-02	1.6285E+00	3.00E+02	5.7

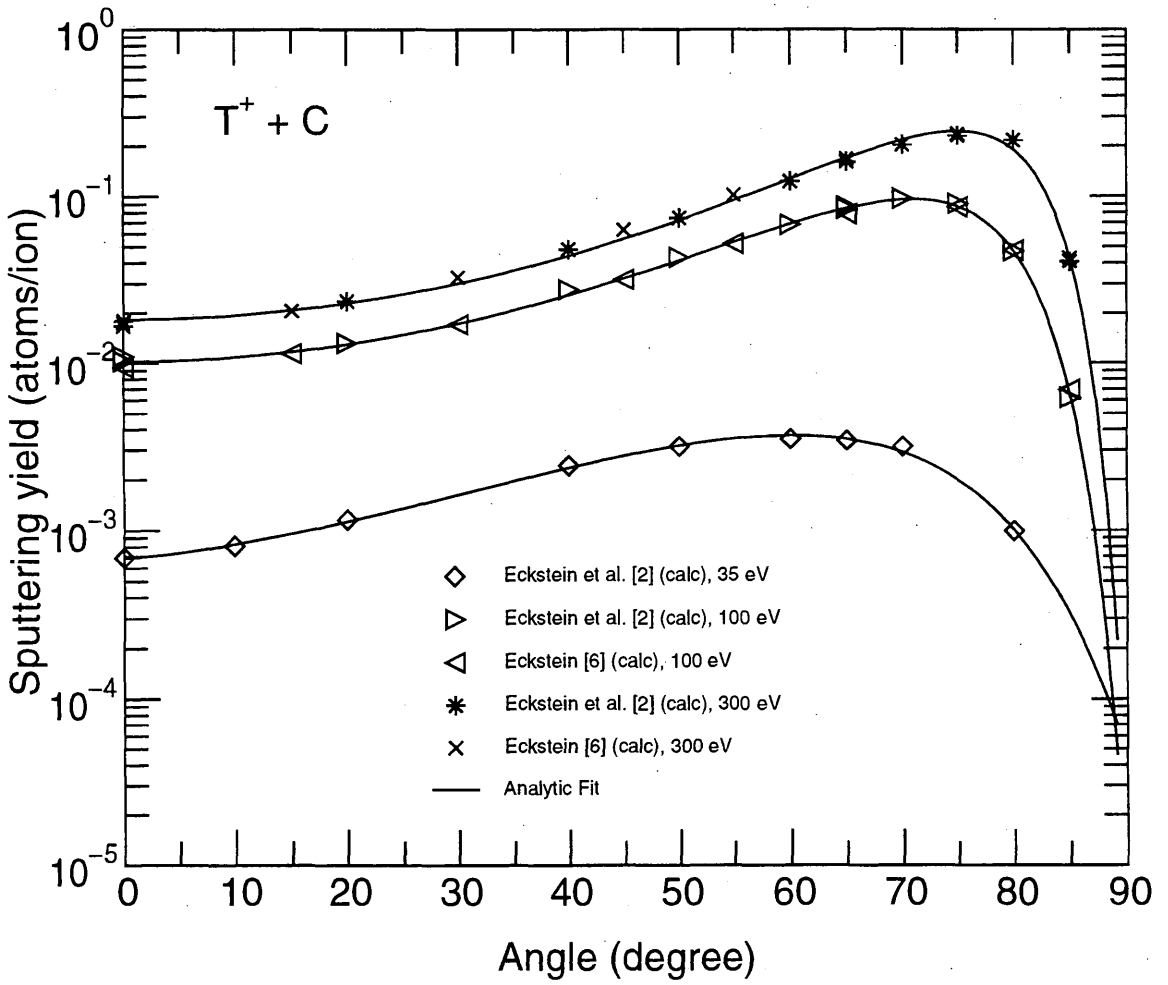

2.2.2.6 $He^+ + C$

Comments: (1) Experimental data for 100 eV are probably affected by chemical erosion or calibration.

Fitting parameters:

Parameter:	f	b	c	$Y(E_0,0)$	α_0 (rad)	E_0 (eV)	Avg. Error (%)
exp	9.5368E-01	2.6235E-10	4.6760E-01	8.3077E-02	1.5708E+00	1.00E+02	4.6
calc	6.7703E+00	2.7530E+00	9.3811E-01	1.9379E-02	1.5708E+00	1.00E+02	5.6
exp	3.7923E+00	1.1947E+00	5.9152E-01	4.6593E-02	1.5708E+00	1.00E+03	8.8
calc	4.6057E+00	1.3002E+00	9.0702E-01	5.5397E-02	1.5708E+00	1.00E+03	6.7

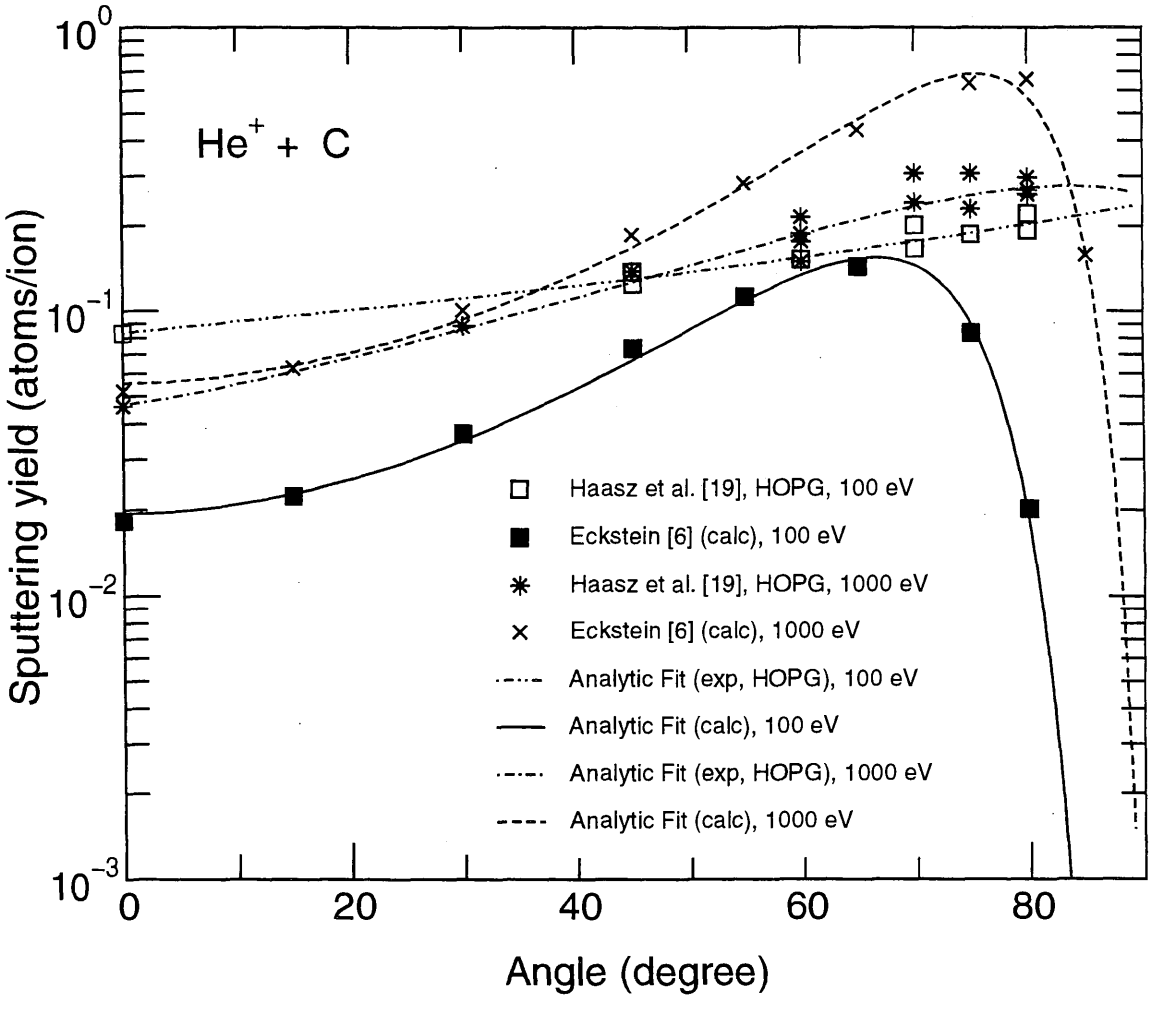

2.2.2.7 $He^+ + C$

Comments: (1) None.

Fitting parameters:

Parameter:	f	b	c	$Y(E_0,0)$	α_0 (rad)	E_0 (eV)	Avg. Error (%)
exp	3.2079E+00	1.0447E+00	7.5637E-01	5.6846E-02	1.5708E+00	3.00E+02	2.7
calc	5.1626E+00	1.6893E+00	9.6371E-01	4.7430E-02	1.5708E+00	3.00E+02	7.6
exp	2.9053E+00	6.5033E-01	7.4351E-01	7.7073E-02	1.5708E+00	2.00E+03	22.4
calc	4.3990E+00	1.1368E+00	8.3733E-01	4.8058E-02	1.5708E+00	2.00E+03	3.3

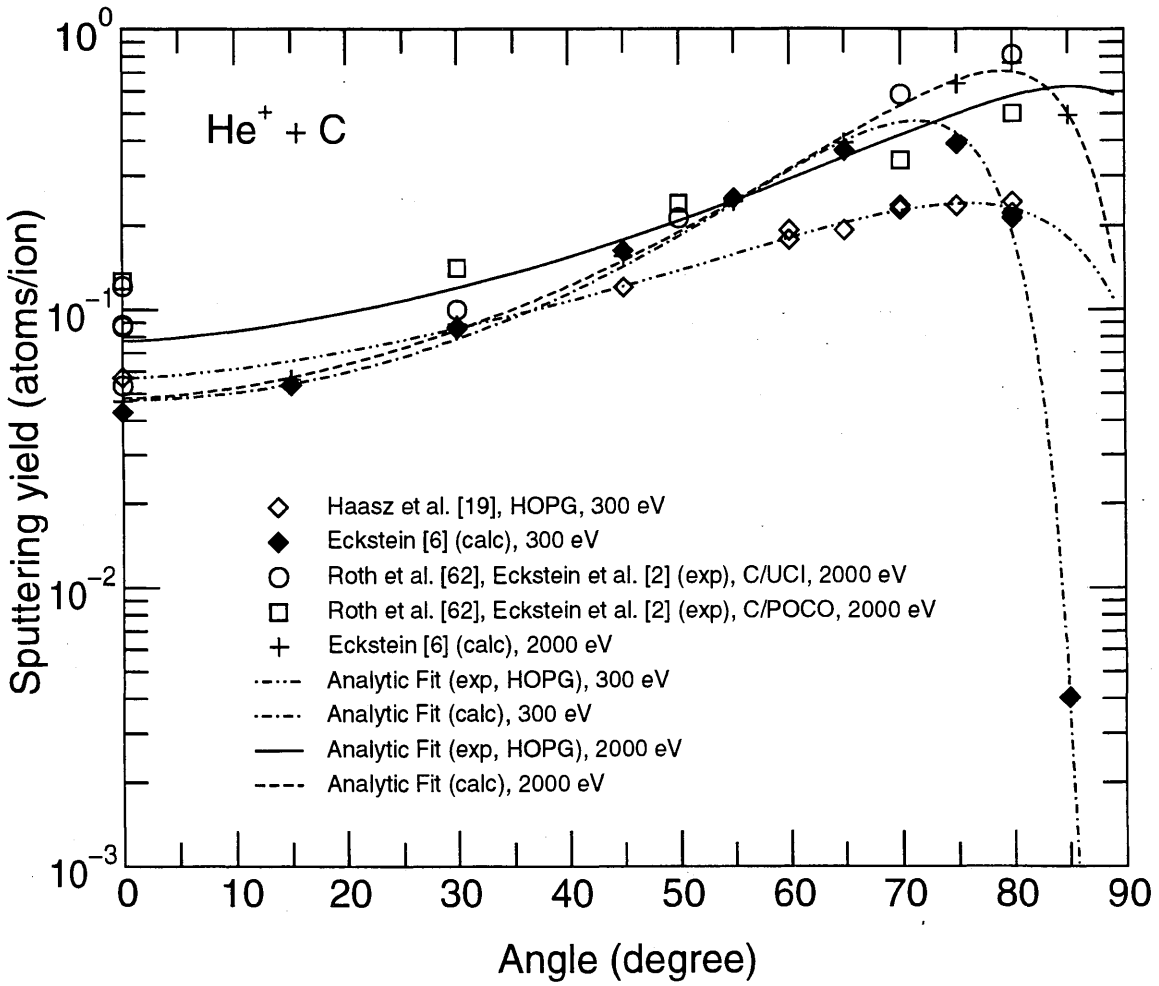

2.2.2.8 $C^+ + C$

Comments: (1) The two calculated data sets at 100 eV are due to different target densities (2.26 g/cm^3 [2] and 1.85 g/cm^3 [6]).

Fitting parameters:

Parameter:	f	b	c	Y(E_0,0)	α_0 (rad)	E_0 (eV)	Avg. Error (%)
calc	2.4975E+01	1.3926E+01	5.3563E-01	8.9983E-03	1.8366E+00	1.00E+02	12.2
calc	1.3228E+01	6.6946E+00	6.8958E-01	7.3702E-02	1.7267E+00	3.00E+02	2.9
exp	2.9598E+00	9.4267E-01	6.7815E-01	3.6893E-01	1.6567E+00	1.00E+03	3.7
calc	6.5477E+00	2.4854E+00	9.4646E-01	2.0964E-01	1.6567E+00	1.00E+03	9.5

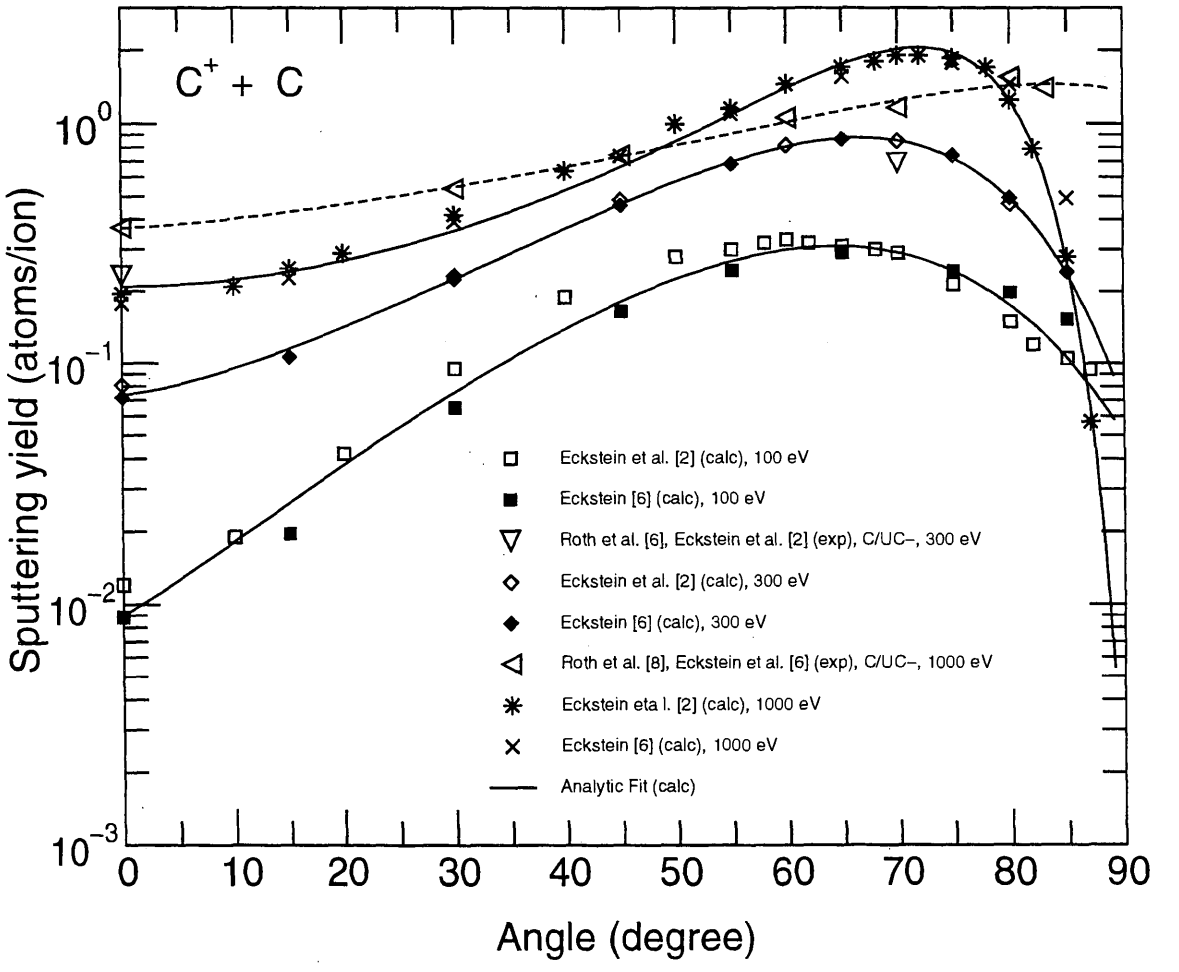

2.2.2.9 $C^+ + C$

Comments: (1) POCO represents a very rough surface.
(2) The region between the two curves is the range of data depending on surface roughness.

Fitting parameters:

Parameter:	f	b	c	$Y(E_0,0)$	α_0 (rad)	E_0 (eV)	Avg. Error (%)
exp	6.0649E+00	3.3386E+00	5.4646E-01	4.4300E-01	1.6205E+00	3.00E+03	0.0
calc	5.0177E+00	1.5887E+00	8.8350E-01	2.6035E-01	1.6205E+00	3.00E+03	4.5

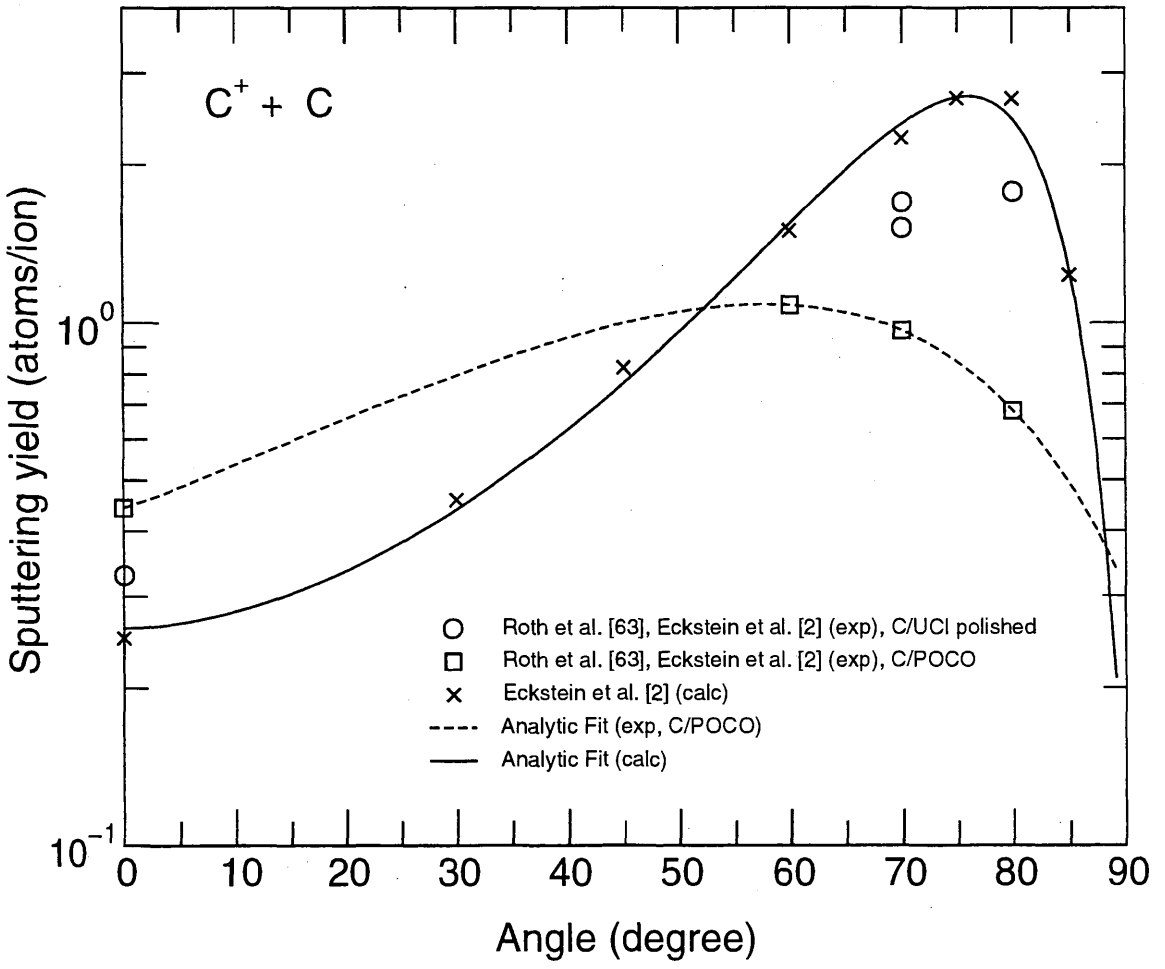

2.2.3.1 $H^+ + W$

Comments: (1) None.

Fitting parameters:

Parameter:	f	b	c	$Y(E_0,0)$	α_0 (rad)	E_0 (eV)	Avg. Error (%)
	1.3323E+00	1.5132E-01	1.0560E+00	2.4010E-03	1.5932E+00	2.00E+03	2.3
	2.9014E+00	4.3111E-01	8.6249E-01	2.0900E-03	1.5866E+00	4.00E+03	0.0

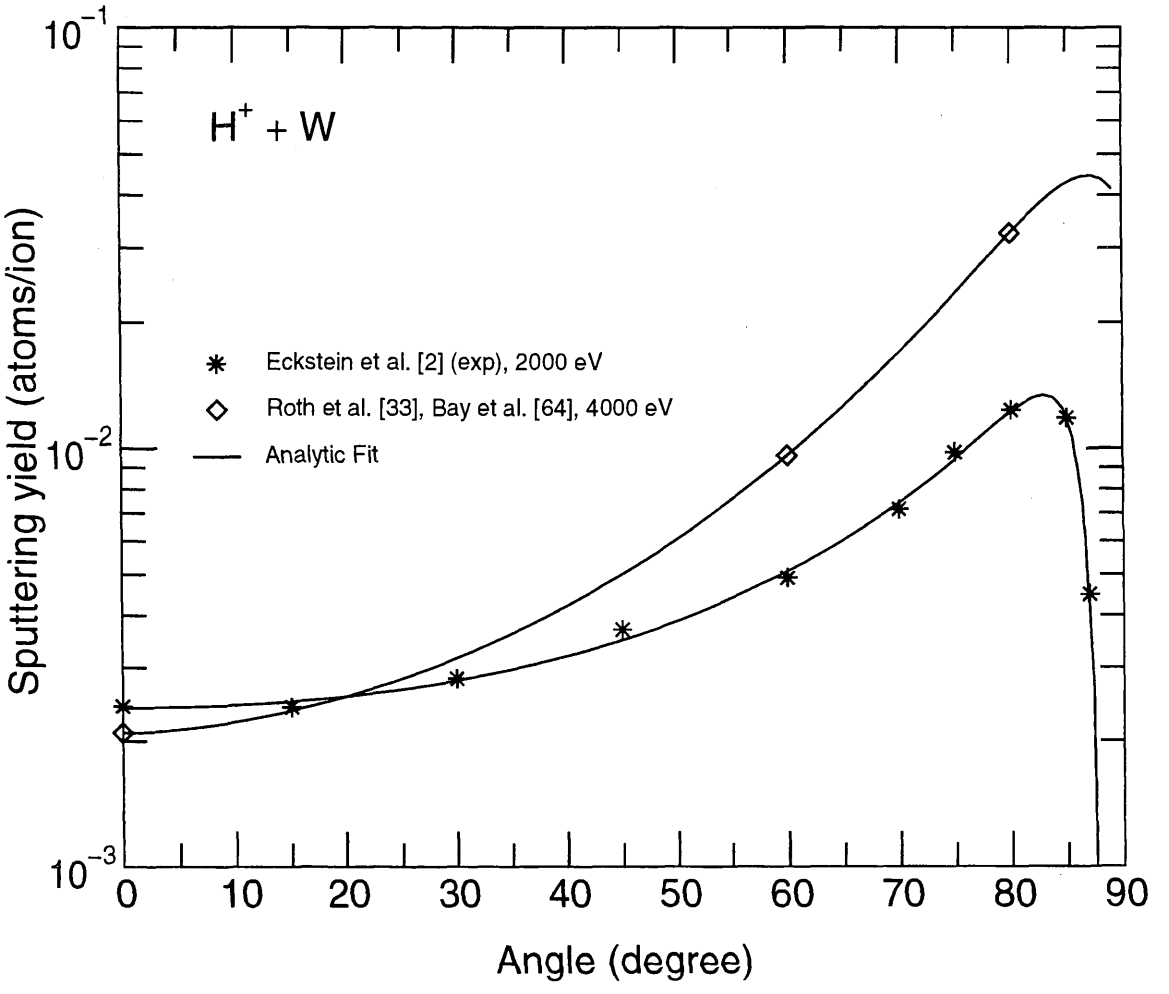

2.2.3.2 OH^+ + W

Comments: (1) This dependence may be affected by chemical effects due to oxide formation.

Fitting parameters:

Parameter:	f	b	c	$Y(E_0,0)$	α_0 (rad)	E_0 (eV)	Avg. Error (%)
	1.9451E+00	6.1980E-01	5.6758E-01	3.7800E-01	1.5837E+00	6.00E+03	0.0

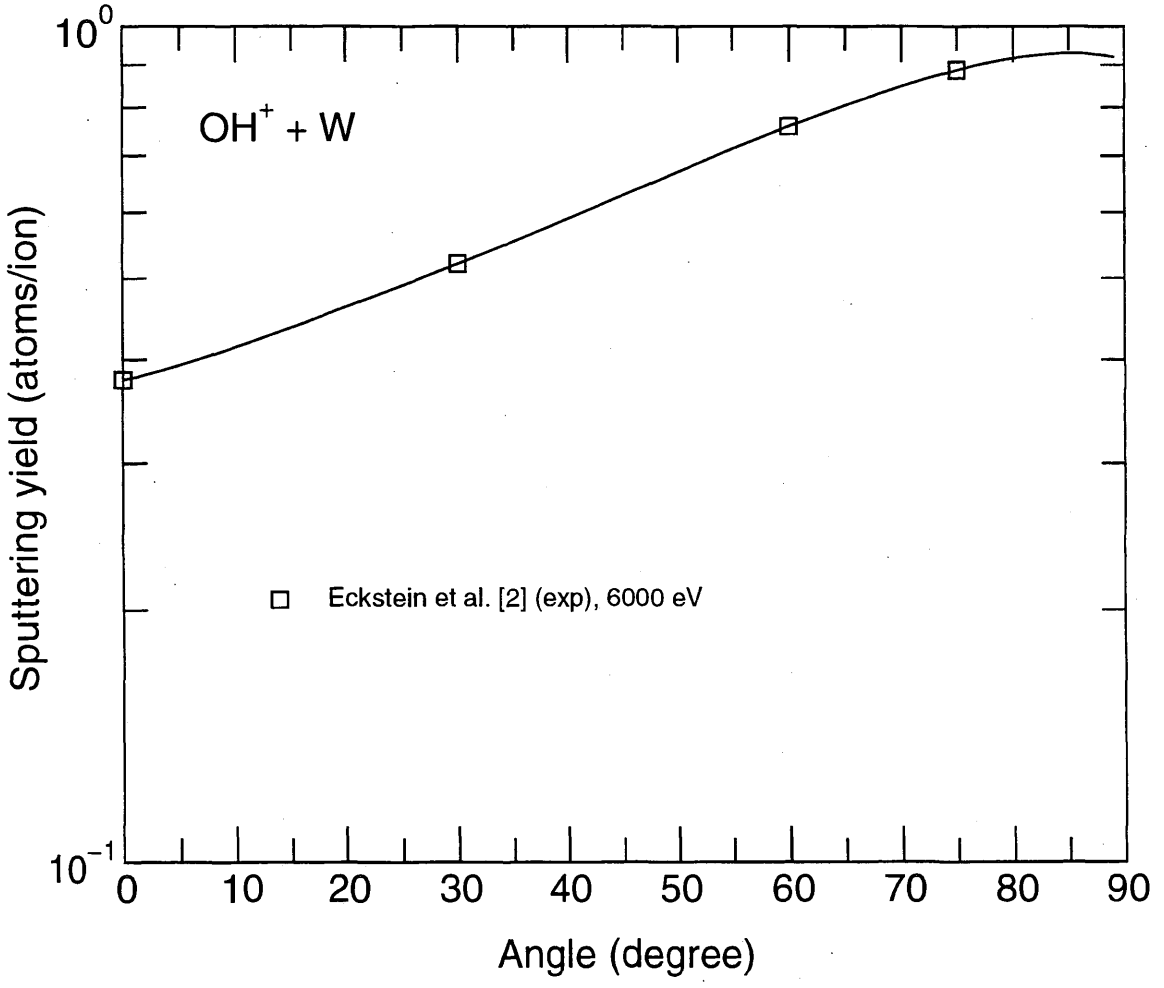

2.2.3.3 $Ar^+ + W$

Comments: (1) Calculated and experimental points fitted together.

Fitting parameters:

Parameter:	f	b	c	$Y(E_0,0)$	α_0 (rad)	E_0 (eV)	Avg. Error (%)
	1.8182E+00	8.6768E-01	9.6698E-01	9.9032E-01	1.5708E+00	1.00E+03	3.9

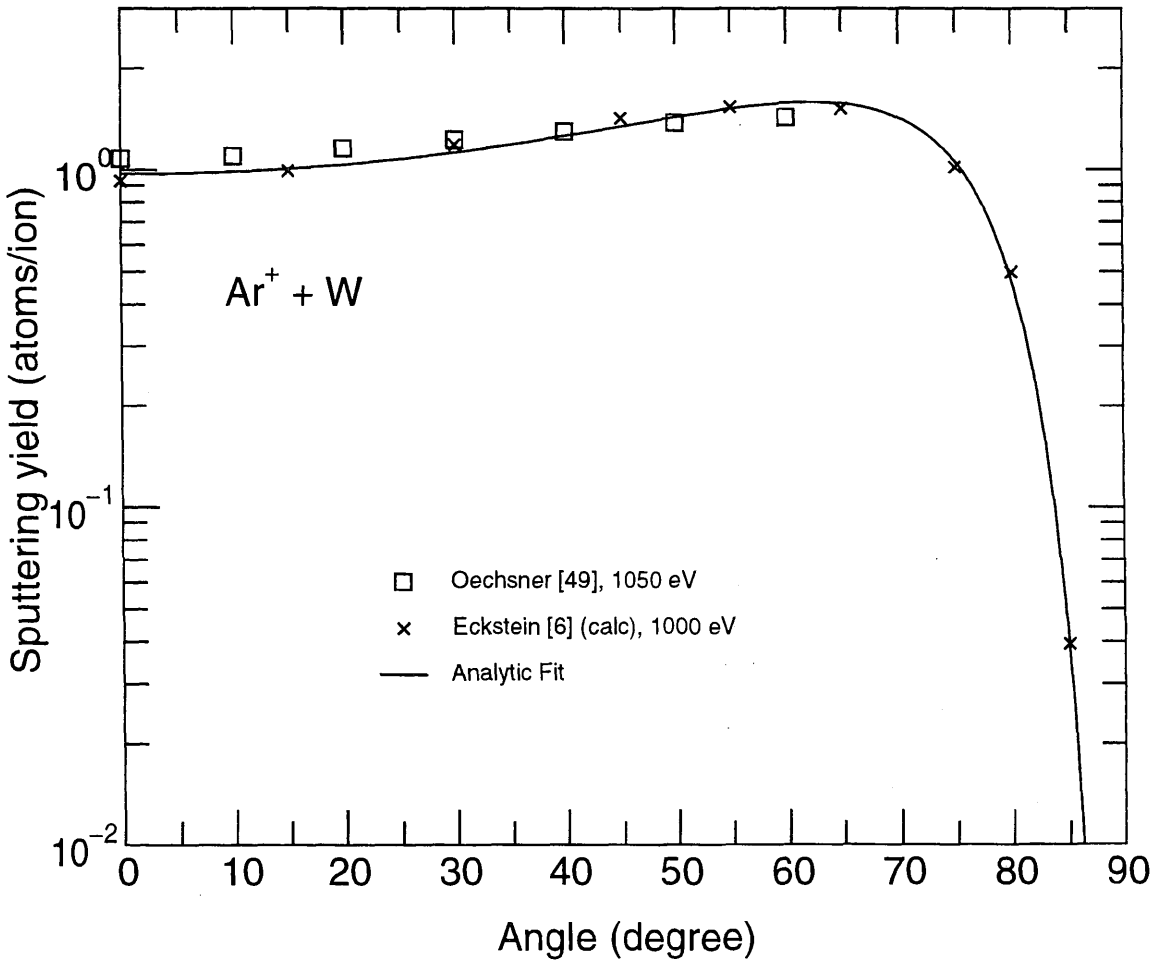

2.2.3.4 $W^+ + W$

Comments: (1) Only calculated values.

Fitting parameters:

Parameter:	f	b	c	Y(E_0,0)	α_0 (rad)	E_0 (eV)	Avg. Error (%)
	3.4680E+01	1.7783E+01	4.8682E-01	8.1551E-06	2.0643E+00	3.00E+01	10.5
	3.1717E+01	1.6512E+01	4.9615E-01	1.6476E-04	1.9656E+00	5.00E+01	9.8
	2.1288E+01	1.1570E+01	4.9913E-01	7.4758E-03	1.8573E+00	1.00E+02	9.6
	1.0065E+01	5.8289E+00	6.1616E-01	2.7884E-01	1.7270E+00	3.50E+02	2.3
	9.1710E+00	5.2962E+00	6.4780E-01	3.5246E-01	1.7171E+00	4.00E+02	1.3

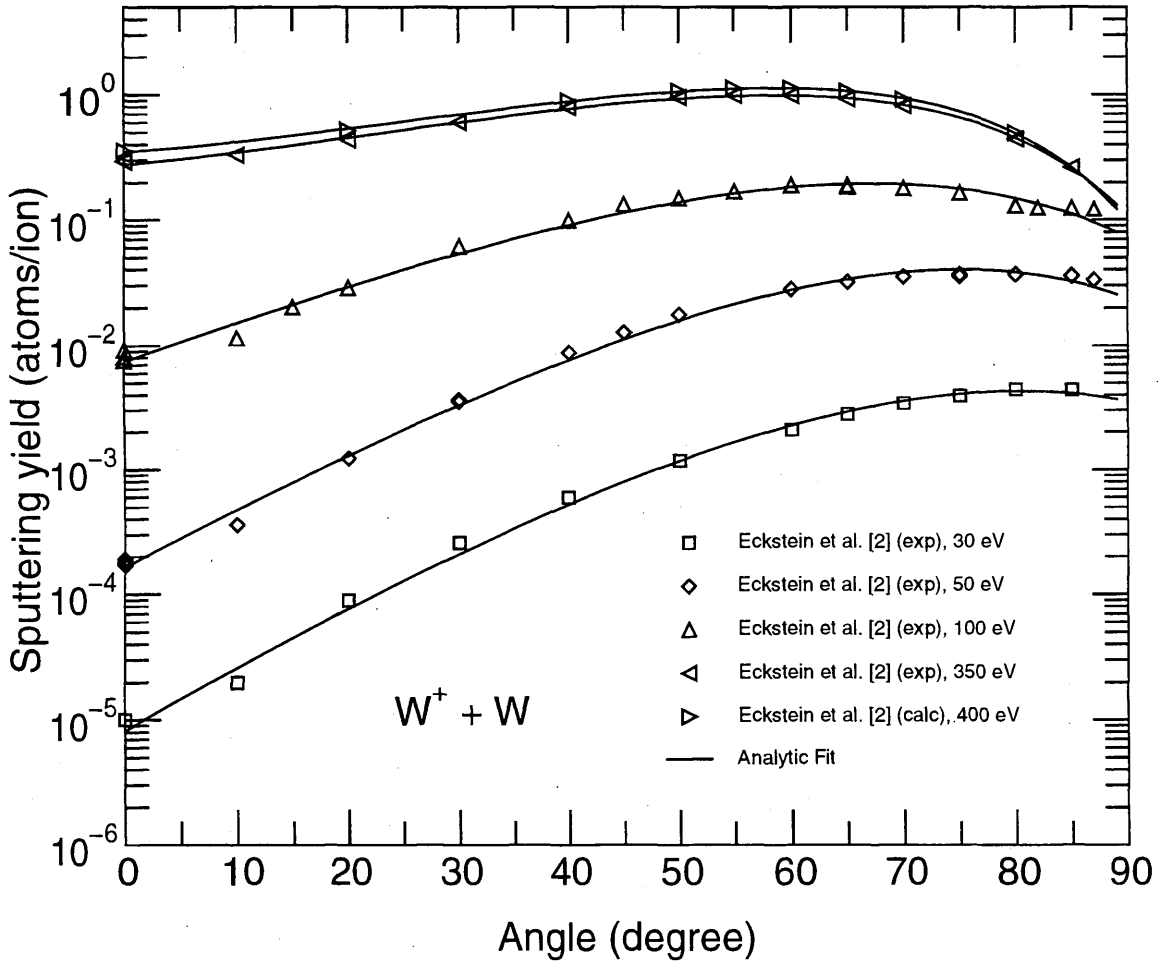

2.2.3.5 $W^+ + W$

Comments: (1) Only calculated values.

Fitting parameters:

Parameter:	f	b	c	$Y(E_0,0)$	α_0 (rad)	E_0 (eV)	Avg. Error (%)
	7.9540E+00	4.5557E+00	6.7639E-01	4.8760E-01	1.7018E+00	5.00E+02	1.7
	5.9865E+00	3.2747E+00	7.5973E-01	8.3829E-01	1.6746E+00	8.00E+02	3.7
	5.6272E+00	3.0811E+00	7.6362E-01	1.0507E+00	1.6637E+00	1.00E+03	3.1
	4.5015E+00	2.3480E+00	7.6259E-01	1.8064E+00	1.6366E+00	2.00E+03	1.0
	3.7958E+00	1.8870E+00	8.4160E-01	2.1735E+00	1.6297E+00	2.50E+03	2.3
	3.6547E+00	1.7164E+00	8.3036E-01	3.1150E+00	1.6124E+00	5.00E+03	2.0

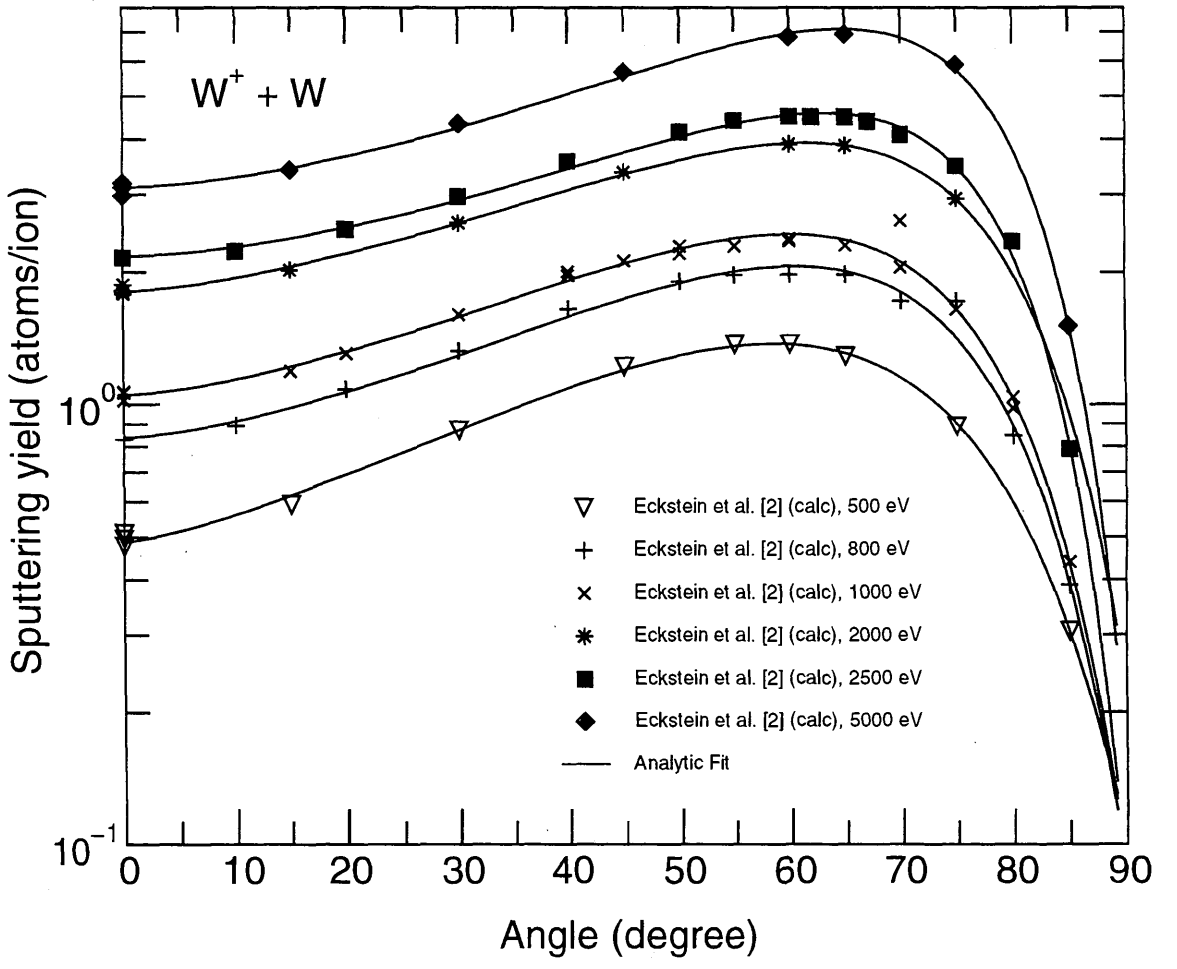

2.2.4.1 $D^+ + B_4C$

Comments: (1) Calculated values are only valid for low fluences due to possible preferential sputtering.

Fitting parameters:

Parameter:	f	b	c	Y(E_0,0)	α_0 (rad)	E_0 (eV)	Avg. Error (%)
exp	2.8411E+00	1.2592E+00	4.9301E-01	2.5545E-02	1.6705E+00	1.00E+02	5.9
calc	6.1226E+00	2.6452E+00	9.8698E-01	1.4152E-02	1.6705E+00	1.00E+02	3.4
exp	4.2466E+00	1.5203E+00	8.9926E-01	3.0116E-02	1.6155E+00	5.00E+02	2.6
calc	4.8576E+00	1.4233E+00	9.7111E-01	2.0388E-02	1.6155E+00	5.00E+02	3.6

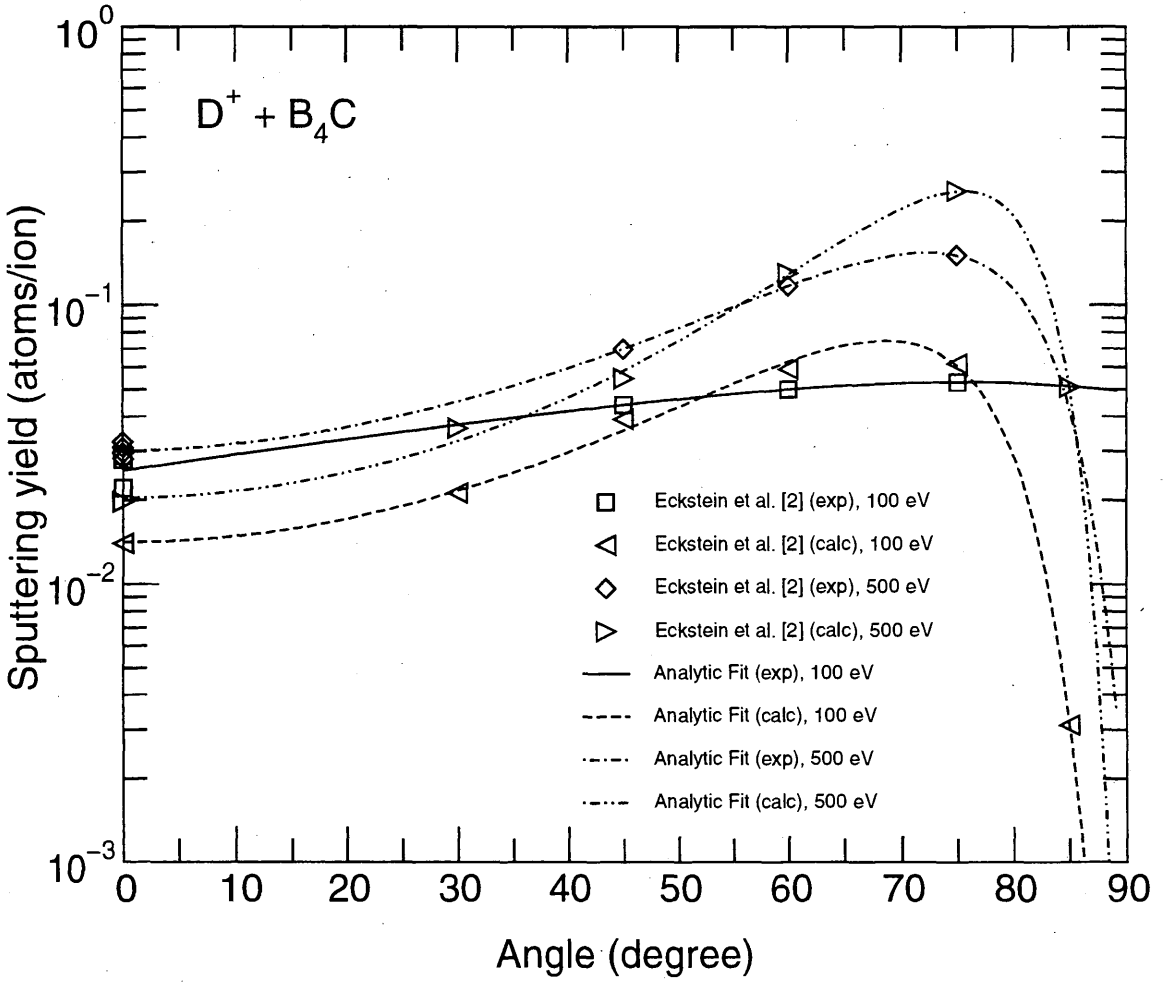

2.2.4.2 He^+, C^+ + B_4C

Comments: (1) Calculated values are only valid for low fluences due to possible preferential sputtering.

Fitting parameters:

Parameter:	f	b	c	Y(E_0,0)	α_0 (rad)	E_0 (eV)	Avg. Error (%)
exp	4.6352E+00	1.9280E+00	5.8969E-01	1.0500E-01	1.5708E+00	8.00E+02	0.0
calc	4.7597E+00	1.4518E+00	9.4177E-01	7.7076E-02	1.5708E+00	8.00E+02	2.9
exp	4.3077E+00	1.6821E+00	4.5537E-01	3.4200E-01	1.6481E+00	1.00E+03	6.1
calc	6.9265E+00	2.7812E+00	8.8457E-01	2.5300E-01	1.6481E+00	1.00E+03	0.0

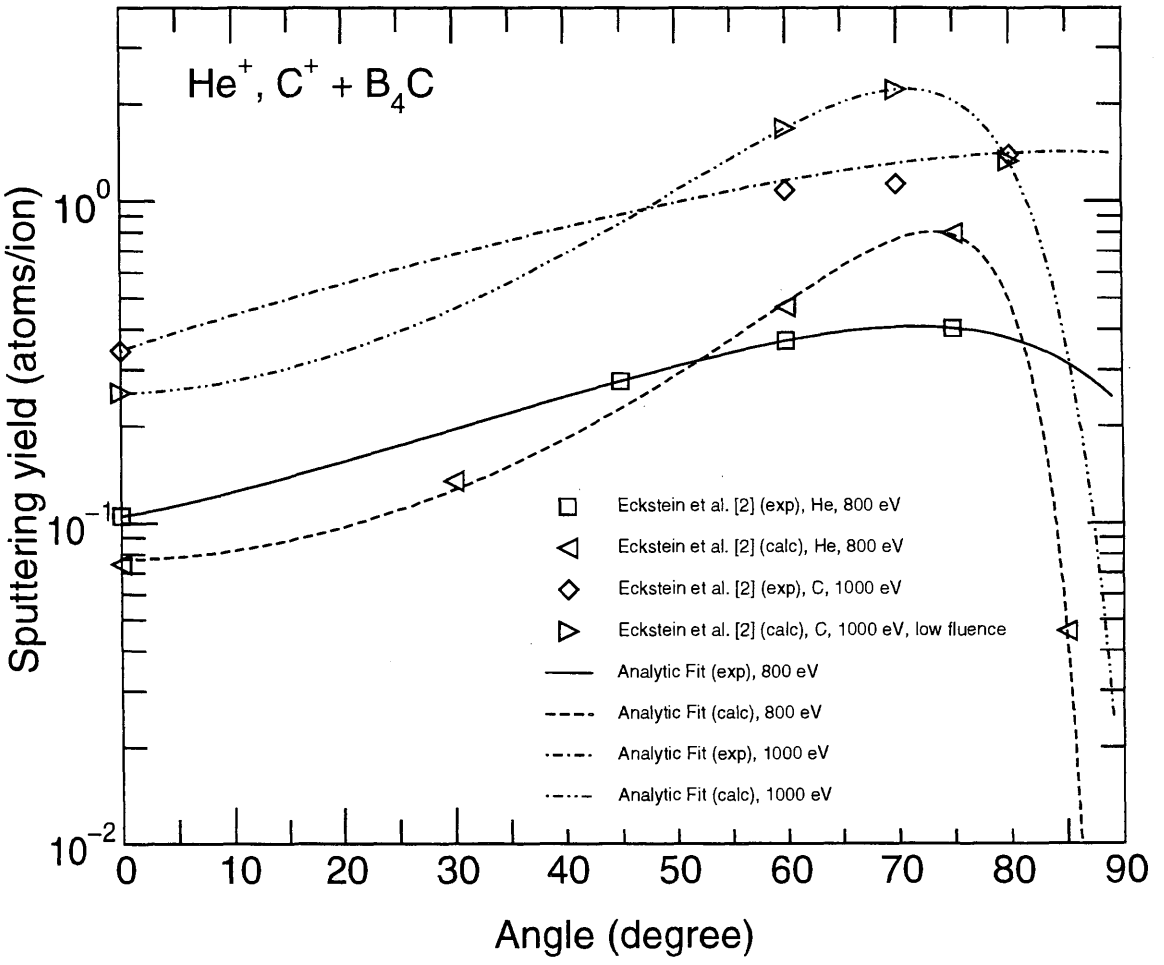

2.2.4.3 H^+, D^+, He^+ + SiC

Comments: (1) Calculated values are only valid for low fluences due to possible preferential sputtering.

Fitting parameters:

Parameter:	f	b	c	$Y(E_0,0)$	α_0 (rad)	E_0 (eV)	Avg. Error (%)
H^+	3.3319E+00	8.8673E-01	8.9729E-01	9.7850E-03	1.5932E+00	2.00E+03	20.4
D^+	2.9040E+00	7.0466E-01	9.7884E-01	2.0971E-02	1.5932E+00	2.00E+03	14.2
He^+	4.4666E+00	1.5655E+00	7.1719E-01	1.0655E-01	1.5708E+00	2.00E+03	13.8

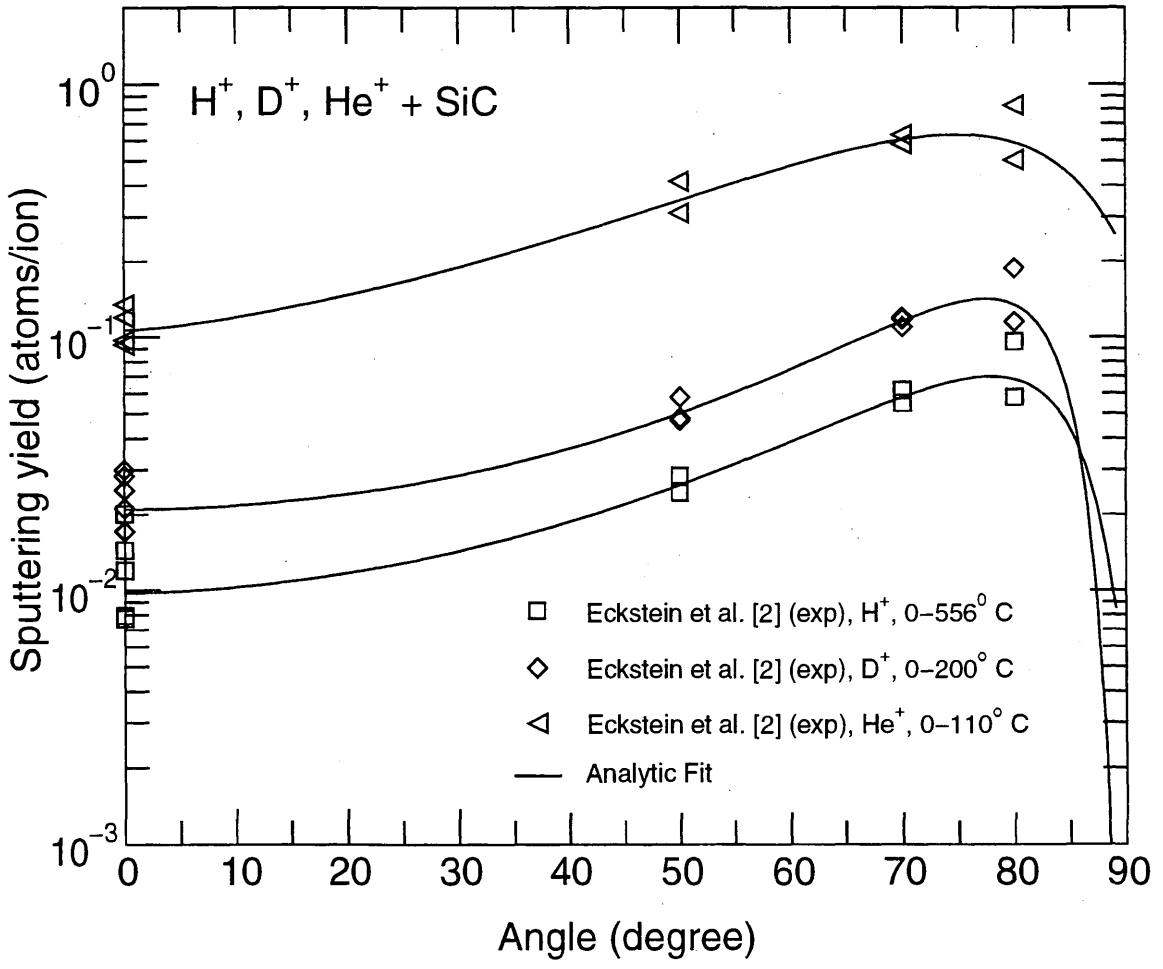

2.2.4.4 H^+ + TiC

Comments: (1) Calculated values are only valid for low fluences due to possible preferential sputtering.

Fitting parameters:

Parameter:	f	b	c	Y(E_0,0)	α_0 (rad)	E_0 (eV)	Avg. Error (%)
sheet	6.6944E-01	5.0919E-02	1.3340E+00	1.3729E-02	1.5932E+00	2.00E+03	5.8
sintered	3.4470E-01	1.3884E-02	1.3715E+00	8.8900E-03	1.5932E+00	2.00E+03	10.3
pl. sprayed	1.3471E+00	6.1387E-01	7.9604E-01	5.8698E-03	1.5932E+00	2.00E+03	16.7

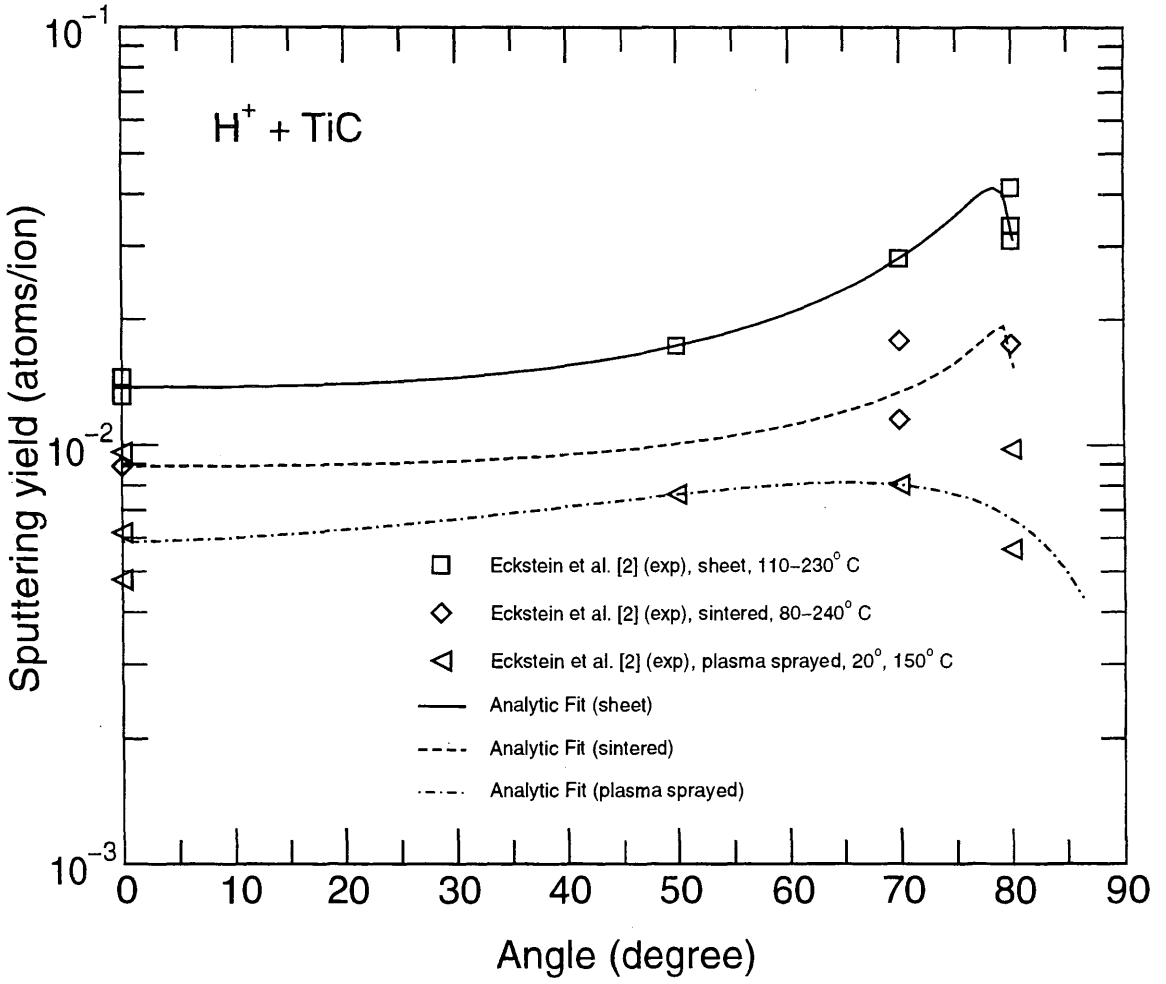

2.2.4.5 D^+ + TiC

Comments: (1) Calculated values are only valid for low fluences due to possible preferential sputtering.

Fitting parameters:

Parameter:	f	b	c	$Y(E_0,0)$	α_0 (rad)	E_0 (eV)	Avg. Error (%)
sheet	3.5734E+00	1.1296E+00	9.4293E-01	1.4555E-02	1.5932E+00	2.00E+03	10.9
sintered	3.4664E+00	1.5457E+00	7.7373E-01	1.5419E-02	1.5932E+00	2.00E+03	14.2
pl. sprayed	5.1042E-01	7.1986E-05	1.5080E-01	1.5843E-02	1.5932E+00	2.00E+03	14.5

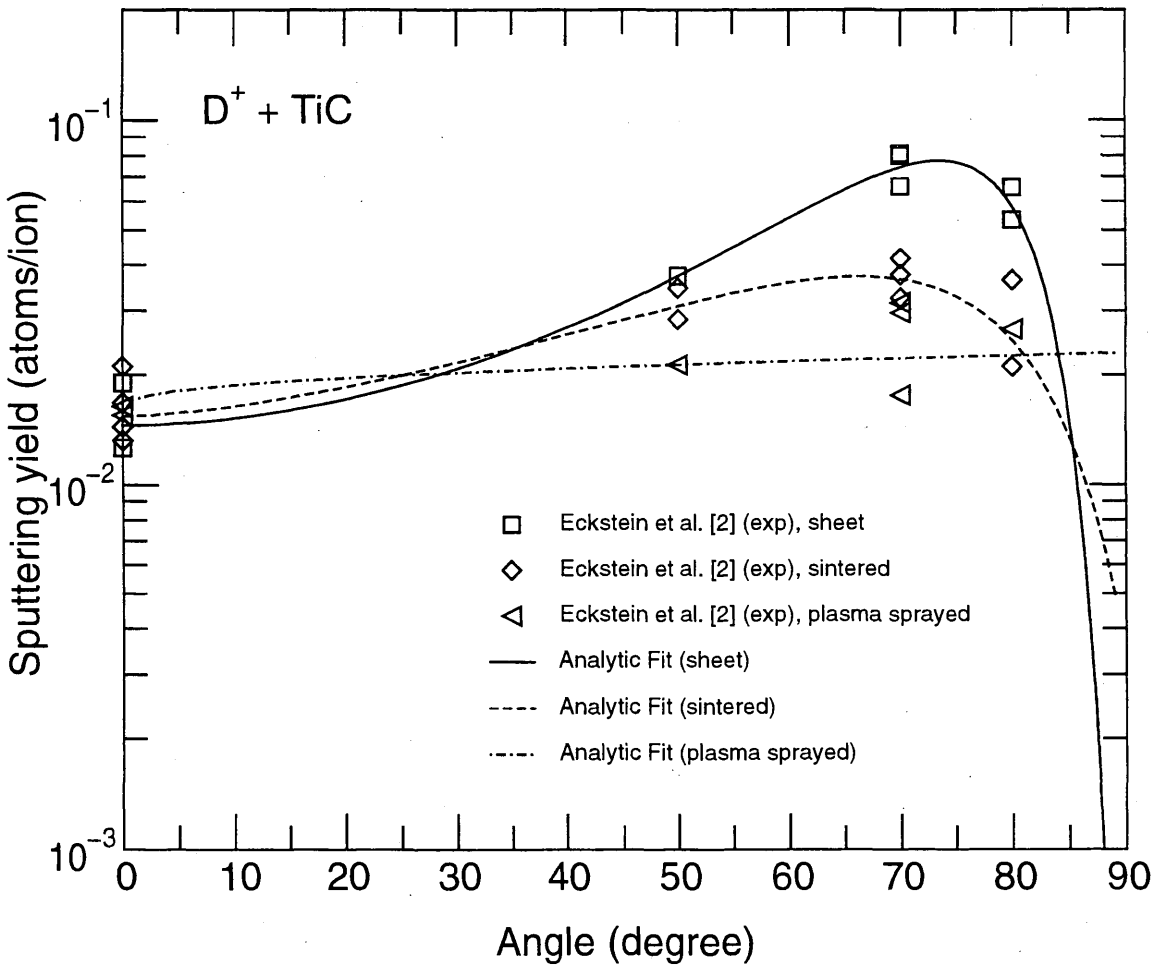

2.2.4.6 He^+ + TiC

Comments: (1) Calculated values are only valid for low fluences due to possible preferential sputtering.

Fitting parameters:

Parameter:	f	b	c	$Y(E_0,0)$	α_0 (rad)	E_0 (eV)	Avg. Error (%)
sheet	4.9956E+00	1.6623E+00	8.3092E-01	5.8725E-02	1.5708E+00	2.00E+03	11.2
sheet	2.0491E+00	2.8804E-08	3.5956E-01	5.5837E-02	1.5708E+00	6.00E+03	7.6
sintered	1.6372E+00	4.9820E-01	8.6877E-01	1.0700E-01	1.5708E+00	6.00E+03	0.0
pl. sprayed	3.0072E+00	1.5655E+00	6.1871E-01	7.5500E-02	1.5708E+00	6.00E+03	0.0

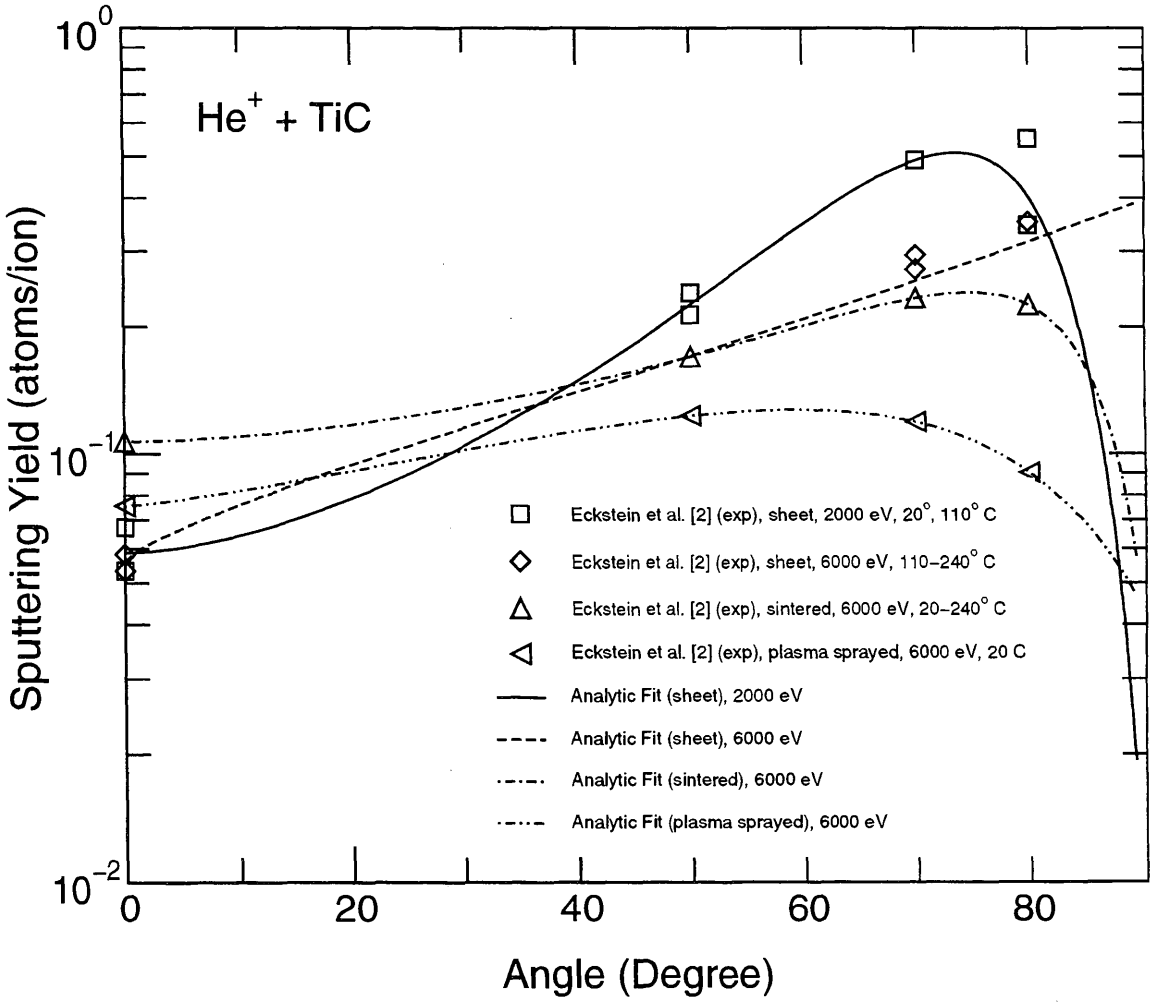

References for Sections 2.1-2.2

[1] BOHDANSKY, J., ROTH, J., OTTENBERGER, W., IPP-JET No. 31, Garching (1985).

[2] ECKSTEIN, W., GARCIA-ROSALES, C., ROTH, J., OTTENBERGER, W., Report IPP 9/82, Garching (1993).

[3] YAMAMURA, Y., TAWARA, H., Report NIFS-DATA-23, Nagoya (1995).

[4] YAMAMURA, Y., SAKAOKA, K., TAWARA, H., Report NIFS-DATA-31, Nagoya (1995).

[5] YAMAMURA, Y., TAWARA, H., Atomic Data and Nuclear Data Tables **62** (1996) 149.

[6] ECKSTEIN, W., Report IPP 9/117, Garching (1998).

[7] ROTH, J., J. Nucl. Mater. **145-147** (1987) 87.

[8] ROTH, J., ECKSTEIN, W., BOHDANSKY, J., J. Nucl. Mater. **165** (1989) 199.

[9] KORSHUNOV, S. N., GUSEVA, M. I., STOLJAROVA, V. G., Proc. 2nd IEA Int. Workshop on Beryllium Technology for Fusion, G. R. Longhurst (ed.), Lockheed Idaho Technologies CONF-9509218, (1995) 285.

[10] ROSENBERG, D., WEHNER, G. K., J. Appl. Phys. **33** (1962) 1842.

[11] FETZ, H., OECHSNER, H., Proc. 6th Int. Conf. Ionization Phenomena in Gases Vol. II, Paris (1963) 39.

[12] GUSEVA, M., GUREEV, V. M., KORSHUNOV, S. N., NEUMOIN, V. E., SOKOLOV, YU. A., STOLYAROVA, V. G., VASILIEV, V. I., RYLOV, S. V., J. Nucl. Mater. **220-222** (1995) 957.

[13] HIROOKA, Y., private communication (1996).

[14] HECHTL, E., ROTH, J., ECKSTEIN, W. WU, C. H., J. Nucl. Mater. **220-222** (1995) 883.

[15] ROTH, J., ECKSTEIN,W., GUSEVA, M., Fusion Engineering and Design **37** (1997) 465.

[16] M. GUSEVA, M., BIRUKOV, A. YU., GUREEV, V. M., DANELJAN, L. S., KORSHUNOV, S. N., MARTYNENKO, YU. V., MOSKOVIN, P. S., SOKOLOV, YU. A., STOLYAROVA, V. G., KALIKAUSKAS, V. S., J. Nucl. Mater. **233-237** (1996) 681.

[17] KÜSTNER, M., ECKSTEIN, W., DOSE, V., ROTH, J., Nucl. Instrum. Meth. B **145** (1998) 320.

[18] LAEGREID, N., WEHNER, G. K., J. Appl. Phys. **32** (1961) 365.

[19] HAASZ, A. A., DAVIS, J. W., WU, C. H., J. Nucl. Mater. **162-164** (1989) 915.

[20] BOHDANSKY, J., ROTH, J., SINHA, M. K., Proc. 9th Symp. Fusion Technol. (1976) 541.

[21] ROTH, J., BOHDANSKY, J., POSCHENRIEDER, W., SINHA, M. K., J. Nucl. Mater. **63** (1976) 222.

[22] BALDEN, M., ROTH, J., J. Nucl. Mater. in press (2000).

[23] BORDERS, J. A., LANGLEY, R. A., WILSON, K. L., J. Nucl. Mater. **76&77** (1978) 168.

[24] GARCÍA-ROSALES, C., GAUTHIER, E., ROTH, J., R. Schwörer and W.Eckstein, J. Nucl. Mater. **189** (1992) 1.

[25] YAMASHITA, M., BABA, S., KINBAR, A., Proc. 4th Symp. Ion Source and Ion Applications (1980) 311.

[26] HECHTL, E., BOHDANSKY, J., ROTH, J., J. Nucl. Mater. **103&104** (1981) 333.

[27] WEHNER, G. K., Phys. Rev. **102** (1956) 690.

[28] HECHTL, E., BOHDANSKY, J., J. Nucl. Mater. **141-143** (1986) 139.

[29] HECHTL, E., BOHDANSKY, J., J. Nucl. Mater. **122&123** (1984) 1431.

[30] BETZ, G., DOBROZEMSKY, R., VIEHBÖCK, F. P., WOTTKE, H., Proc. 9th Int. Conf. Phenomenon Ionized Gases (1969) 91.

[31] SMITH, J. N., JR., MAYER, C. H., JR., LAYTON, J. K., Nucl. Technol. **29** (1976) 318.

[32] ROTH, J., BOHDANSKY, J., OTTENBERGER, W., Report IPP 9/26, Garching, 1979

[33] ROTH, J., BOHDANSKY, J., MARTINELLI, A. P., Radiat. Eff. **48** (1980) 213.

[34] BOHDANSKY, J., CHEN, G. L., ECKSTEIN, W., ROTH, J., SCHERZER, B. M. U., BEHRISCH, R., J. Nucl. Mater. **111&112** (1982) 717.

[35] ECKSTEIN, W., LÁSZLÓ, J., J. Nucl. Mater. **183** (1991) 19.

[36] GUSEVA, M. I., MARTYNENKO, Y. V. Fiz. Plaz. (USSR) **2** (1976) 593.

[37] ZIEGLER, J. F., CUOMO, J. J., ROTH, J., Appl. Phys. Lett. **30** (1977) 268.

[38] HECHTL, E., BOHDANSKY, J., ROTH, J., Proc. Symp. on Sputtering, ed. P. Varga, G. Betz and F. P. Viehböck, Inst. für Allg. Physik, Techn. Univ. Vienna (1980) 834.

[39] BADER, M., WITTERBONE, F. C., SNOUSE, T. W., Nasa Tech. Report R105 (1961).

[40] TSUNOYAMA, K., SUZUKI, T., OHASHI, Y., KISHIDAKA, H., Surface Interface Analysis **2** (1980) 212.

[41] HECHTL, E., ECKSTEIN, W., ROTH, J., LÁSZLÓ, J., J. Nucl. Mater. **179 - 181** (1991) 290.

[42] ALMÉN, O., BRUCE, G., Nucl. Instrum. Methods **11** (1961) 257.

[43] STUART, R. V., WEHNER, G. K., J. Appl. Phys. **33** (1962) 2345.

[44] WINTERS, H. F., HORNE, D., Phys. Rev. B **10** (1974) 55.

[45] SCHIRRWITZ, H., Beiträge aus der Plasmaphysik **2** (1962) 188.

[46] GURMIN, B. M., MARTYNENKO, T. P., RYZHOV, YU. A., Sov. Phys. - Solid State **10** (1968) 324.

[47] KOSHKIN, V. K., RYSOV, J. A., SHKARBAN, I. I., GOURMIN, B. M., Proc. 9th Int. Conf. Phenomenon Ionized Gases (1969) 92.

[48] NAVINSEK, B., CARTER, G., SPIG, Hercegnovi, 1970, p.65.

[49] OECHSNER, H., Z. Physik **261** (1973) 37.

[50] SMITH, J. N., JR., MAYER, C. H., JR., LAYTON, J. K., Trans. Am. Nucl. Soc. **22** (1975) 29.

[51] SAIDOH M., SONE, K., Jap. J. Appl. Phys. **22** (1983) 1361.

[52] HECHTL, E., YANG, H. R., WU, C. H., ECKSTEIN, W., J. Nucl. Mater. **176 & 177** (1990) 874.

[53] BOHDANSKY, J., BAY, H. L., OTTENBERGER, W., J. Nucl. Mater. **76 & 77** (1978) 163.

[54] ONO, T., KAWAMURA, T., ISHII, K., YAMAMURA, Y., Report NIFS-DATA-34, Nagoya (1995).

[55] ONO, T., KAWAMURA, T., ISHII, K., YAMAMURA, Y., J. Nucl. Mater. **232** (1996) 52.

[56] GAUTHIER, E., ECKSTEIN, W., LÁSZLÓ, J., ROTH, J., J. Nucl. Mater. **176 & 177** (1990) 438.

[57] ROTH, J., BOHDANSKY, J., BLEWER, R. S., OTTENBERGER, W., J. Nucl. Mater. **85 & 86** (1979) 1077.

[58] HIROOKA, Y., WON, J., BOIVIN, R., SZE, D., NEUMOIN, V., J. Nucl. Mater. **228** (1996) 148, 173.

[59] BALDEN, M., ROTH, J., WU, C. H., J. Nucl. Mater. **258-263** (1998) 740.

[60] RUZIC, D. N., SMITH, P. C., TURKOT, R. B., JR., J. Nucl. Mater. **241-243** (1997) 1170.

[61] UEDA, S., OHSAKA, T., KUWAJIMA, S., J. Nucl. Mater. **258 - 263** (1998) 713.

[62] ROTH, J. in *Physics of Plasma-Wall Interactions in Controlled Fusion*, eds. D. E. Post, R. Behrisch, Plenum (1986) 351.

[63] ROTH, J., ECKSTEIN, W., GAUTHIER, E., LÁSZLÓ, J., J. Nucl. Mater. **179-181** (1991) 34.

[64] BAY, H. L., BOHDANSKY, J., HOFER, W. O., ROTH, J. Appl. Phys. **21** (1980) 327.

3 Radiation-Enhanced Sublimation: Data Collection

Radiation-enhanced sublimation is an erosion mechanism peculiar to carbon-based materials, and affects only carbon atoms within those materials. It is similar to physical sputtering in that it does not involve chemical reactions, and that it does require incident particles to have sufficient energy to dislodge carbon atoms from their lattice sites. But, the process does not require that carbon atoms be ejected from the surface via momentum transfer alone, as in the case of physical sputtering. Once in interstitial spaces, the carbon atoms may diffuse to a surface, where they are weakly bound. The atoms may leave the surface by a thermal mechanism, such that there is an exponential increase in their release with increasing temperature. The activation energy for this release, that is, the atom binding energy to the surface, is generally in the range 0.5-1 eV [1-10] significantly less than the sublimation energy for carbon, 7.4 eV. This basic understanding of the processes involved in RES has been established for many years, and a review of these concepts is presented in [11]. Models of the RES process have been reasonably successful [7, 10, 12, 13], however, some questions remain with regard to the flux density dependence, see below.

Several fundamental aspects of RES have been investigated experimentally, the most obvious of these is the temperature dependence, and thus the activation energy for the carbon atom release. The fact that the activation energy is about 10% of that for thermal sublimation, clearly separates the two mechanisms. The released carbon atoms do, however, have a near thermal energy distribution which is similar to that seen for thermal sublimation. The time-of-flight spectra of carbon atoms released due to 5 keV Ar^+ bombardment of carbon at 2000 K is presented in Fig. 1 [14, 15]. There are two clear groups of atoms leaving the surface; a fast group, attributed to physical sputtering, and a thermal group attributed to RES; the two groups are clearly distinguishable. This provides solid evidence that carbon atoms released by RES involve a thermal process. In addition, measurements [1] have shown that the C atoms are released with nearly a cosine distribution, as would be expected for a thermal release process.

A further feature which separates RES from physical sputtering and thermal sublimation is the fraction of carbon released as C_2 and C_3 molecules. In RES, the carbon is almost entirely released as single atoms (see Fig. 2 [11]), while for physical sputtering only about 80% is released as a C_1, the rest being released as C_2 and C_3. In thermal sublimation, the fraction released as C_2 and C_3 increases with temperature, with single carbon atoms accounting for less than 20% at 2500 K. The predominant release of single carbon atoms in RES is a natural consequence of the mechanism which involves the transport of individual carbon atoms through interstitial spaces to the surface.

There are also differences in the angular dependence of the RES erosion yield as compared to physical sputtering. For example, as shown in Fig. 3, the total erosion yield due to 1 keV C^+ shows a smaller increase with angle than the physical sputtering yield. In fact, most of the increase shown for the total yield at 1500 K is attributable to the physical sputtering component. More recent results on the RES angular dependence [16] show a similar weak dependence. The weak angular dependence is, again, a natural consequence of the RES mechanism. At large angles of incidence, carbon interstitials would simply be created closer to the surface; pro-

vided the mean diffusional range of the interstitials is less than the ion range, the number of C atoms emitted from the surface will not be affected.

A large number of experiments have been performed investigating the temperature dependence of RES erosion yields for various pure and doped graphites. There is general agreement on the exponential nature of the temperature dependence, of the form: $Y \propto \exp^{-E/T}$. For this reason, data are often presented in an Arrhenius plot. Experiments have primarily been performed with light ions, including H^+, D^+, He^+ and C^+, as well as some heavier incident species, e.g., Ar^+. It is noted that erosion yields for C^+ self-sputtering can exceed unity [21], thus leading to the possibility of runaway erosion. The data presented in Section 3.1 generally falls into two categories, depending on the experimental technique used. Mass loss experiments provide an absolute measure of the total erosion yield, while line-of-sight mass spectroscopy measurements may be scaled to other results, or provide data as relative units. Data presented here are generally in the form that appears in the original publication.

Generally, reductions in RES yields due to dopants have been found to be minor [26], except in a couple of cases, where Ti-doping has made a significant impact [9, 17]. It is becoming apparent that the mechanism by which the dopants are introduced, and the structure of the near-surface layers imposed by the manufacturing technique have an impact on the erosion yield. The RES yield for one specimen with a particular concentration of a dopant may vary substantially from another with the same dopant concentration, but different structure.

The dependence of RES erosion yields on incident ion energy and on the incident flux density have been much less studied than the temperature dependence. For fusion materials selection, however, these are critical issues. In Fig. 4, RES erosion yields are presented as a function of ion energy. It is important to note the clear indication of a threshold energy, similar to that observed for physical sputtering. In Fig. 5, we have compiled data on the flux dependence of RES erosion. While most models of RES have generally predicted reductions in erosion yield with increasing flux on the order of $Y \propto \phi^{-0.25}$ [7, 10, 12, 13], experimental results have tended to be closer to $Y \propto \phi^{-0.1}$. An exception to the experimental trends are the highest flux measurements for 5 keV Ar^+ impact (which have the damage equivalence of a D^+ flux 50 times larger [10]) which show a dependence much closer to the model prediction [10, 18]. This leads to the possibility that ion beam experiments are simply at too low of a flux density to see the decrease, but the decrease may result in the yields being small in comparison to physical sputtering in a tokamak environment. This observation is in line with the results of the test limiter observations in TEXTOR as discussed in Vol. 7, Part A, p15 of this series. Obtaining more high flux results in plasma-simulation devices, under well controlled conditions, will be essential for confirming this trend at high fluxes.

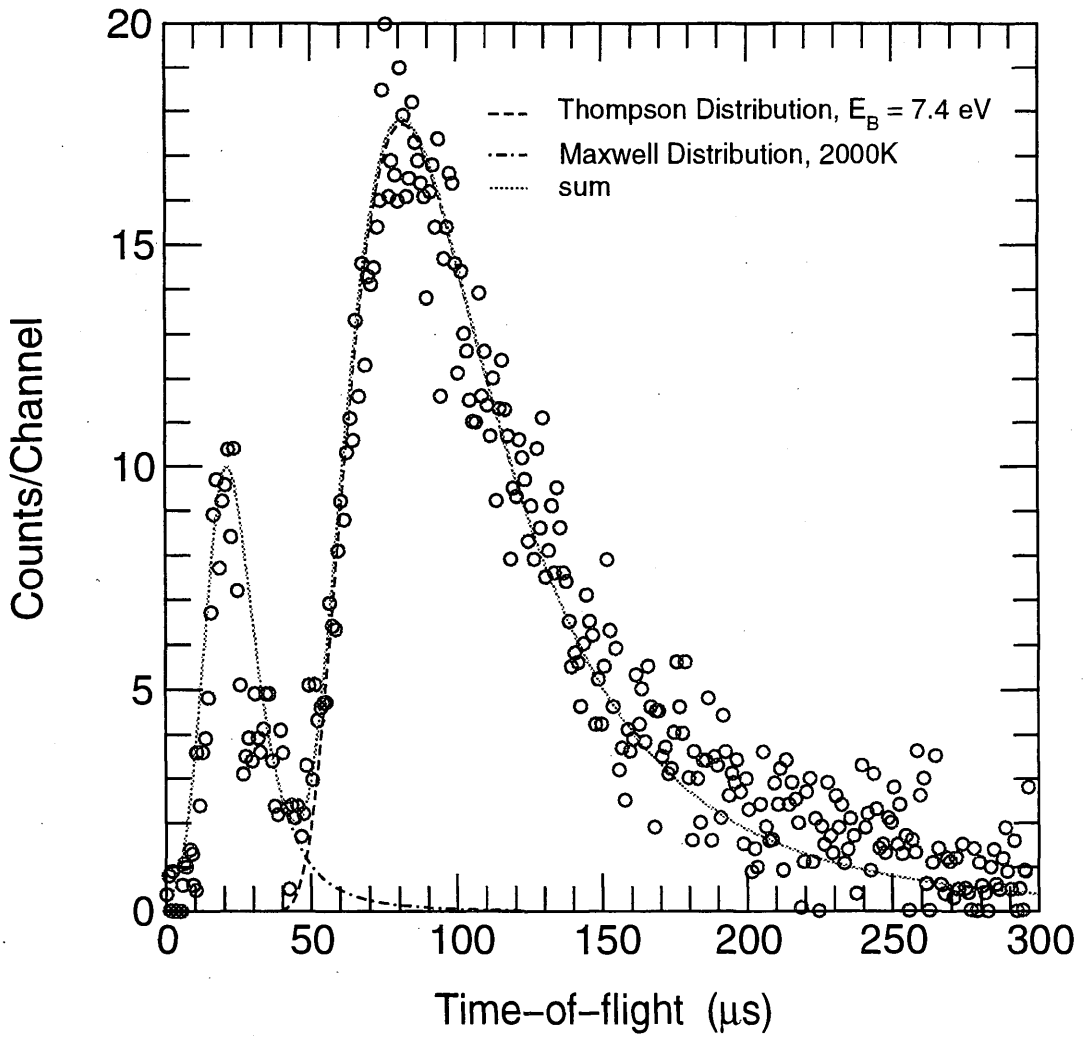

Figure 1: Time-of-flight spectrum of emitted carbon atoms under 5 keV Ar+ bombardment of carbon at 2000 K. Physically sputtered carbon atoms appear around 20μs, and RES-emitted carbon atoms appear at times in agreement with a Maxwellian velocity distribution corresponding to the target temperature [14].

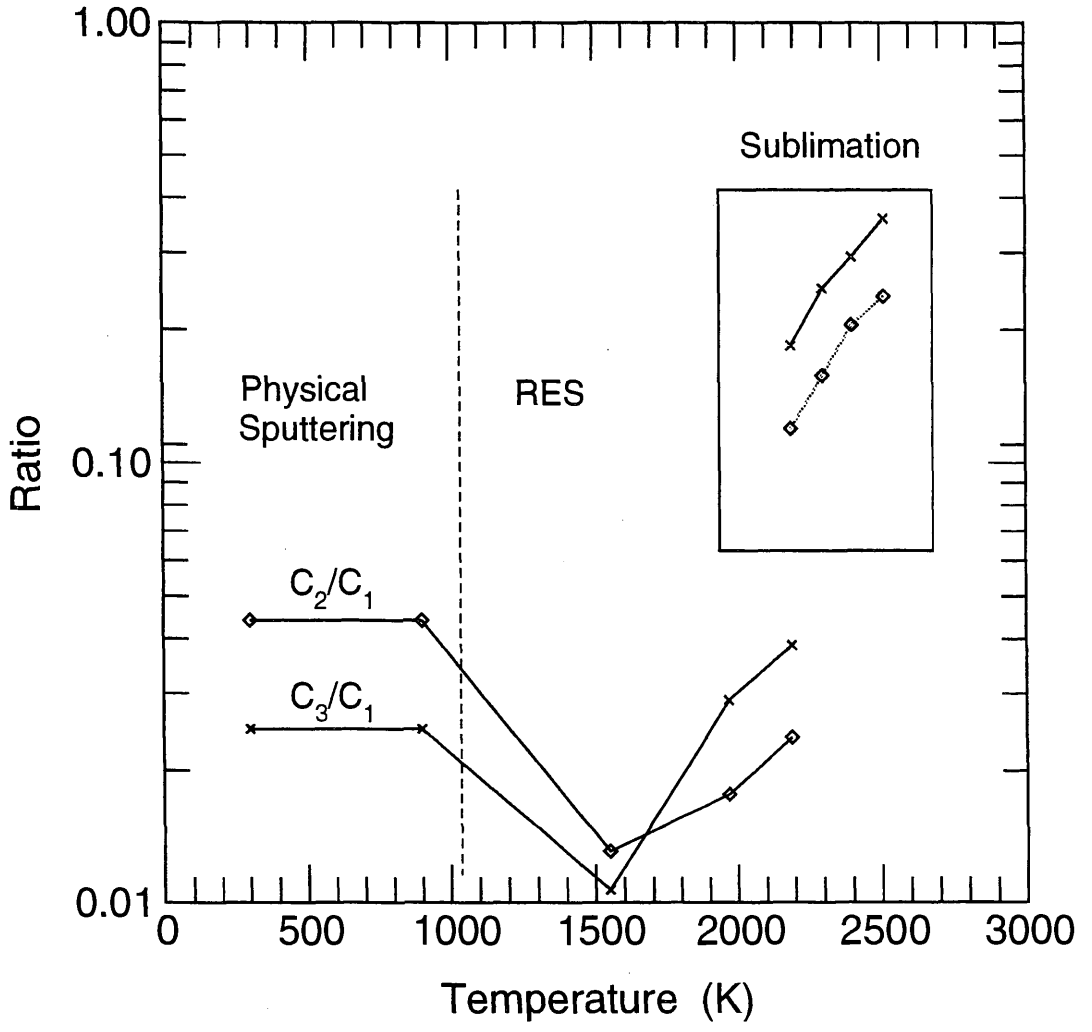

Figure 2: Temperature dependence of the ratio of emitted C_2/C_1 and C_3/C_1 under 5 keV Ar^+ bombardment of graphite. Data for T > 2200 K (in the insert) are obtained during thermal sublimation alone, i.e., with the ion beam off. The ratio of the ionization cross sections needed for mass spectroscopic detection has been taken from theoretical calculations for C_2 and C_3 (H. Deutsch et al., Int. J. Mass Spectrom., **197** (2000) 37) and experimental result for C_1 [19] to be at an electron energy of 70 eV: $C_2/C_1 = 1.85$ and $C_3/C_1 = 2.4$. The data of carbon sputtering (with energy distributions) in [20] were corrected with the cross section ratios given above. For the determination of RES and thermal evaporation data, Maxwell distributions have been taken for all components (unpublished results of E. Vietzke 1994) and the mass dependent sensitivity as above.

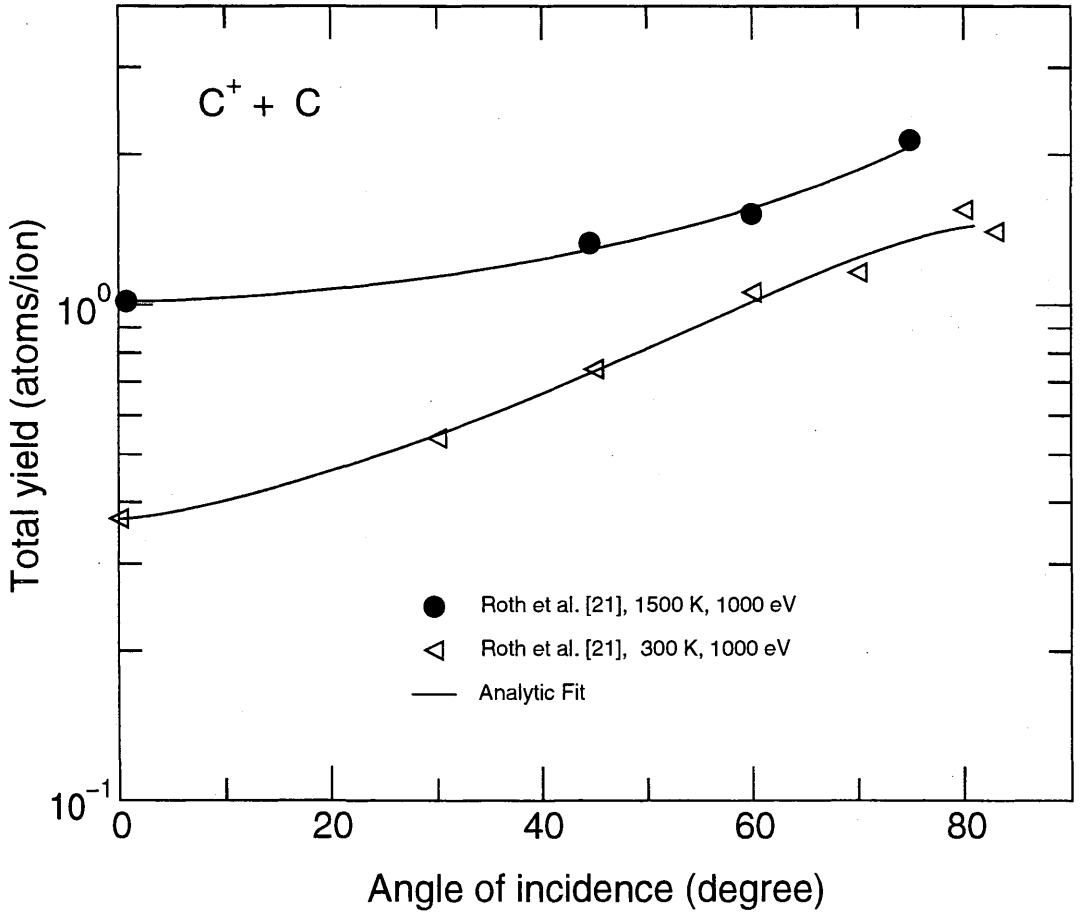

Figure 3: Angular dependence of physical sputtering and radiation-enhanced sublimation.

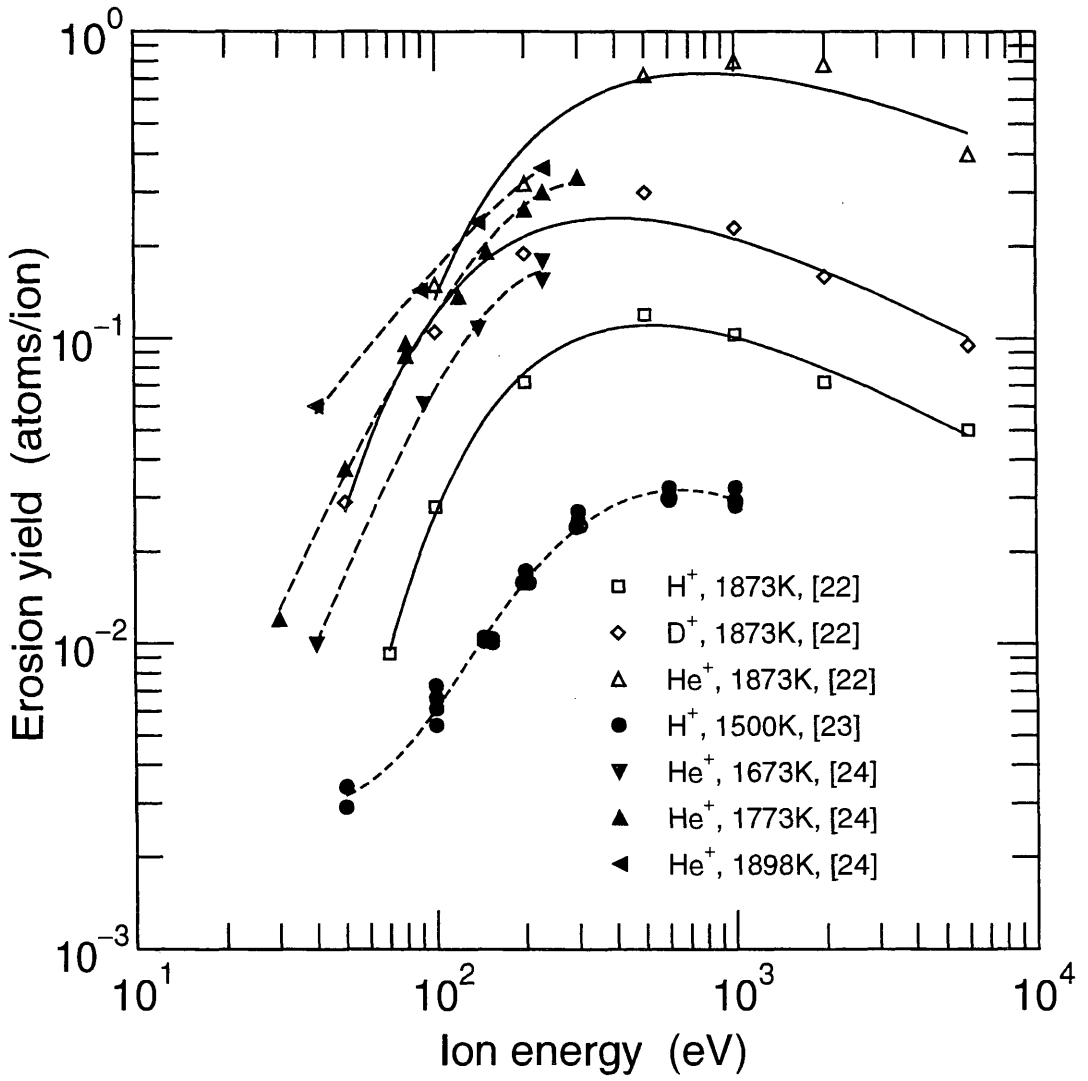

Figure 4: Energy dependence of radiation-enhanced sublimation, from several sources.

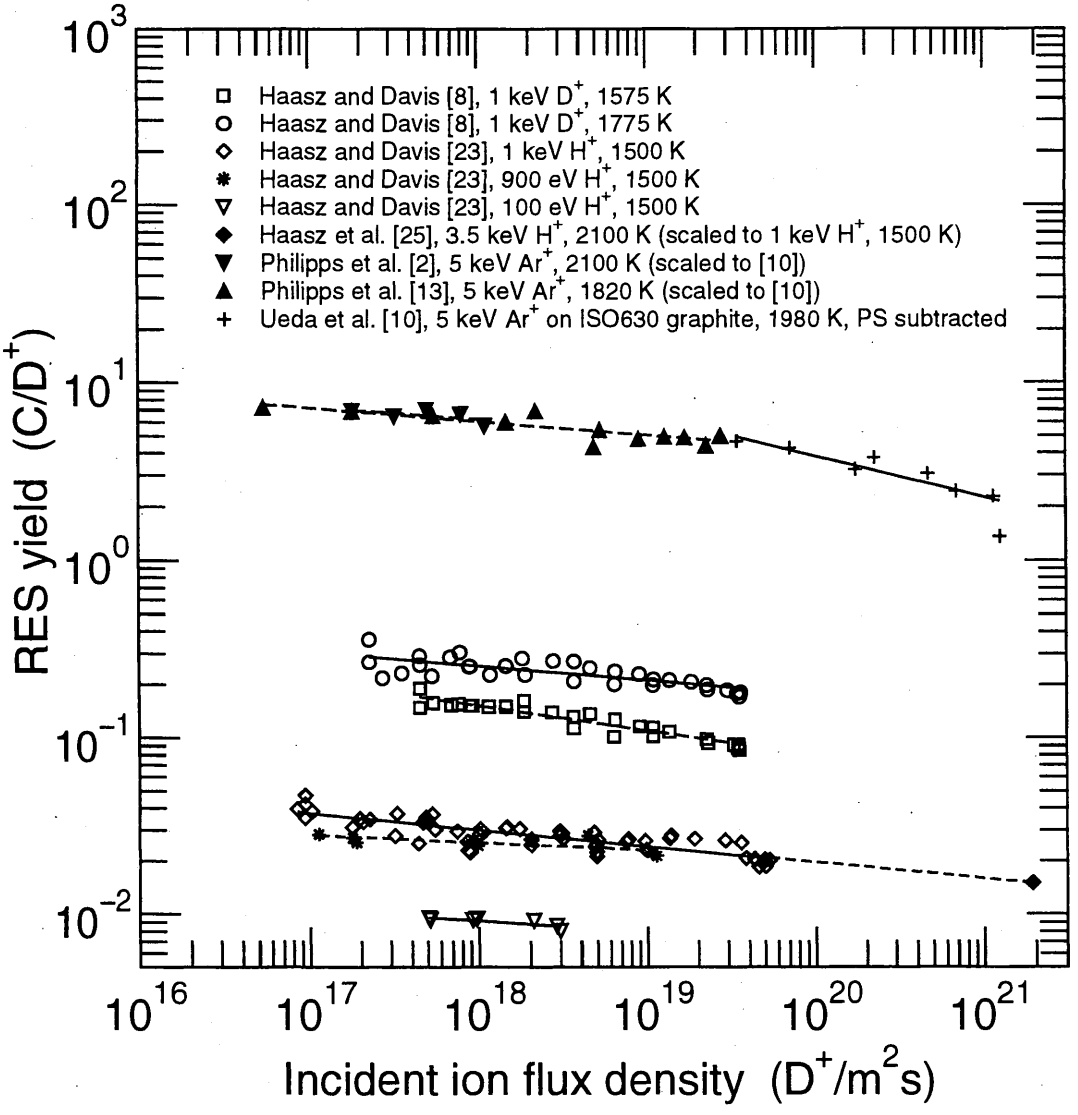

Figure 5: Flux dependence of RES. Unless otherwise indicated, the specimens were pyrolytic graphite.

References for Section 3

[1] ROTH, J., BOHDANSKY, J., WILSON, K. L., J. Nucl. Mater. **111&112** (1982) 775.

[2] PHILIPPS, V., FLASKAMP, K., VIETZKE, E., J. Nucl. Mater. **111&112** (1982) 781.

[3] NYGREN, R. E., BOHDANSKY, J., POSPIESZCZYK, LEHMER, R., RA, Y., CONN, R. W., DOERNER, R., HIROOKA, Y., LEUNG, W. K., SCHMITZ, L., J. Vac. Sci. Technol. **111&112** (1982) 781.

[4] ROTH, J., BOHDANSKY, J., WILSON, K. L., J. Nucl. Mater. **122&123** (1984) 1447.

[5] HIROOKA, Y., CONN, R. W., CAUSEY, R., CROESSMANN, D., DOERNER, R., HOLLAND, D., KHANDAGLE, M., MATSUDA, T., SMOLIK, G., SOGABE, T., WHITLEY, J., WILSON, K., J. Nucl. Mater. **176&177** (1990) 473.

[6] HINO, T., YAMASHITA, T., J. Nucl. Mater. **196&198** (1992) 531.

[7] FRANZEN, P., DAVIS, J. W., HAASZ, A. A., J. Appl. Phys. **78** (1995) 817.

[8] HAASZ, A. A., DAVIS, J. W., J. Nucl. Mater. **224** (1995) 141.

[9] FRANZEN, P., HAASZ, A. A., DAVIS, J. W., J. Nucl. Mater. **226** (1995) 15.

[10] UEDA, Y., NAKANO, K., OHTSUKA, Y., ISOBE, M., GOTO, S., NISHIKAWA, M., J. Nucl. Mater. **227** (1996) 251.

[11] ECKSTEIN, W., PHILIPPS, V., Physical Processes of the Interaction of Fusion Plasmas with Solids, eds. W. O. Hofer and J. Roth, Academic Press, Amsterdam (1996) 93.

[12] ROTH, J., MÖLLER, W., Nucl. Instrum. Meth. B **7/8** (1985) 788.

[13] PHILIPPS, V., VIETZKE, E., SCHORN, R. P., TRINKAUS, H., J. Nucl. Mater. **155-157** (1988) 319.

[14] PHILIPPS, V., VIETZKE, E., TRINKAUS, H., J. Nucl. Mater. **179-181** (1991) 25.

[15] PHILIPPS, V., VIETZKE, E., ERDWEG, M., FLASKAMP, K., Plasma Phys. Contrl. Fusion **31** (1989) 1685.

[16] UEDA, Y., SHIOTA, K., OHTSUKA, Y., ISOBE, M., NISHIKAWA, M., Fusion Eng. Des. **41** (1998) 55.

[17] BEGRAMBEKOV, L. B., BUZHINSKIJ, O. I., KOKUSHKIN, B. YA., NIKOLSKIJ, M. V., OTHOSHCHENKO, V. G., PUSTOBAEF, A. A., RAZUMOV, TEL'KOVSKIJ, V. G., FEDEROV, YU. V., SHLENOV, I. D., J. Nucl. Mater. **170** (1990) 101.

[18] OHTSUKA, Y., UEDA, Y., ISOBE, M., NISHIKAWA, M., J. Nucl. Sci. Tech. **34** (1997) 792.

[19] BROOK, E., HARRISON, M. F. A., SMITH, A. C. H., J. Phys. B: Atom. Molec. Phys. **11** (1978) 3115.

[20] VIETZKE, E., REFKE, A., PHILIPPS, V., HENNES, M., J. Nucl. Mater. **241-243** (1997) 810.

[21] ROTH, J., ECKSTEIN, W., BOHDANSKY, J., J. Nucl. Mater. **165** (1989) 199.

[22] BOHDANSKY, J., ROTH, J., Proc. 15th Symposium Fusion Technology, Volume 1, Elsevier, (1989) 889.

[23] HAASZ, A. A., DAVIS, J. W., J. Nucl. Mater. **151** (1987) 77.

[24] NYGREN, R. E., BOHDANSKY, J., POSPIESZCZYK, LEHMER, R., RA, Y., CONN, R. W., DOERNER, R., LEUNG, W. K., SCHMITZ, L., J. Nucl. Mater. **176&177** (1990) 445.

[25] HAASZ, A. A., DAVIS, J. W., CROESSMANN, C. D., DOYLE, B. L., NYGREN, R. E., WALSH, D. S., WATKINS, J. G., WHITLEY, J. B., J. Nucl. Mater. **173** (1990) 108.

[26] VIETZKE, E., PHILIPPS, V., FLASKAMP, K., WINTER, J., VEPREK, S., J. Nucl. Mater. **176&177** (1990) 481.

List of Reactions for Section 3

3 Radiation enhanced sublimation of carbon

3.1 Temperature dependence

3.1.1 H^+ + graphite (pyrolytic) → C

3.1.2 H^+, D^+, He^+ + graphite (pyrolytic) → C

3.1.3 H^+ + graphite (MPG-8, USB-15) → C

3.1.4 H^+ + graphite (USB-15, B_4C/B) → C

3.1.5 H^+ + graphite (POCO-AXF5Q, GB-103) → C

3.1.6 H^+, H_3^+ + graphite (Papyex, USB-15, C/SiC) → C

3.1.7 H_3^+, D_3^+, He^+ + graphite (Papyex) → C

3.1.8 H_3^+ + graphite (HPG99) → C

3.1.9 H_3^+ + graphite (HPG99, EK98, CKC base and edge planes) → C

3.1.10 H_3^+ + graphite (HPG99, EK98, CKC base and edge planes) → C

3.1.11 H_3^+ + graphite (IG-110U, ISO-880U, ISO-630U) → C

3.1.12 H_3^+ + graphite (IG-110U, ISO-630U, ISO-890U, CX-2002U, pyroid) → C

3.1.13 H_3^+ + graphite (GB-100, GB-103, GB-110, GB-120) → C

3.1.14 H_3^+ + graphite (V doped) → C

3.1.15 D^+ + graphite (pyrolytic, GB-100, GB-110, GB-120, GB-130, CCB-407) → C

3.1.16 D_3^+ + graphite (pyrolytic, USB-15, GB-120), B_4C → C

3.1.17 D^+ + graphite (diamond, pyrolytic, various B doped) → C

3.1.18 D^+, C^+ + graphite (pyrolytic) → C

3.1.19 D^+, C^+ + graphite, B_4C → C

3.1.20 D_3^+ + graphite (pyrolytic, RG-Ti91, USB-15) → C

3.1.21 D_3^+ + graphite (CKC-Si, base plane) → C

3.1.22 D_3^+ + graphite (CKC-Si, base plane) → C

3.1.23 D_3^+ + graphite (CKC-B, base plane) → C

3.1.24 D_3^+ + graphite (CKC-B, base plane) → C

3.1.25 D_3^+ + graphite (CKC-B, edge plane) → C

3.1.26 D_3^+ + graphite (CKC-B, edge plane) → C

3.1.27 D_3^+ + graphite (CKC-Ti, base plane) → C

3.1.28 D_3^+ + graphite (CKC-Ti, base plane) → C

3.1.29 D_3^+ + graphite (CKC-Ti, edge plane) → C

3.1.30 D_3^+ + graphite (CKC-Ti, edge plane) → C

3.1.31 He^+ + graphite (POCO) → C

3.1.32 He^+ + graphite (pyrolytic, POCO) → C

3.1.33 He^+ + graphite (gravimol C/C, MPG-9, KUP-VM, KUP-VM Ti, Si doped) → C

3.1.34 C^+, O^+, Ar^+ + graphite (Papyex) → C

3.1.35 Ar^+ + graphite (pyrolytic) → C

3.1.36 Ar^+ + graphite (pyrolytic) → C

3.1.37 Ar^+ + graphite (ISO-630) → C

3.1.38 Ar^+ + graphite (pyrolytic, Toyo Tanso, Carbone Lorraine, USB-15) → B, C

3.1.39 Ar^+ + graphite (USB-15) → B, C

3.1.40 Ar^+ + graphite (pyrolytic, Toyo Tanso, Carbone Lorraine, USB-15) → B, C

3.1.41 Ar^+ + graphite (pyrolytic, a-C:H, a-C/B:H, diamond) → B, C

3.2 Energy dependence

3.2.1 H_3^+ + graphite (pyrolytic) → C

3.2.2 D^+ + graphite (pyrolytic) → C

3.2.3 D_3^+ + graphite (Papyex) → C

3.2.4 He^+ + graphite (POCO) → C

3.2.5 H^+, D^+, He^+ + graphite (pyrolytic) → C

3.2.6 H^+, D^+, C^+, Ar^+ + graphite (Papyex) → C

3.2.7 He^+, Ar^+ + graphite (pyrolytic) → C

3.3 Angle dependence

3.3.1 D_3^+ + graphite (Papyex) → C

3.3.2 D^+, C^+ + graphite (pyrolytic, Papyex) → C

3.3.3 Ar^+ + graphite (pyrolytic, IG-430) → C

3.4 Flux dependence

3.4.1 H_3^+ + graphite (pyrolytic) → C

3.4.2 D^+ + graphite (pyrolytic) → C

3.4.3 Ar^+ + graphite (pyrolytic) → C

3.4.4 Ar^+ + graphite (pyrolytic) → C

3.4.5 Ar^+ + graphite (IG-430) → total, C

3.4.6 Ar^+ + graphite (ISO-630) → total, C

3.4.7 Ar^+ + graphite (pyrolytic, RG-Ti, ISO-630) → C

3.1.1 H^+ + graphite (pyrolytic) → C

Source: J. Bohdansky and J. Roth, Fusion Technology, Proc. 15th Symposium on Fusion Technology, Vol. 1, 889 (1988).

Accuracy: Yield (abs.): ±15%; T: ±20K.

Comments: (1) Yield for total erosion measured by mass loss.
(2) Specimen: pyrolytic graphite.
(3) H_3^+ ions: mass-analyzed accelerator.

Analytic fitting:

Analytic fit for reaction A (○).

Fitting parameters A_1-A_2

A	3.7458E-01	6.9326E+03

ALADDIN hierarchical labelling and evaluation function:

A: RES H [+1] GRAPHITE T=PYG C [+0] #EYIELD2EN

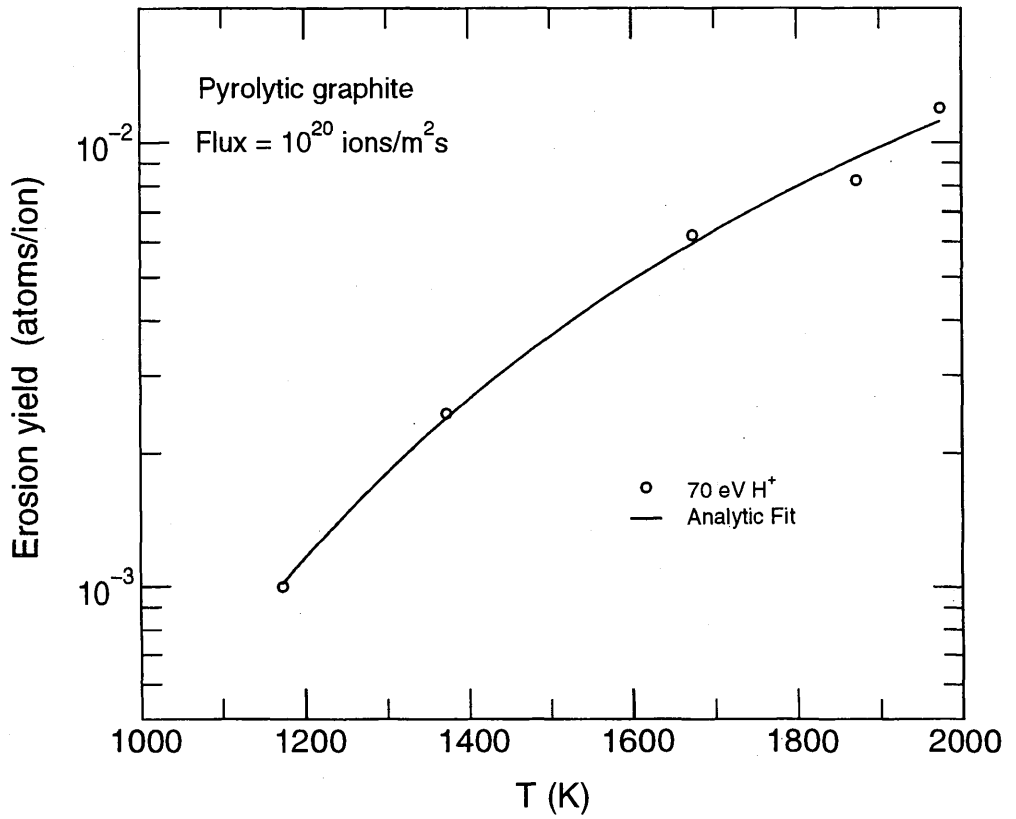

3.1.2 H^+, D^+, He^+ + graphite (pyrolytic) → C

Source: J. Bohdansky and J. Roth, Fusion Technology, Proc. 15th Symposium on Fusion Technology, Vol. 1, 889 (1988).

Accuracy: Yield (abs.): ±15%; T: ±20K.

Comments: (1) Yield for total erosion measured by mass loss.
(2) Specimen: pyrolytic graphite.
(3) H_3^+, D_3^+ and He^+ ions: mass-analyzed accelerator.

Analytic fitting:

Analytic fits for reactions A (○), B (△) and C (∗).

Fitting parameters A_1-A_2

A	7.8037E+00	7.6683E+03
B	1.4124E+01	7.2293E+03
C	2.8131E+01	7.0639E+03

ALADDIN hierarchical labelling and evaluation function:

A: RES H [+1] GRAPHITE T=PYG C [+0] #EYIELD2EN
B: RES D [+1] GRAPHITE T=PYG C [+0] #EYIELD2EN
C: RES He [+1] GRAPHITE T=PYG C [+0] #EYIELD2EN

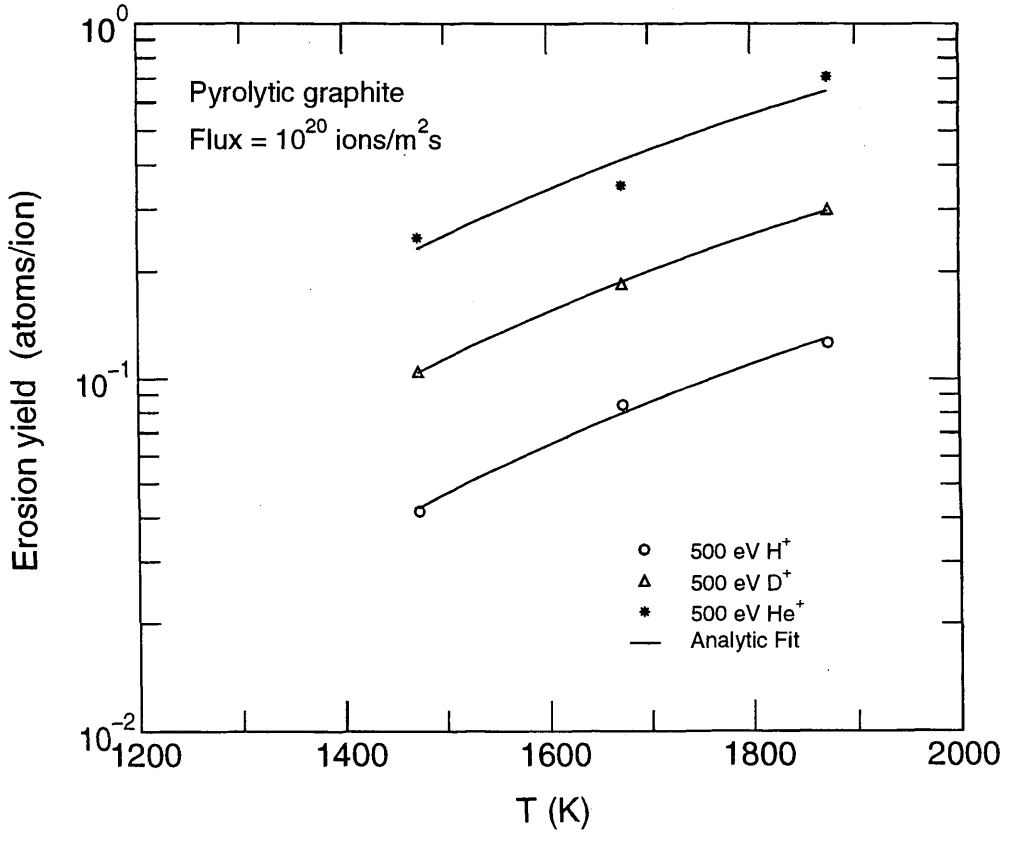

3.1.3 H^+ + graphite (MPG-8, USB-15) → C

Source: M. I. Guseva, S. M. Ivanov and A. N. Mansurova, Atomnaya Energiya **55**, 336 (1982).

Accuracy: Yield (rel.): Indeterminate.

Comments: (1) H^+ ions: mass-analyzed ion beam.
(2) Weight loss measurements.
(3) Specimens: MPG-8 graphite and USB-15 boron-doped graphite.

Analytic fitting:

Analytic fits for reactions A (△) and B (○).

Fitting parameters A_1-A_{10}

A	6.4507E-03	7.8217E+02	1.0381E+04	3.4195E-01	4.0254E-03	-1.6237E-03
	1.3319E-01	-1.2074E+02	1.5443E+04	-1.0297E-02		
B	5.1733E-07	7.1205E+02	4.2854E+03	1.5424E+00	-3.5107E-09	-4.5366E-03
	1.3618E+00	5.4133E+01	9.5760E+03	5.4752E-03		

ALADDIN hierarchical labelling and evaluation function:

A: RES H [+1] GRAPHITE T=MPG-8 C [+0] #EYIELD10AN
B: RES H [+1] GRAPHITE T=USB-15 C [+0] #EYIELD10AN

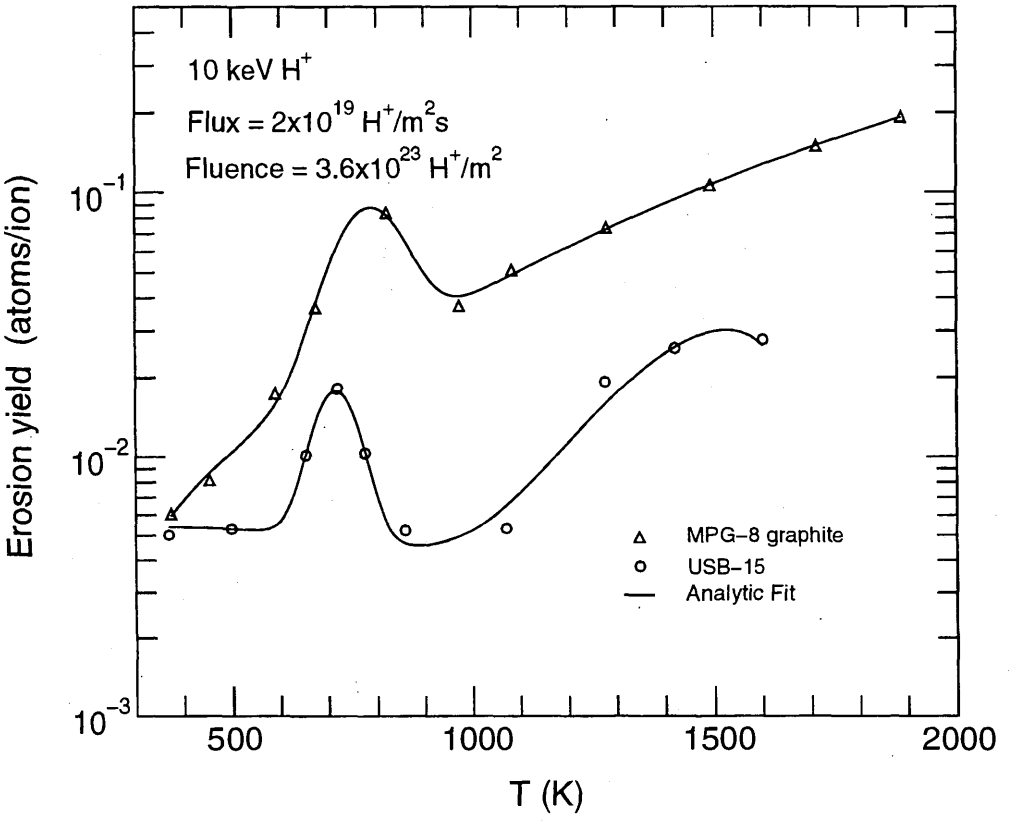

3.1.4 H^+ + graphite (USB-15, B_4C/B) → C

Source: O. I. Buzhinskiy, M. I. Guseva, G. V. Gordeeva, V. M. Gureev, P. N. Orlov, E. S. Ionova, S. V. Mirnov, R. Un. Mametiev, E. V. Tupitsina, B. N. Sharupin and V. E. Neumoin, J. Nucl. Mater. **175**, 262 (1990).

Accuracy: Yield (rel.): Indeterminate.

Comments: (1) H^+ ions: mass-analyzed ion beam.
(2) Weight loss measurements.
(3) Specimen: MPG-8 graphite with 100-500μm B_4C film coating.
(4) Results for USB-15 are shown for comparison (reference unavailable).

Analytic fitting:

Analytic fits for reactions A (o) and B (△).

Fitting parameters A_1-A_{10}

A	5.7718E-04	6.9424E+02	7.3518E+03	3.5733E-01	5.4435E-03	-1.6541E-05
	2.0764E-01	2.1888E+01	9.5699E+03	-1.5303E-02		
B	5.5337E-25	4.5679E+02	2.1843E+04	8.0661E+00	2.2000E-03	5.7108E-04
	4.8865E-01	6.9487E+01	1.4951E+04	-3.1367E-02		

ALADDIN hierarchical labelling and evaluation function:

A: RES H [+1] GRAPHITE T=USB-15 C [+0] #EYIELD10AN
B: RES H [+1] GRAPHITE T=B4C-B C [+0] #EYIELD10AN

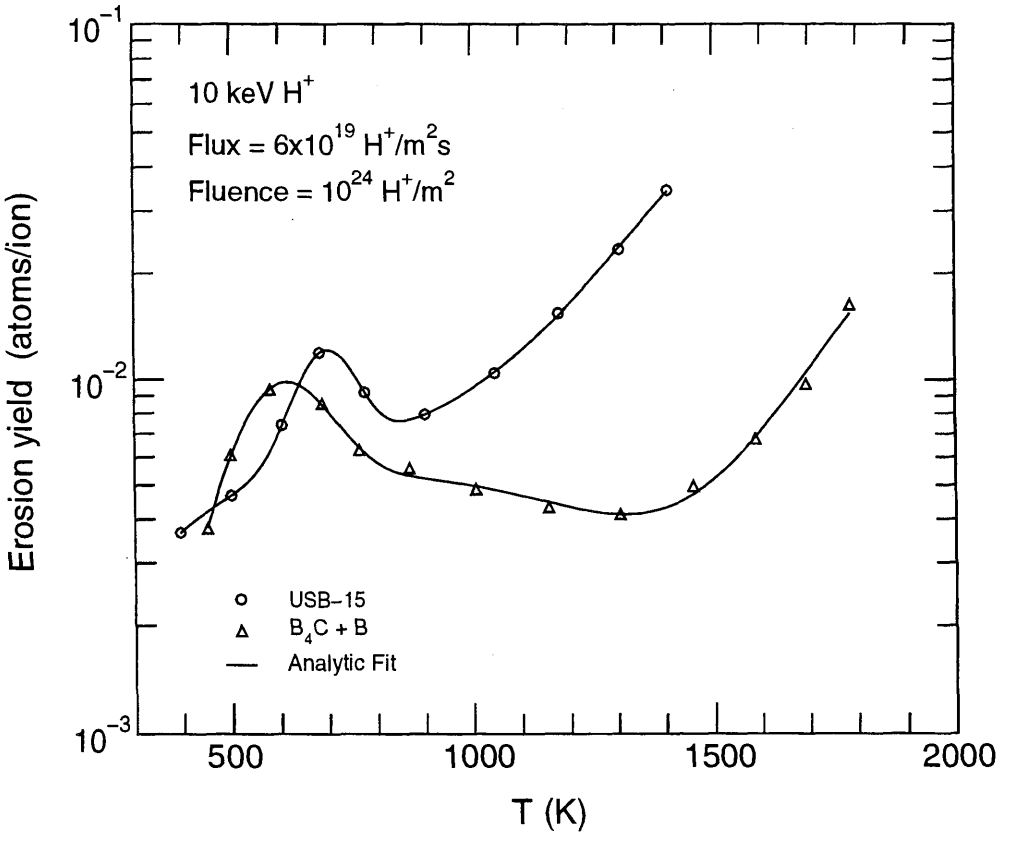

3.1.5 H^+ + graphite (POCO-AXF5Q, GB-103) → C

Source: Y. Hirooka, R. W. Conn, T. Sketchley, W. K. Leung, G. Chevalier, R. Doerner, J. Elverum, D. M. Goebel, G. Gunner, M. Khandagle, B. Labombard, R. Lehmer, P. Luong, Y. Ra, L. Schmitz and G. Tynan, J. Vac. Sci. Technol. **A8**, 1790 (1990).

Accuracy: Yield (rel.): ±10%-15%.

Comments: (1) Weight loss measurements.
(2) Specimens: POCO-AXF5Q isotropic fine grain graphite and GB-103 bulk-boronized graphite (Toyo Tanso).
(3) Minimal redeposition effects (i.e. low T_e, n_e).
(4) A factor of 2-3 reduction found for bulk-boronized graphite only.
(5) High intensity steady-state plasma source.

Analytic fitting:

Analytic fits for reactions A (○) and B (●). The data was fitted only for T > 1280 K where RES occurs.

Fitting parameters A_1-A_3

A	1.2546E+01	1.1871E+04	1.1953E-03
B	1.2291E-01	2.8151E+02	-9.4067E-02

ALADDIN hierarchical labelling and evaluation function:

A: RES H [+1] GRAPHITE T=POCO-AXF5Q C [+0] #EYIELD3BN
B: RES H [+1] GRAPHITE T=GB-103 C [+0] #EYIELD3BN

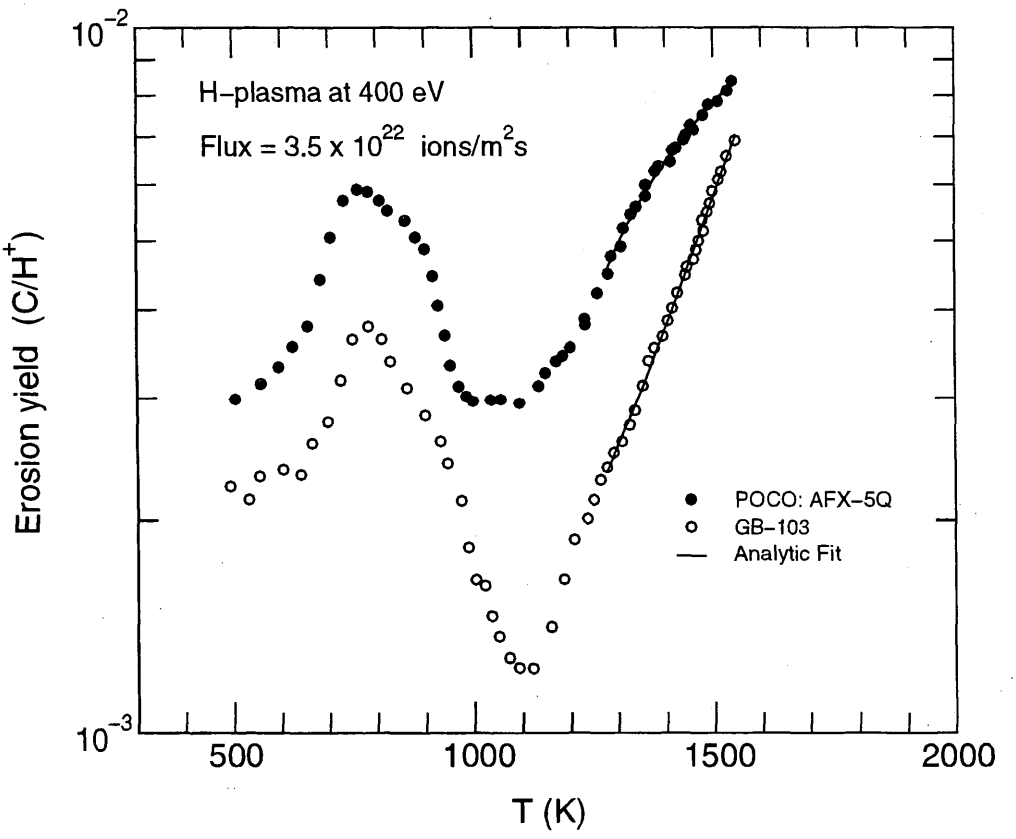

3.1.6 H^+, H_3^+ + graphite (Papyex, USB-15, C/SiC) → C

Source: J. Roth, J. Bohdansky and J. B. Roberto, J. Nucl. Mater. **128&129**, 534 (1984).

Accuracy: Yield (abs.): ±15%, T: ±20K.

Comments: (1) Yield for total erosion measured by mass loss.
(2) Specimens: Papyex graphite, SiC-dopped graphite.
(3) H_3^+ ions: mass-analyzed accelerator.
(4) USB-15 data from USSR contribution to PHASE IIA of the INTOR Workshop, Vol. 2, (Oct. 1982).

Analytic fitting:

Analytic fits for reactions A (△) and B (•). The 3 keV H_3^+ data and fit are given in reaction 3.1.7.

Fitting parameters A_1-A_8

A	5.5226E-03	7.4325E+02	5.4888E+03	1.3181E-01	1.1098E-06	-1.0160E-02
	-8.8131E-01	5.0404E-03				
B	1.5063E-02	9.1293E+02	4.6649E+04	-6.6448E-02	7.0179E-05	-3.9734E-03
	5.1637E-02	6.0040E-03				

ALADDIN hierarchical labelling and evaluation function:

A: RES H [+1] GRAPHITE T=USB C [+0] #EYIELD8CN
B: RES H {3} [+1] GRAPHITE T=C-SiC C [+0] #EYIELD8CN

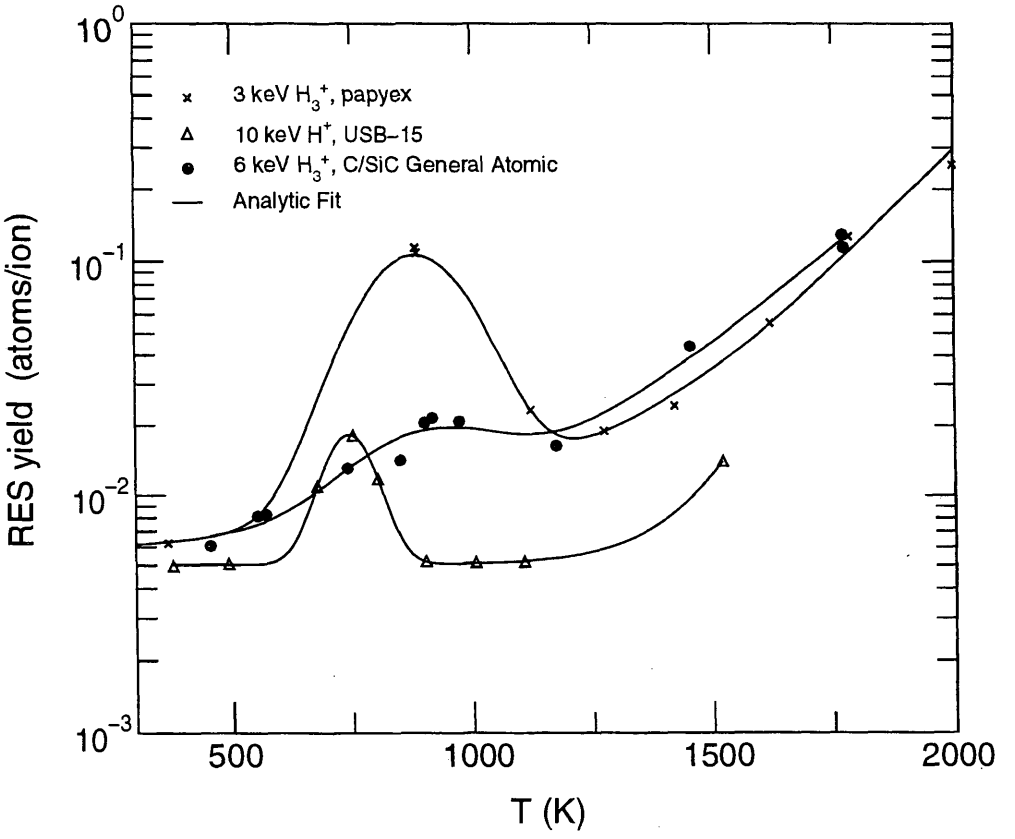

3.1.7 H_3^+, D_3^+, He^+ + graphite (Papyex) → C

Source: J. Roth, J. Bohdansky and K. L. Wilson, J. Nucl. Mater. **111&112**, 775 (1982).

Accuracy: Yield (abs.): ±15%; T: ±20K.

Comments: (1) Yield for total erosion measured by mass loss.
(2) Specimen: papyex graphite.
(3) H_3^+, D_3^+ and He^+ ions: mass-analyzed accelerator.

Analytic fitting:

Analytic fits for reactions A (x), B (o) and C (△).

Fitting parameters A_1-A_{10}

A	2.5000E-02	8.8000E+02	2.5000E+04	2.0000E-01	1.2000E-03	-3.0000E-03
	-2.0000E-01	1.1000E+04	2.2000E+04	5.2000E-03		
B	2.5000E-02	8.6000E+02	2.0000E+04	2.0000E-01	2.0000E-03	-3.4000E-03
	-2.0000E-01	9.0000E+03	2.2000E+04	1.9000E-02		
C	4.2473E+01	7.6560E+03	5.9328E-02			

ALADDIN hierarchical labelling and evaluation function:

A: RES H {3} [+1] GRAPHITE T=PAPYEX C [+0] #EYIELD10AN
B: RES D {3} [+1] GRAPHITE T=PAPYEX C [+0] #EYIELD10AN
C: RES He [+1] GRAPHITE T=PAPYEX C [+0] #EYIELD3BN

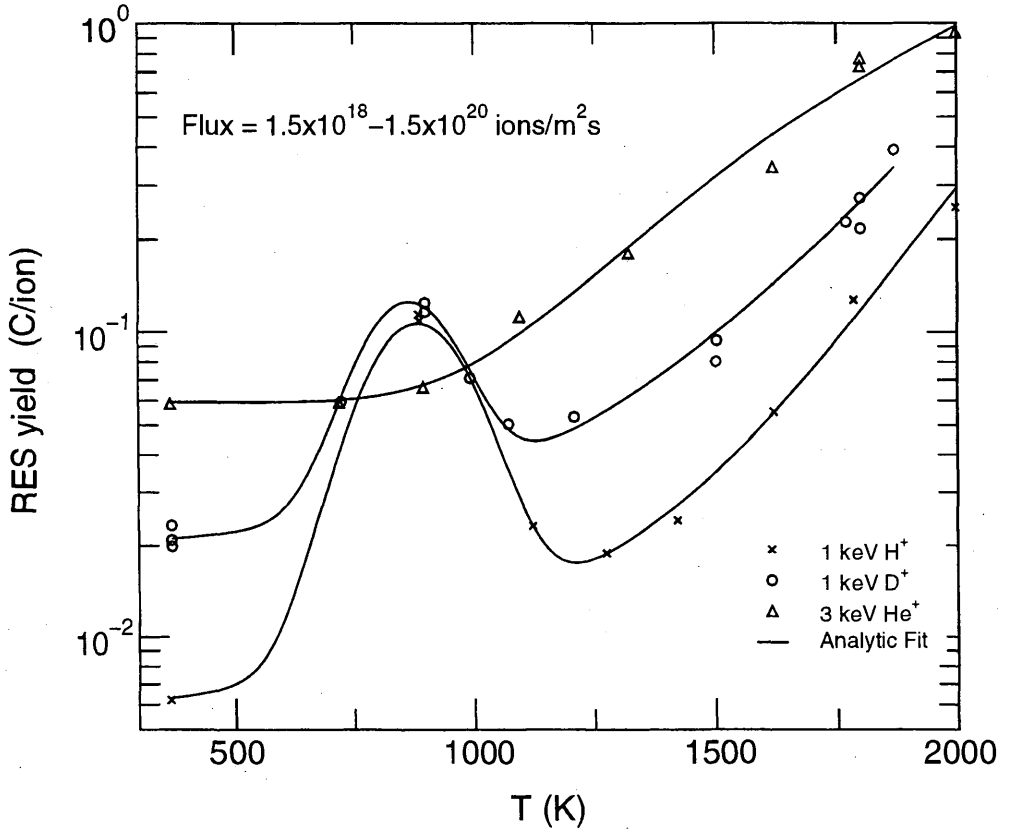

3.1.8 H_3^+ + graphite (HPG99) → C

Source: P. Franzen, J. W. Davis and A. A. Haasz, J. Appl. Phys. **78**, 817 (1995).

Accuracy: Yield (rel.): ±10%; T: ±25K.

Comments: (1) Specimen: HPG99 pyrolytic graphite (Union Carbide).
(2) Incident ion energy: 3 keV H_3^+ (1 keV/H^+); flux: 10^{19} ions/m^2s.
(3) Ions produced by a mass-analyzed ion accelerator.
(4) Absolute yields determined by comparison with mass-loss results in Roth et al., J. Nucl. Mater. **111&112** 775 (1982) and Roth et al., J. Nucl. Mater. **122&123** 1447 (1984).
(5) Carbon atoms were detected by phase-sensitive line-of-sight QMS.

Analytic fitting:

Analytic fit for reaction A (○).

Fitting parameters A_1-A_4

A	7.3831E-03	6.2811E+02	5.6638E+01	1.0906E+04

ALADDIN hierarchical labelling and evaluation function:

A: RES H {3} [+1] GRAPHITE T=HPG99 C [+0] #EYIELD4GN

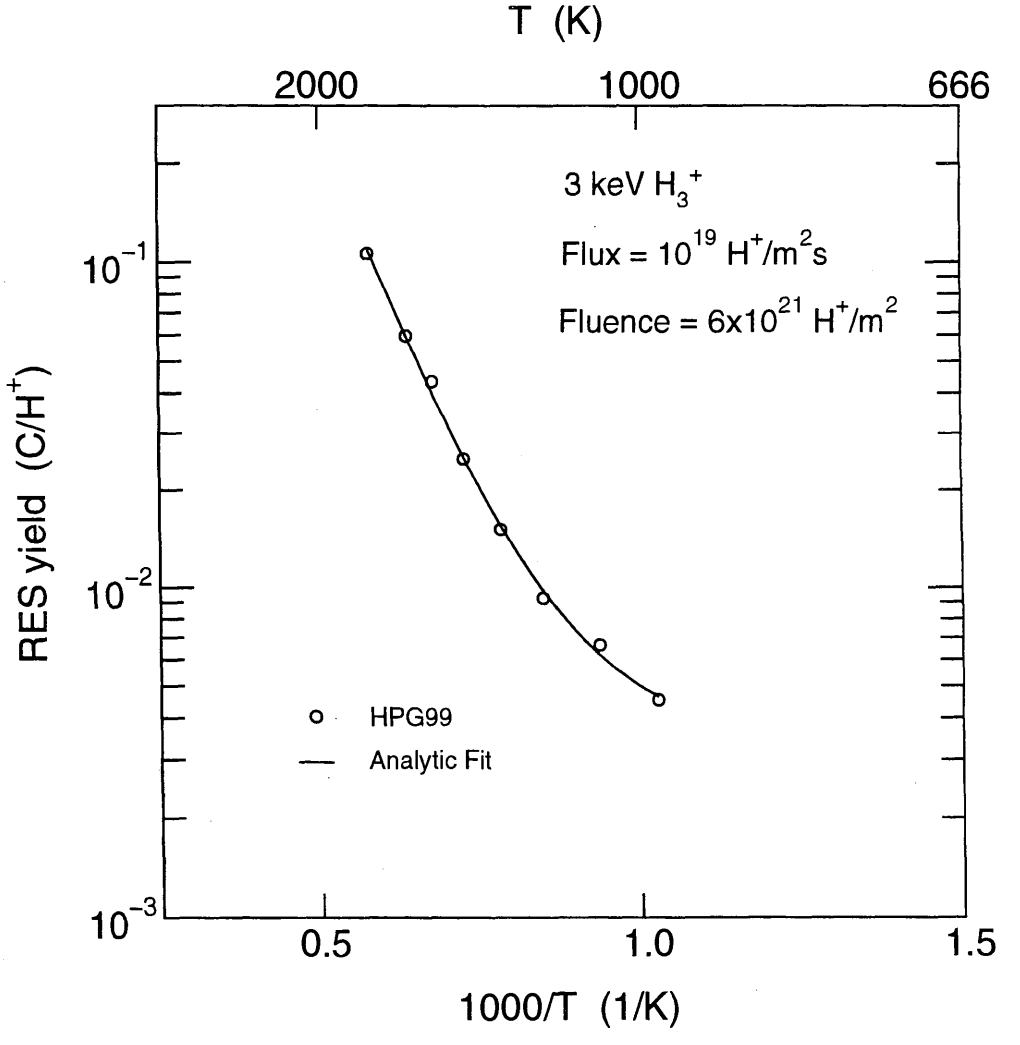

3.1.9 H_3^+ + graphite (HPG99, EK98, CKC base and edge planes) → C

Source: P. Franzen, J. W. Davis and A. A. Haasz, J. Appl. Phys. **78**, 817 (1995).

Accuracy: Yield (rel.): ±10%; T: ±25K.

Comments: (1) Specimens: HPG99 pyrolytic graphite (Union Carbide), EK98 isotropic graphite (Ringsdorff) and CKC isostatically compressed anisotropic graphite (CKC).
(2) Incident ion energy: 3 keV D_3^+ (1 keV/D^+); flux: 10^{19} ions/m^2s.
(3) Ions produced by a mass-analyzed ion accelerator.
(4) Carbon atoms were detected by phase-sensitive line-of-sight QMS.
(5) Absolute yields determined by comparison with mass-loss results in Roth et al., J. Nucl. Mater. **111&112** 775 (1982) and Roth et al., J. Nucl. Mater. **122&123** 1447 (1984).

Analytic fitting:

Analytic fits for reactions A (○), B (●), C (△) and D (▽). The data fits are from the paper.

Fitting parameters A_1-A_4

A	1.0342E-02	7.3760E+02	4.4800E+01	9.8988E+03
B	3.5216E-02	1.3726E+03	5.2192E+01	1.0850E+04
C	1.3522E-02	6.8370E+02	1.3010E+01	8.2105E+03
D	1.2373E-02	5.5060E+02	2.0715E+01	9.2716E+03

ALADDIN hierarchical labelling and evaluation function:

A: RES D {3} [+1] GRAPHITE T=HPG99 C [+0] #EYIELD4GN
B: RES D {3} [+1] GRAPHITE T=EK98 C [+0] #EYIELD4GN
C: RES D {3} [+1] GRAPHITE T=CKC O=BASE-PL C [+0] #EYIELD4GN
D: RES D {3} [+1] GRAPHITE T=CKC O=EDGE-PL C [+0] #EYIELD4GN

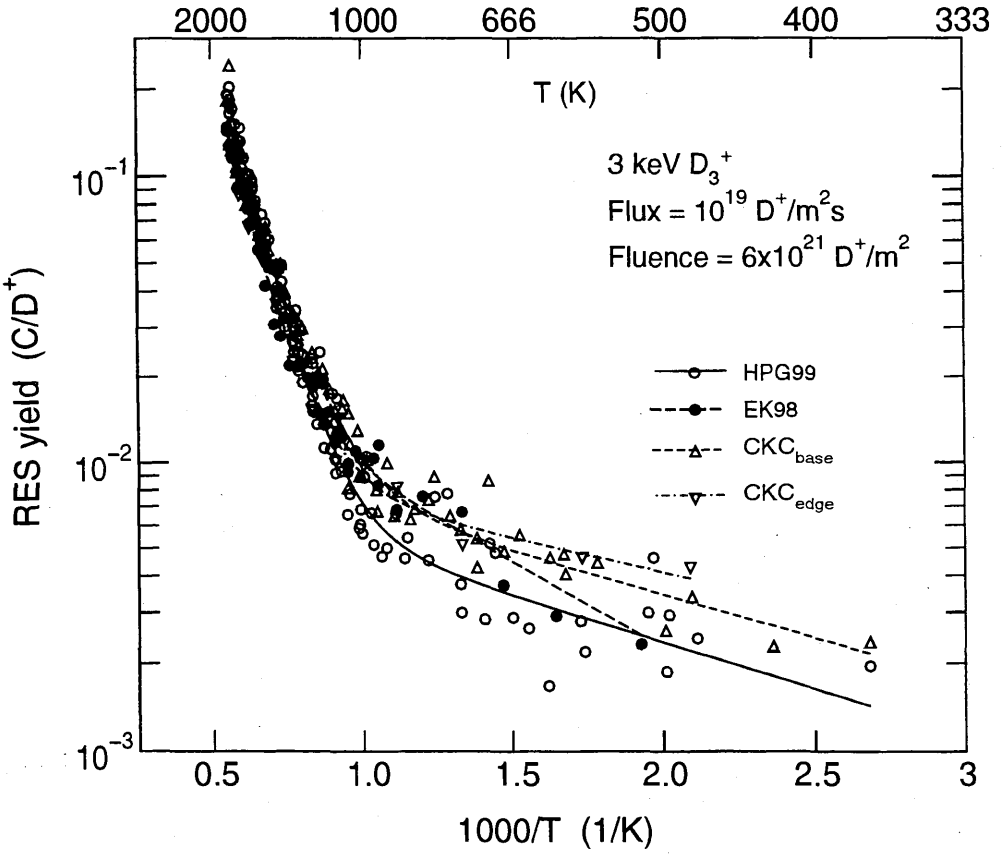

3.1.10 H_3^+ + graphite (HPG99, EK98, CKC base and edge planes) → C

Source: P. Franzen, J. W. Davis and A. A. Haasz, J. Appl. Phys. **78**, 817 (1995).

Accuracy: Yield (rel.): ±10%; T: ±25K.

Comments: (1) Specimens: HPG99 pyrolytic graphite (Union Carbide), EK98 isotropic graphite (Ringsdorff) and CKC isostatically compressed anisotropic graphite (CKC).
(2) Incident ion energy: 3 keV D_3^+ (1 keV/D^+); flux: 10^{19} ions/m^2s.
(3) Ions produced by a mass-analyzed ion accelerator.
(4) Carbon atoms were detected by phase-sensitive line-of-sight QMS.
(5) Absolute yields determined by comparison with mass-loss results in Roth et al., J. Nucl. Mater. **111&112** 775 (1982) and Roth et al., J. Nucl. Mater. **122&123** 1447 (1984).

Analytic fitting:

The analytic fits for reactions A (○), B (●), C (△) and D (▽) are have been replotted using data from the preceeding page. The data fits are from the paper.

Fitting parameters A_1-A_4

A	1.0342E-02	7.3760E+02	4.4800E+01	9.8988E+03
B	3.5216E-02	1.3726E+03	5.2192E+01	1.0850E+04
C	1.3522E-02	6.8370E+02	1.3010E+01	8.2105E+03
D	1.2373E-02	5.5060E+02	2.0715E+01	9.2716E+03

ALADDIN hierarchical labelling and evaluation function:

A: RES D {3} [+1] GRAPHITE T=HPG99 C [+0] #EYIELD4GN
B: RES D {3} [+1] GRAPHITE T=EK98 C [+0] #EYIELD4GN
C: RES D {3} [+1] GRAPHITE T=CKC O=BASE-PL C [+0] #EYIELD4GN
D: RES D {3} [+1] GRAPHITE T=CKC O=EDGE-PL C [+0] #EYIELD4GN

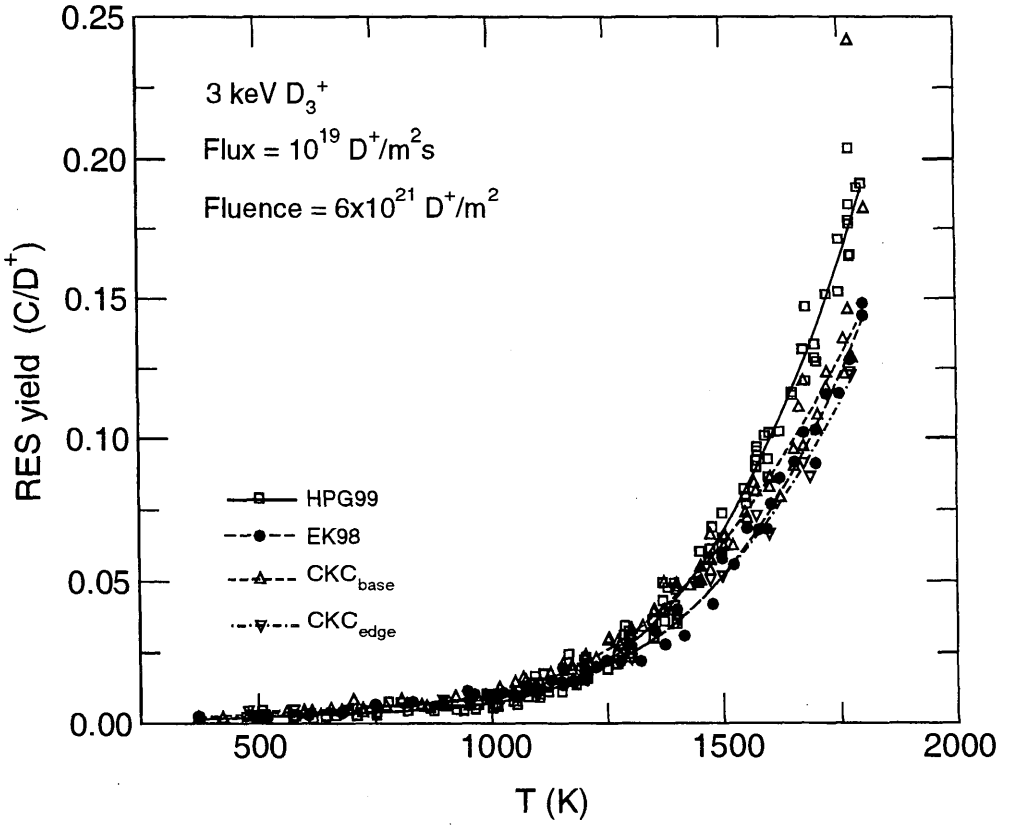

3.1.11 H_3^+ + graphite (IG-110U, ISO-880U, ISO-630U) → C

Source: T. Hino, T. Yamashina, S. Fukuda and Y. Takasugi, J. Nucl. Mater. **186**, 54 (1991).

Accuracy: Yield (rel.): Indeterminate.

Comments: (1) Yield for total erosion measured by mass loss.
(2) Specimens: isotropic graphites IG-110U, ISO-630U and ISO-880U.
(3) H_3^+ ions: mass-analyzed accelerator.

Analytic fitting:

Analytic fits for reactions A (○), B (△) and C (+).

Fitting parameters A_1-A_8

A	3.4312E+00	8.0413E+02	1.7692E+04	-5.0173E-01	3.6720E-02	-3.3344E-03
	-6.4994E-01	6.9794E-03				
B	3.7894E+02	1.5913E+04	3.8427E-02			
C	4.8665E+00	7.7540E+03	3.7173E-02			

ALADDIN hierarchical labelling and evaluation function:

A: RES H {3} [+1] GRAPHITE T=IG-110U C [+0] #EYIELD8CN
B: RES H {3} [+1] GRAPHITE T=ISO-880U C [+0] #EYIELD3BN
C: RES H {3} [+1] GRAPHITE T=ISO-630U C [+0] #EYIELD3BN

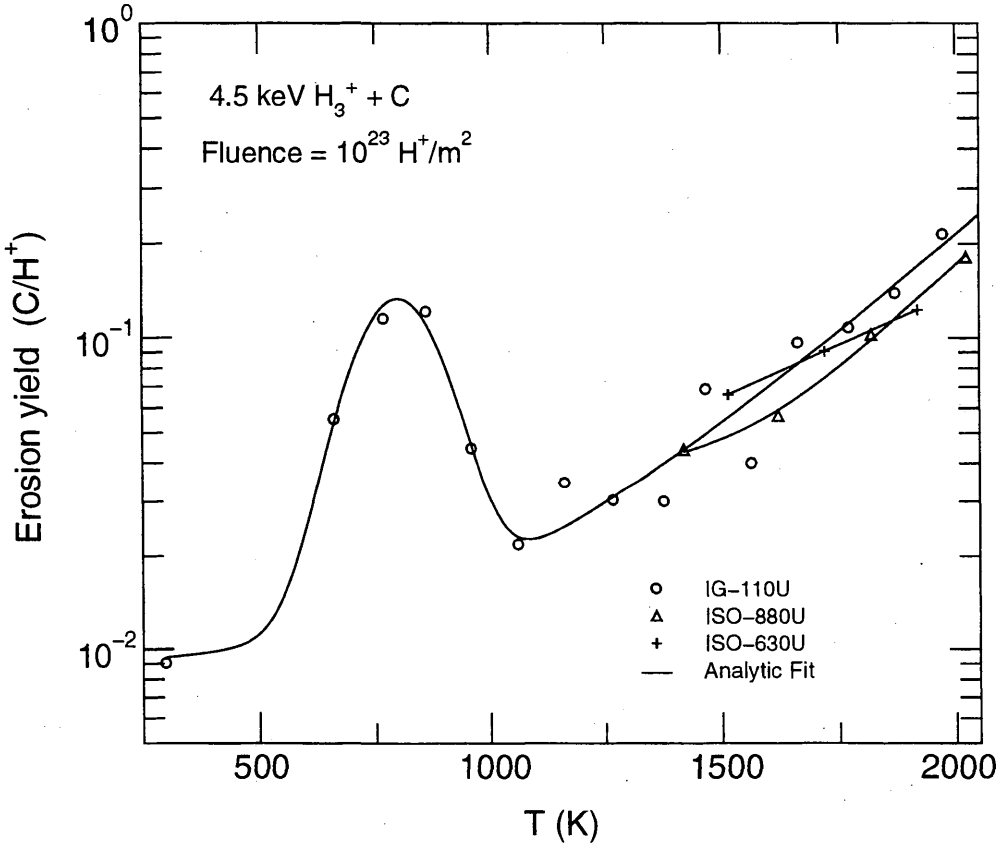

3.1.12 H_3^+ + graphite (IG-110U, ISO-630U, ISO-890U, CX-2002U, pyroid) → C

Source: T. Hino and T. Yamashina, J. Nucl. Mater. **196&198**, 531 (1992).

Accuracy: Yield (rel.): Indeterminate.

Comments: (1) Yield for total erosion measured by mass loss.
(2) Specimens: isotropic graphites IG-110U, ISO-630U and ISO-880U; pyrolytic graphite "pyroid"; carbon/carbon composite CX-2002U; and boron-doped graphites, 1, 3, 20 at% (GB-series, Toyo Tanso).
(3) H_3^+ ions: mass-analyzed accelerator.

Analytic fitting:

The analytic fit is taken from the source.

Fitting parameters A_1-A_2

1.1334E+01	7.0950E-01

ALADDIN hierarchical labelling and evaluation function:

RES H {3} [+1] GRAPHITE T=VARIOUS C [+0] #EYIELD2E

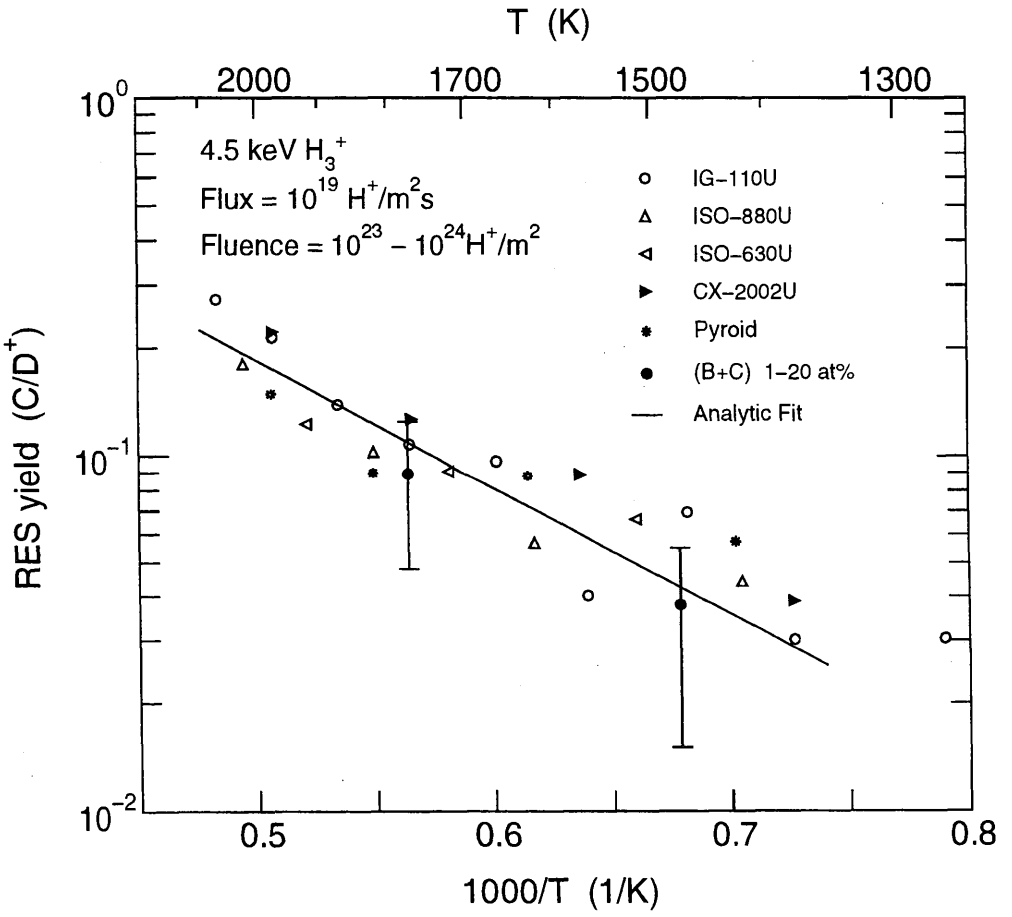

3.1.13 H_3^+ + graphite (GB-100, GB-103, GB-110, GB-120) → C

Source: T. Hino, K. Ishio, Y. Hirohata, T. Yamashina, T. Sogabe, M. Okada and K. Kuroda, J. Nucl. Mater. **211**, 30 (1994).

Accuracy: Yield (rel.): Indeterminate.

Comments: (1) Yield for total erosion measured by mass loss.
(2) Specimens: boron-doped isotropic graphites, 3, 10 and 20 at% B (GB-series, Toyo Tanso).
(3) H_3^+ ions: mass-analyzed accelerator.

Analytic fitting:

Analytic fits for reactions A (•), B (△) and C (∗).

Fitting parameters A_1-A_8

A	3.2115E-03	8.3386E+02	2.2572E+04	5.2248E-01	6.3217E-08	-2.4231E-03
	1.3657E+00	8.6000E-03				
B	1.3886E-02	8.5901E+02	4.3371E+04	1.1841E-01	1.6328E-02	7.5147E+03
	8.1519E-01	4.7862E-03				
C	2.7964E-01	5.9690E+02	2.2347E+05	-1.1160E-01	2.1656E-04	-2.6917E-04
	9.2115E-01	-2.1320E-01				

ALADDIN hierarchical labelling and evaluation function:

A: RES H {3} [+1] GRAPHITE T=GB-100 C [+0] #EYIELD8CN
B: RES H {3} [+1] GRAPHITE T=GB-103 C [+0] #EYIELD8DN
C: RES H {3} [+1] GRAPHITE T=GB-120 C [+0] #EYIELD8CN

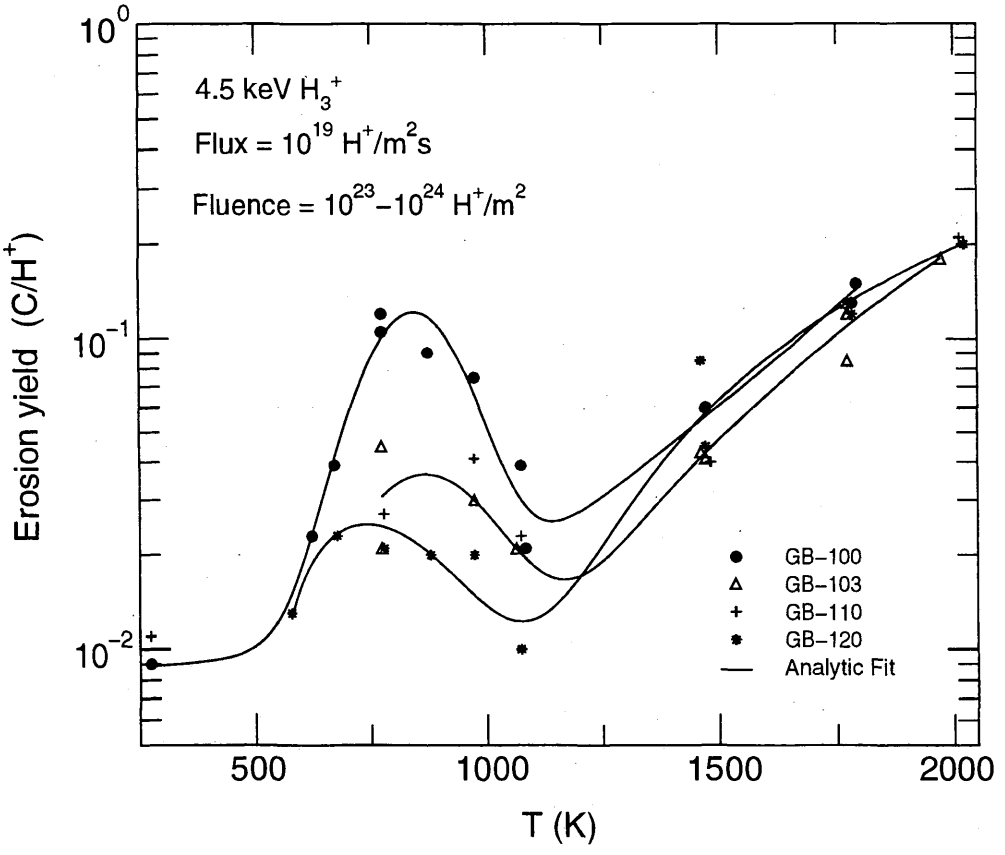

3.1.14 H_3^+ + graphite (V doped) → C

Source: T. Hino, K. Ishio, Y. Hirohata, T. Yamashina, T. Sogabe, M. Okada and K. Kuroda, J. Nucl. Mater. **211**, 30 (1994).

Accuracy: Yield (rel.): Indeterminate.

Comments: (1) Yield for total erosion measured by mass loss.
(2) Specimens: vanadium-doped isotropic graphites (TC-series, Toyo Tanso).
(3) H_3^+ ions: mass-analyzed accelerator.

Analytic fitting:

Analytic fits for reactions A (+) and B (▷).

Fitting parameters A_1-A_2

A	9.2129E+00	7.7439E+03
B	3.5175E+01	9.0392E+03

ALADDIN hierarchical labelling and evaluation function:

A: RES H {3} [+1] GRAPHITE T=PYG C [+0] #EYIELD2EN
B: RES H {3} [+1] GRAPHITE T=PYG D=V C [+0] #EYIELD2EN

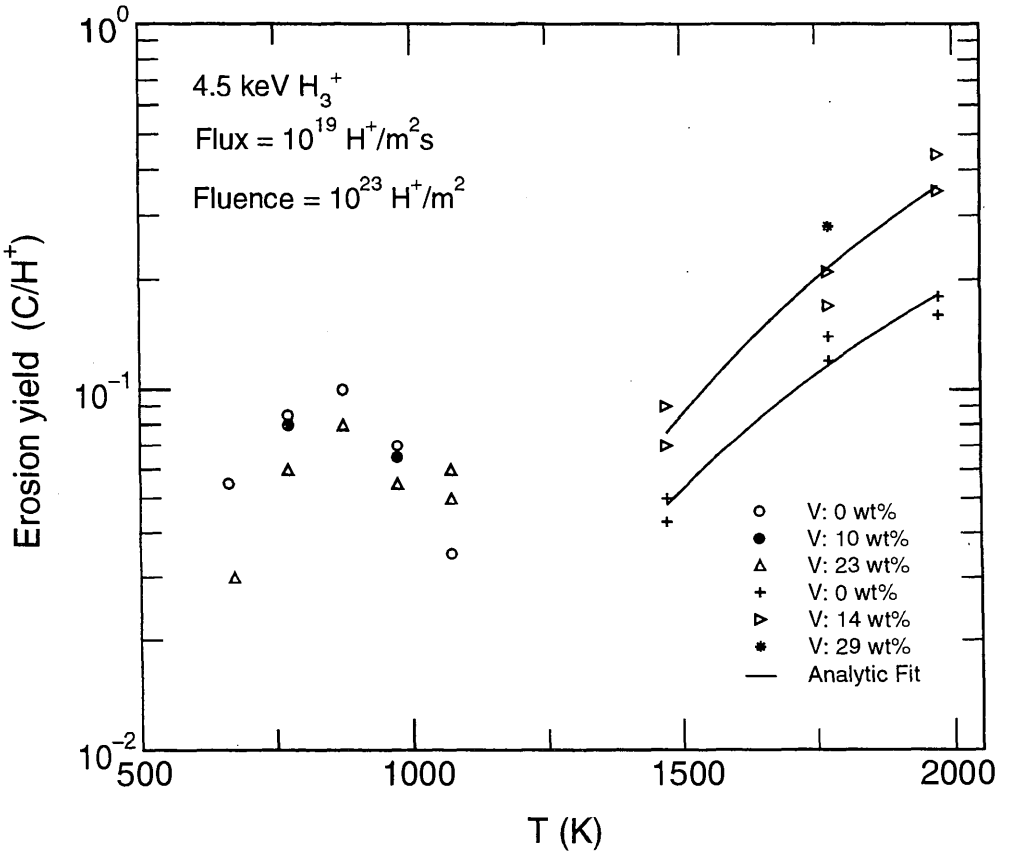

3.1.15 D^+ + graphite (pyrolytic, GB-100, GB-110, GB-120, GB-130, CCB-407) → C

Source: Y. Hirooka, R. W. Conn, R. Causey, D. Croessman, R. Doerner, D. Holland, M. Khandagle, T. Matsuda, G. Smolik, T. Sogabe, J. Whitley and K. Wilson, J. Nucl. Mater. **176&177**, 473 (1990).

Accuracy: Yield (rel.): ±10%-15%.

Comments: (1) Weight loss measurements.
(2) Specimens: bulk-boronized graphites and CC composites (Toyo Tanso).
(3) Minimal redeposition effects (i.e. low T_e, n_e).
(4) A factor of 2-3 reduction found for bulk-boronized graphite only.
(5) High intensity staedy-state plasma source.

Analytic fitting:

Analytic fits for reactions A (○, ∗, x) and B (•, △, ▽).

Fitting parameters A_1-A_8

A	1.0417E+77	1.1871E+03	2.4859E+04	-2.6152E+01	1.5300E-09	-7.5011E-03
	7.2562E-01	4.3324E-03				
B	1.1356E+46	1.1698E+03	4.0220E+04	-1.5996E+01	1.6318E+00	-9.9105E-03
	-2.7381E+00	3.4818E-04				

ALADDIN hierarchical labelling and evaluation function:

A-B: RES He [+1] GRAPHITE T=VARIOUS C [+0] #EYIELD8CN

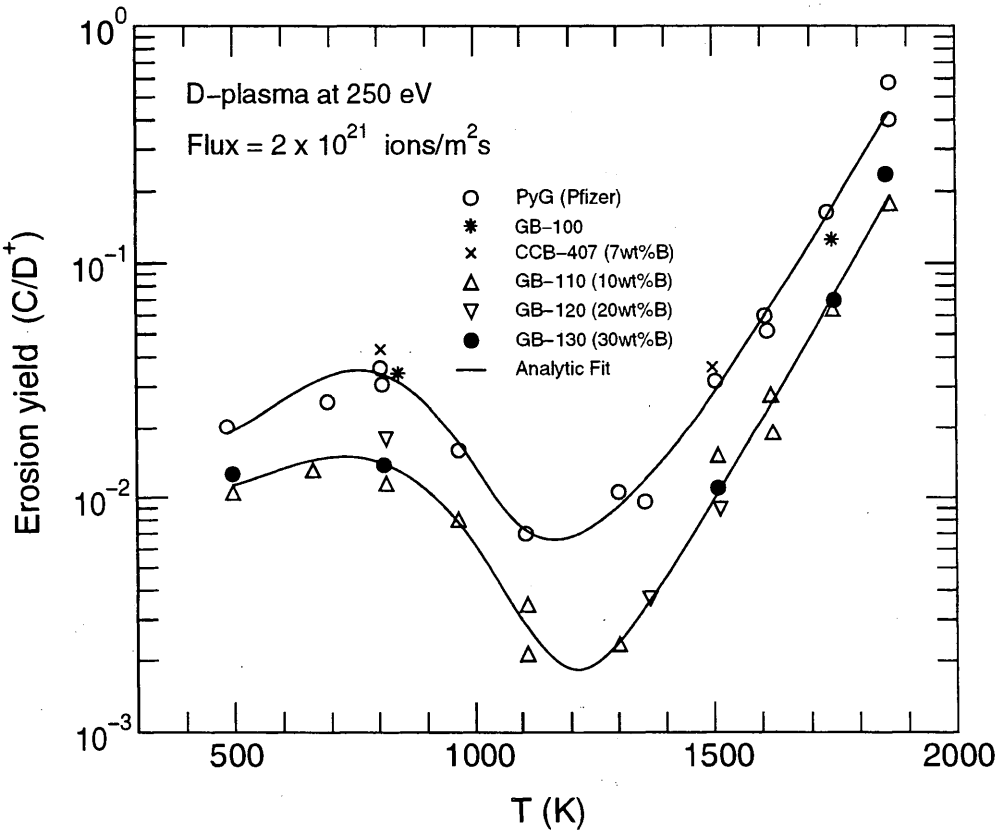

3.1.16 D_3^+ + graphite (pyrolytic, USB-15, GB-120), $B_4C \rightarrow C$

Source: C. Garcia-Rosales, E. Gauthier, J. Roth, R. Schwörer and W. Eckstein, J. Nucl. Mater. **189**, 1 (1992).

Accuracy: Yield (abs.): ±15%, T: ±20K.

Comments: (1) Total erosion yields determined by mass loss.
(2) Specimens: pyrolytic graphite, B_4C, USB-15 boron-doped graphite, and GB120 boron-doped graphite.
(3) D_3^+ ions: mass-analyzed accelerator.

Analytic fitting:

Analytic fits for reactions A (•), B (+), C (◇) and D (△, ▽).

Fitting parameters A_1-A_5

A	3.3680E+02	1.2404E+04	4.5321E-02		
B	1.8728E+00	5.9322E+03	5.2174E+09	4.2715E+04	3.6763E-02
C	2.5404E+05	2.3346E+04	4.7389E-02		
D	1.2178E-35	4.3669E-02	3.4127E-02	8.2830E+02	1.8676E-02

ALADDIN hierarchical labelling and evaluation function:

A: RES D [+1] GRAPHITE T=PYG C [+0] #EYIELD3BN
B: RES D [+1] GRAPHITE T=USB C [+0] #EYIELD5BN
C: RES D [+1] GRAPHITE T=GB C [+0] #EYIELD3BN
D: RES D [+1] B{4}C C [+0] #EYIELD5EN

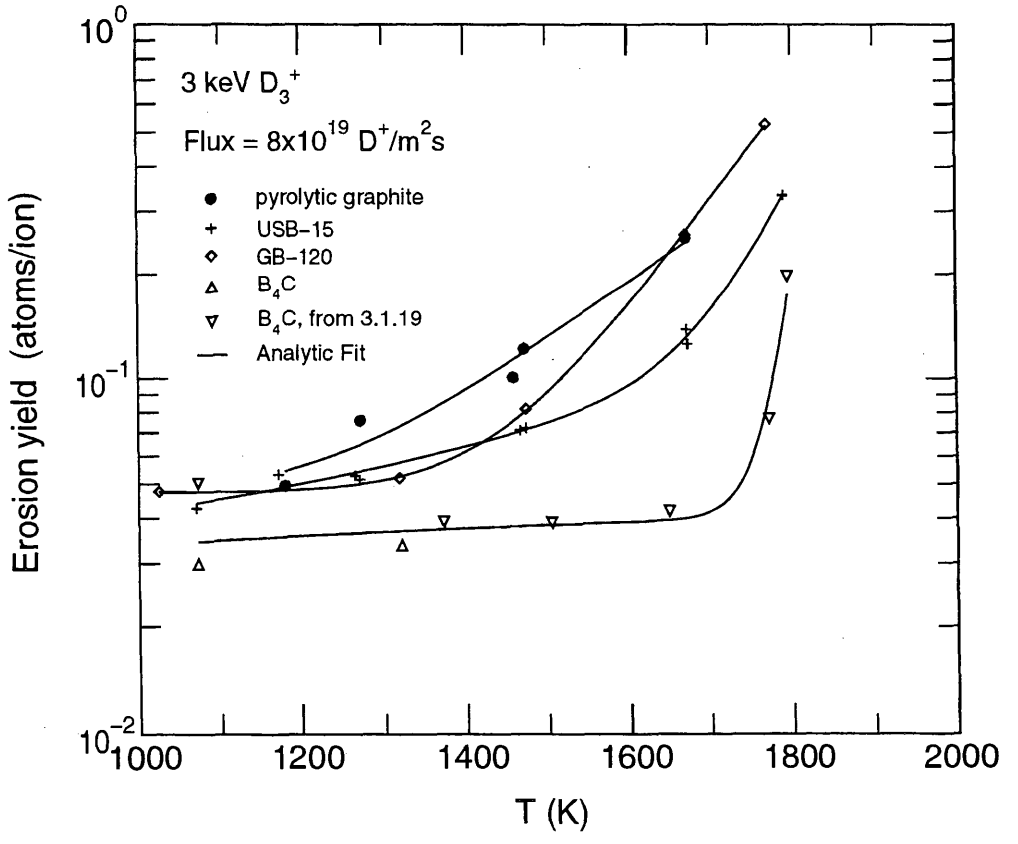

3.1.17 D^+ + graphite (diamond, pyrolytic, various B doped) → C

Source: J. Roth, C. Garcia-Rosales, R. Behrisch and W. Eckstein, J. Nucl. Mater. **191-194**, 45 (1992).

Accuracy: Yield (abs.): ±15%, T: ±20 K.

Comments:
(1) Total erosion yields determined by mass loss.
(2) D^+ ions: mass-analyzed accelerator.
(3) Comparison of erosion yield for diamond, pyrolytic graphite and boron containing materials at three temperatures.
(4) All erosion data is compiled from values given in Table 1 of the source.
(5) The data was originally presented in C. Garcia-Rosales et al., J. Nucl. Mater. **189**, 1 (1992).

Analytic fitting:

Not fitted.

ALADDIN hierarchical labelling and evaluation function:

A-O: RES D [+1] GRAPHITE T=type C [+0] #TAB2D

where 'type' = DIAMOND, PYG, CX-2002, GB100, DPE, S2508, SEP-CFC, GB110, USB15, GB120, GB130, S1325, M019AII, B4C-CL5890, and B4C.

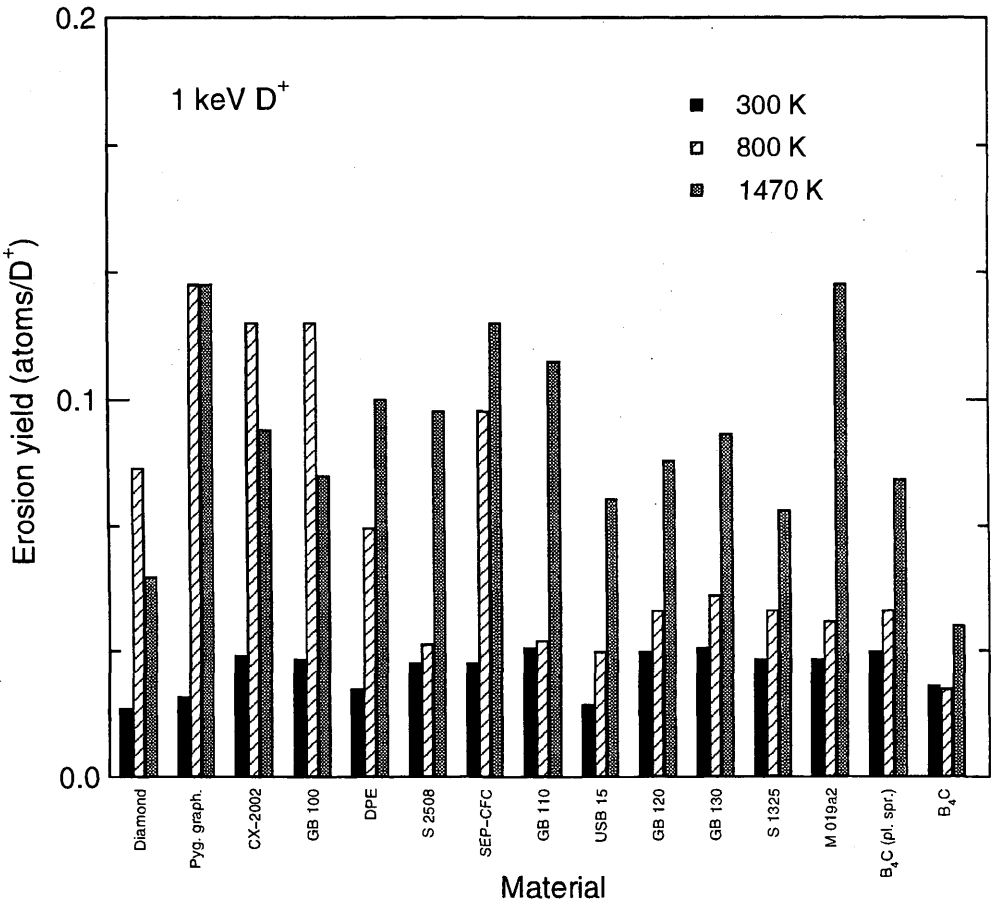

3.1.18 D^+, C^+ + graphite (pyrolytic) → C

Source: J. Roth, J. Bohdansky and W. Ottenberger, J. Nucl. Mater. **165**, 193 (1989).

Accuracy: Yield (abs.): ±15%, T: ±20K.

Comments: (1) Yields determined by the mass change of target.
(2) Specimen: pyrolytic graphite.
(3) D^+ and C^+ ions: mass-analyzed accelerator.

Analytic fitting:

Analytic fits for reactions A (+), B (○), C (△), D (▷), E (•) and F (x). The data point for C^+ at 100 eV (∗) is (T, Y) = (1857, 0.91).

Fitting parameters A_1-A_3

A	9.0026E+01	1.2631E+04	6.5995E-03
B	2.5529E+01	9.4504E+03	3.9732E-02
C	1.4701E+01	7.2232E+03	
D	7.7508E+00	3.5894E+03	
E	1.1493E+02	6.9603E+03	
F	2.3016E+03	1.2303E+04	8.0619E-01

ALADDIN hierarchical labelling and evaluation function:

A: RES D [+1] GRAPHITE T=PYG C [+0] #EYIELD3BN
B: RES D [+1] GRAPHITE T=PYG C [+0] #EYIELD3BN
C: RES D [+1] GRAPHITE T=PYG C [+0] #EYIELD2EN
D: RES C [+1] GRAPHITE T=PYG C [+0] #EYIELD2EN
E: RES C [+1] GRAPHITE T=PYG C [+0] #EYIELD2EN
F: RES C [+1] GRAPHITE T=PYG C [+0] #EYIELD3BN

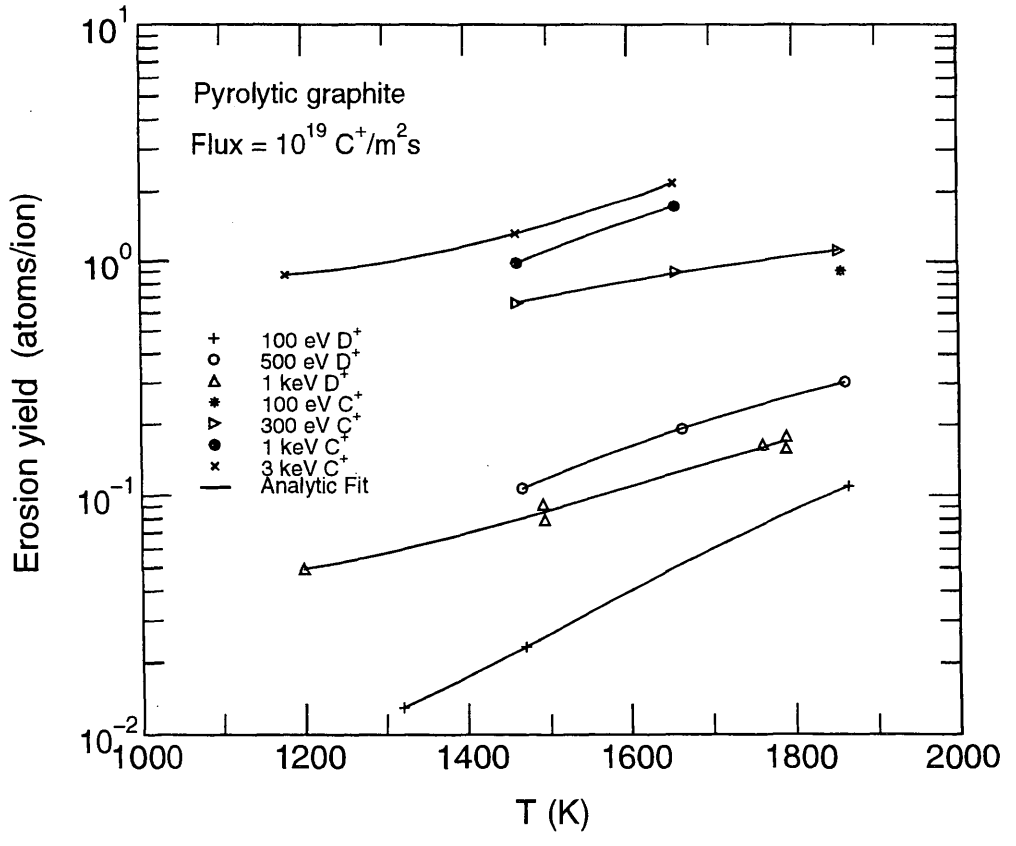

3.1.19 D^+, C^+ + graphite, $B_4C \rightarrow C$

Source: E. Gauthier, W. Eckstein, J. László and J. Roth, J. Nucl. Mater. **176&177**, 438 (1990).

Accuracy: Yield (abs.): ±15%, T: ±20K.

Comments: (1) Yields determined by the mass change of target.
(2) The 1 keV D^+ on graphite results are from the source of 3.1.7.
(3) Specimens: pyrolytic graphite and USB-15 boron-doped graphite.
(4) D_3^+ and C^+ ions: mass-analyzed accelerator.

Analytic fitting:

Analytic fits for reactions A (△) and B (○, +).

Fitting parameters A_1-A_8

A	2.2189E-06	8.6770E+02	3.7113E+05	1.3615E+00	3.3999E-16	-2.3704E-02
	-1.2559E+00	2.1979E-02				
B	3.0022E+02	8.7726E+03	1.4463E+00			

ALADDIN hierarchical labelling and evaluation function:

A: RES D {3} [+1] B{4}C C [+0] #EYIELD8CN
B: RES C [+1] GRAPHITE C [+0] #EYIELD3BN

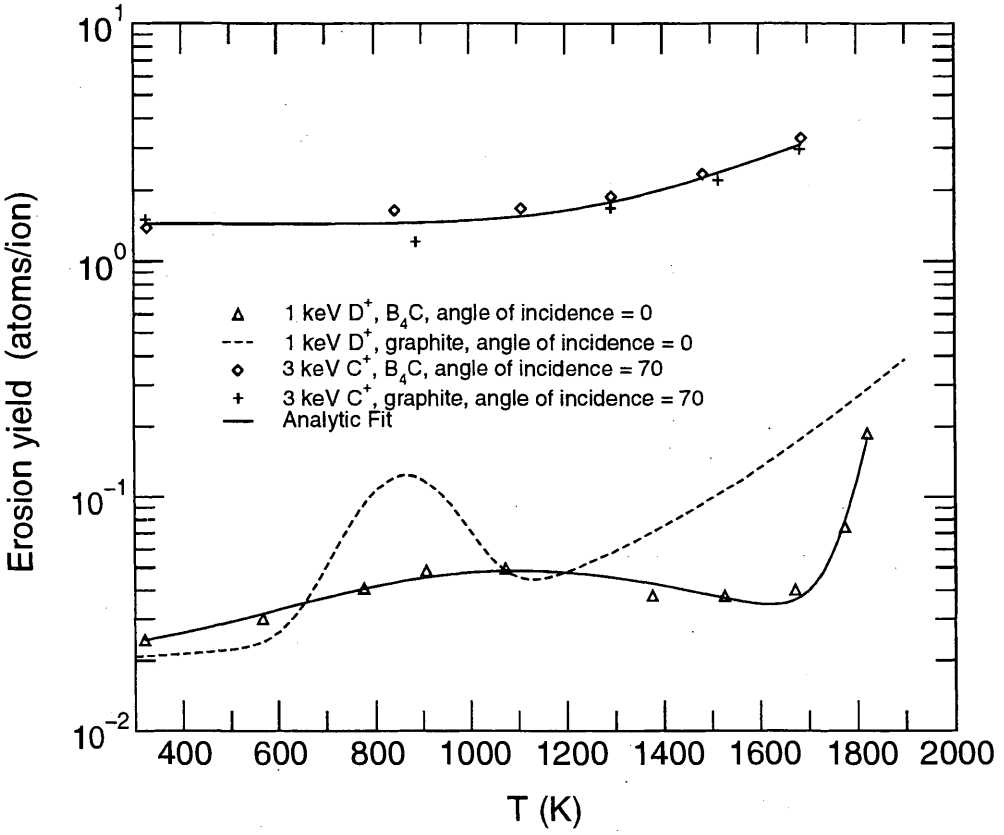

3.1.20 D_3^+ + graphite (pyrolytic, RG-Ti91, USB-15) → C

Source: C. Garcia-Rosales, J. Roth and R. Behrisch, J. Nucl. Mater. **212-215**, 1211 (1992).

Accuracy: Yield (abs.): ±15%, T: ±20K.

Comments: (1) Total erosion yields determined by mass loss.
(2) Specimen: RG-Ti91 titanium-doped graphite (1.7 at% Ti).
(3) D_3^+ ions: mass-analyzed accelerator.
(4) The PG and USB15 results are from 3.1.16.

Analytic fitting:

Analytic fit for reaction A (•). The dashed curves are data taken from reaction 3.1.17.

Fitting parameters A_1-A_3

8.3185E-07	7.1298E-03	5.7514E-02

ALADDIN hierarchical labelling and evaluation function:

A: RES D {3} [+1] GRAPHITE T=RG-Ti91 C [+0] #EYIELD3CN

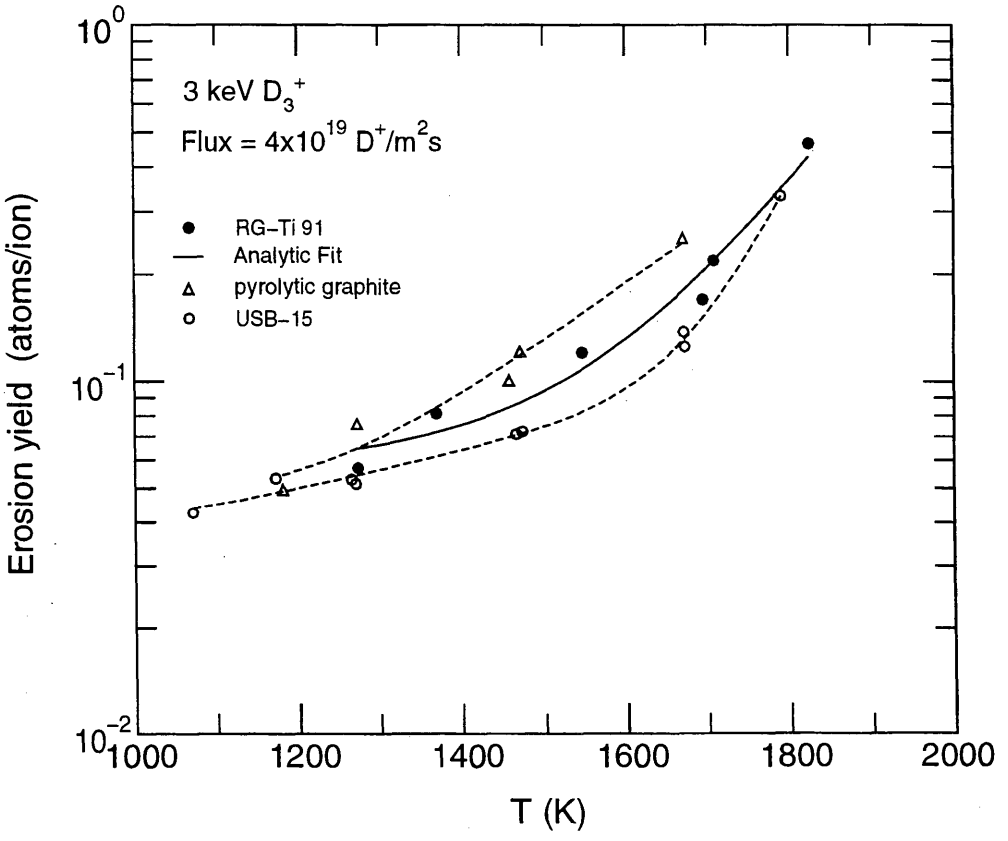

3.1.21 D_3^+ + graphite (CKC-Si, base plane) → C

Source: P. Franzen, A. A. Haasz and J. W. Davis, J. Nucl. Mater. **226**, 15 (1995).

Accuracy: Yield (rel.): ±10%; T: ±25K.

Comments: (1) Specimens: Si-doped CKC isostatically compressed anisotropic graphite (CKC), base orientation (cut parallel to graphite planes). Bulk concentrations: 3.0, 7.5 and 14.0 at% Si, corresponding to surface concentrations of 0.7, 1.9 and 3.8 at% Si.
(2) Incident ion energy: 3 keV D_3^+ (1 keV/D^+); flux: 10^{19} ions/m^2s.
(3) Ions produced by a mass-analyzed ion accelerator.
(4) Carbon atoms were detected by phase-sensitive line-of-sight QMS
(5) Absolute yields for pure graphites determined by comparison with mass-loss results in Roth et al., J. Nucl. Mater. **111&112** 775 (1982) and Roth et al., J. Nucl. Mater. **122&123** 1447 (1984).

Analytic fitting:

Analytic fits for reactions A (○), B (△) and C (▽). The data and fit for zero doping is given in reaction 3.1.9. Data fits are from the paper.

Fitting parameters A_1-A_4

A	3.6077E-02	1.3958E+03	3.5248E+01	1.0232E+04
B	1.7056E-02	7.7404E+02	6.5277E+01	1.1469E+04
C	1.7827E-02	8.9553E+02	1.7900E+01	9.7146E+03

ALADDIN hierarchical labelling and evaluation function:

A-C: RES D [+1] GRAPHITE T=CKC D=Si O=BASE-PL C [+0] #EYIELD4GN

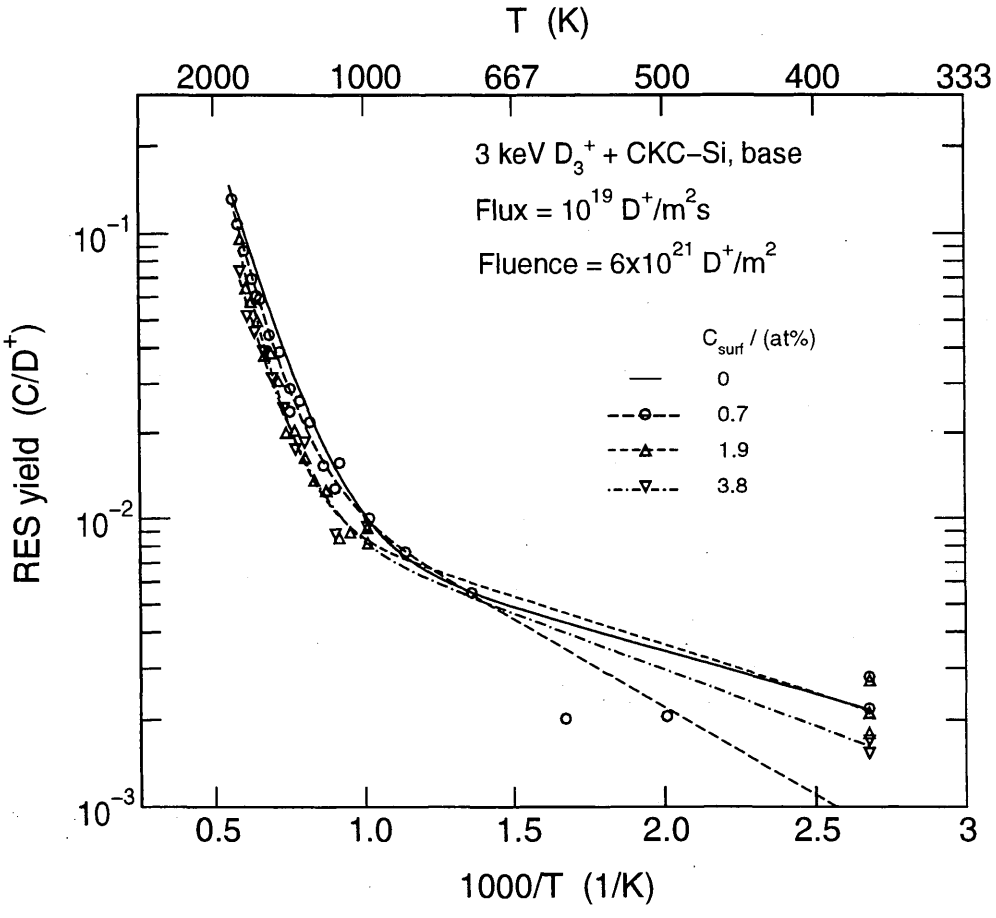

3.1.22 D_3^+ + graphite (CKC-Si, base plane) → C

Source: P. Franzen, A. A. Haasz and J. W. Davis, J. Nucl. Mater. **226**, 15 (1995).

Accuracy: Yield (rel.): ±10%; T: ±25K.

Comments: (1) Specimens: Si-doped CKC isostatically compressed anisotropic graphite (CKC), base orientation (cut parallel to graphite planes). Bulk concentrations: 3.0, 7.5 and 14.0 at% Si, corresponding to surface concentrations of 0.7, 1.9 and 3.8 at% Si.
(2) 3 keV D_3^+ (1 keV/D^+); flux: 10^{19} ions/m^2s.
(3) Ions produced by a mass-analyzed ion accelerator.
(4) Carbon atoms were detected by phase-sensitive line-of-sight QMS.
(5) Absolute yields for pure graphites determined by comparison with mass-loss results in Roth et al., J. Nucl. Mater. **111&112** 775 (1982) and Roth et al., J. Nucl. Mater. **122&123** 1447 (1984).

Analytic fitting:

The analytic fits for reactions A (○), B (△) and C (▽) have been replotted using data from the preceeding page. The data and fit for zero doping is given in reaction 3.1.10. Data fits are from the paper.

Fitting parameters A_1-A_4

A	3.6077E-02	1.3958E+03	3.5248E+01	1.0232E+04
B	1.7056E-02	7.7404E+02	6.5277E+01	1.1469E+04
C	1.7827E-02	8.9553E+02	1.7900E+01	9.7146E+03

ALADDIN hierarchical labelling and evaluation function:

A-C: RES D [+1] GRAPHITE T=CKC D=Si O=BASE-PL C [+0] #EYIELD4GN

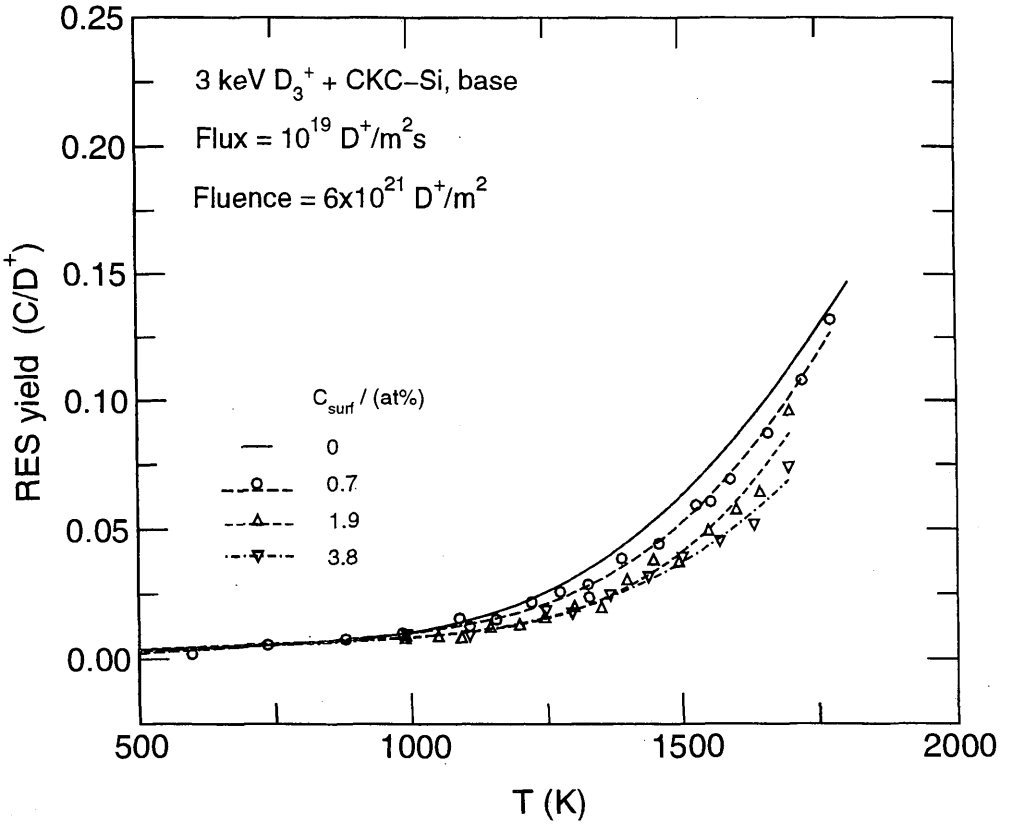

3.1.23 D_3^+ + graphite (CKC-B, base plane) → C

Source: P. Franzen, A. A. Haasz and J. W. Davis, J. Nucl. Mater. **226**, 15 (1995).

Accuracy: Yield (rel.): ±10%; T: ±25K.

Comments: (1) Specimens: B-doped CKC isostatically compressed anisotropic graphite (CKC), base orientation (cut parallel to graphite planes). Bulk concentrations: 2.0, 9.4 and 20.1 at% B, corresponding to surface concentrations of 1.2, 7.9 and 13.8 at% B.
(2) 3 keV D_3^+ (1 keV/D^+); flux: 10^{19} ions/m^2s.
(3) Ions produced by a mass-analyzed ion accelerator.
(4) Carbon atoms were detected by phase-sensitive line-of-sight QMS.
(5) Absolute yields for pure graphites determined by comparison with mass-loss results in Roth et al., J. Nucl. Mater. **111&112** 775 (1982) and Roth et al., J. Nucl. Mater. **122&123** 1447 (1984).

Analytic fitting:

Analytic fits for reactions A (○), B (△) and C (▽). The data and fit for zero doping is given in reaction 3.1.9. Data fits are from the paper.

Fitting parameters A_1-A_4

A	2.0880E-02	7.3737E+02	6.6987E+01	1.0422E+04
B	4.6878E-03	3.8904E+02	6.3331E+00	8.0901E+03
C	5.3678E-03	2.7007E+02	1.9275E+00	6.2243E+03

ALADDIN hierarchical labelling and evaluation function:

A-C: RES D [+1] GRAPHITE T=CKC D=B O=BASE-PL C [+0] #EYIELD4GN

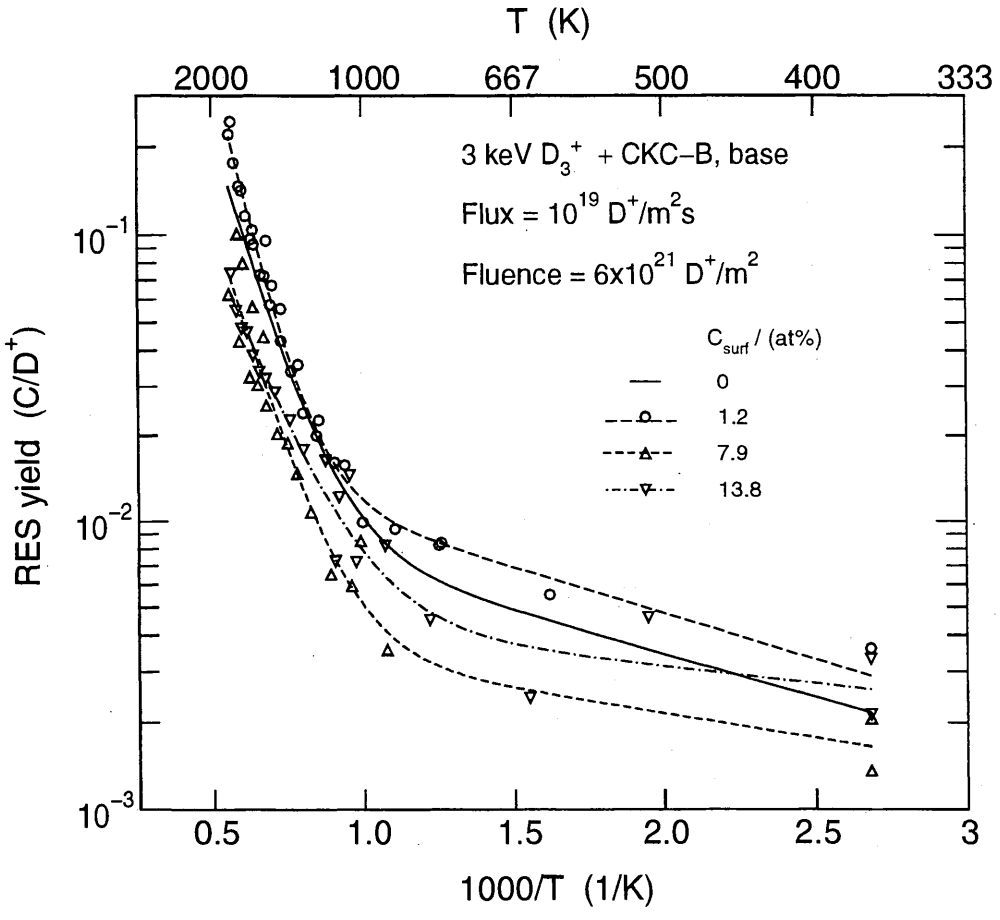

3.1.24 D_3^+ + graphite (CKC-B, base plane) → C

Source: P. Franzen, A. A. Haasz and J. W. Davis, J. Nucl. Mater. **226**, 15 (1995).

Accuracy: Yield (rel.): ±10%; T: ±25K.

Comments: (1) Specimens: B-doped CKC isostatically compressed anisotropic graphite (CKC), base orientation (cut parallel to graphite planes). Bulk concentrations: 2.0, 9.4 and 20.1 at% B, corresponding to surface concentrations of 1.2, 7.9 and 13.8 at% B.
(2) 3 keV D_3^+ (1 keV/D^+); flux: 10^{19} ions/m^2s.
(3) Ions produced by a mass-analyzed ion accelerator.
(4) Carbon atoms were detected by phase-sensitive line-of-sight QMS.
(5) Absolute yields for pure graphites determined by comparison with mass-loss results in Roth et al., J. Nucl. Mater. **111&112** 775 (1982) and Roth et al., J. Nucl. Mater. **122&123** 1447 (1984).

Analytic fitting:

The analytic fits for reactions A (○), B (△) and C (▽) have been replotted using data from the preceeding page. The data and fit for zero doping is given in reaction 3.1.10. Data fits are from the paper.

Fitting parameters A_1-A_4

A	2.0880E-02	7.3737E+02	6.6987E+01	1.0422E+04
B	4.6878E-03	3.8904E+02	6.3331E+00	8.0901E+03
C	5.3678E-03	2.7007E+02	1.9275E+00	6.2243E+03

ALADDIN hierarchical labelling and evaluation function:

A-C: RES D [+1] GRAPHITE T=CKC D=B O=BASE-PL C [+0] #EYIELD4GN

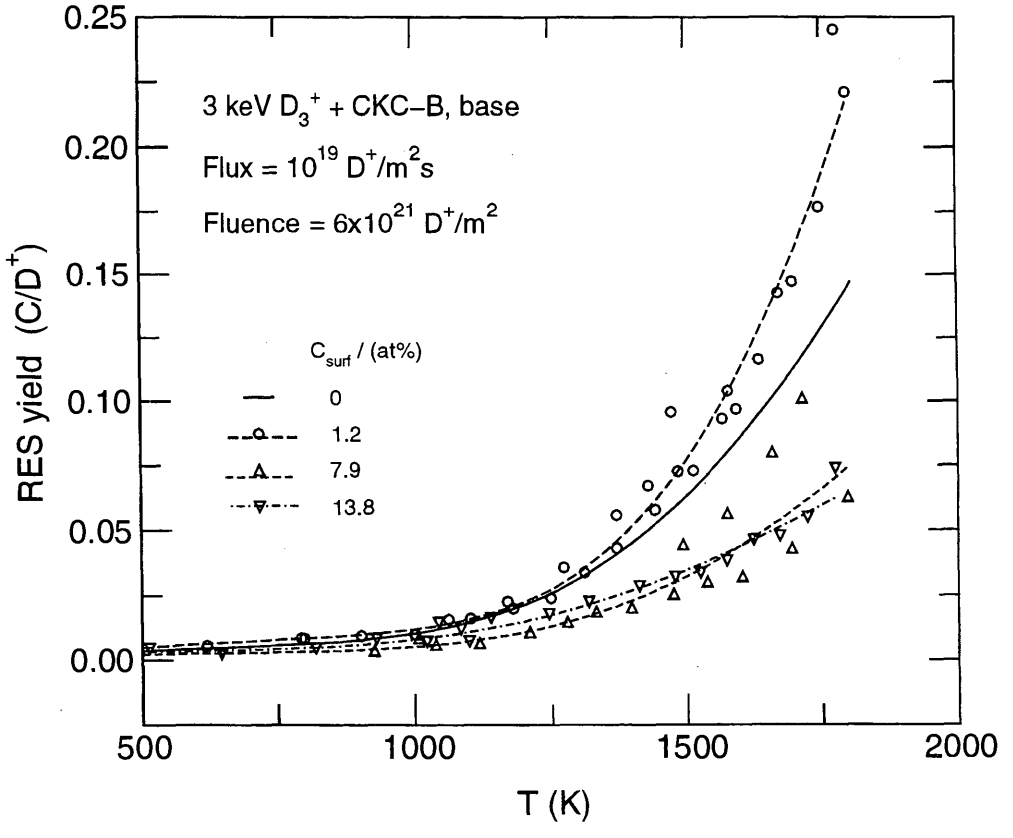

3.1.25 D_3^+ + graphite (CKC-B, edge plane) → C

Source: P. Franzen, A. A. Haasz and J. W. Davis, J. Nucl. Mater. **226**, 15 (1995).

Accuracy: Yield (rel.): ±10%; T: ±25K.

Comments: (1) Specimens: B-doped CKC isostatically compressed anisotropic graphite (CKC), base orientation (cut parallel to graphite planes). Bulk concentrations: 2.0, 9.4 and 20.1 at% B, corresponding to surface concentrations of 1.2, 7.9 and 13.8 at% B.
(2) 3 keV D_3^+ (1 keV/D^+); flux: 10^{19} ions/m^2s.
(3) Ions produced by a mass-analyzed ion accelerator.
(4) Carbon atoms were detected by phase-sensitive line-of-sight QMS.
(5) Absolute yields for pure graphites determined by comparison with mass-loss results in Roth et al., J. Nucl. Mater. **111&112** 775 (1982) and Roth et al., J. Nucl. Mater. **122&123** 1447 (1984).

Analytic fitting:

Analytic fits for reactions A (o), B (△) and C (▽). The data and fit for zero doping is given in reaction 3.1.9. Data fits are from the paper.

Fitting parameters A_1-A_4

A	9.0849E-03	5.5089E+02	6.5354E+00	7.8331E+03
B	1.0162E-02	6.4888E+02	2.0765E+01	9.3491E+03
C	1.2857E-02	6.4474E+02	1.0547E+01	9.6032E+03

ALADDIN hierarchical labelling and evaluation function:

A-C: RES D [+1] GRAPHITE T=CKC D=B O=EDGE-PL C [+0] #EYIELD4GN

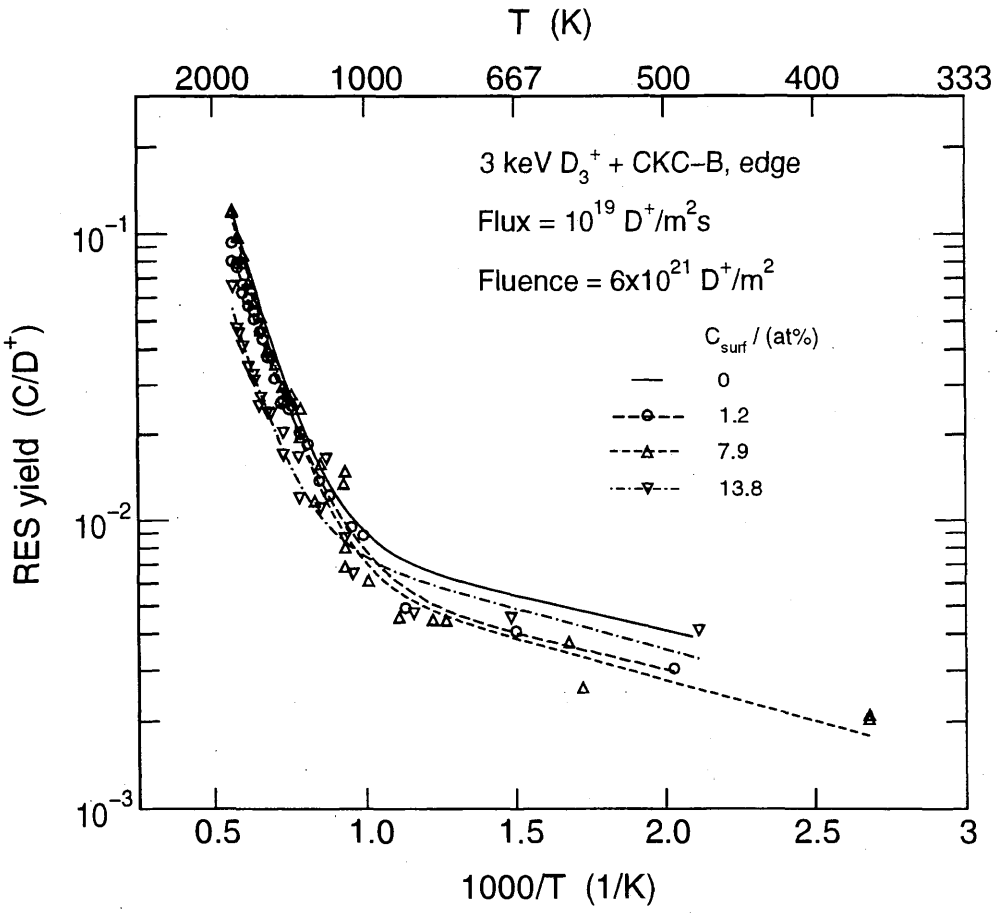

3.1.26 D_3^+ + graphite (CKC-B, edge plane) → C

Source: P. Franzen, A. A. Haasz and J. W. Davis, J. Nucl. Mater. **226**, 15 (1995).

Accuracy: Yield (rel.): ±10%; T: ±25K.

Comments: (1) Specimens: B-doped CKC isostatically compressed anisotropic graphite (CKC), edge orientation (cut perpendicular to graphite planes). Bulk concentrations: 2.0, 9.4 and 20.1 at% B, corresponding to surface concentrations of 1.2, 7.9 and 13.8 at% B.
(2) 3 keV D_3^+ (1 keV/D^+); flux: 10^{19} ions/m^2s.
(3) Ions produced by a mass-analyzed ion accelerator.
(4) Carbon atoms were detected by phase-sensitive line-of-sight QMS.
(5) Absolute yields for pure graphites determined by comparison with mass-loss results in Roth et al., J. Nucl. Mater. **111&112** 775 (1982) and Roth et al., J. Nucl. Mater. **122&123** 1447 (1984).

Analytic fitting:

The analytic fits for reactions A (○), B (△) and C (▽) have been replotted using data from the preceeding page. The data and fit for zero doping is given in reaction 3.1.10. Data fits are from the paper.

Fitting parameters A_1-A_4

A	9.0849E-03	5.5089E+02	6.5354E+00	7.8331E+03
B	1.0162E-02	6.4888E+02	2.0765E+01	9.3491E+03
C	1.2857E-02	6.4474E+02	1.0547E+01	9.6032E+03

ALADDIN hierarchical labelling and evaluation function:

A-C: RES D [+1] GRAPHITE T=CKC D=B O=EDGE-PL C [+0] #EYIELD4GN

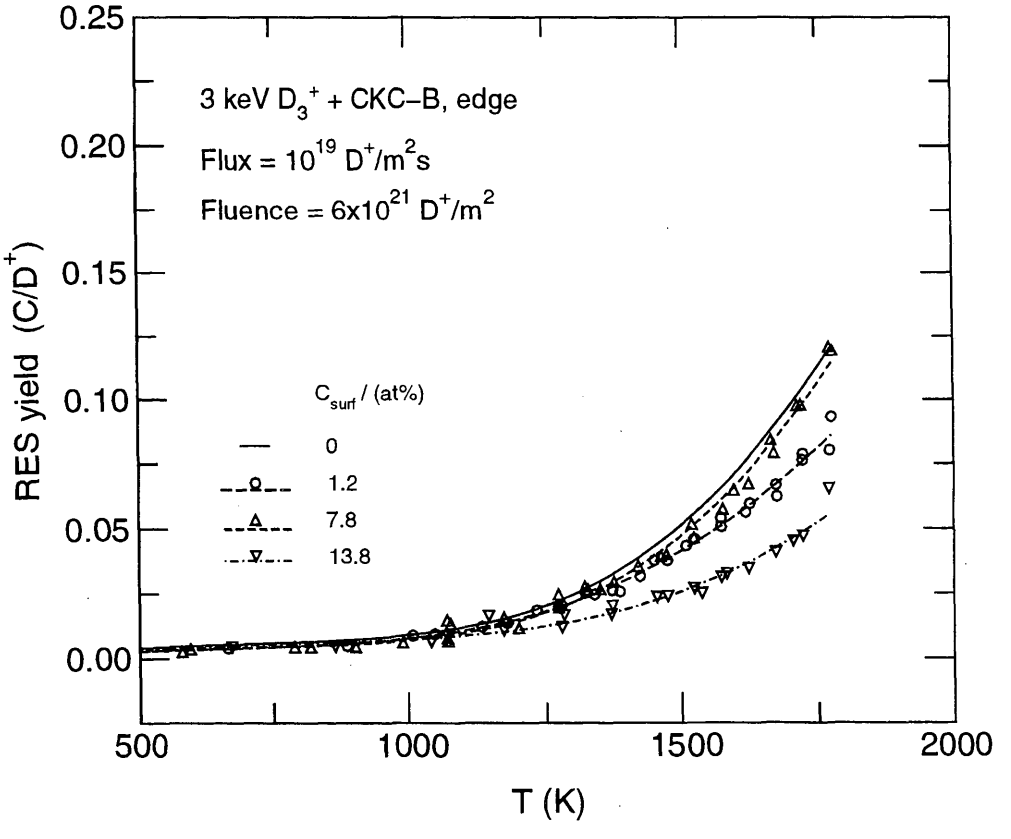

3.1.27 D_3^+ + graphite (CKC-Ti, base plane) → C

Source: P. Franzen, A. A. Haasz and J. W. Davis, J. Nucl. Mater. **226**, 15 (1995).

Accuracy: Yield (rel.): ±10%; T: ±25K.

Comments: (1) Specimens: Ti-doped CKC isostatically compressed anisotropic graphite (CKC), base orientation (cut parallel to graphite planes). Bulk concentrations: 2.0, 8.5 and 16.0 at% Ti, corresponding to surface concentrations of 0.7, 3.2 and 5.0 at% Ti.
(2) 3 keV D_3^+ (1 keV/D^+); flux: 10^{19} ions/m^2s.
(3) Ions produced by a mass-analyzed ion accelerator.
(4) Carbon atoms were detected by phase-sensitive line-of-sight QMS.
(5) Absolute yields for pure graphites determined by comparison with mass-loss results in Roth et al., J. Nucl. Mater. **111&112** 775 (1982) and Roth et al., J. Nucl. Mater. **122&123** 1447 (1984).

Analytic fitting:

Analytic fits for reactions A (○), B (△) and C (▽). The data and fit for zero doping is given in reaction 3.1.9. Data fits are from the paper.

Fitting parameters A_1-A_4

A	2.5141E-02	8.2275E+02	1.9240E+01	8.8153E+03
B	1.9155E-02	7.4955E+02	8.7691E+01	1.1730E+04
C	5.7521E-03	3.6278E+02	2.2711E-01	3.4781E+03

ALADDIN hierarchical labelling and evaluation function:

A-C: RES D [+1] GRAPHITE T=CKC D=Ti O=BASE-PL C [+0] #EYIELD4GN

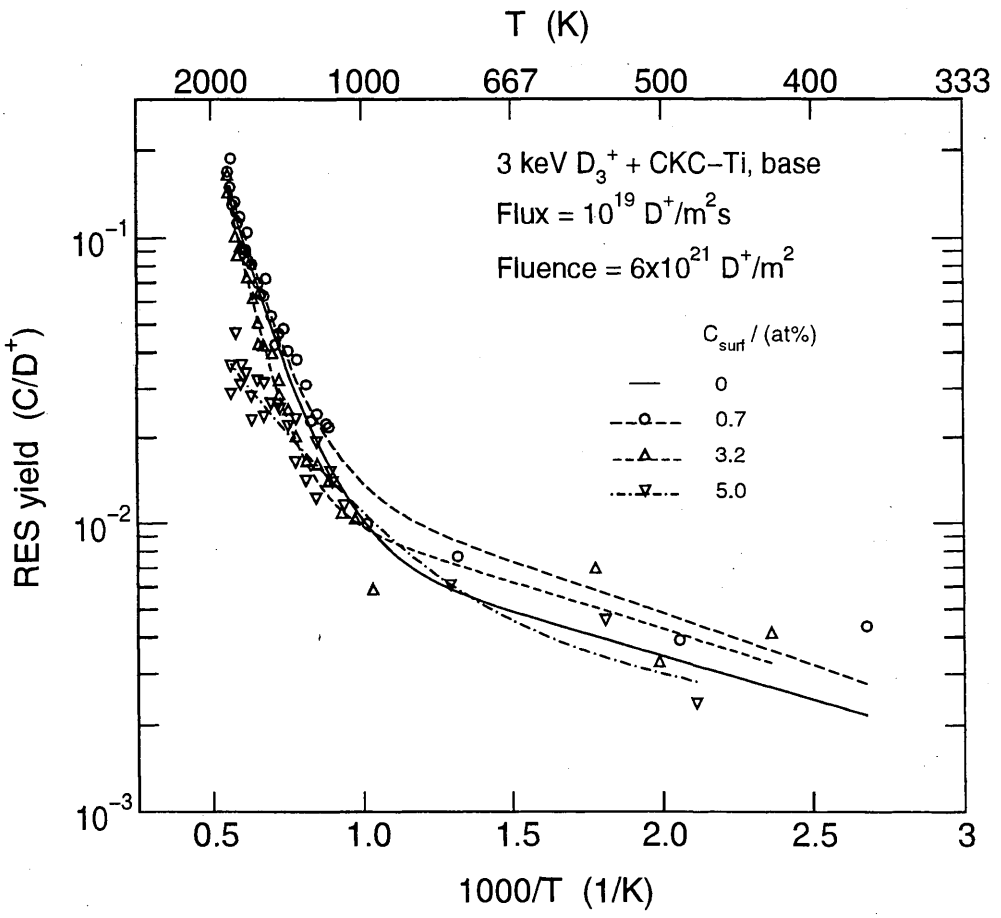

3.1.28 D_3^+ + graphite (CKC-Ti, base plane) → C

Source: P. Franzen, A. A. Haasz and J. W. Davis, J. Nucl. Mater. **226**, 15 (1995).

Accuracy: Yield (rel.): ±10%; T: ±25K.

Comments: (1) Specimens: Ti-doped CKC isostatically compressed anisotropic graphite (CKC), base orientation (cut parallel to graphite planes). Bulk concentrations: 2.0, 8.5 and 16.0 at% Ti, corresponding to surface concentrations of 0.7, 3.2 and 5.0 at% Ti.
(2) 3 keV D_3^+ (1 keV/D^+); flux: 10^{19} ions/m^2s.
(3) Ions produced by a mass-analyzed ion accelerator.
(4) Carbon atoms were detected by phase-sensitive line-of-sight QMS.
(5) Absolute yields for pure graphites determined by comparison with mass-loss results in Roth et al., J. Nucl. Mater. **111&112** 775 (1982) and Roth et al., J. Nucl. Mater. **122&123** 1447 (1984).

Analytic fitting:

The analytic fits for reactions A (○), B (△) and C (▽) have been replotted using data from the preceeding page. The data and fit for zero doping is given in reaction 3.1.10. Data fits are from the paper.

Fitting parameters A_1-A_4

A	2.5141E-02	8.2275E+02	1.9240E+01	8.8153E+03
B	1.9155E-02	7.4955E+02	8.7691E+01	1.1730E+04
C	5.7521E-03	3.6278E+02	2.2711E-01	3.4781E+03

ALADDIN hierarchical labelling and evaluation function:

A-C: RES D [+1] GRAPHITE T=CKC D=Ti O=BASE-PL C [+0] #EYIELD4GN

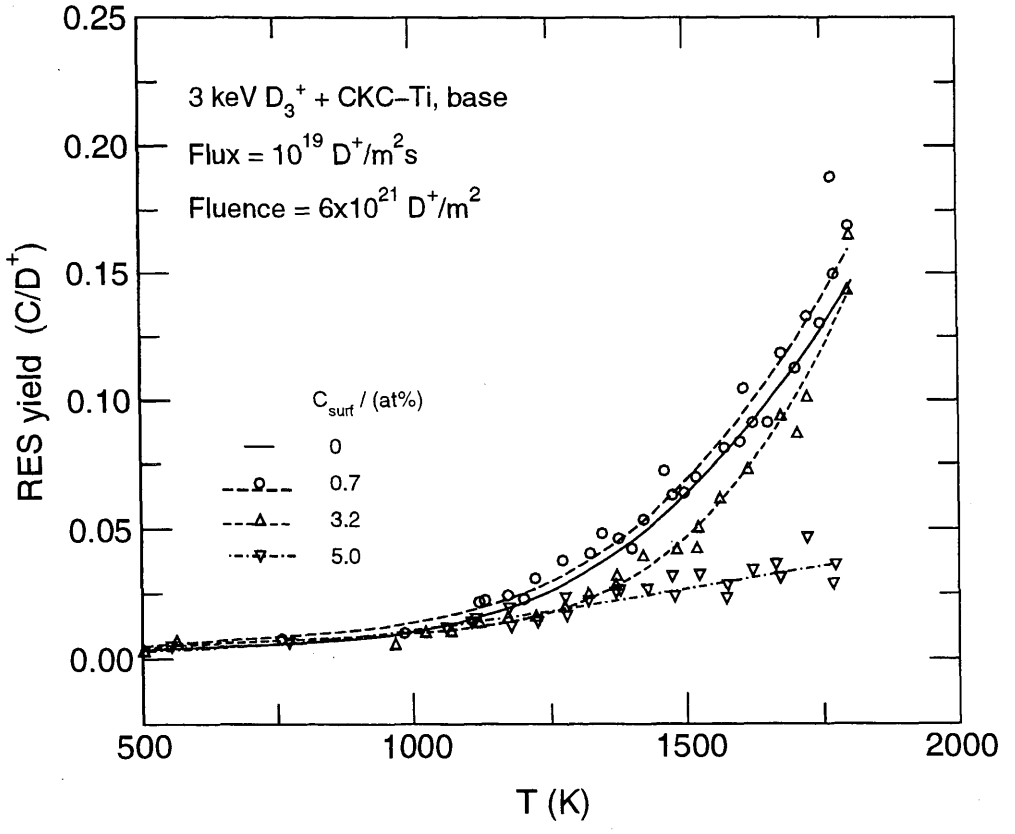

3.1.29 D_3^+ + graphite (CKC-Ti, edge plane) → C

Source: P. Franzen, A. A. Haasz and J. W. Davis, J. Nucl. Mater. **226**, 15 (1995).

Accuracy: Yield (rel.): ±10%; T: ±25K.

Comments: (1) Specimens: Ti-doped CKC isostatically compressed anisotropic graphite (CKC), edge orientation (cut perpendicular to graphite planes). Bulk concentrations: 2.0, 8.5 and 16.0 at% Ti, corresponding to surface concentrations of 0.7, 3.2 and 5.0 at% Ti.
(2) 3 keV D_3^+ (1 keV/D^+); flux: 10^{19} ions/m^2s.
(3) Ions produced by a mass-analyzed ion accelerator.
(4) Carbon atoms were detected by phase-sensitive line-of-sight QMS.
(5) Absolute yields for pure graphites determined by comparison with mass-loss results in Roth et al., J. Nucl. Mater. **111&112** 775 (1982) and Roth et al., J. Nucl. Mater. **122&123** 1447 (1984).

Analytic fitting:

Analytic fits for reactions A (○), B (△) and C (▽). The data and fit for zero doping is given in reaction 3.1.9. Data fits are from the paper.

Fitting parameters A_1-A_4

A	2.6442E-02	8.9261E+02	2.6811E+01	9.1189E+03
B	4.2234E-03	0.0000E+00	1.6099E+00	5.7414E+03
C	1.1558E-02	4.1678E+02	1.0200E+01	9.0262E+03

ALADDIN hierarchical labelling and evaluation function:

A-C: RES D [+1] GRAPHITE T=CKC D=Ti O=EDGE-PL C [+0] #EYIELD4GN

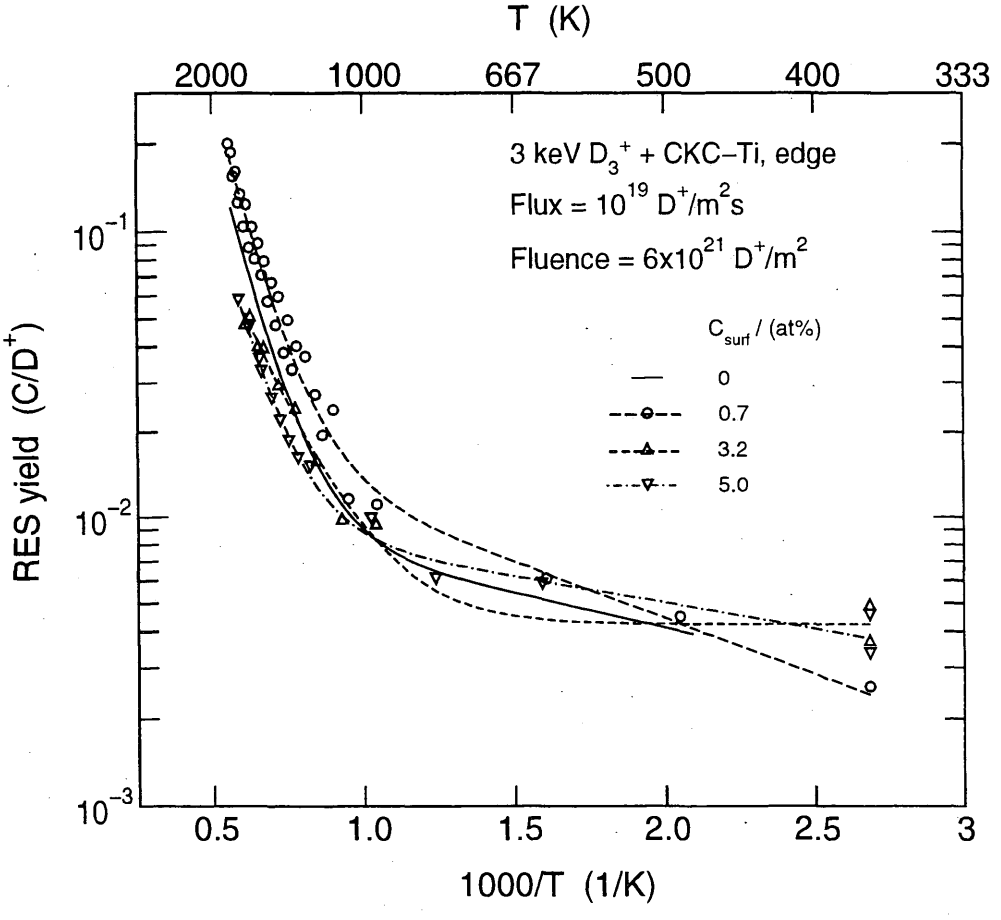

3.1.30 D_3^+ + graphite (CKC-Ti, edge plane) → C

Source: P. Franzen, A. A. Haasz and J. W. Davis, J. Nucl. Mater. **226**, 15 (1995).

Accuracy: Yield (rel.): ±10%; T: ±25K.

Comments: (1) Specimens: Ti-doped CKC isostatically compressed anisotropic graphite (CKC), edge orientation (cut perpendicular to graphite planes). Bulk concentrations: 2.0, 8.5 and 16.0 at% Ti, corresponding to surface concentrations of 0.7, 3.2 and 5.0 at% Ti.
(2) 3 keV D_3^+ (1 keV/D^+); flux: 10^{19} ions/m^2s.
(3) Ions produced by a mass-analyzed ion accelerator.
(4) Carbon atoms were detected by phase-sensitive line-of-sight QMS.
(5) Absolute yields for pure graphites determined by comparison with mass-loss results in Roth et al., J. Nucl. Mater. **111&112** 775 (1982) and Roth et al., J. Nucl. Mater. **122&123** 1447 (1984).

Analytic fitting:

The analytic fits for reactions A (○), B (△) and C (▽) have been replotted using data from the preceeding page. The data and fit for zero doping is given in reaction 3.1.10. Data fits are from the paper.

Fitting parameters A_1-A_4

A	2.6442E-02	8.9261E+02	2.6811E+01	9.1189E+03
B	4.2234E-03	0.0000E+00	1.6099E+00	5.7414E+03
C	1.1558E-02	4.1678E+02	1.0200E+01	9.0262E+03

ALADDIN hierarchical labelling and evaluation function:

A-C: RES D [+1] GRAPHITE T=CKC D=Ti O=EDGE-PL C [+0] #EYIELD4GN

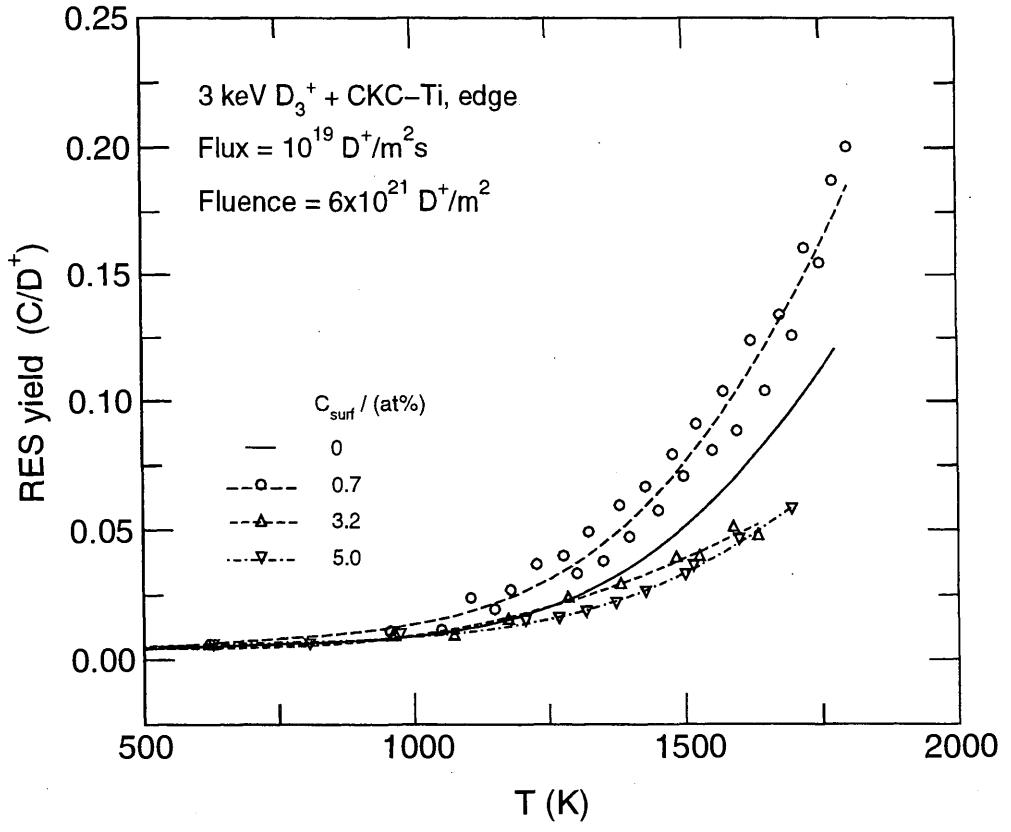

3.1.31 He^+ + graphite (POCO) → C

Source: R. E. Nygren, J. Bohdansky, A. Pospieszczyk, R. Lehmer, Y. Ra, R. W. Conn, R. Doerner, W. K. Leung and L. Schmitz, J. Nucl. Mater. **176&177**, 445 (1990).

Accuracy: Yield (rel.): ±20%.

Comments: (1) Spectroscopic measurements, using C-I, calibrated by the weight loss method.
(2) Specimen: POCO graphite (resistively heated).
(3) High intensity steady-state source.

Analytic fitting:

Analytic fits for reactions A (○), B (△), C (∗) and D (▽).

Fitting parameters A_1-A_3

A	5.0542E+02	2.0464E+04	5.7174E-03
B	1.4868E+02	1.5485E+04	7.9551E-03
C	6.7124E+02	1.5389E+04	4.7882E-02
D	4.2235E+01	8.8563E+03	-4.2477E-02

ALADDIN hierarchical labelling and evaluation function:

A-D: RES He [+1] GRAPHITE T=POCO C [+0] #EYIELD3BN

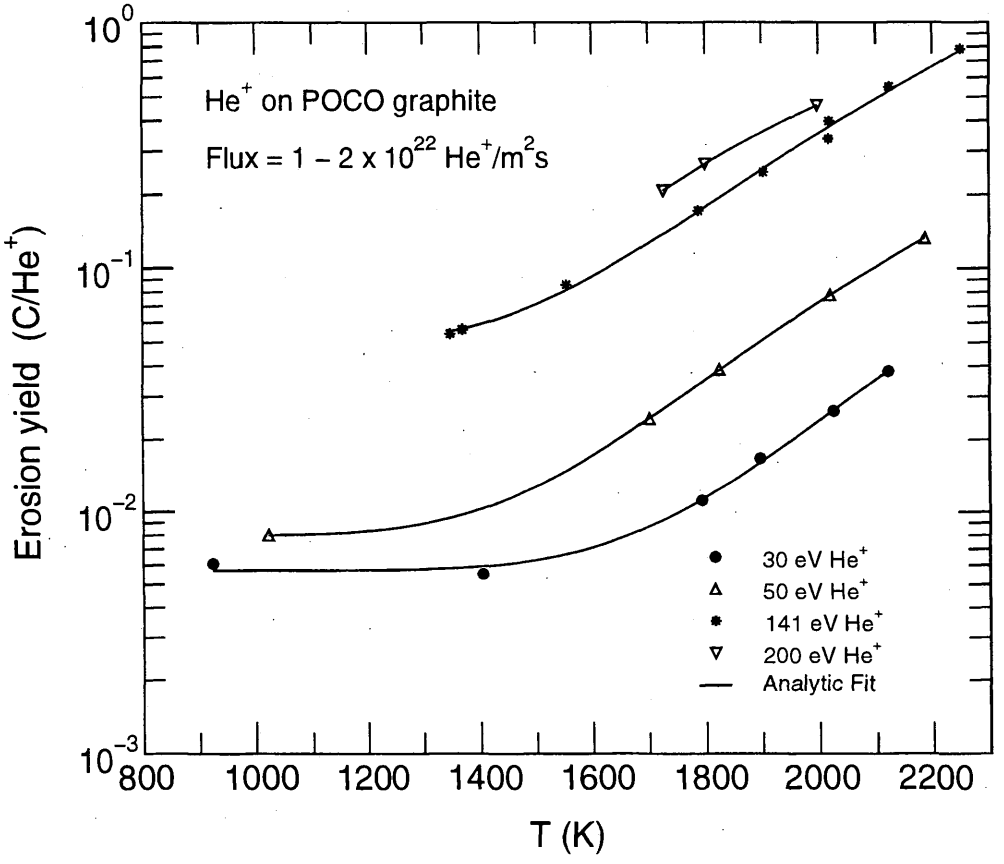

3.1.32 He^+ + graphite (pyrolytic, POCO) → C

Source: R. E. Nygren, J. Bohdansky, A. Pospieszczyk, R. Lehmer, Y. Ra, R. W. Conn, R. Doerner, Y. Hirooka, W. K. Leung and L. Schmitz, J. Vac. Sci. Technol. **A8**, 1778 (1990).

Accuracy: Yield (rel.): ±20%.

Comments: (1) Spectroscopic measurements, using C-I, calibrated by the weight loss method.
(2) Specimens: POCO graphite, pyrolytic graphite (resistively heated).
(3) High intensity steady-state plasma source.

Analytic fitting:

The data is reported as (T (K), Y(C/He^+)) pairs below for A (○), B (△) and C (∗). There were insufficient points for an analytic fit.

Data points

A	(1199, 0.032)	(1213, 0.035)	(2023, 0.184)	(2023, 0.159)
B	(1693, 0.025)	(2023, 0.072)	(2048, 0.078)	
C	(1848, 0.083)			

ALADDIN hierarchical labelling and evaluation function:

A: RES He [+1] GRAPHITE T=POCO C [+0] #TAB2D
B: RES He [+1] GRAPHITE T=POCO C [+0] #TAB2D
C: RES He [+1] GRAPHITE T=PYG C [+0] #TAB2D

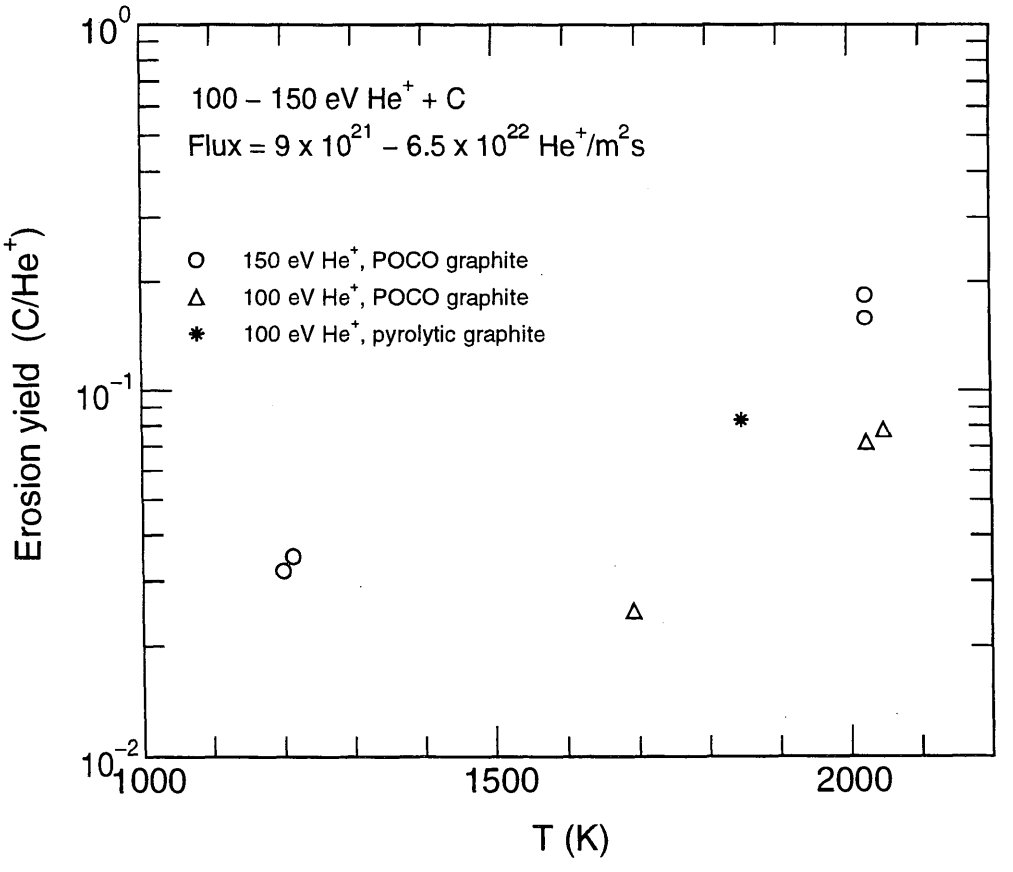

3.1.33 He^+ + graphite (gravimol C/C, MPG-9, KUP-VM, KUP-VM Ti, Si doped) → C

Source: L. B. Begrambekov, O. I. Buzhinskij, B. Ya. Kokushkin, M. V. Nikolskij, V. G. Othoshchenko, A. A. Pustobaef, L. L. Razumov, V. G. Telkovskij, Yu. V.Federov and I. D. Shlenov, J. Nucl. Mater. **170**, 101 (1990).

Accuracy: Yield (rel.): Indeterminate.

Comments: (1) Monoenergetic He^+ ion beam.
(2) Erosion measurements by secondary ion mass spectrometry (SIMS), recording C^+ signals.
(3) Specimens: MPG-8 graphite, gravimol and KUP-VM carbon/carbon composites, and KUP-VM modified by doping with Ti and Si.

Analytic fitting:

Analytic fits for reactions A (•), B (△) and C (○). The fit for reaction D (*) is given by the constant $Y = 2.76$.

Fitting parameters A_1-A_5

A	2.4585E+10	3.6634E+04	1.6394E+00		
B	1.1627E+06	1.9445E+04	1.8577E+00		
C	1.1868E+02	3.4474E+03	2.6665E+08	2.8854E+04	5.0512E+00

ALADDIN hierarchical labelling and evaluation function:

A: RES He [+1] GRAPHITE T=GRAVIMOL C [+0] #EYIELD3BN
B: RES He [+1] GRAPHITE T=MPG-8 C [+0] #EYIELD3BN
C: RES He [+1] GRAPHITE T=KUP-VM C [+0] #EYIELD5BN
D: RES He [+1] GRAPHITE T=KUP-VM D=Ti,Si C [+0] #TAB2D

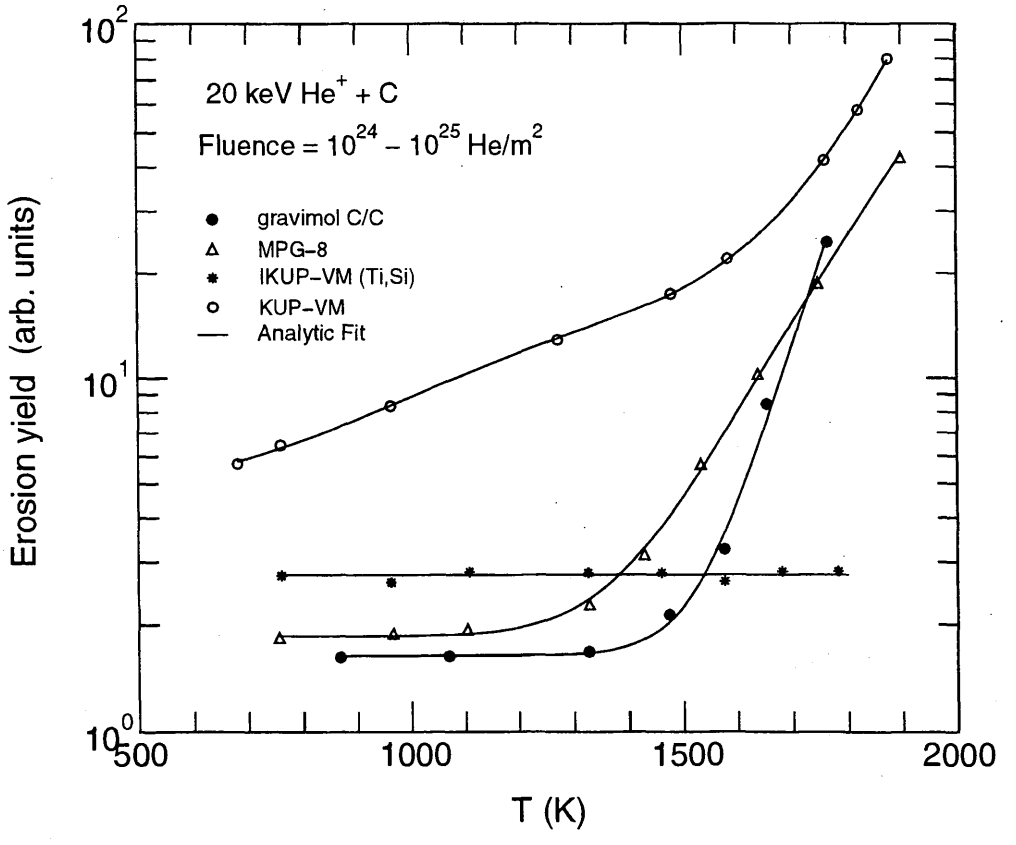

3.1.34 C^+, O^+, Ar^+ + graphite (Papyex) → C

Source: J. Roth, J. B. Roberto and K. L. Wilson, J. Nucl. Mater. **122&123**, 1447 (1984).

Accuracy: Yield (abs.): +100%-50%; Yield (rel): ±30%; T: ±20K.

Comments: (1) Absolute yield for total erosion measured by mass loss.
(2) Relative yields determined by in situ analysis of C atoms collected on Si catchers in front of the specimen using resonant backscattering of 1.75 MeV H^+.
(3) Specimen: papyex graphite.
(4) Ar^+, C^+ and O^+ ions: mass-analyzed accelerator.

Analytic fitting:

Analytic fits for reactions A (•), B (△) and C (○).

Fitting parameters A_1-A_3

A	3.7373E+01	5.8786E+03	3.4024E-01
B	2.8003E+02	7.5279E+03	8.6245E-01
C	3.3627E+02	6.9705E+03	1.5394E+00

ALADDIN hierarchical labelling and evaluation function:

A: RES C [+1] GRAPHITE T=PAPYEX C [+0] #EYIELD3BN
B: RES O [+1] GRAPHITE T=PAPYEX C [+0] #EYIELD3BN
C: RES Ar [+1] GRAPHITE T=PAPYEX C [+0] #EYIELD3BN

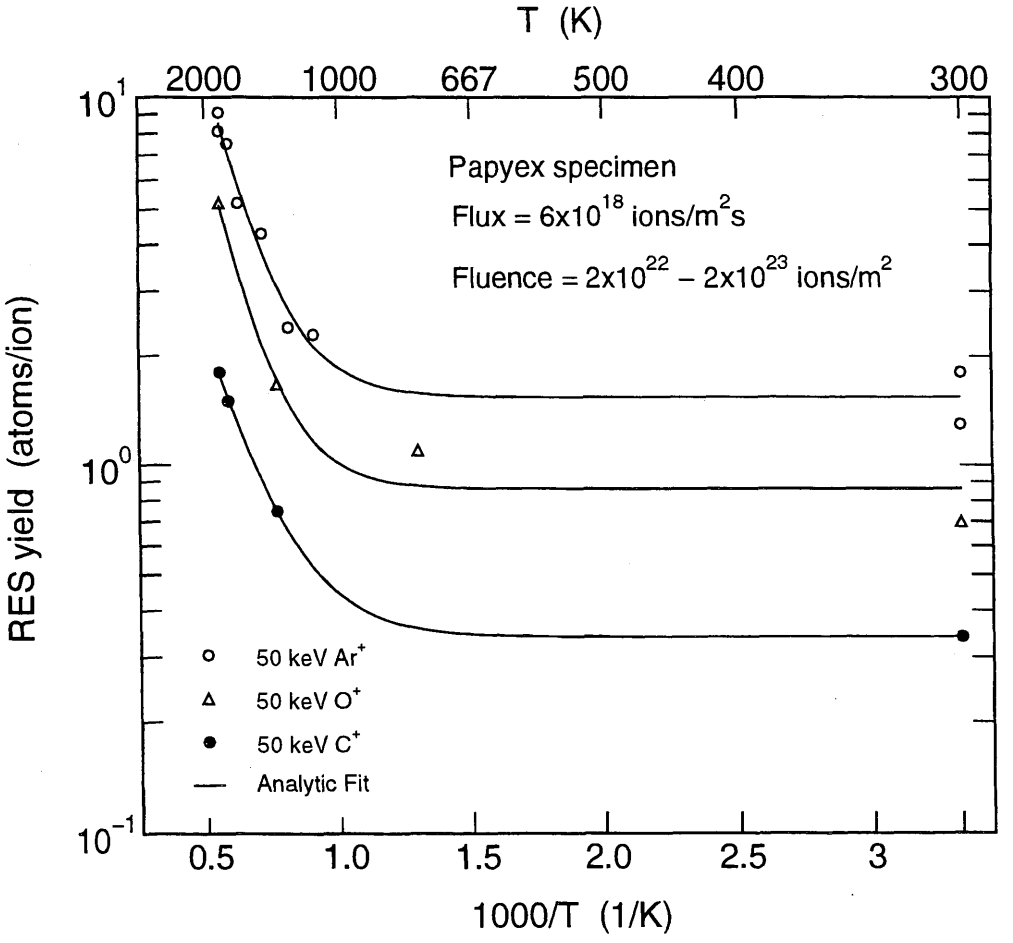

3.1.35 Ar^+ + graphite (pyrolytic) → C

Source: V. Philipps, K. Flaskamp and E. Vietzke, J. Nucl. Mater. **111&112**, 781 (1982).

Accuracy: Yield: 50%.

Comments: (1) RES and sputter signals of Ar^+ (5 keV) on pyrolytic graphite.
(2) Particles detected by line-of-sight QMS.
(3) No corrections made for different velocities.
(4) Specimen: pyrolytic graphite 50x3x0.2 mm^3, resistively heated.

Analytic fitting:

Analytic fits for reactions A (•), B (△) and C (○).

Fitting parameters A_1-A_3

A	5.6647E+12	6.2200E+04	3.6258E-01
B	8.7385E+28	1.4055E+05	
C	1.2703E+03	7.6003E+03	1.0992E+00

ALADDIN hierarchical labelling and evaluation function:

A: SAT Ar [+1] GRAPHITE T=PYG C [+0] #EYIELD3B
B: SAT Ar [+1] GRAPHITE T=PYG C {2} [+0] #EYIELD2E
C: RES Ar [+1] GRAPHITE T=PYG C [+0] #EYIELD3BN

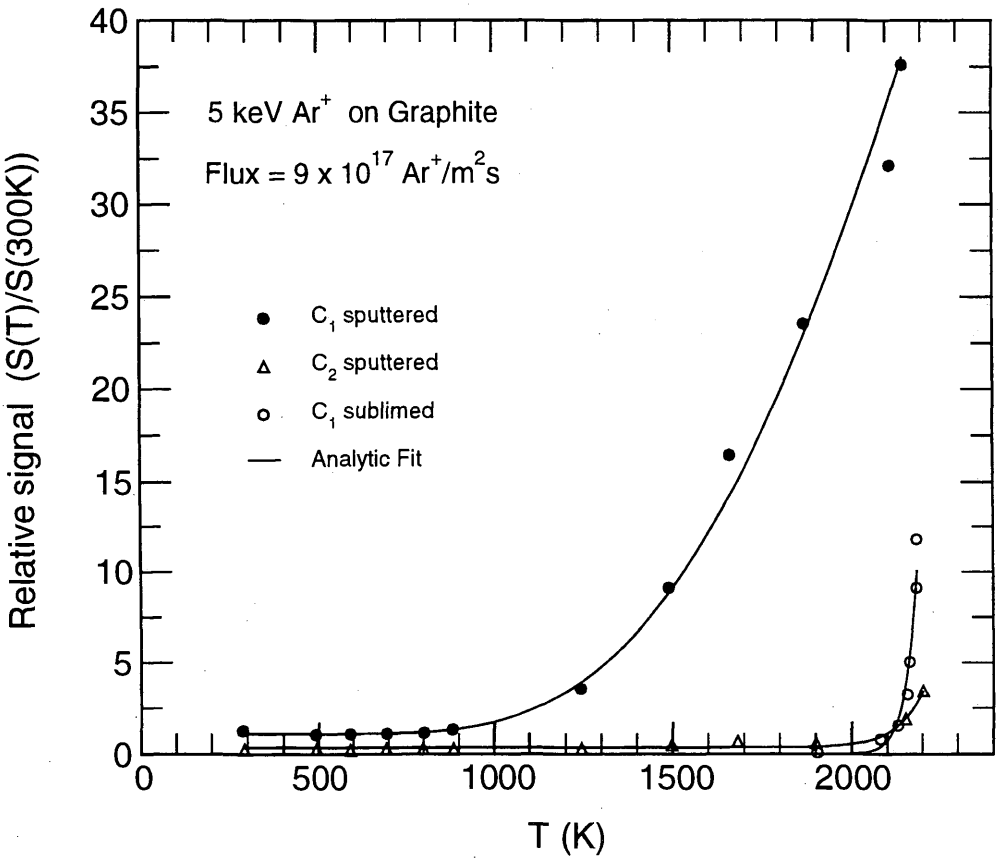

3.1.36 Ar^+ + graphite (pyrolytic) → C

Source: V. Philipps, E. Vietzke, R. P. Schorn and H. Trinkaus, J. Nucl. Mater. **155&157**, 319 (1988).

Accuracy: Yield: 50%.

Comments: (1) RES and sputter yields of C by Ar^+ (5 keV) on pyrolytic graphite for two different flux densities.
(2) C atoms detected by lin-of-sight QMS.
(3) Yield determined assuming a sputter distribution at 300K of E_B = 8.3 eV and a thermal distribution for RES.
(4) Specimen: pyrolytic graphite, machined to 50x3x0.2 mm^3, resistively heated.

Analytic fitting:

Analytic fit for reaction A (o, x).

Fitting parameters A_1-A_3

A	4.3714E+02	9.4301E+03	1.0089E+00

ALADDIN hierarchical labelling and evaluation function:

A: RES Ar [+1] GRAPHITE T=PYG C [+0] #EYIELD3BN

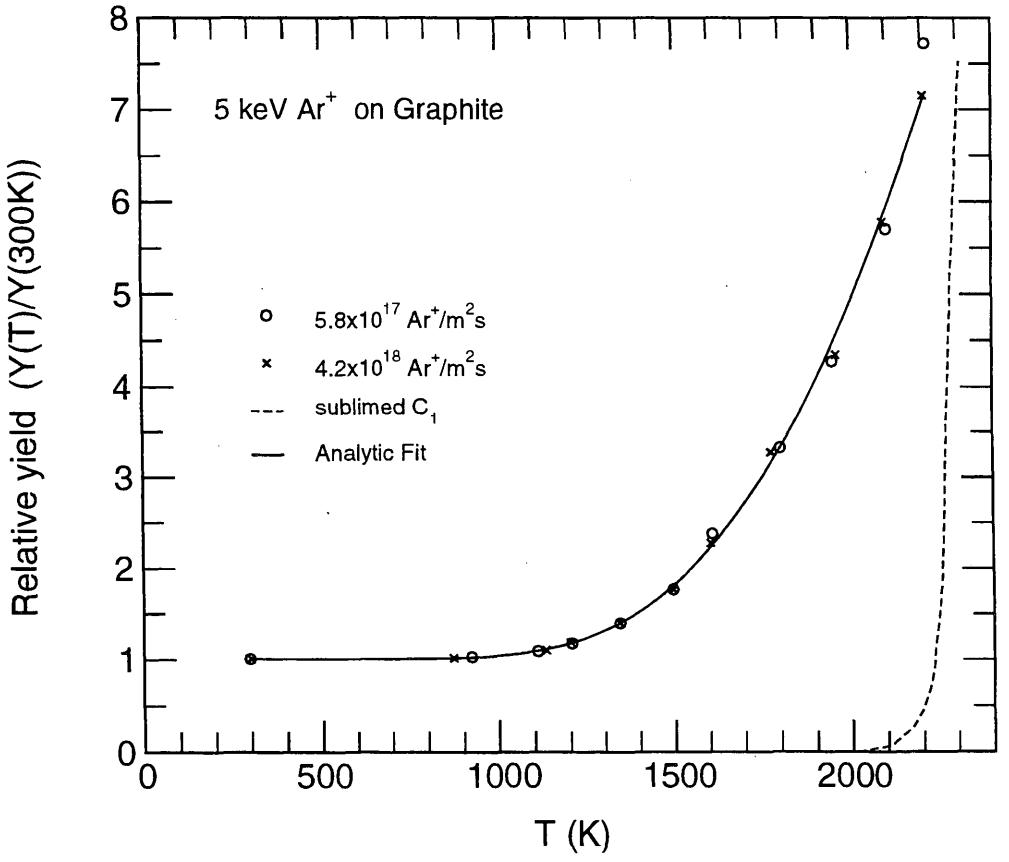

3.1.37 Ar^+ + graphite (ISO-630) → C

Source: Y. Ueda, K. Nakano, Y. Ohtsuka, M. Isobe, S. Goto and M. Nishikawa, J. Nucl. Mater. **227**, 251 (1996).

Accuracy: Yield: ±15%.

Comments: (1) Yield for total erosion measured by mass loss.
(2) Specimen: ISO-630 isotropic gaphite.
(3) High-flux, non-mass-analyzed Ar^+ ion source, operated in pulsed mode.
(4) Impurity content of beam < 6% (H, C, O).

Analytic fitting:

Analytic fit for reaction A (△).

Fitting parameters A_1-A_3

A	1.9770E+02	8.3824E+03	1.2983E+00

ALADDIN hierarchical labelling and evaluation function:

A: RES Ar [+1] GRAPHITE T=ISO-630 C [+0] #EYIELD3BN

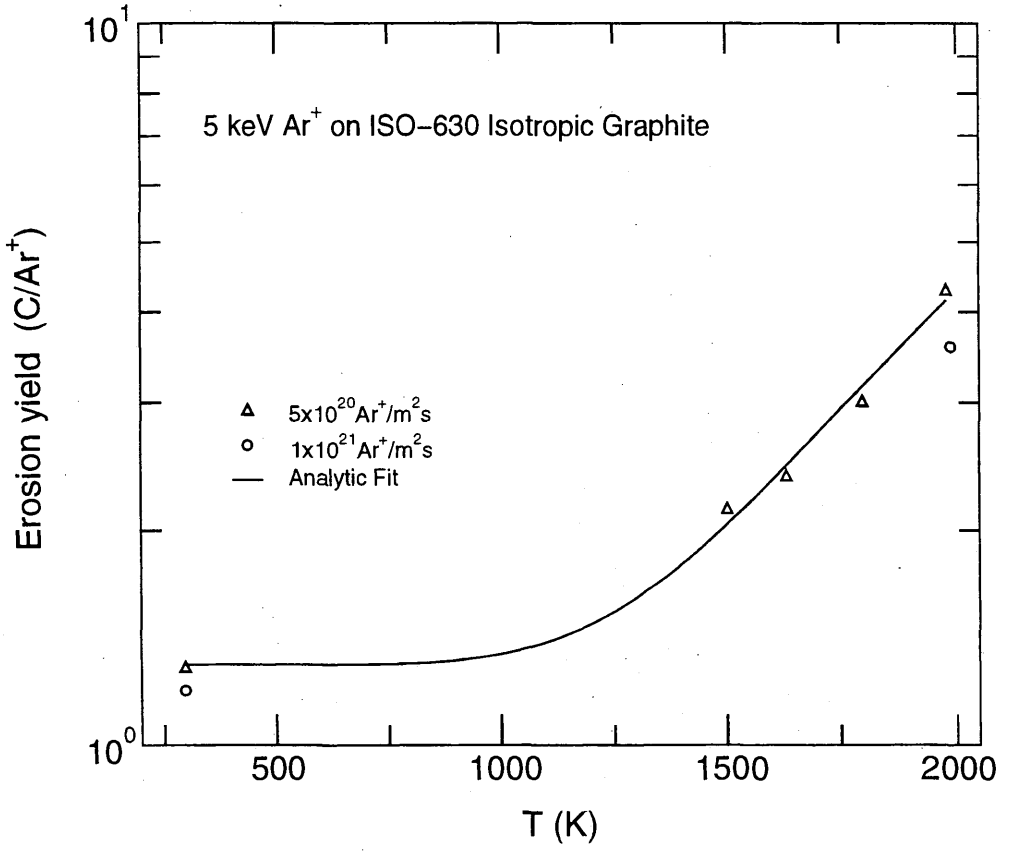

3.1.38 Ar^+ + graphite (pyrolytic, Toyo Tanso, Carbone Lorraine, USB-15) → B, C

Source: E. Vietzke, V. Philipps, K. Flaskamp, J. Winter and S. Veprek, J. Nucl. Mater. **176&177**, 481 (1990).

Accuracy: Yield: 50%.

Comments: (1) RES and sputter signals by 5 keV Ar^+ on diverse carbon materials.
(2) Atoms detected by line-of-sight QMS.
(3) Machined specimens (50x3x0.2 mm^3), resistively heated.

Analytic fitting:

Analytic fits for reactions A (x), B (o), C (*), D (◇), E (△), F (+) and G (•).

	Fitting parameters A_1-A_5				
A	1.6349E+01	7.6762E+03	5.0226E+02	7.6737E+03	3.0517E-02
B	8.2861E-01	2.1156E+03	5.2409E+03	1.3022E+04	1.8916E-01
C	3.2655E+08	3.9161E+04			
D	3.9394E+02	8.6558E+03	1.3799E+06	2.5828E+04	1.5981E-01
E	1.9586E-01	2.2507E+02	4.4032E+09	4.1715E+04	
F	6.5646E+01	7.8699E+03	6.9068E+10	4.6574E+04	1.2288E-01
F	1.0467E+08	3.4528E+04			

ALADDIN hierarchical labelling and evaluation function:

A: RES Ar [+1] GRAPHITE T=PYG C [+0] #EYIELD5B
B: RES Ar [+1] GRAPHITE T=TT C [+0] #EYIELD5BN
C: RES Ar [+1] GRAPHITE T=TT B [+0] #EYIELD2E
D: RES Ar [+1] GRAPHITE T=CLOR C [+0] #EYIELD5BN
E: RES Ar [+1] GRAPHITE T=CLOR B [+0] #EYIELD4GN
F: RES Ar [+1] GRAPHITE T=USB-15 C [+0] #EYIELD5BN
F: RES Ar [+1] GRAPHITE T=USB-15 B [+0] #EYIELD2E

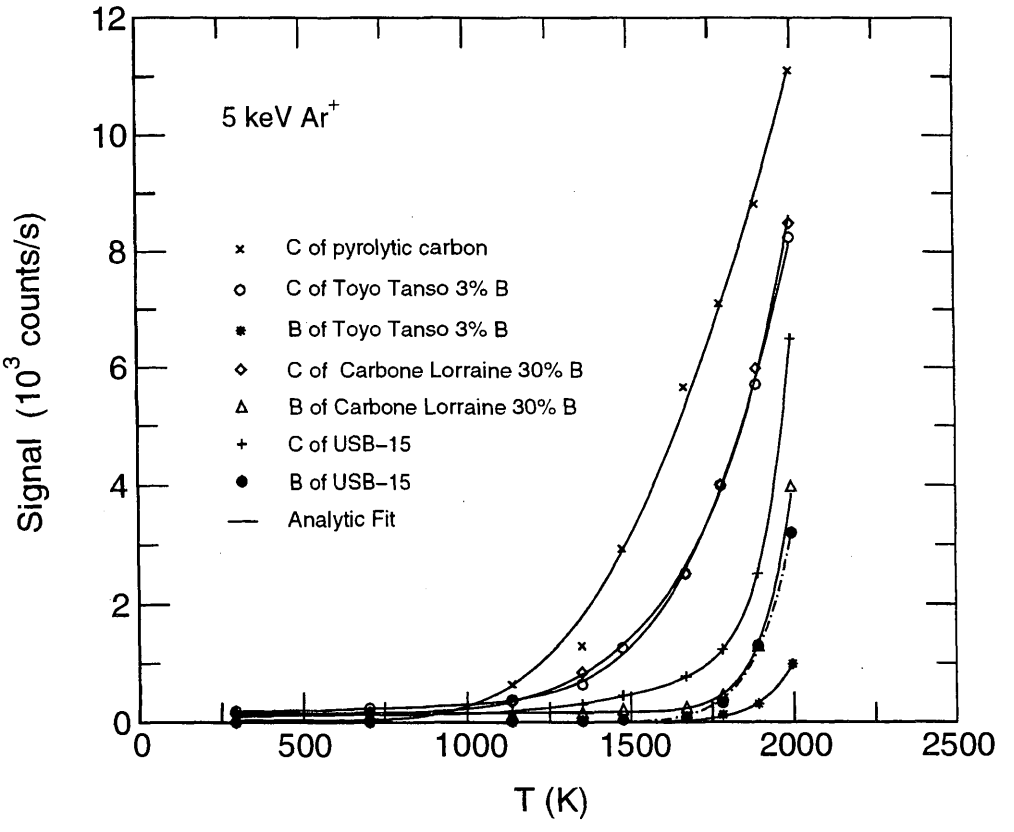

3.1.39 Ar^+ + graphite (USB-15) → B, C

Source: E. Vietzke, V. Philipps, K. Flaskamp, J. Winter and S. Veprek, J. Nucl. Mater. **176&177**, 481 (1990).

Accuracy: Yield: 50%.

Comments: (1) Main RES sputter signals by 5 keV Ar^+ on USB15.
(2) Particles detected by line-of-sight QMS.
(3) Specimen: USB15 [graphitized fine crystallite of B_4C (size 10 nm)], machined, resistively heated.

Analytic fitting:

Analytic fits for reactions A (+), B (o), C (◇), D (△) and E (x).

Fitting parameters A_1-A_8

A	1.2350E+02	2.5466E+01	6.4739E+04	7.8470E+03		
B	-3.8818E+00	1.6755E+03	2.6963E+04	1.7063E-01	1.0323E-09	-1.9938E-03
	2.4244E+00	5.9896E+01				
C	3.4132E+02	-8.6220E+00	3.6684E+03	5.4084E+03	-3.0853E+02	
D	1.3953E+03	2.2504E-01	2.1802E+14	4.8755E+04	-1.3598E+03	
E	1.7998E+02	2.9073E+03	1.5272E+07	2.2036E+04	1.1753E+01	

ALADDIN hierarchical labelling and evaluation function:

A: RES Ar [+1] GRAPHITE T=USB-15 C [+1] #EYIELD4GN
B: RES Ar [+1] GRAPHITE T=USB-15 BC [+1] #EYIELD8CN
C: RES Ar [+1] GRAPHITE T=USB-15 C {3} [+1] #EYIELD5BN
D: RES Ar [+1] GRAPHITE T=USB-15 B [+1] #EYIELD5BN
E: RES Ar [+1] GRAPHITE T=USB-15 C {2} [+1] #EYIELD5BN

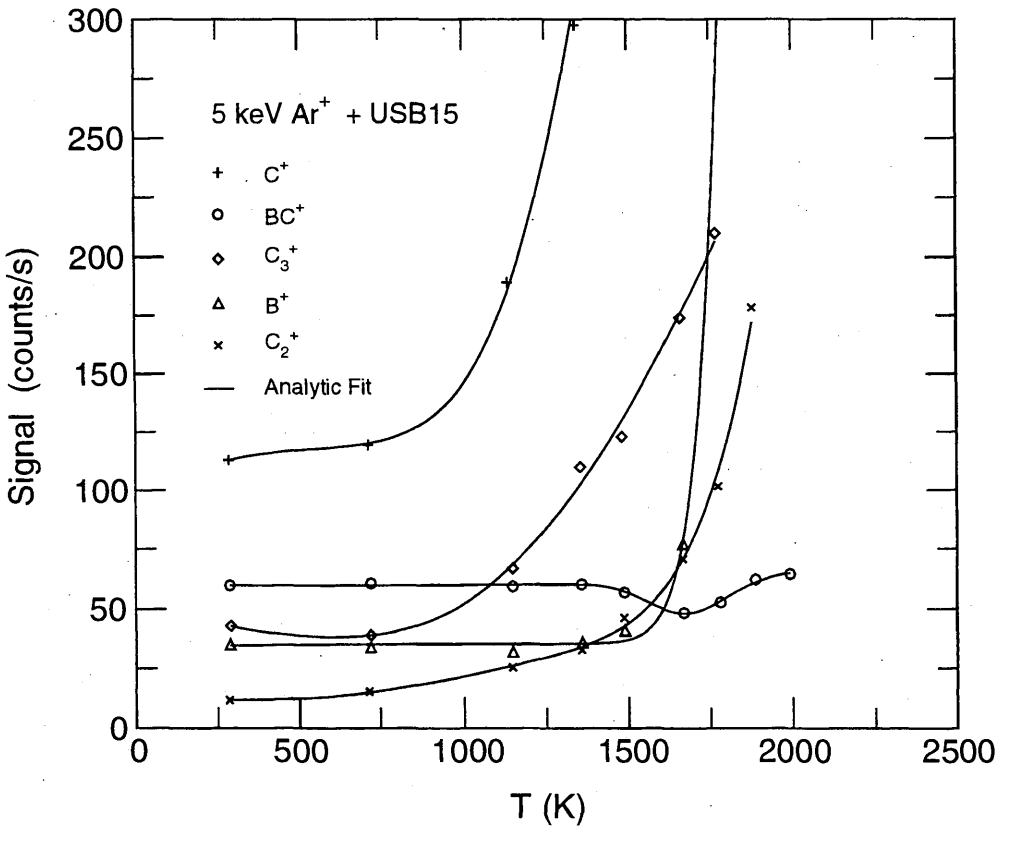

3.1.40 Ar^+ + graphite (pyrolytic, Toyo Tanso, Carbone Lorraine, USB-15) → B, C

Source: E. Vietzke, V. Philipps, K. Flaskamp, J. Winter and S. Veprek, J. Nucl. Mater. **176&177**, 481 (1990).

Accuracy: Yield: 50%.

Comments: (1) Total yield (RES and physical sputtering) of 5 keV Ar^+ on different carbon materials.
(2) Particles are detected by line-of-sight QMS.
(3) The erosion yield is determined from signals (see 3.1.40 and 3.1.43) by assuming a sputter distribution at 300 K of E_B = 8.3 eV and a thermal velocity distribution for RES.

Analytic fitting:

Analytic fits for reactions A (•), B (+), C (*), D (o) and E (x).

Fitting parameters A_1-A_5

A	3.0820E+02	8.4333E+03	1.0001E+00		
B	2.1646E+01	5.7634E+03	1.8745E+05	2.2470E+04	9.8930E-01
C	2.3743E+01	5.7434E+03	7.3101E+06	2.9170E+04	9.6544E-01
D	3.4151E+00	4.8205E+03	2.2955E+08	3.6010E+04	8.2890E-01
E	1.5672E+09	4.2531E+04			

ALADDIN hierarchical labelling and evaluation function:

A: RES Ar [+1] GRAPHITE T=PYG C [+0] #EYIELD3BN
B: RES Ar [+1] GRAPHITE T=TT D=B C [+0] #EYIELD5BN
C: RES Ar [+1] GRAPHITE T=CLOR D=B C [+0] #EYIELD5BN
D: RES Ar [+1] GRAPHITE T=USB-15 C [+0] #EYIELD5BN
E: RES Ar [+1] GRAPHITE T=USB-15 B [+0] #EYIELD2E

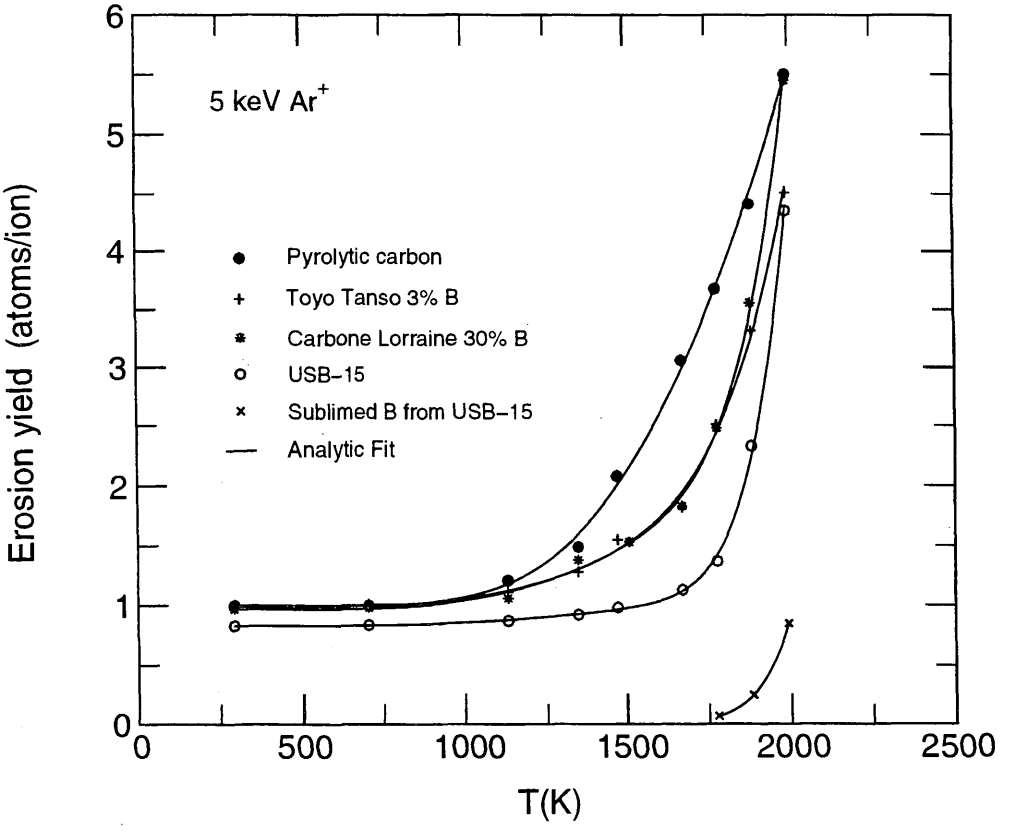

3.1.41 Ar^+ + graphite (pyrolytic, a-C:H, a-C/B:H, diamond) → B, C

Source: E. Vietzke, V. Philipps, K. Flaskamp, J. Winter and S. Veprek, J. Nucl. Mater. **176&177**, 481 (1990).

Accuracy: Yield: 50%.

Comments: (1) RES and sputter signal of C by 5 keV Ar^+ on diverse carbon materials.
(2) C atoms detected by line-of-sight QMS.
(3) C signals from diamond flim vanishes above 1500K (MoC formation).

Analytic fitting:

Analytic fits for reactions A (x), B (◇), C (△), D (▷), E (○), F (◁) and G (●).

Fitting parameters A_1-A_5

A	7.3496E+02	8.0486E+03	8.8752E+11	4.8543E+04	2.1960E-01
B	7.0047E-01	1.4356E+03	3.5488E+03	1.1312E+04	9.3478E-02
C	3.9641E+03	1.1672E+04	4.5955E-02		
D	1.8809E+01	6.3809E+03	6.3016E+12	5.6685E+04	
E	3.1780E-01	1.0117E+02	1.1249E+03	9.4729E+03	
F	9.9381E+14	6.6757E+04			
G	5.3063E+13	7.1157E+04			

ALADDIN hierarchical labelling and evaluation function:

A: RES Ar [+1] GRAPHITE T=PYG C [+0] #EYIELD5B
B: RES Ar [+1] GRAPHITE T=A-CH-FILM C [+0] #EYIELD5BN
C: RES Ar [+1] GRAPHITE T=A-CB-FILM C [+0] #EYIELD3B
D: RES Ar [+1] GRAPHITE T=A-CB-FILM C [+0] #EYIELD4GN
E: RES Ar [+1] GRAPHITE T=DIAM-FILM C [+0] #EYIELD4GN
F: RES Ar [+1] GRAPHITE T=A-CB-FILM B [+0] #EYIELD2E
G: RES Ar [+1] GRAPHITE T=A-CB-FILM C [+0] #EYIELD2E

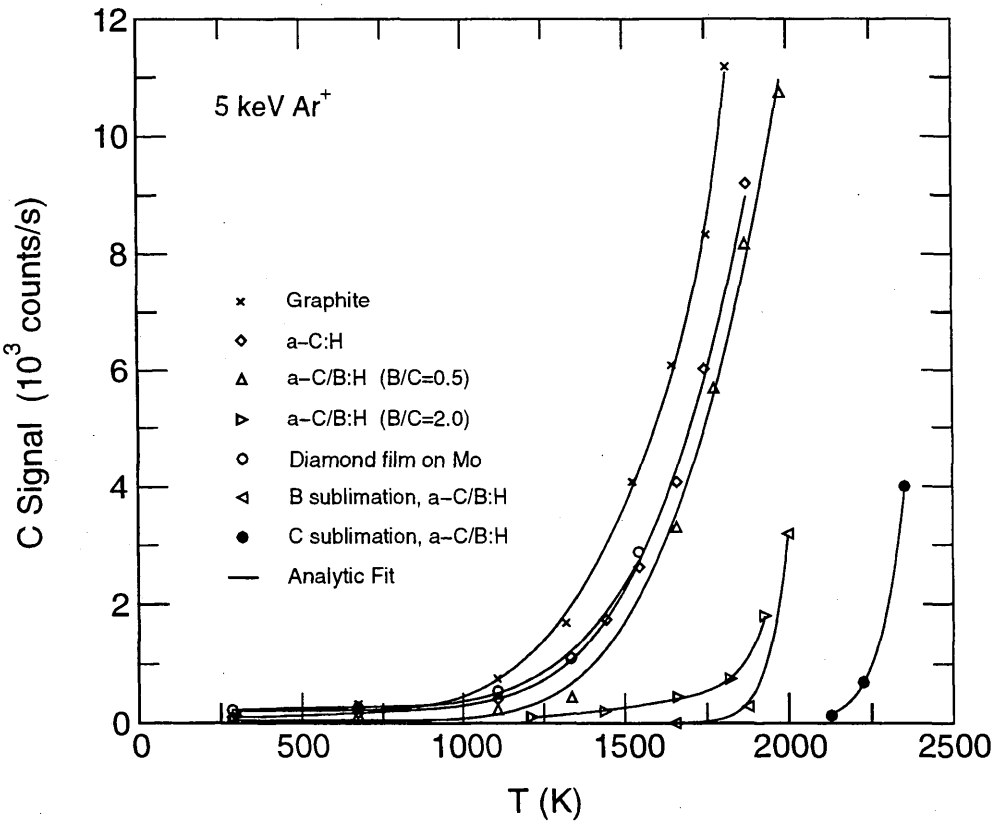

3.2.1 H_3^+ + graphite (pyrolytic) → C

Source: A. A. Haasz and J. W. Davis, J. Nucl. Mater. **151**, 77 (1987).

Accuracy: Yield (rel.): ±10%; T: ±25K.

Comments: (1) Specimen: HPG99 pyrolytic graphite (Union Carbide).
(2) Incident ion energy: 150 eV H_3^+ (50 eV/H^+) to 3 keV H_3^+ (1 keV/H^+).
(3) Ions produced by a mass-analyzed ion accelerator.
(4) Carbon atoms were collected on surfaces near specimen, and converted to methane molecules by a large flux of atomic hydrogen. Methane molecules were detected by QMS-RGA.

Analytic fitting:

Analytic fit for reaction A (○, △).

Fitting parameters A_1-A_7

A	1.0621E+01	-1.8356E+04	3.4850E+07	7.0393E-01	-5.5071E-05	1.3176E-02
	1.4007E+00					

ALADDIN hierarchical labelling and evaluation function:

A: RES H {3} [+1] GRAPHITE T=PYG C [+0] #EYIELD7AN

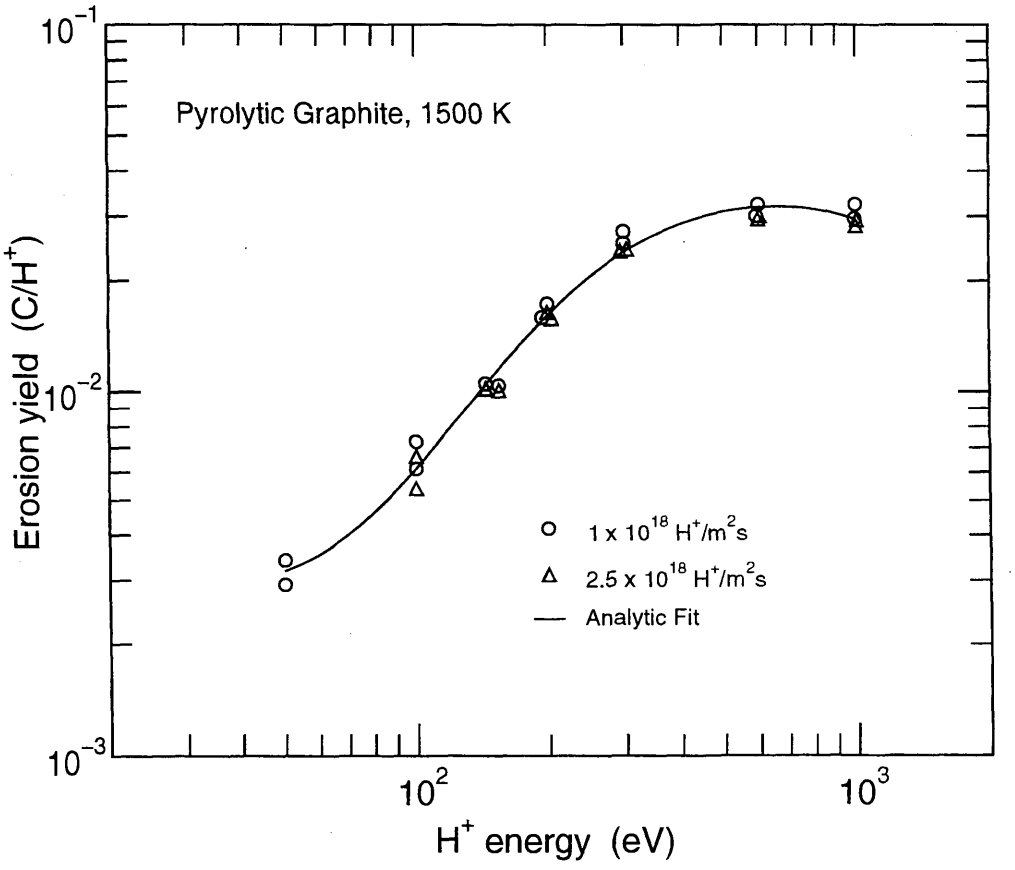

3.2.2 D^+ + graphite (pyrolytic) → C

Source: J. Bohdansky and J. Roth, Fusion Technology, Proc. 15th Symposium on Fusion Technology, Vol. 1, 889 (1988).

Accuracy: Yield (abs.): ±15%, T: ±20K.

Comments: (1) Yield for total erosion measured by mass loss.
(2) Specimen: pyrolytic graphite.
(3) D^+, D_2^+ and D_3^+ ions: mass-analyzed accelerator.
(4) D^+ ions used above 3 keV, D_2^+ ions used above 1 keV, and D_3^+ ions used for 1 keV and below.

Analytic fitting:

Analytic fit for reaction A (o) at 1473 K. The data and fit for 1873 K is given in reaction 3.2.5.

Fitting parameters A_1-A_5

A	7.0400E+00	3.2598E+09	-4.8666E+02	-2.4785E+00	-9.6786E-01

ALADDIN hierarchical labelling and evaluation function:

A: RES D [+1] GRAPHITE T=PYG C [+0] #EYIELD5DN

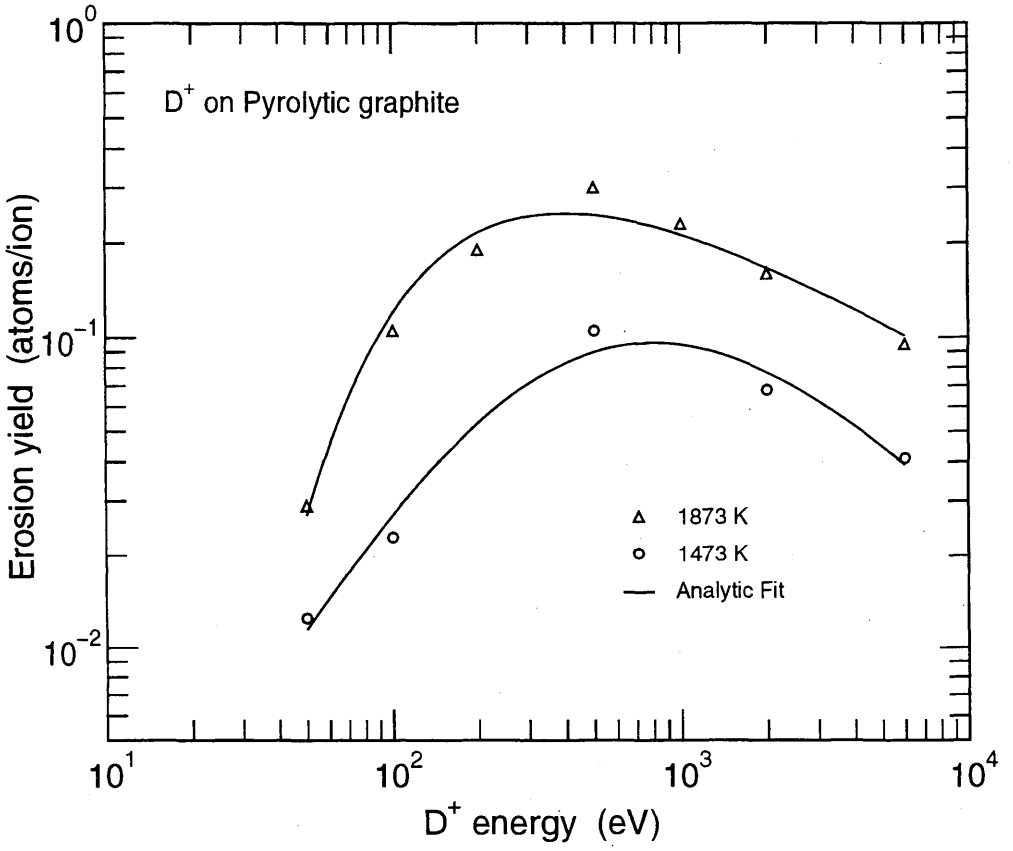

3.2.3 D_3^+ + graphite (Papyex) → C

Source: J. Roth, J. Bohdansky and K. L. Wilson, J. Nucl. Mater. **111&112**, 775 (1982).

Accuracy: Yield (abs.): ±15%, T: ±20K.

Comments: (1) Yield for total erosion measured by mass loss.
(2) Specimen: papyex graphite.
(3) D_3^+ ions: mass-analyzed accelerator.

Analytic fitting:

Analytic fit for reaction A (+).

Fitting parameters A_1-A_2

A	2.2219E-01	-3.8765E-05

ALADDIN hierarchical labelling and evaluation function:

A: RES D {3} [+1] GRAPHITE T=PAPYEX C [+0] #EYIELD2B

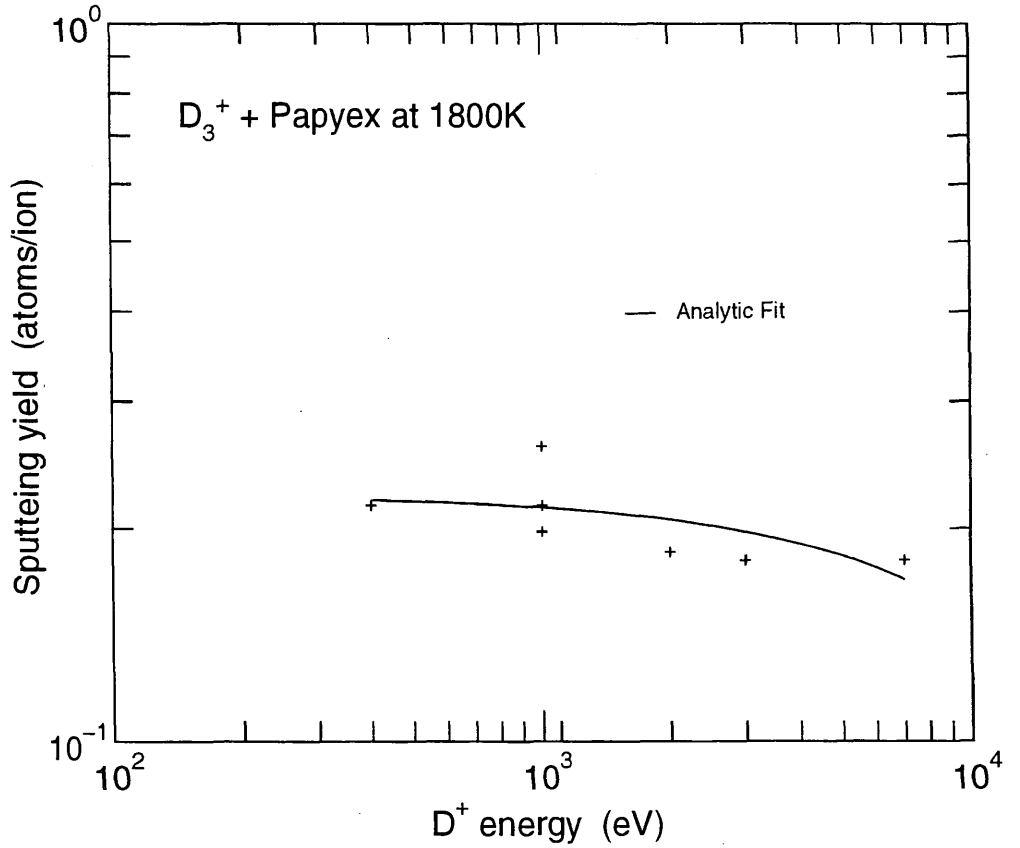

3.2.4 He^+ + graphite (POCO) → C

Source: R. E. Nygren, J. Bohdansky, A. Pospieszczyk, R. Lehmer, Y. Ra, R. W. Conn, R. Doerner, W. K. Leung and L. Schmitz, J. Nucl. Mater. **176&177**, 445 (1990).

Accuracy: Yield (rel.): ±20%.

Comments: (1) Spectroscopic measurements, using C-I, calibrated by the weight loss method.
(2) Specimen: POCO graphite (resistively heated).
(3) High intensity steady-state plasma source.

Analytic fitting:

Analytic fits for reactions A (∗), B (∘) and C (△).

Fitting parameters A_1-A_3

A	4.7167E-07	1.1209E-02	2.8233E+00
B	6.8625E-06	7.5689E-03	2.2838E+00
C	4.1119E-04	2.8550E-03	1.3669E+00

ALADDIN hierarchical labelling and evaluation function:

A-B: RES He [+1] GRAPHITE T=POCO C [+0] #EYIELD3AN
C: RES He [+1] GRAPHITE T=POCO C [+0] #EYIELD3A

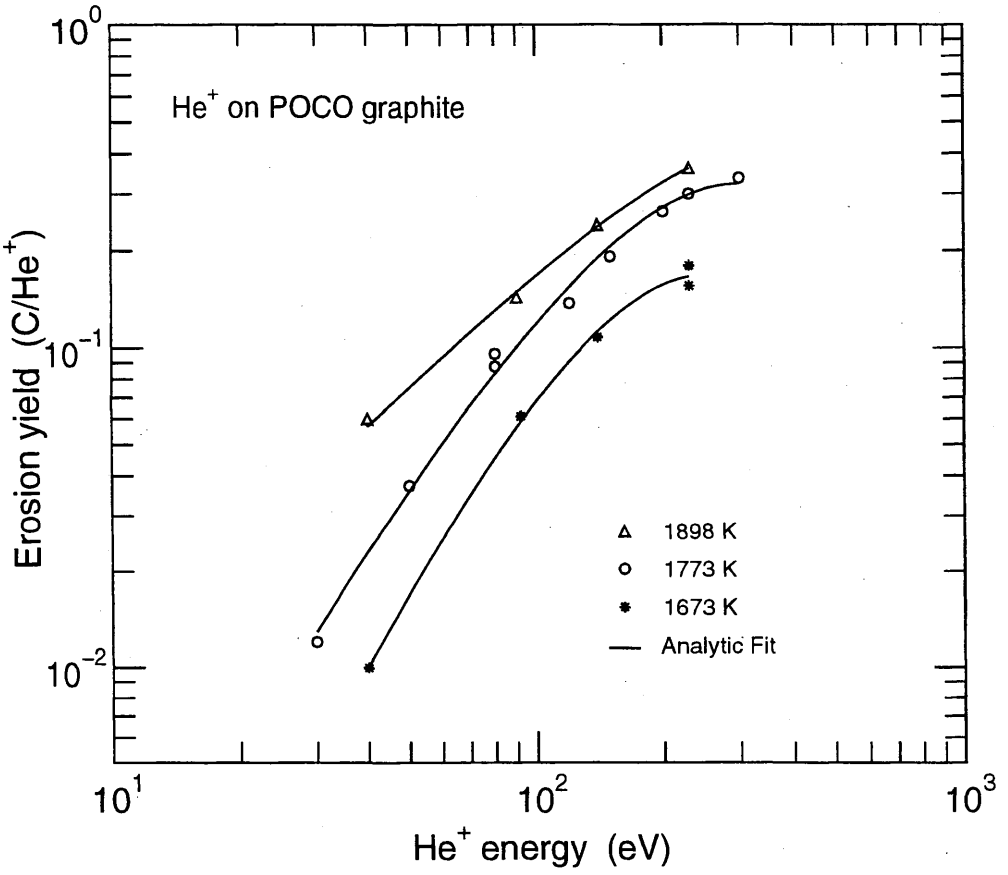

3.2.5 H^+, D^+, He^+ + graphite (pyrolytic) → C

Source: J. Bohdansky and J. Roth, Fusion Technology, Proc. 15th Symposium on Fusion Technology, Vol. 1, 889 (1988).

Accuracy: Yield (abs.): ±15%, T: ±20K.

Comments: (1) Yield for total erosion measured by mass loss.
(2) Specimen: pyrolytic graphite.
(3) H^+, H_2^+, H_3^+, D^+, D_2^+, D_3^+ and He+ ions: mass-analyzed accelerator.
(4) H^+ and D^+ ions were used above 3 keV, H_2^+ and D_2^+ ions were used above 1 keV, and H_3^+ and D_3^+ ions were used for 1 keV and below.

Analytic fitting:

Analytic fits for reactions A (○), B (△) and C (∗).

Fitting parameters A_1-A_5

A	4.5190E-01	1.6094E+05	-2.1538E-01	-1.3344E+03	-6.0068E-01
B	5.8027E+00	9.1556E-02	3.5988E-02	4.3778E+03	-6.7423E-01
C	1.1498E+01	5.0317E-02	2.0219E-02	1.1532E+04	-5.6391E-01

ALADDIN hierarchical labelling and evaluation function:

A: RES H [+1] GRAPHITE T=PYG C [+0] #EYIELD5DN
B: RES D [+1] GRAPHITE T=PYG C [+0] #EYIELD5DN
C: RES He [+1] GRAPHITE T=PYG C [+0] #EYIELD5DN

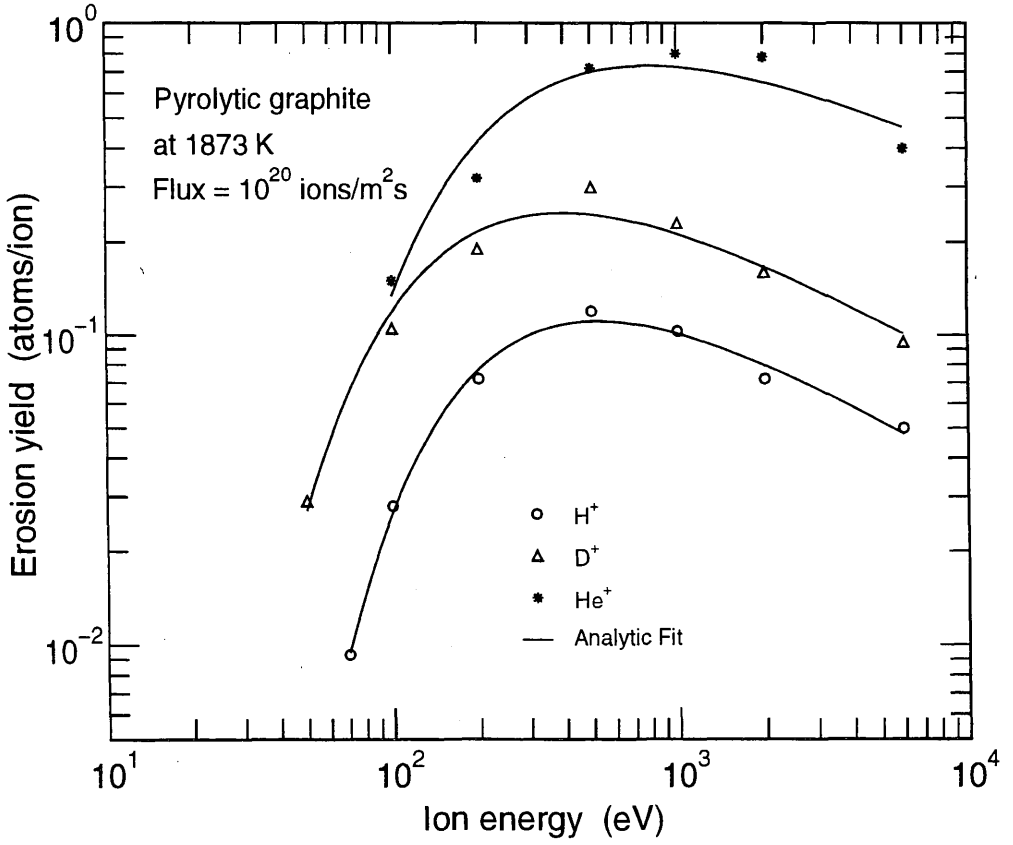

3.2.6 H^+, D^+, C^+, Ar^+ + graphite (Papyex) → C

Source: J. Roth, J. B. Roberto and K. L. Wilson, J. Nucl. Mater. **122&123**, 1447 (1984).

Accuracy: Yield (abs.): +100%-50%; Yield (rel): ±30%; T: ±20K.

Comments: (1) Absolute yield for total erosion measured by mass loss.
(2) Relative yields determined by in situ analysis of C atoms collected on Si catchers in front of the specimen using resonant backscattering of 1.75 MeV H^+.
(3) Specimen: papyex graphite.
(4) Ar^+, C^+ and O^+ ions: mass-analyzed accelerator.
(5) D^+ data is from sheet 3.2.3.

Analytic fitting:

Analytic fits for reactions A (•) and B (▽). Data for C^+ were not fitted.

Fitting parameters A_1-A_4

A	4.7301E-03	2.5835E+14	6.1293E-02	-6.7551E-01
B	-1.2799E-02	9.4619E+00		

ALADDIN hierarchical labelling and evaluation function:

A: RES H [+1] GRAPHITE T=PAPYEX C [+0] #EYIELD4FN
B: RES Ar [+1] GRAPHITE T=PAPYEX C [+0] #EYIELD2A

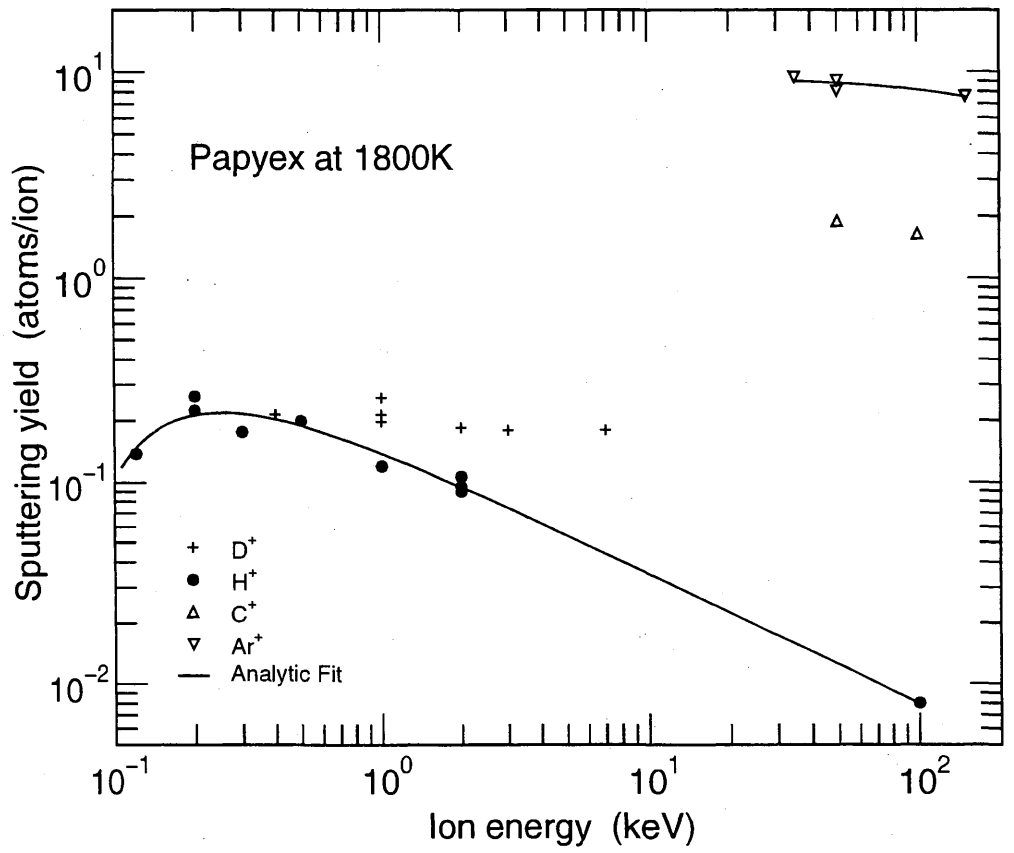

3.2.7 He^+, Ar^+ + graphite (pyrolytic) → C

Source: V. Philipps, K. Flaskamp and E. Vietzke, J. Nucl. Mater. **111&112**, 781 (1982).

Accuracy: Yield: 50%.

Comments: (1) RES and sputter yields of C by Ar^+, He^+ (5 keV) on pyrolytic graphite for 2-5 keV at 1800K.
(2) C atoms detected by line-of-sight QMS.

Analytic fitting:

The data for reaction A (○) is given by the constant yield $Y = 1.767$. Analytic fit for reaction B (●).

Fitting parameters A_1-A_3

-2.3702E-01	2.6087E+00	-8.0414E-01

ALADDIN hierarchical labelling and evaluation function:

A: RES He [+1] GRAPHITE T=PYG C [+0] #TAB2D
B: RES Ar [+1] GRAPHITE T=PYG C [+0] #EYIELD3BN

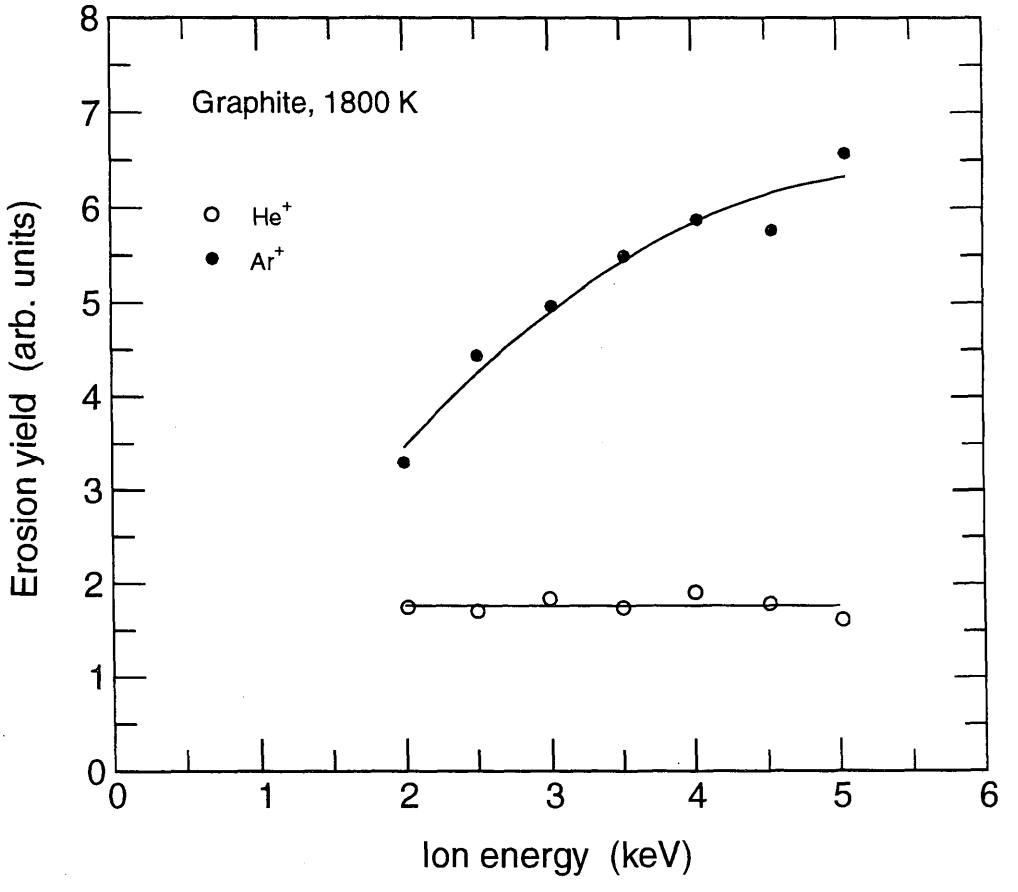

3.3.1 D_3^+ + graphite (Papyex) → C

Source: J. Roth, J. Bohdansky and K. L. Wilson, J. Nucl. Mater. **111&112**, 775 (1982).

Accuracy: Yield (abs.): ±15%, T: ±20K.

Comments: (1) Yield for total erosion measured by mass loss.
(2) Specimen: papyex graphite.
(3) D_3^+ ions: mass-analyzed accelerator.

Analytic fitting:

The yield for reaction A (○) at 1800 K was represented by a constant of 0.21. The fit coefficents for reaction B (△) at 300 K below correspond to parameters f, b, c, $Y(E_0,0)$ and α_0, respectively, in the fitting function.

Fitting parameters

B	4.3140E+00	1.0822E+00	9.2234E-01	1.7410E-02	1.6024E+00

ALADDIN hierarchical labelling and evaluation function:

A-B: RES D {3} [+1] GRAPHITE T=PAPYEX C [+0] #SPTAEX

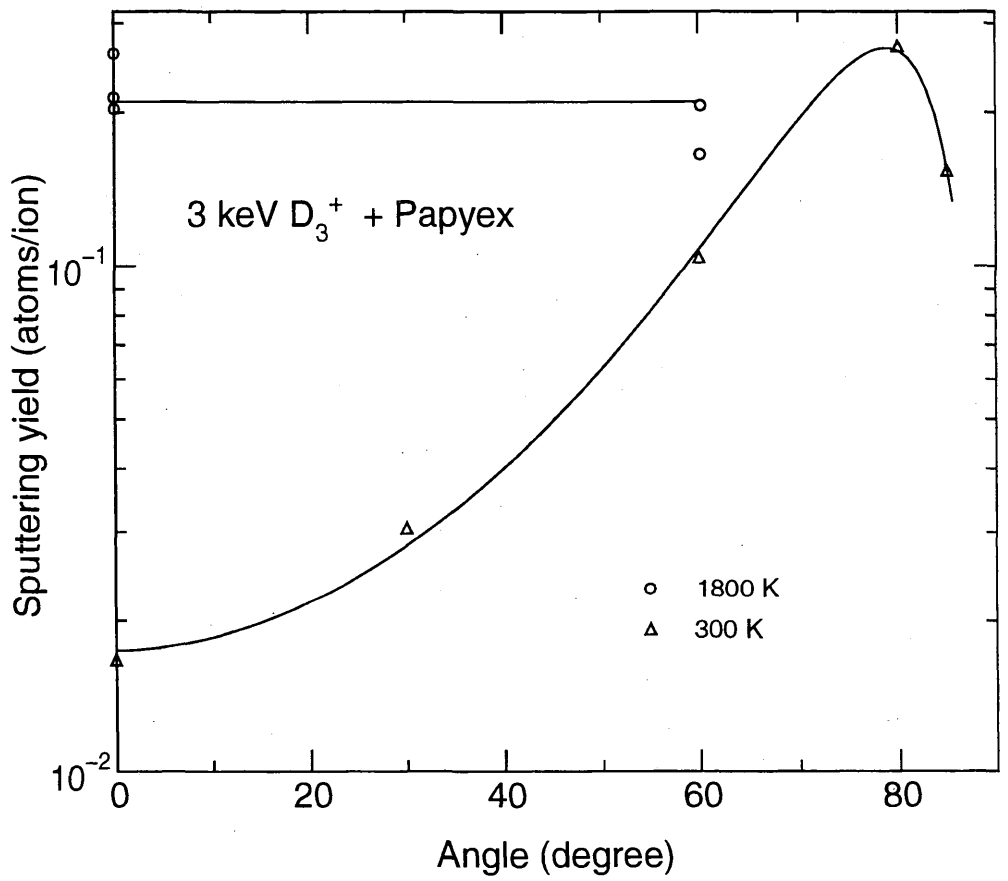

3.3.2 D^+, C^+ + graphite (pyrolytic, Papyex) → C

Source: J. Roth, J. Bohdansky and W. Ottenberger, J. Nucl. Mater. **165**, 193 (1989).

Accuracy: Yield (abs.): ±15%; T: ±20 K.

Comments: (1) Yields determined by the mass change of target.
(2) Specimens: pyrolytic graphite, papyex.
(3) D^+ and C^+ ions: mass-analyzed accelerator.
(4) The results for D^+ on papyex are from the previous page 3.3.1.

Analytic fitting:

Analytic fits for reactions A (○), B (●), C (△) and D (◇, +, x). The parameters A_1-A_5 for sets A-C correspond to f, b, c, $Y(E_0,0)$ and α_0, respectively, in the function SPTAEX (see Appendix B).

Fitting parameters A_1-A_5

A	6.9722E-01	6.6600E-06	8.5212E-01	9.4104E-01	1.7267E+00
B	7.1144E-01	6.6600E-06	8.3611E-01	1.0149E+00	1.6567E+00
C	1.1548E+00	2.0775E-01	9.9179E-01	1.3605E+00	1.6205E+00
D	5.8920E-04	2.0080E-01			

ALADDIN hierarchical labelling and evaluation function:

A-C: RES C [+1] GRAPHITE T=PYG C [+0] #SPTAEX
D: RES D [+1] GRAPHITE T=PAPYEX C [+0] #EYIELD2A

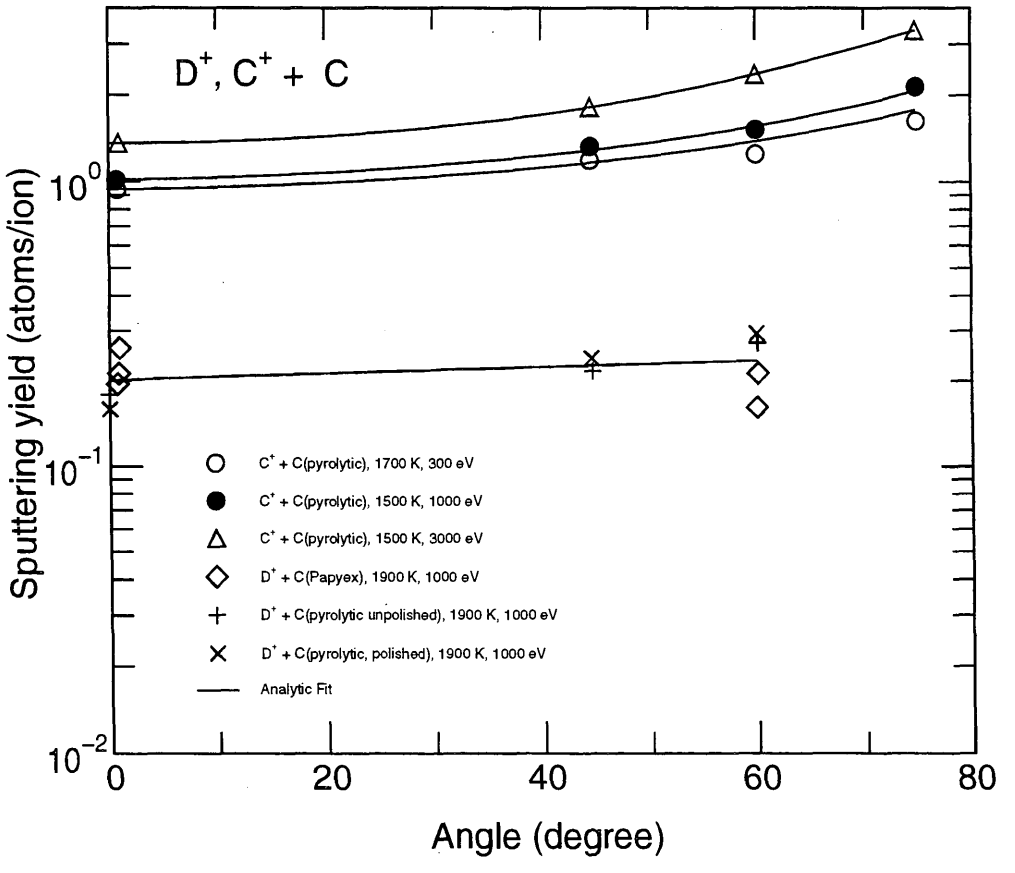

3.3.3 Ar^+ + graphite (pyrolytic, IG-430) → C

Source: Y. Ueda, K. Shiota, Y. Kitamura, Y. Ohtsuka, M. Isobe and M. Nishikawa, Fusion Eng. and Des. **41**, 55 (1998).

Accuracy: Yield (RES): 0.1-1 C/Ar^+; Yield (PS): 0.1 C/Ar^+; T: ±25 K.

Comments: (1) Yield for total erosion measured by mass loss.
(2) Specimens: IG-430 isotropic graphite, pyrolytic graphite.
(3) High-flux, non-mass-analyzed Ar^+ ion source, operated in pulsed mode.

Analytic fitting:

The data for reactions A (◇), B (•), C (○) and D (△) are reported as (Y (atoms/ion), Angle (deg.)).

Fitting parameters A_1-A_2

A	(0.0, 6.09)	(60.0, 7.32)	(75.0, 6.9)		
B	(0.0, 4.17)	(45.0, 3.5)	(45.0, 3.64)	(60.0, 3.47)	(60.0, 4.31)
C	(0.0, 1.11)	(45.0, 1.65)	(60.0, 1.82)	(75.0, 1.91)	
D	(0.0, 1.16)	(60.0, 1.89)			

ALADDIN hierarchical labelling and evaluation function:

A-C: RES Ar [+1] GRAPHITE T=IG-430 C [+0] #TAB2D
D: RES Ar [+1] GRAPHITE T=PYG C [+0] #TAB2D

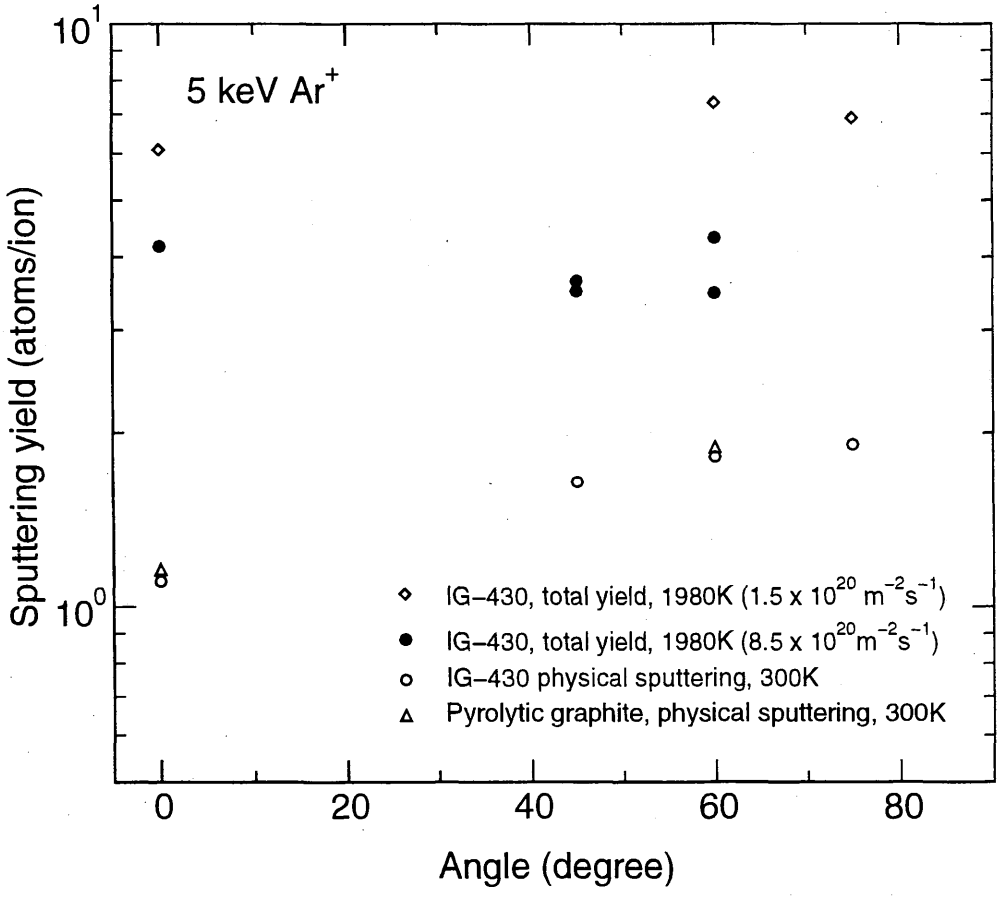

3.4.1 H_3^+ + graphite (pyrolytic) → C

Source: A. A. Haasz and J. W. Davis, J. Nucl. Mater. **151**, 77 (1987).

Accuracy: Yield (rel.): ±10%; T: ±25K.

Comments: (1) Specimen: HPG99 pyrolytic graphite (Union Carbide) at 1500 K.
(2) Incident ion energies: 300 eV H_3^+ (100 eV/H^+), 900 eV H_3^+ (300 eV/H^+), and 3 keV H_3^+ (1 keV/H^+).
(3) Ions produced by a mass-analyzed ion accelerator.
(4) Carbon atoms were collected on surfaces near specimen, and converted to methane molecules by a large flux of atomic hydrogen. Methane molecules were detected by QMS-RGA.

Analytic fitting:

Analytic fits for reactions A (•), B (△) and C (○).

Fitting parameters A_1-A_2

A	1.4108E-01	6.5953E-02
B	1.6920E-01	4.5718E-02
C	1.3027E+00	9.1175E-02

ALADDIN hierarchical labelling and evaluation function:

A-C: RES H {3} [+1] GRAPHITE T=PYG C [+0] #EYIELD2DN

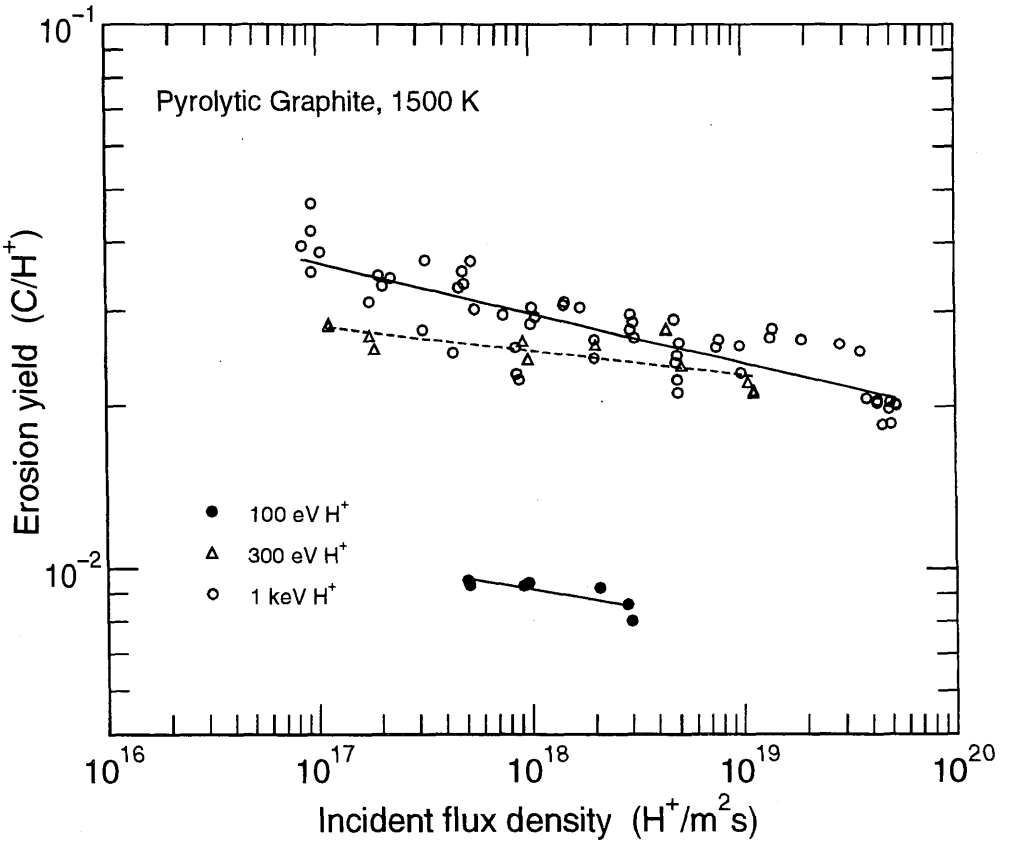

3.4.2 D^+ + graphite (pyrolytic) → C

Source: A. A. Haasz and J. W. Davis, J. Nucl. Mater. **224**, 141 (1995).

Accuracy: Yield (rel.): ±10%; T: ±25K.

Comments: (1) Specimen: HPG99 pyrolytic graphite (Union Carbide).
(2) Incident ion energy: 3 keV D_3^+ (1 keV/D^+).
(3) Ions produced by a mass-analyzed ion accelerator.
(4) Carbon atoms were detected by phase-sensitive line-of-sight QMS.
(5) Absolute yields determined by comparison with mass-loss results in Roth et al., J. Nucl. Mater. **111&112** 775 (1982) and Roth et al., J. Nucl. Mater. **122&123** 1447 (1984).

Analytic fitting:

Analytic fits for reactions A (○) and B (●).

Fitting parameters A_1-A_2

A	6.9407E+01	1.4757E-01
B	7.6591E+00	8.2189E-02

ALADDIN hierarchical labelling and evaluation function:

A-B: RES D [+1] GRAPHITE T=PYG C [+0] #EYIELD2DN

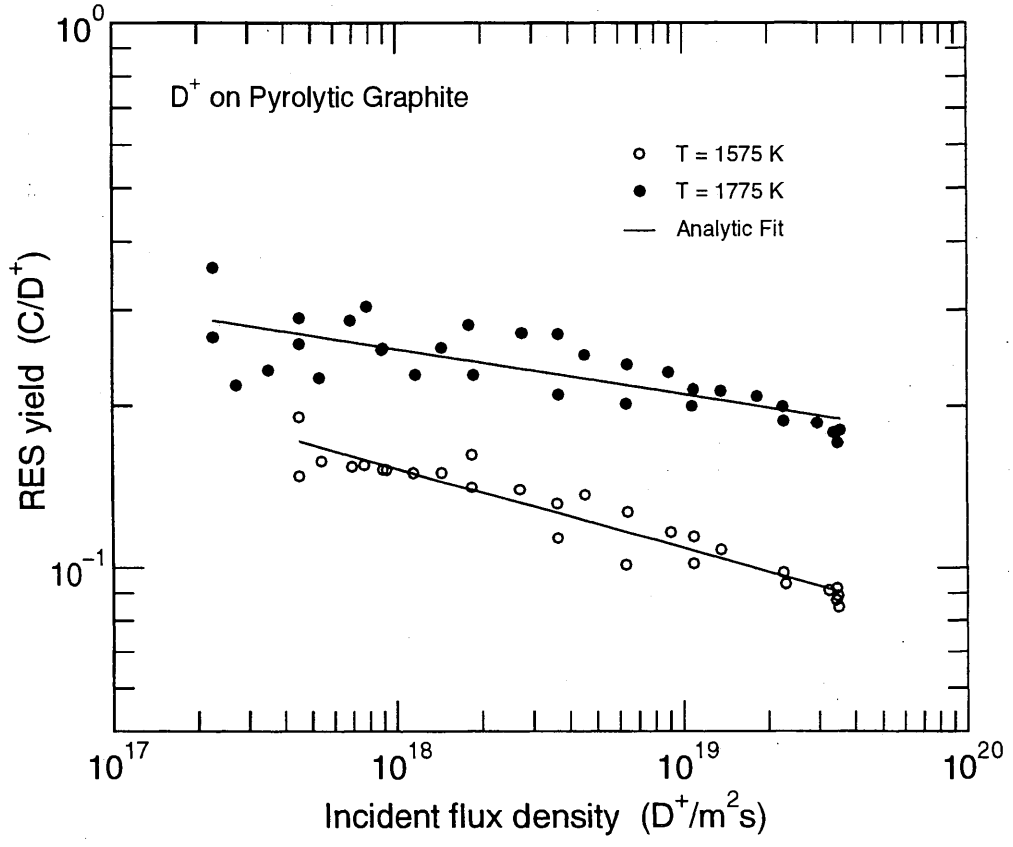

3.4.3 Ar^+ + graphite (pyrolytic) → C

Source: V. Philipps, K. Flaskamp and E. Vietzke, J. Nucl. Mater. **111&112**, 781 (1982).

Accuracy: Yield (rel.): 50%.

Comments: (1) RES signals for 5 keV Ar^+ on pyrolytic graphite.
(2) C atoms (C_1) and C_2 radicals detected by line-of-sight QMS.

Analytic fitting:

Analytic fits for reactions A (•) and B (x).

Fitting parameters A_1-A_2

A	4.6365E-16	-9.2701E-01
B	4.1819E-15	-8.0448E-01

ALADDIN hierarchical labelling and evaluation function:

A: RES Ar [+1] GRAPHITE T=PYG C {1} [+0] #EYIELD2D
B: RES Ar [+1] GRAPHITE T=PYG C {2} [+0] #EYIELD2D

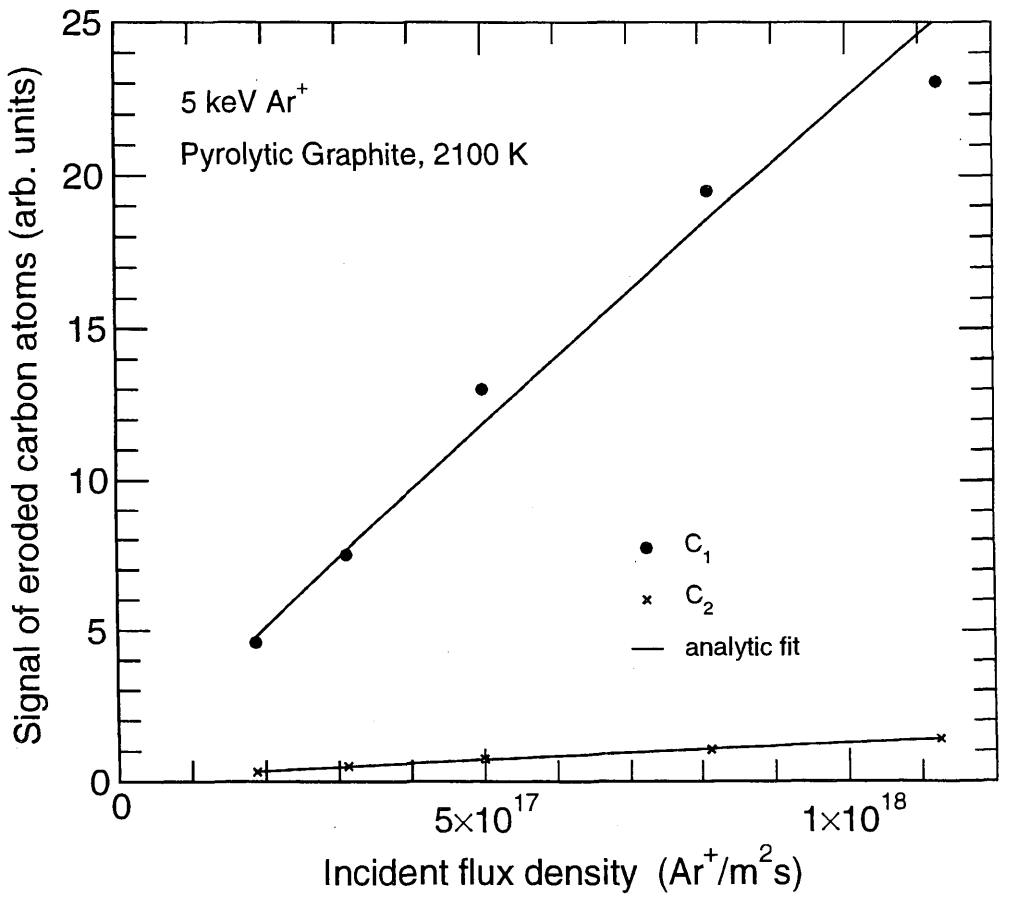

3.4.4 Ar^+ + graphite (pyrolytic) → C

Source: V. Philipps, E. Vietzke, R. P. Schorn and H. Trinkaus, J. Nucl. Mater. **155&157**, 319 (1988).

Accuracy: Yield (rel.): 50%.

Comments: (1) Flux dependence of RES and physical sputtering for 5 keV Ar^+ on pyrolytic graphite.
(2) C atoms detected by line-of-sight QMS.
(3) Analytic fit is based on both low and high flux data.

Analytic fitting:

Analytic fits for reactions A (•, *) and B (○, △).

Fitting parameters A_1-A_2

A	6.7413E-14	-9.2146E-01
B	2.1649E-16	-9.7941E-01

ALADDIN hierarchical labelling and evaluation function:

A, B: RES Ar [+1] GRAPHITE T=PYG C {1} [+0] #EYIELD2D

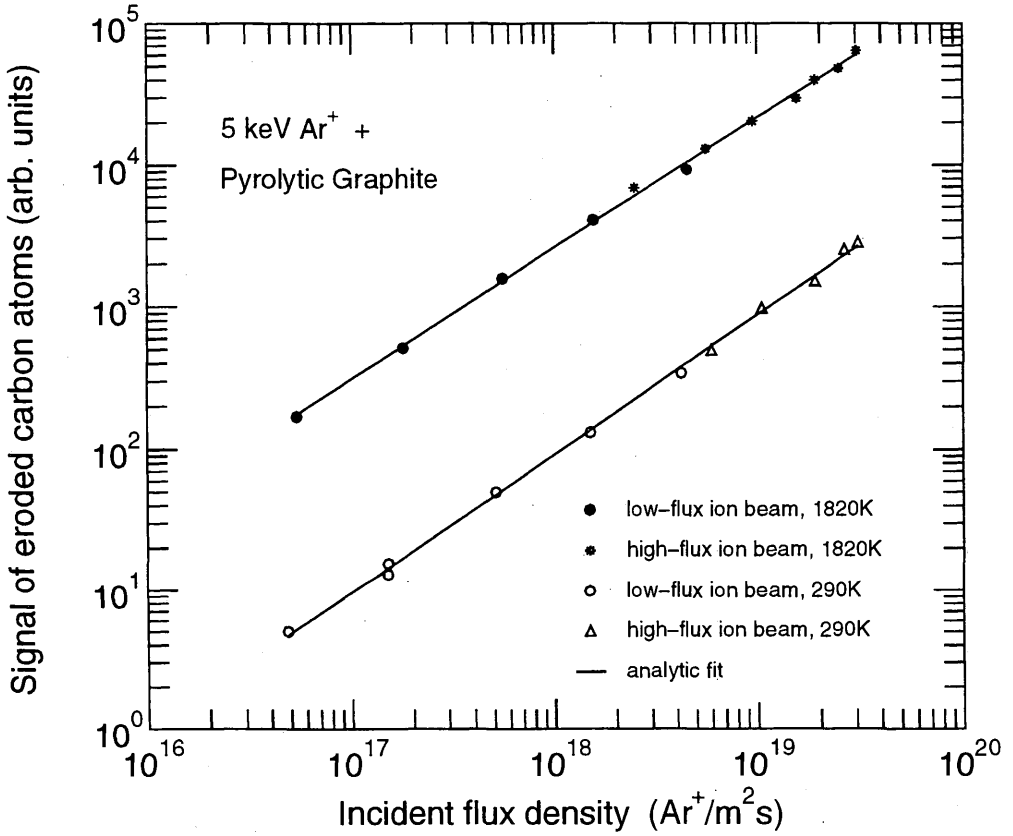

3.4.5 Ar^+ + graphite (IG-430) → C

Source: Y. Ueda, K. Shiota, Y. Kitamura, Y. Ohtsuka, M. Isobe and M. Nishikawa, Fusion Eng. and Des. **41**, 55 (1998).

Accuracy: Yield: 0.5-1 C/Ar^+; T: ±25 K.

Comments: (1) Yield for total erosion measured by mass loss.
(2) Specimens: IG-430 isotropic graphite.
(3) High-flux, non-mass-analyzed Ar^+ ion source, operated in pulsed mode.
(4) Yield measurements for specimens with 0 and 60 degrees angles of incidence.

Analytic fitting:

Analytic fits for reactions A (○) and B (●).

Fitting parameters A_1-A_2

A	2.4291E+06	2.7748E-01
B	3.6968E+06	2.8503E-01

ALADDIN hierarchical labelling and evaluation function:

RES Ar [+1] GRAPHITE T=PYG C [+0] #EYIELD2DN

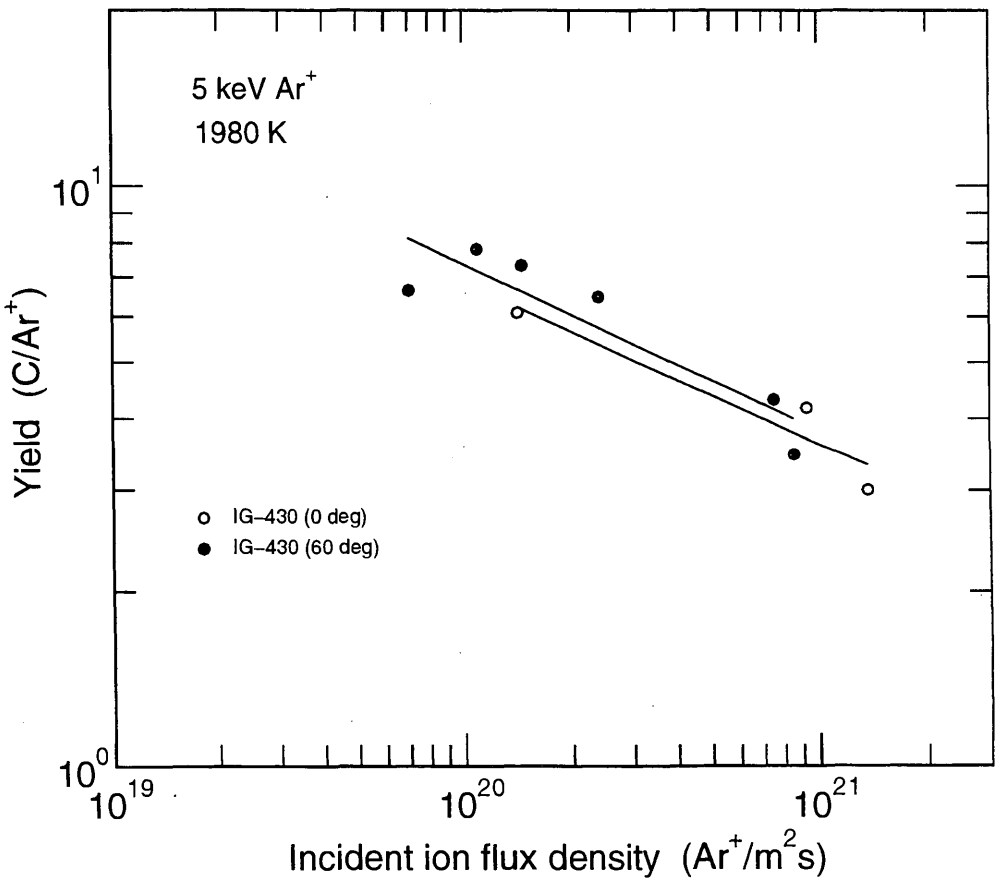

3.4.6 Ar^+ + graphite (ISO-630) → total, C

Source: Y. Ueda, K. Nakano, Y. Ohtsuka, M. Isobe, S. Goto and M. Nishikawa, J. Nucl. Mater. **227**, 251 (1996).

Accuracy: Yield: 0.3-0.5 C/Ar^+.

Comments: (1) Yield for total erosion measured by mass loss.
(2) RES yield calculated by subtracting a physical sputtering yield as measured at room temperature, 1.3 C/Ar^+, from total erosion yield.
(3) Specimen: ISO-630 isotropic gaphite.
(4) High-flux, non-mass-analyzed Ar^+ ion source, operated in pulsed mode.
(5) Impurity content of beam < 6% (H, C, O).

Analytic fitting:

Analytic fits for reactions A (○) and B (●).

Fitting parameters A_1-A_2

A	5.8827E+04	2.0335E-01
B	1.1105E+06	2.7266E-01

ALADDIN hierarchical labelling and evaluation function:

A: RES Ar [+1] GRAPHITE T=ISO-630 C [+0] #EYIELD2DN
B: RES Ar [+1] GRAPHITE T=ISO-630 C [+0] #EYIELD2DN

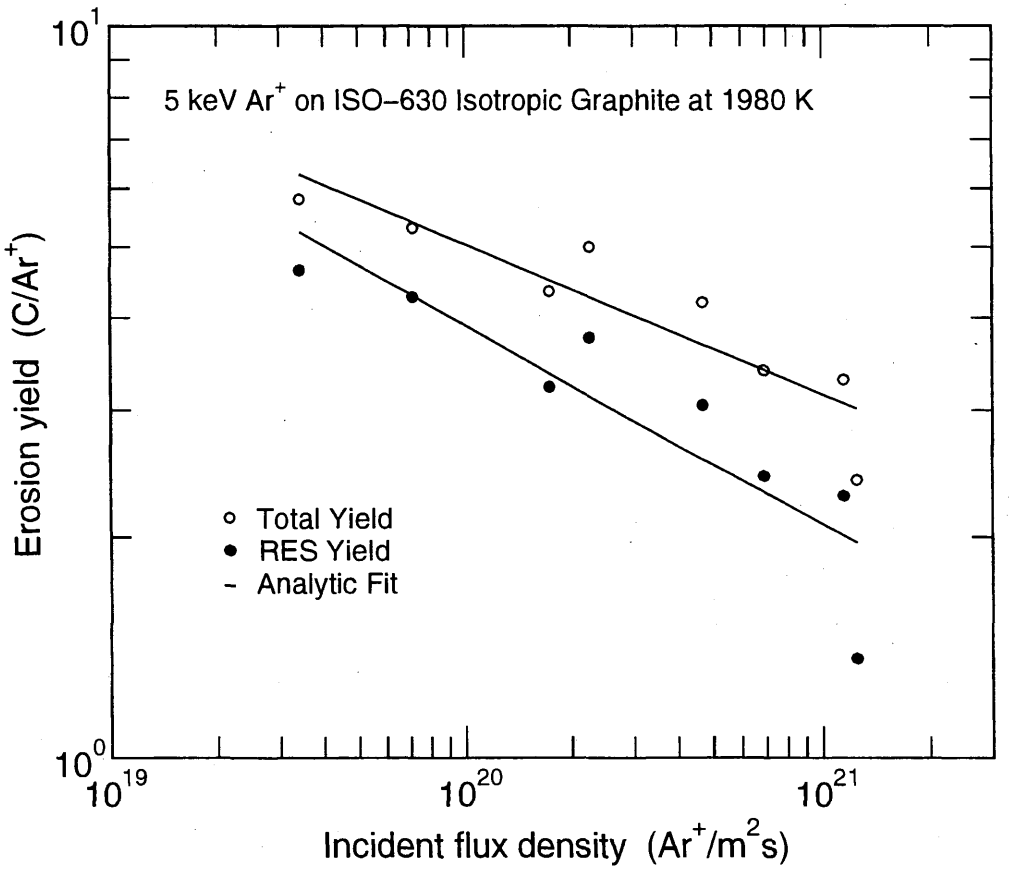

3.4.7 Ar^+ + graphite (pyrolytic, RG-Ti, ISO-630) → C

Source: Y. Ohtsuka, Y. Ueda, M. Isobe, S. Goto and M. Nishikawa, J. Nucl. Sci. Tech. **34**, 792 (1997).

Accuracy: Yield: 0.3-0.5 C/Ar^+.

Comments: (1) Yield for total erosion measured by mass loss.
(2) Specimens: pyrolytic graphite, RG-Ti titanium-doped graphite, and ISO-630 graphite.
(3) High-flux, non-mass-analyzed Ar^+ ion source, operated in pulsed mode.
(4) Impurity content of beam < 6% (H, C, O).

Analytic fitting:

Analytic fits for reactions A (o) and B (•). Data for ISO-630 graphite is shown and fitted on the previous page, 3.4.6.

Fitting parameters A_1-A_2

A	8.1346E+05	2.5353E-01
B	2.0251E+05	2.4271E-01

ALADDIN hierarchical labelling and evaluation function:

A: RES Ar [+1] GRAPHITE T=PYG C [+0] #EYIELD2DN
B: RES Ar [+1] GRAPHITE T=RG-Ti C [+0] #EYIELD2DN

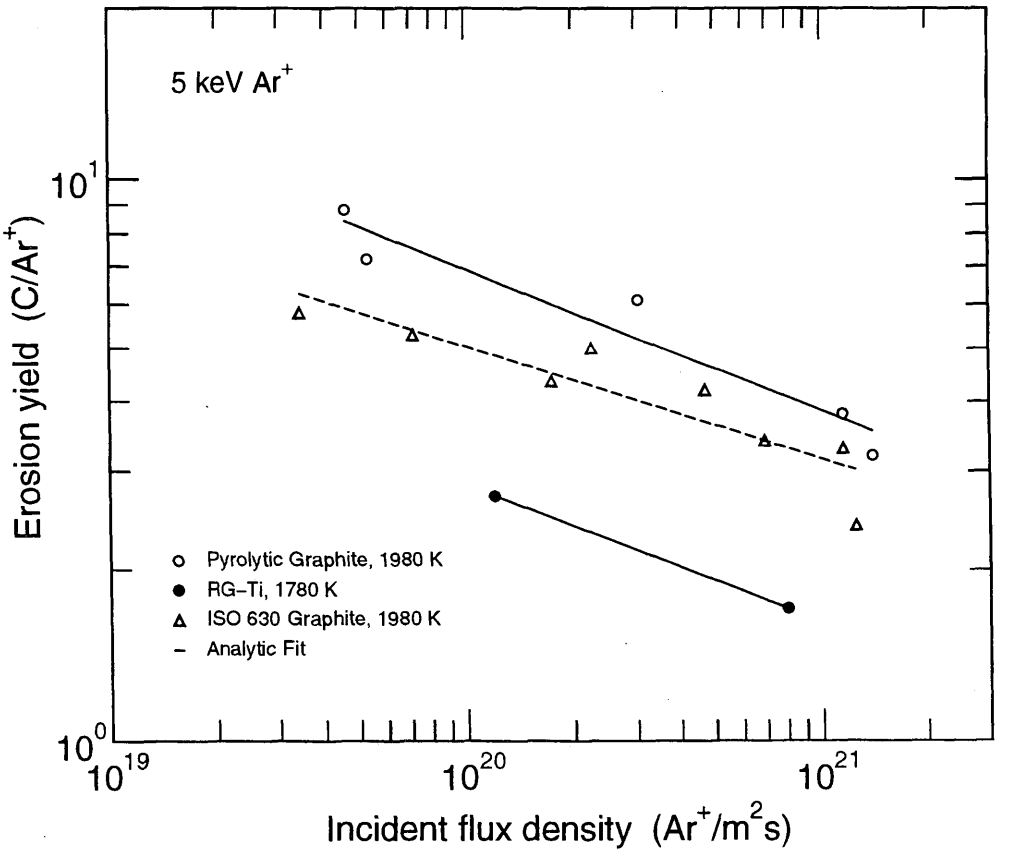

Appendix A: List of Abbreviations

Abbreviations used for experimental techniques and facilities:

JET - Joint European Torus
NRA - nuclear reaction analysis
PISCES - Plasma Interactive Surface Component Experimental Station
RGA - residual gas analysis
TEXTOR - Tokamak Experiment for Technology Oriented Research
TFTR - Tokamak Fusion Test Reactor
QMS - quadrupole mass spectrometer

Abbreviations used in graph labels:

Y - generic erosion yield (physical sputtering, RES, chemical erosion, or the sum)
T - target temperature

Abbreviations used for material descriptions and ALADDIN hierarchical labels:

A-CH-FILM - a-C:H (amorphous hydrogenated carbon film)
A-CB-FILM - a-C/B:H, (amorphous hydrogenated carbon/boron film)
B4C - boron carbide
B4C-CL5890 - B_4C plasma sprayed on CL5890, 80% Boron, SNMI (France)
BASAL-PL - basal-plane orientation
BASE-PL - base-plane orientation
BASAL-PL-CL - basal-plane orientation, cleaved
BASAL-PL-MI - milled-plane orientation, milled
C-SiC - C-SiC coated graphite
CKC - Ceramics Kingston Ceramiques, Inc. (Canada)
CLOR - 5829 graphite, Carbone Lorraine (France)
CX-2002U - carbon fiber composite
D - dopant material
DIAM-FILM - diamond film deposited on a substrate
DPE - boronized isotropic graphite, 0.5% Boron, UKAEA (United Kingdom)
EDGE-PL - edge-plane orientation
EK98 - isotropic fine grain graphite (Ringsdorff)
GB - boronized graphite, structure: as in GB-100, Toyo Tanso (Japan)
GRAPHITE - graphite material, generic
GRAVIMOL - carbon/carbon composite
HPG - pyrolytic graphite, anisotropic, Union Carbide (USA)
HPG99 - polycrystalline pyrolytic graphite, Union Carbide (USA)
HPG-PI - pyrolytic graphite, preirradiated
IG-110U, IG-430, ISO-630U, ISO-880U - isotropic graphite, Toyo Tanso (Japan)
KUP-VM - carbon/carbon composite
M019AII - isotropic graphite, 41% Boron, Toyo Tanso (Japan)
MPG-8,9 - MPg-8,9 graphite
O - sample orientation
PAPYEX - compressed graphite tape
POCO - low-impurity, high-density (low-porosity) isotropic graphite

POCO-AXF5Q - POCO graphite (product number AXF5Q)
PFG - pyrolytic graphite, Pfizer (USA)
PYG - pyrolytic graphite, generic
RES - radiation enhanced sublimation yield
PYROID - pyrolytic graphite
RG-Ti - Recrystallized graphite containing 1.7 at%Ti
SAT - sputtering by atoms leading to molecule and atom emission (physical + chemical erosion)
SEP-CFC - carbon fiber composite, SEP (France)
S1325 - isotropic graphite, 32% Boron, Carbone Lorraine (France)
S2508 - anisotropic graphite, 3% Boron, Carbone Lorraine (France)
T - material type
TFTR-REDEP - TFTR redeposited graphite
TT - Toyo Tanso
USB15 - boronized isotropic graphite, NII Grafit (Russia)

Appendix B: List of Analytic Fitting Functions

The following analytic functions are used to represent erosion data as functions of the variable X. In this work X may represent target temperature, incident particle kinetic energy, or incident particle flux. The function names EYIELD2E, EYIELD3B, etc., refer to the relevant ALADDIN evaluation function. If "N" is attached to the end of the function name, e.g. EYIELD3BN, a logarithmic fit was performed. The functions for fitting the yields in Section 3 were implemented using the MINPACK subroutine LMDIF1, which minimizes the sum of squares of M nonlinear functions in N variables using a modified Levenberg-Marquardt algorithm. Convergence was reached when the relative error in the sum of squares was at most 10^{-3}-10^{-4}, or the relative error between the estimated solution vector and the final solution vector was at most 10^{-3}-10^{-4}.

$$Y = A_1 X + A_2 \qquad \text{[EYIELD2A]}$$

$$Y = A_1 \exp(A_2 X) \qquad \text{[EYIELD2B]}$$

$$Y = A_1 X^{-A_2} \qquad \text{[EYIELD2D]}$$

$$Y = A_1 \exp(-A_2/X) \qquad \text{[EYIELD2E]}$$

$$Y = A_1 \exp(-A_2 X) X^{A_3} \qquad \text{[EYIELD3A]}$$

$$Y = A_1 \exp(-A_2/X) + A_3 \qquad \text{[EYIELD3B]}$$

$$Y = A_1 \exp(-A_2 X) + A_3 \qquad \text{[EYIELD3C]}$$

$$Y = A_1 \exp(-(X - A_2)^2/A_3) X^{A_4} \qquad \text{[EYIELD4B]}$$

$$Y = A_1 \ln(A_2 X)(1 - A_3/X)^2 X^{A_4} \qquad \text{[EYIELD4F]}$$

$$Y = A_1 \exp(-A_2/X) + A_3 \exp(-A_4/X) \qquad \text{[EYIELD4G]}$$

$$Y = A_1 \exp(-A_2/X) + A_3 \exp(-A_4/X) + A_5 \qquad \text{[EYIELD5B]}$$

$$Y = A_1 \ln(A_2 X)(1 - A_3/X)^{A_4} X^{A_5} \qquad \text{[EYIELD5D]}$$

$$Y = A_1 \exp(-A_2 X) + A_3 \exp(-A_4/X) + A_5 \qquad \text{[EYIELD5E]}$$

$$Y = A_1 \exp(-(X - A_2)^2/A_3) X^{A_4} + A_5 \exp(-A_6 X) X^{A_7} \qquad \text{[EYIELD7A]}$$

$$Y = A_1 \exp(-(X - A_2)^2/A_3) X^{A_4} + A_5 \exp(-A_6 X) X^{A_7} + A_8 \qquad \text{[EYIELD8C]}$$

$$Y = A_1 \exp(-(X - A_2)^2/A_3) X^{A_4} + A_5 \exp(-A_6/X) X^{A_7} + A_8 \qquad \text{[EYIELD8D]}$$

$$Y = A_1 \exp(-(X - A_2)^2/A_3) X^{A_4} + A_5 \exp(-A_6 X) X^{A_7} + A_8 \exp(-A_9/X) + A_{10} \qquad \text{[EYIELD10A]}$$

$$Y(E_0) = 0.5Q\frac{\left(\frac{E_0}{E_{th}}-1\right)^{\mu}\ln(1+1.2288\varepsilon)}{\lambda+\left(\frac{E_0}{E_{th}}-1\right)^{\mu}\left[\varepsilon+0.1728\sqrt{\varepsilon}+0.008\varepsilon^{0.1504}\right]} \qquad \text{[SPTEEX]}$$

$$Y(E_0,\alpha) = Y(E_0,0)\left\{\cos\left[\left(\frac{\alpha}{\alpha_0}\frac{\pi}{2}\right)^{c}\right]\right\}^{-f}\exp\left\{b\left(1-\frac{1}{\cos\left[\left(\frac{\alpha}{\alpha_0}\frac{\pi}{2}\right)^{c}\right]}\right)\right\} \qquad \text{[SPTAEX]}$$

Contents of previous volumes of Atomic and Plasma–Material Interaction Data for Fusion

Volume 1 (1991)

Volume 2 (1992)

Volume 3 (1992)

Volume 4 (1993)

Volume 5 (1994)

Volume 6 (1995)

Volume 7/A (1998)

No. 11, June 2000

WHERE TO ORDER IAEA PUBLICATIONS

In the following countries IAEA publications may be purchased from the sources listed below, or from major local booksellers. Payment may be made in local currency or with UNESCO coupons.

AUSTRALIA
Hunter Publications, 58A Gipps Street, Collingwood, Victoria 3066
Telephone: +61 3 9417 5361 • Fax: +61 3 9419 7154 • *E-mail: jpdavies@ozemail.com.au*

BELGIUM
Jean de Lannoy, avenue du Roi 202, B-1060 Brussels • Telephone: +32 2 538 43 08 • Fax: +32 2 538 08 41
E-mail: jean.de.lannoy@infoboard.be • Web site: http://www.jean-de-lannoy.be

BRUNEI
Parry's Book Center Sdn. Bhd., 60 Jalan Negara, Taman Melawati, 53100 Kuala Lumpur, Malaysia
Telephone: +60 3 4079176, 4079179, 4087235, 4087528 • Fax: +60 3 407 9180
E-mail: haja@pop3.jaring.my • Web site: http://www.mol.net.my/~parrybook/parrys.htm

CANADA
Renouf Publishing Company Ltd., 1-5369 Canotek Rd., Ottawa, Ontario, K1J 9J3
Telephone: +613 745 2665 • Fax +613 745 7660
E-mail: order.dept@renoufbooks.com • Web site: http://www.renoufbooks.com

CHINA
IAEA Publications in Chinese: China Nuclear Energy Industry Corporation, Translation Section, P.O. Box 2103, Beijing

DENMARK
Munksgaard Direct, Postbox 173, DK-1005 København K
Telephone: +45 77 33 33 33 • Fax: +45 77 33 33 77
E-mail: direct@munksgaarddirect.dk • Web site: http://www.munksgaarddirect.dk

FRANCE
Nucléon, Immeuble Platon, Parc les Algorithmes,F-91194 Gif-sur-Yvette, Cedex
Telephone: +33 1 69 353636 • Fax +33 1 69 350099 • *E-mail: nucleon@wanadoo.fr*

GERMANY
UNO-Verlag, Vertriebs- und Verlags GmbH, Am Hofgarten 10, D-53113 Bonn
Telephone: +49 228 94 90 20 • Fax: +49 228 94 90 222
E-mail: unoverlag@aol.com • Web site: http://www.uno-verlag.de

HUNGARY
Librotrade Ltd., Book Import, P.O. Box 126, H-1656 Budapest
Telephone: +36 1 257 7777 • Fax: +36 1 257 7472 • *E-mail: books@librotrade.hu*

INDIA
Allied Publishers Limited, 1-13/14, Asaf Ali Road, New Delhi 110002
Telephone: +91 11 3233002, 004 • Fax: +91 11 3235967
E-mail: aplnd@del2.vsnl.net.in • Web site: http://www.alliedpublishers.com

ISRAEL
YOZMOT Ltd., 3 Yohanan Hasandlar St., P.O. Box 56055, IL-61560 Tel Aviv
Telephone: +972 3 5284851 • Fax: +972 3 5285397

ITALY
Libreria Scientifica Dott. Lucio di Biasio "AEIOU", Via Coronelli 6, I-20146 Milan
Telephone: +39 2 48 95 45 52 or 48 95 45 62 • Fax: +39 2 48 95 45 48

JAPAN
Maruzen Company, Ltd., P.O. Box 5050, 100-3191 Tokyo International
Telephone: +81 3 3275 8539 • Fax: +81 3 3275 0657
E-mail: journal@maruzen.co.jp • Web site: http://www.maruzen.co.jp

MALAYSIA
Parry's Book Center Sdn. Bhd., 60 Jalan Negara, Taman Melawati, 53100 Kuala Lumpur,
Telephone: +60 3 4079176, 4079179, 4087235, 4087528 • Fax: +60 3 407 9180
E-mail: haja@pop3.jaring.my • Web site: http://www.mol.net.my/~parrybook/parrys.htm

NETHERLANDS
Martinus Nijhoff International, P.O. Box 269, NL-2501 AX The Hague
Telephone: +31 793 684 400 • Fax: +31 793 615 698 • *E-mail: info@nijhoff.nl • Web site: http://www.nijhoff.nl*

Swets and Zeitlinger b.v., P.O. Box 830, NL-2160 SZ Lisse
Telephone: +31 252 435 111 • Fax: +31 252 415 888 • *E-mail: infoho@swets.nl • Web site: http://www.swets.nl*

POLAND
Ars Polona, Book Department/Import, P.O. Box 1001, PL-00-950 Warsaw
Telephone: +48 22 826 1201 ext. 147, 151, 159, 167 • Fax: +48 22 826 4763
E-mail: ksiazki@arspolona.com.pl • books119@arspolona.com.pl • Web site: http://www.arspolona.com.pl

SINGAPORE
Parry's Book Center Pte. Ltd., 528 A MacPherson Rd., Singapore 1336
Telephone: +65 744 8673 • Fax: +65 744 8676
E-mail: haja@pop3.jaring.my • Web site: http://www.mol.net.my/~parrybook/parrys.htm

SLOVAKIA
Alfa Press, s.r.o, Račianska 20, SQ-832 10 Bratislava • Telephone/Fax: +421 7 566 0489

SPAIN
Díaz de Santos, S.A., c/ Juan Bravo, 3A, E-28006 Madrid
Telephone: +34 91 781 94 80 • Fax: +34 91 575 55 63 • *E-mail: compras@diazdesantos.es • carmela@diazdesantos.es barcelona@diazdesantos.es • julio@diazdesantos.es • Web site: http://www.diazdesantos.es*

UNITED KINGDOM
The Stationery Office Ltd, International Sales Agency, 51 Nine Elms Lane, London SW8 5DR
Telephone: +44 171 873 9090 • Fax: +44 171 873 8463
E-mail: Orders to: book.orders@theso.co.uk • Enquiries to: ipa.enquiries@theso.co.uk
Web site: http://www.the-stationery-office.co.uk

UNITED STATES OF AMERICA
Bernan Associates, 4611-F Assembly Drive, Lanham, MD 20706-4391, USA
Telephone: 1-800-274-4447 (toll-free) • Fax: (301) 459-0056 / 1-800-865-3450 (toll-free)
E-mail: query@bernan.com • Web site: http://www.bernan.com

Renouf Publishing Company Ltd., 812 Proctor Ave., Ogdensburg, New York, 13669
Telephone: +888 551 7470 (toll-free) • Fax +888 568 8546 (toll-free)
E-mail: order.dept@renoufbooks.com • Web site: http://www.renoufbooks.com

Orders and requests for information may also be addressed directly to:

Sales and Promotion Unit, International Atomic Energy Agency
Wagramer Strasse 5, P.O. Box 100, A-1400 Vienna, Austria
Telephone: +43 1 2600 22529 (or 22530) • Facsimile: +43 1 2600 29302
E-mail: sales.publications@iaea.org • Web site: http://www.iaea.org/worldatom/Books